THE UNIVERSITY *of* EDINBURGH

The Proteomic Response to Metabolic Stress and Cellular Dysfunction in Relation to Alzheimer's disease

Abigail Herrmann BSc (Hons)

April 2014

A thesis submitted for the degree of Doctor of Philosophy to the College of Medicine and Veterinary Medicine, University of Edinburgh

Centre for Cognitive and Neural Systems
1 George Square
Edinburgh, EH8 9JZ

Acknowledgements

First and foremost, I offer my sincerest thanks to my supervisors, Professor James McCulloch and Dr Ruth Deighton, for their guidance, encouragement and scientific enthusiasm. I am forever grateful to you both for getting me on a solid track and keeping me there.

I also wish to extend my gratitude and appreciation to the talented scientists that I have been privileged enough to collaborate with during my PhD. Thank you to the team at SynthSys, Dr Lorraine Kerr, Dr Sarah Martin and particularly Dr Thierry Le Bihan, who ensured this proteomic research was carried out to the highest standard, and answered my endless questions with insight and humour – I couldn't have done this without you. To Mailis McCulloch, an artist with an electron microscope, thank you for providing such beautiful images, and for painstakingly helping me turn them into dreary numbers! I am also grateful for the generosity of Dr Trudi Gillespie in sharing her immunofluorescence knowledge with me.

Sincere thanks are given to Professor Mike Cousin and his lab members for making me welcome, imparting their extensive scientific knowledge, and letting me share their bench space. I am particularly appreciative of Dr Sarah Gordon, for being an excellent mentor, and for keeping me calm in the face of experimental adversity...!

A special mention must be given to my fellow lab members who have come and gone over the years. I am grateful for the time spent with Dr Severine Launay and Jocelyn Kemp, for their support early in my scientific career, and for encouraging me to undertake this PhD. Also to Ian Heron for his patience in introducing me to the world of cell culture. I am endlessly thankful to Dr Luke Searcy, Callum Johnston and Jamie McQueen, who together provided onsite scientific and personal therapy, and have kept my feet firmly on the ground at all times. I also want to thank the talented Will Herrmann for his help in designing the figures contained within this thesis.

Latterly, I am hugely appreciative of the support of Dr Tara Spires-Jones in getting me over the PhD finish line, and being such a consistently kind and generous person, thank you. Thanks also to Dr Paul Skehel for helping me navigate the challenges of the PhD process, and for testing my scientific thinking. I must also acknowledge the Medical Research Council for providing the financial support for my research, and enabling me to attend national and international conferences.

Finally, I am truly thankful to my family for all their support and encouragement. Above all, I am grateful to Mum and Dad, who have been a constant source of assurance in their unwavering belief in me over the years.

I dedicate this thesis to you both.

Declaration

I declare that this thesis contains my own original work, solely carried out by me, except where acknowledged in the text. The contents of this thesis have not been submitted previously for any other degree or professional qualification. All sources of data and information have been specifically referenced.

Abigail Herrmann

Table of Contents

Chapter 3: Investigating the Proteomics of Metabolic Stress and Mitochondrial Dysfunction in an *in vitro* model of the Vascular Contribution to Alzheimer's disease

Chapter 4: Examining ABAD Interacting Proteins and their Response to Metabolic Stress

Chapter 5: Investigating a Possible Role for ABAD in APP Processing

Chapter 6: Discussing the Utility of the Present Studies and Future Proteomic Investigations in enhancing our Understanding of Alzheimer's disease

References, Appendices & Publications

List of Tables

List of Figures

Chapter 1

Chapter 2

Chapter 3

Chapter 4

Chapter 5

Chapter 6

Abbreviations

2-DG	2-Deoxyglucose
2-DE	2-dimensional electrophoresis
ABAD	amyloid binding alcohol dehydrogenase
AD	Alzheimer's disease
APOE	apolipoprotein E
APP	amyloid precursor protein
ATP	adenosine triphosphate
Aβ	aggregated amyloid-beta
BCAS	bilateral common carotid artery stenosis
BCCAO	bilateral common carotid artery occlusion
CATCH	critically attained threshold of cerebral hypoperfusion
CCH	chronic cerebral hypoperfusion
CSF	cerebral spinal fluid
DAVID	database for annotation, visualization and integrated discovery
DMEM	dulbecco's modified eagle medium
EIFs	eukaryotic translation initiation factors
ELISA	enzyme linked immunosorbent assay
EM	electron microscopy
ER	endoplasmic reticulum
ETC	electron transport chain
FBS	fetal bovine serum
FT	flow through
GO	gene ontology
GRPs	glucose-regulated proteins
GWAS	genome-wide association studies
HPLC	high performance – liquid chromatography

ICAT	isotope-coded affinity tags
IP	immunoprecipitation
IPA	ingenuity pathway analysis
IP-MS	immunoprecipitation – mass spectrometry
iTRAQ	isobaric tags for relative and absolute quantification
LC-MS	liquid chromatography – mass spectrometry
MAM	mitochondrial associated membrane
MCI	mild cognitive impairment
MCU	mitochondrial calcium uniporter
MRI	magnetic resonance imaging
mtDNA	mitochondrial DNA
NFTs	neurofibrillary tangles
NMDA	N-methyl-D-aspartate
OD	optical density
OGD	oxygen-glucose deprivation
PBS	phosphate buffered saline
PET	positron emission tomography
PFL	protein frequency library
Prxs	peroxiredoxins
PTP	permeability transition pore
ROS	reactive oxygen species
sAPP	soluble APP
SDS-PAGE	sodium dodecyl sulfate polyacrylamide gel electrophoresis
SILAC	stable isotope labelling by amino acids in cell culture
SUMO	small ubiquitin-like modifier protein
UPR	unfolded protein response
VDAC	voltage dependent anion channels

Abstract

Vascular risk factors inducing a state of chronic cerebral hypoperfusion and metabolic stress are thought to influence the onset and progression of Alzheimer's disease (AD). To investigate the complex molecular changes underpinning cellular adaptation to metabolic stress, the first aim of this thesis was to define the proteomic response of the SH-SY5Y human neuroblastoma cell line after exposure to the metabolic challenge of oxygen glucose deprivation (OGD). 958 proteins across multiple subcellular compartments were detected and quantified by label-free liquid chromatography mass spectrometry (LC-MS). The levels of 130 proteins were significantly increased ($P<0.01$) after OGD and the levels of 63 proteins were significantly decreased ($P<0.01$) while expression of the majority of proteins (765) was not altered. Ingenuity Pathway Analysis identified novel protein-protein interactomes involved with mitochondrial energy production, protein folding, and protein degradation, indicative of coherent and integrated proteomic responses to the metabolic challenge. Approximately one third (61) of the differentially expressed proteins were associated with the endoplasmic reticulum and mitochondria. Electron microscopic analysis of these subcellular structures showed morphologic changes consistent with the identified proteomic alterations.

Pertinent to AD research, amyloid binding alcohol dehydrogenase (ABAD) was found to be significantly increased in response to OGD. ABAD is emerging as a key player in mitochondrial dysfunction in AD, yet full understanding of the biochemical pathways in which this protein is involved remain elusive. Using immunoprecipitation coupled to LC-MS (IP-MS), the second aim of the thesis was to characterise the ABAD protein interactome in SH-SY5Y cells and its response to metabolic stress. 67 proteins were identified as potential ABAD interactors under control conditions, and 69 proteins were identified as potential ABAD interactors under OGD conditions. The Database for Annotation, Visualization and Integrated Discovery (DAVID) was used to

determine the subcellular locations and biological functions of the ABAD interacting proteins in control and OGD conditions. DAVID identified the nuclei and mitochondria to contain the greatest number of changes in ABAD interacting proteins following OGD. "Glucose Metabolic Process" (GO:0006006) was the top functional cluster for ABAD interacting proteins in both control and OGD conditions. Independent immunoprecipitations, western blotting, immunohistochemistry and electron microscopy were used to validate specific protein interactions.

OGD was found to initiate a novel interaction between ABAD and glucose-regulated protein 75 (GRP75), a finding confirmed in human AD tissue. GRP75 is a mitochondrial protein and marker of the mitochondrial associated membrane (MAM), a specialised region between the mitochondria and the ER. The MAM is known to be enriched with presenilin proteins, involved in the proteolytic cleavage of amyloid precursor protein (APP). These data were used to generate an "*ABAD-GRP75-MAM hypothesis of mitochondrial dysfunction in AD*", which might provide a novel link between chronic metabolic stress, ABAD, mitochondrial dysfunction and the onset / progression of AD. The third aim of the thesis was to test this novel hypothesis. Western blotting revealed APP to be significantly decreased following OGD, concurrent with an increase in ABAD protein levels. Over-expression of ABAD protein in SH-SY5Y cells was used to test whether the increased levels of ABAD following OGD were the driving force behind APP down-regulation. ABAD over-expression in SH-SY5Y cells was found to have no detectable effect on APP. Conversely, electron microscopy revealed a dynamic response of the MAM to metabolic stress. This result, along with the interaction of ABAD with GRP75, and the enrichment of presenilins at the MAM, suggests that this specialised membrane region may have an important role to play in AD.

The data presented within this thesis provide the first comprehensive analysis of the proteomic and morphologic response of human SH-SY5Y cells to prolonged metabolic challenge. The lack of acute ischemic cell death in this *in vitro* model makes the data particularly pertinent to the compromised energy metabolism associated with slowly evolving neurodegenerative disorders, including Alzheimer's disease. The generation of novel hypotheses from highly descriptive proteomic investigations provides a powerful platform for discovery based research, a strategy that is becoming increasingly important for the advancement of neurodegenerative research.

Chapter 1: Introducing Alzheimer's Disease, Mitochondria and Proteomics

Chapter 1: Introducing Alzheimer's disease, the Mitochondria, and Proteomics

1.1 Dementia, Ageing and Cognitive Decline: A Historical Perspective

Dementia, derived from the Latin de- (meaning without) and -mens (meaning mind), is not a modern disorder. Historical texts as early as those of Plato saw descriptions of forgetfulness as a natural human disorder of ageing. At the end of the 19th century, despite ageing and cognitive decline having been on the scientific and philosophical agenda since 400 B.C., the term "dementia" was still being used to describe any unspecific psychological decline. When this dementia was seen in the elderly, it was described simply as "senile dementia" (Berrios, 1990). However, from the 1860's onwards, work attempting to separate features of "dementia" and "senile dementia" was beginning to emerge. Of particular importance was the work of Marcé (1863), who described the gross structure of the ageing demented brain to be altered, with significant softening and shrinkage, thus providing the first descriptions of cerebral atrophy in dementia.

The modern definition of dementia is the loss or decline in memory and other cognitive abilities which have a significant negative impact on daily functioning (Qiu et al., 2007). Dementia is now broken down and classified into different subtypes, including Vascular Dementia, Dementia with Lewy Bodies, and Alzheimer's Disease (AD). It can be challenging to distinguish between these different types of dementia due to the overlap in cognitive symptoms. However, advances in neuropsychological evaluation and neuroimaging markers are beginning to provide a more accurate basis for differentiating between AD and the other major dementia subtypes (Karantzoulis and Galvin, 2011).

1.2 Alzheimer's Disease: Prevalence and Pathophysiology

1.2.1 Incidence and Classification of Alzheimer's disease

AD is the most common and most severe form of dementia. It is predicted by the Alzheimer's Association that if treatments for AD don't drastically improve, the number of people suffering from this disease worldwide will increase from approximately 26 million sufferers currently, to over 100 million by the year 2050. AD brains exhibit extensive neuronal degeneration, which is grossly manifested in the significant atrophy and shrinkage of the brain (Figure 1.1). These changes in gross structure are accompanied by progressive cognitive dysfunctions, including memory loss, language difficulties, and psychiatric changes such as depression, delusions and agitation (Burns and Iliffe, 2009).

AD is broadly categorised into two types: early onset AD and late onset AD. Early onset AD occurs in younger patients (usually less than 60 years of age), and accounts for less than 5% of all AD cases in Western population (Heckmann et al., 2004). Early onset AD is caused by mutations in genes encoding the amyloid precursor protein (APP) and presenilin proteins (PS1 and PS2). Mutations in these genes are penetrant and, if present, will result in the early onset of AD (Tanzi and Bertram, 2005). The identification and mapping of the APP and presenilin genes aberrant in early onset AD have been invaluable in extending our understanding of the pathological mechanisms underpinning the neurodegeneration seen in AD, and formed the basis of the "amyloid cascade hypothesis" of AD, discussed in more detail below.

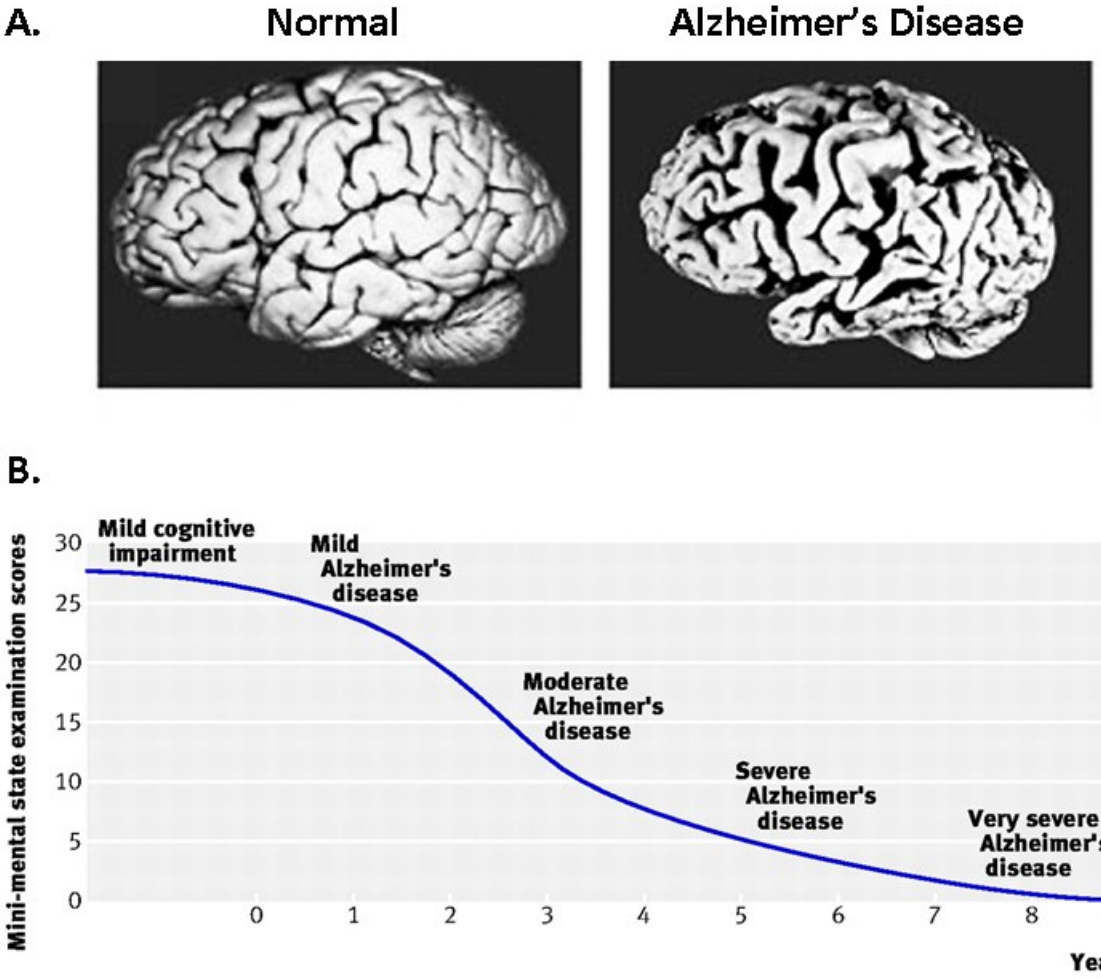

Figure 1.1 Structural and cognitive characterisation of Alzheimer's disease. **A.** Gross structural analysis of AD brains shows significant atrophy and shrinkage compared to normal, healthy brains. Adapted from (Mattson, 2004). **B.** Details of the progressive cognitive decline from initial mild cognitive impairments to very severe AD (Burns and Iliffe, 2009).

The majority of AD cases are of the late-onset variety, the causes of which are not yet understood, but are likely to be a combination of genetic, environmental and social risk factors. Genetic risk factors for late-onset AD are widely investigated, however the apolipoprotein E (APOE) gene remains the best characterised. Carriers of the E4 allele of the APOE gene are at significantly higher risk of developing AD compared to APOE3 carriers (the allele which appears to have little effect on AD risk) and APOE2 carriers (the allele affording some protection against AD) (Kim et al., 2009). The dawn of genome-wide association studies (GWAS) has enabled screening for many other genetic risk factors for AD, the results of which are collated in the publicly available AlzGene database (Bertram et al., 2007).

Epidemiological studies have identified numerous environmental and social risk factors for late onset AD including traumatic head injury (Plassman et al., 2000), education level (Ngandu et al., 2007), dietary factors (Luchsinger and Mayeux, 2004) and environmental pollutants. Indeed, a recent study has shown that levels of dichlorodiphenyldichloroethylene (DDE), the metabolite of the pesticide dichlorodiphenyltrichloroethane (DDT) that has been banned in the United States since 1972, were elevated in patients suffering AD (Richardson et al., 2014). In order to fully understand the interplay between so many potential risk factors for AD, large-scale longitudinal population based studies are needed. One such study is the Lothian Birth Cohort, which will provide social, medical and biochemical insight into the various features required for healthy cognitive aging from data collated over individual lifetimes (Deary et al., 2007)

Despite the large number of potential genetic, environmental and social risk factors for late-onset AD, it is believed that the biggest risk factor for this devastating condition is ageing itself. One theory proposed to explain aging as a risk factor for AD is that young brains contain higher levels of growth factors and effective cell repair mechanisms that afford provide protection against neurodegeneration (Mucke, 2009).

Another plausible explanation for the link between ageing and AD is the increased incidence of vascular disorders in aged individuals (Breteler, 2000). Vascular disorders including hypertension, atrial fibrillation, high cholesterol and atherosclerosis induce a sub-lethal state of cerebral hypoperfusion, thereby reducing the delivery of oxygen, glucose and other nutrients required for energy metabolism. This state of chronic cerebral hypoperfusion (CCH) disrupts normal cell function and results in a state of metabolic stress that is thought to significantly increase the risk of developing late-onset AD (de la Torre, 2002b). The link between vascular disorders and AD has led to the proposal of the Vascular hypothesis of AD, discussed in more detail in Section 1.3.2. Research focussed on understanding the biochemical changes underpinning cellular dysfunction in response to metabolic stress will be important in the pursuit of therapeutic interventions to alter the course of hypoperfusion related neurodegenerative processes.

1.2.2 Key Pathological Features of Alzheimer's disease

The standard pathological hallmarks of AD were first described by Alois Alzheimer in 1906. Macroscopically, there is clear evidence of extensive brain atrophy (Figure 1.1). Microscopically, the three major pathological hallmarks of AD are: loss of neuronal integrity, extracellular amyloid plaques and intracellular neurofibrillary tangles (Holtzman et al., 2011). The presentation of these pathologies occur at different time points in the aging process, and are often present before the onset of cognitive symptoms (Figure 1.2). It is therefore proposed that these AD biomarkers act in concert, and when a threshold of pathologies is met, the cognitive decline into AD begins (Perrin et al., 2009).

Found in the extracellular space, amyloid plaques are traditionally considered to be the classic hallmark of AD (Figure 1.2). Plaques are composed of aggregated amyloid-beta (Aβ) peptides produced from the pathological cleavage of APP by β- and γ- secretase enzymes (Figure 1.3). Alternatively, APP can be processed through the non-amyloidogenic pathway, where α-secretase cleaves APP within the Aβ peptide domain, preventing Aβ generation (Querfurth and LaFerla).

Amyloidogenic and non-amyloidogenic APP processing takes place in different locations throughout the cell. Following transcription and translation, nascent APP moves from the ER to the plasma membrane. At the cell membrane, APP is either cleaved non-amyloidogenically by α-secretases, or is endocytosed. Amyloidogenic processing of APP occurs during its transit from the plasma membrane through the endocytic organelles, where the β- and γ-secretases are located. Alternatively, endocytosed APP can be recycled back to the plasma membrane or degraded in lysosomes (Haass et al., 2012). Inhibiting APP endocytosis through mutations in the YENPTY c-terminal motif inhibits APP endocytosis, and decreases the production of Aβ. This finding suggests a functional endocytic system is integral to amyloidogenic-APP processing (Perez et al., 1999).

On the basis of the abundant accumulations of amyloid plaques in AD brains, the amyloid cascade hypothesis of AD was proposed (Hardy and Higgins, 1992). This hypothesis states that amyloid plaques are the driving force behind AD pathophysiology, with neuronal cell death and synapse loss occurring downstream of plaque formation. The details of this hypothesis and the controversies surrounding it are discussed in detail below.

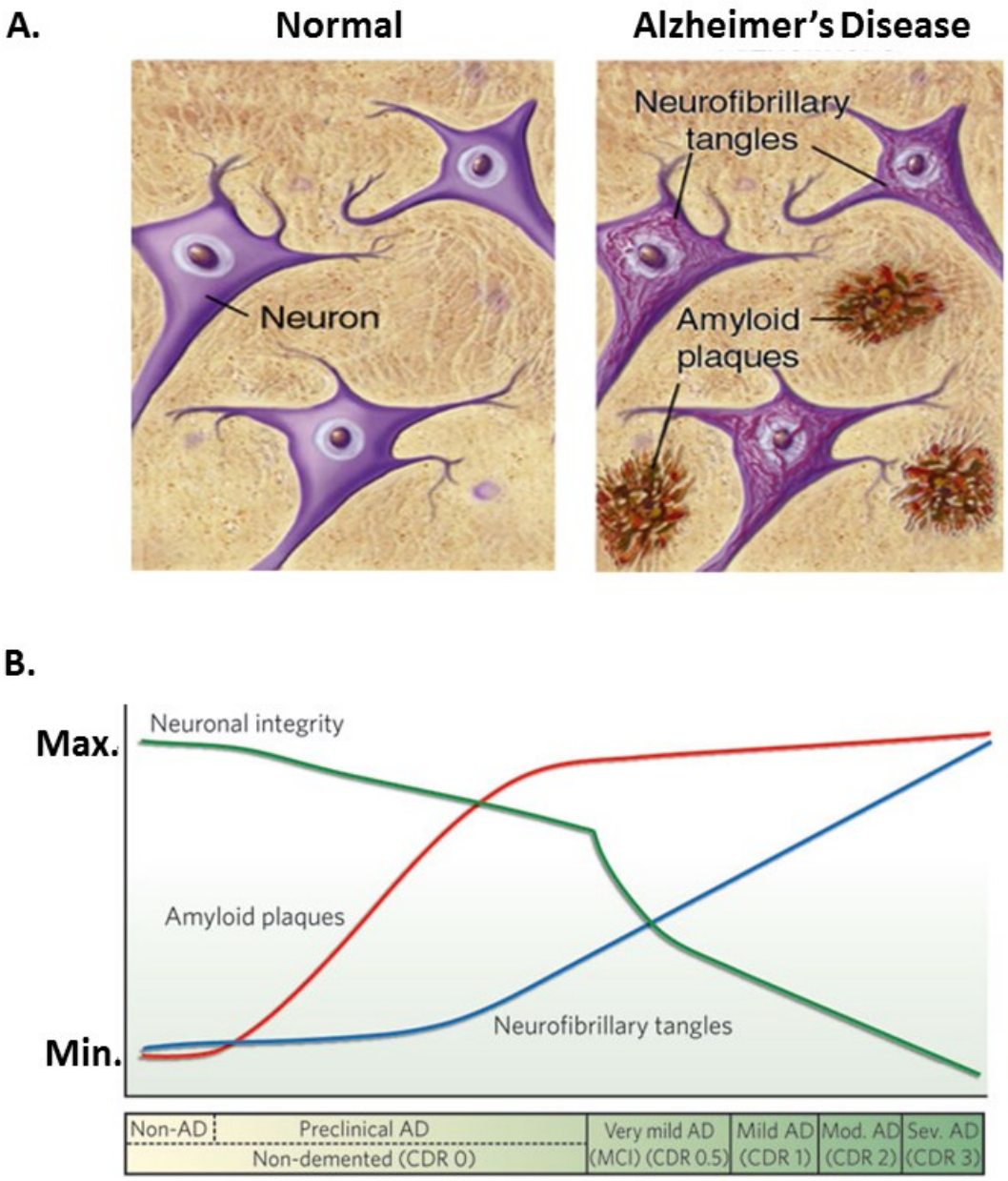

Figure 1.2 The pathological hallmarks of Alzheimer's disease. **A.** Characteristic hallmarks of AD include the extracellular accumulation of amyloid plaques and the presence of intracellular tangles of hyperphosphorylated tau. (from *BrightFocus Foundation, 2000 – 2013)* **B.** The progressive cognitive decline associated with AD from mild cognitive impairment (MCI) to mild, moderate (Mod.) and severe (Sev.) cognitive dysfunction corresponds to clinical dementia ratings (CDR) 0 – 3, as shown. These cognitive changes are associated with heavy amyloid plaque burden (red line), increasing abundance of neurofibrillary tangles (blue line) and synapse and neuronal loss (green line). Adapted from (Perrin et al., 2009)

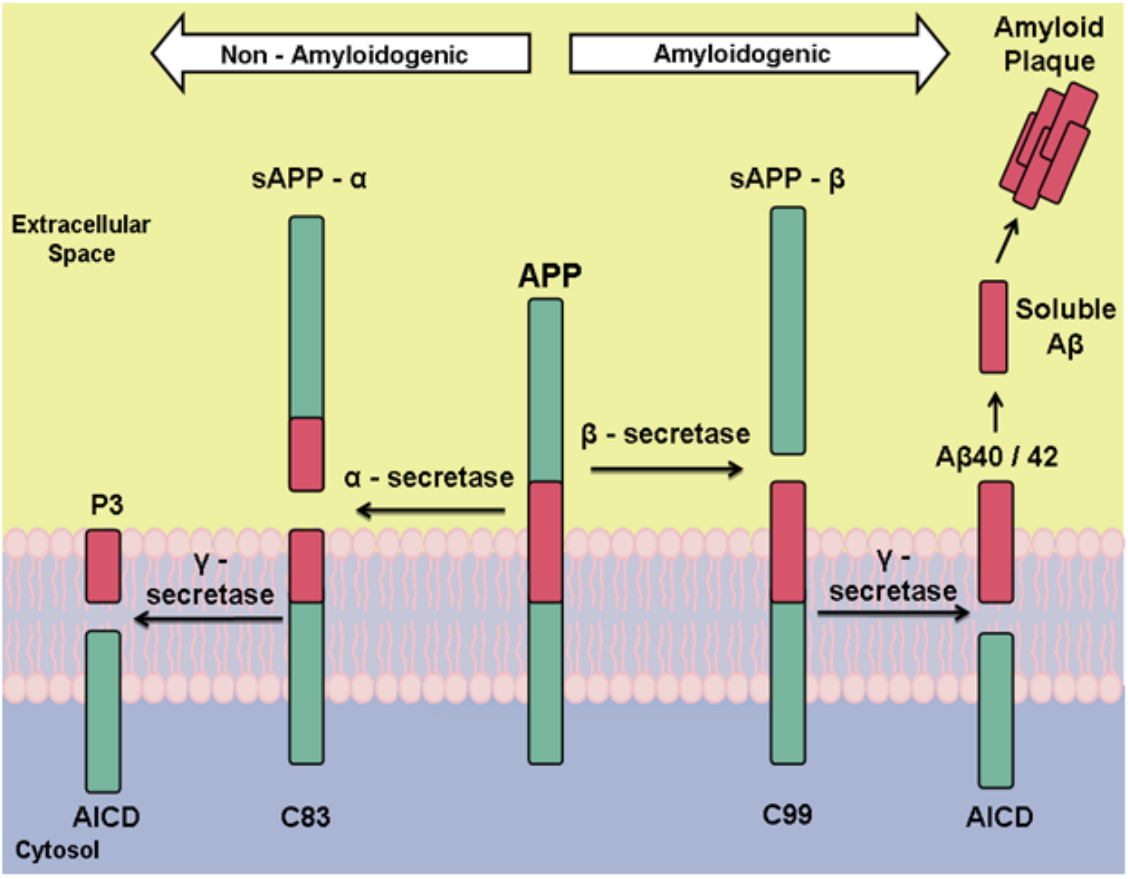

Figure 1.3 APP processing pathways. In the non-amyloidogenic pathway, APP is cleaved by α-secretase within the amyloid sequence, producing non-toxic sAPPα and a C-terminal fragment C83. C83 is then cleaved by γ-secretase to produce p3 and the APP intracellular domain (AICD). Amyloidogenic cleavage of APP by β-secretase produces sAPP-β and the C99 fragment. γ-Secretase then cleaves C99, releasing neurotoxic Aβ

In addition to amyloid plaque formation, the other major pathological hallmark of AD is the presence of intracellular neurofibrillary tangles (NFTs). The major component of NFTs is the microtubule associated protein tau. Under physiological conditions, tau plays an important role in the stabilisation of microtubules and the maintenance of effective axonal transport of signalling molecules, organelles and other essential cellular components. Tau protein moves on and off microtubules in a dynamic equilibrium, controlled by the kinases and phosphatases that determine its phosphorylation state (Ballatore et al., 2007).

Under pathological conditions, tau becomes hyperphosphorylated, detaches from microtubules and aggregates into NFTs. This process can disrupt axonal transport and adversely affect normal cell functioning, ultimately resulting in neuronal cell death (Spires-Jones et al., 2009). NFTs have been shown to develop in a hierarchical pattern through brain regions associated with learning and memory. The entorhinal cortex is the first brain region affected by NFTs, with the pathology sequentially spreading through the regions of the hippocampus, and finally to the neocortex. The NFT induced loss of neurons in these distinct brain regions is thought to result in disconnection of neuronal signalling circuits, inducing the defects in memory and higher functioning that is characteristic of AD (Pooler et al., 2013).

Linked to this tau induced disconnection of neural circuits, loss of neuronal integrity is the third common pathological hallmark of AD (Figure 1.2). Neuronal atrophy in vulnerable brain regions, including the hippocampus and the cerebral cortex, causes regional decreases in volume, a feature that is detectable with magnetic resonance imaging (MRI). Indeed, MRI studies have revealed that medial temporal lobe atrophy is an early marker of AD, present in individuals suffering only very mild cognitive symptoms, and the rate of this early atrophy can be indicative of later cognitive decline (Jack et al., 1997, Fox et

al., 1999). Progression from MCI to severe AD is also characterised by significant loss of synapses. This synaptic loss has been shown to be the pathological hallmark of AD that correlates most robustly with pre-mortem symptoms of cognitive decline (Selkoe, 2002). Synapse loss in AD can be caused as a direct result of neuronal death, but recent research also suggests that soluble Aβ and tau (as opposed to the aggregated forms of these proteins)are also heavily involved (Koffie et al., 2011, Pooler et al., 2014).

AD can also be characterised neurochemically. In the early 1970s, it was reported that there were substantial deficits in choline acetyltransferase, the enzyme responsible for the synthesis of the neurotransmitter acetylcholine, in the amygdala, hippocampus and cortex of AD brains (Davies and Maloney, 1976). This research was extended in the 1978 landmark study by Perry et al. which showed a significant correlation between post-mortem cholinergic neuronal loss and AD patients' pre-mortem mental state scores (Perry et al., 1978). These findings formed the basis of the "cholinergic hypothesis" of AD, which states that the disorders of learning and memory seen in AD may be attributable to dysfunctions of the cholinergic neurons in the basal forebrain (Muir, 1997). The cholinergic hypothesis forms the foundation of three of the four commercially available drug treatments of AD, discussed in more detail below.

Understanding the evolution of the pathological hallmarks of AD, and being able to identify these in the clinic, is an important step towards early diagnosis of this devastating disorder. However, in order to develop novel neuroprotective treatment strategies, the causes of the neuronal and synaptic degeneration need to be understood.

1.3 Conflicting Theories on the Causes of Alzheimer's disease

1.3.1 The Amyloid Cascade Hypothesis

The amyloid cascade hypothesis of AD proposes that the cerebral accumulation of neurotoxic Aβ is the initial event in AD pathophysiology. Other features of AD, such as the formation of NFTs, cognitive decline and neuronal cell death, are thought to be by-products of the preceding Aβ deposition (Hardy and Higgins, 1992). The strongest evidence for this hypothesis comes from the identification of mutations in the APP and presenilin genes, which if present, cause early onset AD. Research shows that expression of these mutations alter APP processing, causing increased production of the 42–43 amino acid form of Aβ, the main component of amyloid plaques found within the AD brain (Hardy, 1997). Clinically, late onset AD cases are almost identical to early onset AD cases, thus suggesting that alterations in APP processing are likely to drive the neurodegenerative processes in both conditions.

Experimental and clinical data have also provided support for the amyloid cascade hypothesis of AD. Pivotal experiments carried out *in vitro* demonstrated that the application of Aβ to neuronal cell cultures was highly toxic (Yankner et al., 1989, Yankner, 1996). Additionally, APP-overexpressing or Aβ–overproducing transgenic mice develop cognitive deficits alongside plaque formation in the hippocampus and the cerebral cortex (German and Eisch, 2004).

Evidence of a direct relationship between APOE genes, (a major risk factor in late onset AD), cerebral amyloid burden and AD provides further support for the amyloid hypothesis of AD. People carrying the APOE4 allele of the gene are at significantly higher risk of developing AD (Kim et al., 2009). A series of experiments carried out in APP transgenic mice showed the human APOE genes to be associated with the level of cerebral Aβ burden, with APOE4 mice having the highest levels of Aβ (Bales et al., 2009).

However, the validity of the amyloid cascade hypothesis has been brought into question in recent years. Despite Aβ plaques being considered to be the main neuropathological hallmark of AD, the accumulation of these plaques correlates poorly with the severity of dementia (Arriagada et al., 1992, Giannakopoulos et al., 2003). Indeed, post-mortem studies have shown cognitively normal individuals to have an Aβ plaque load sufficient for AD diagnosis (Katzman et al., 1988). Moreover, drug trials directed at the clearance of amyloid plaques in the hope of treating AD patients have repeatedly failed, adding to the scepticism surrounding the relationship between amyloid pathology and late onset AD.

The amyloid hypothesis also fails to fully acknowledge the role of hyperphosphorylated tau protein in the pathogenesis of AD. Importantly, where there is an apparent lack of correlation between amyloid plaque density and severity of cognitive dysfunction, the spatiotemporal pattern of NFT accumulation correlates much more closely with dementia severity (Gomez-Isla et al., 1997, Braak and Braak, 1995, Giannakopoulos et al., 2003). An elegant study using the entorhinal-hippocampal systems, analysed the spatial and temporal evolution of plaque and tangle formation in the human brain. In early stages of the disease, NFTs were seen before the development of plaques, and in none of the cases were plaques seen before tangles (Schonheit et al., 2004, Braak and Del Tredici, 2011). This finding conflicts with the postulation of the amyloid hypothesis that the formation of NFTs occurs as a by-product of amyloid plaque formation.

In light of the criticisms associated with the traditional amyloid hypothesis, it is now suggested that soluble Aβ species (dimers, trimers and dodecamers – collectively known as amyloid-derived diffusible ligands , ADDLs) may be the culprit neurotoxic amyloid species involved in AD (Klein et al., 2001). ADDLs are found at increased concentrations in the cerebral spinal fluid of AD patients compared to non-demented age-matched controls (Georganopoulou et al., 2005), and cerebral microinjection of these oligomeric amyloid species induces

significant disruption of long-term potentiation in the rat hippocampus (Walsh et al., 2002). More recently, research showed amyloid dimers (the most abundant form of soluble oligomeric Aβ isolated in AD cortical tissue) to induce tau hyperphosphorylation and microtubule disruption in cultured rat hippocampal neurons, a phenomenon averted in tau siRNA cultures (Jin et al., 2011). These data suggest that oligomeric Aβ might be an upstream driver of tau pathology, and a key feature of the neuronal dysfunction associated with AD.

Despite the arguments for and against the amyloid cascade hypothesis, and the recent efforts to update the thinking in this field, the reality remains that despite more than two decades of amyloid based research, there is still a severe lack of effective AD treatments. Many view this as evidence of a fundamental error in our understanding of AD pathogenesis, forcing researchers to look for alternative theories to explain the causes and progression of late onset AD.

1.3.2 The Vascular Hypothesis

The central dogma associated with vascular theories of AD is that atherosclerosis and other vascular disorders evolving with advancing age reduce blood flow to the brain over many years (chronic cerebral hypoperfusion, CCH). De la Torre captures the culmination of vascular disorders and CCH on the brain in his *Critically Attained Threshold of Cerebral Hypoperfusion* (CATCH) hypothesis of neurodegeneration (de la Torre, 2000). CATCH is the point at which brain circulation is impaired to an extent where oxygen, glucose and other nutrients are delivered sub-optimally to neurons, leading to a downward spiral of metabolic and cognitive decline, with the accompanying pathology associated with AD. The CATCH associated disruption of glucose uptake and usage in AD brains has been well documented by positron emission tomography (PET). PET studies have shown glucose uptake in AD brains to be massively reduced compared to normal, aged matched controls, with a significant correlation found between glucose uptake and scores on mini-mental state examination (Kadir et al., 2011) (Figure 1.4).

Once CATCH is initiated, the onset and progression of cognitive symptoms and neurodegeneration are thought to be based on a culmination of factors relating to each individual, including:

- Genetic profile - APOE4 carriers at significantly higher risk of developing AD (Kim et al., 2009)
- Gender - AD has an increased prevalence in women, thought to be linked to the sudden drop in oestrogen following the menopause, however the increased life expectancy of women compared to men has hindered interpretation of the epidemiological data (Barron and Pike, 2012)
- Lifestyle choices - including alcohol intake, smoking, fitness level and diet. See (Pope et al., 2003) for a review.

The culmination of vascular disorders that results in CATCH leads to a cascade of cellular events that are detrimental to brain function, including mitochondrial dysfunction, oxidative stress, decreased production of adenosine triphosphate (ATP), signal transduction defects, and neurotransmission failure (Aliev et al., 2003) (Figure 1.4). A CATCH induced energy crisis is also associated with an increased production of reactive oxygen species (ROS). Mitochondria are a natural source of ROS, and under CATCH conditions, mitochondrial production of ROS increases, which in turn induces further damage to mitochondrial proteins (discussed in more detail below).

Increased ROS in the cell can cause damage and misfolding of proteins, which accumulate in the endoplasmic reticulum, and induce the unfolded protein response (UPR). The UPR is mediated by glucose-regulated proteins (GRPs), the most common of which are GRP78 (also referred to as BiP) and GRP94. These proteins are up-regulated in response to the accumulation of misfolded proteins

in the ER lumen (Zhang and Kaufman, 2006). The UPR is integral to cell survival as excessive accumulation of these damaged proteins in the ER lumen can prevent the timely inactivation of UPR, resulting in prolonged reductions in protein synthesis (Ron and Walter, 2007). Importantly, research has shown the key chaperones involved in the UPR to decrease in abundance with advancing age (Naidoo et al., 2008), suggesting a reduced ability for elderly brains to deal with the accumulations of damaged proteins under CATCH conditions.

Evidence supporting a connection between oxidative stress and the pathological protein hallmarks of AD is beginning to emerge. An *in vitro* model of oxidative stress involving the application of Hydroxynonenal (HNE) (a product of lipid peroxidation) to the human NT-2 cell line induced a significant increase in BACE1 protein, (the β-secretase enzyme involved in amyloidogenic processing of APP to produce neurotoxic Aβ) with consequent increase in Aβ peptides (Tamagno et al., 2005). In addition, *in vivo* studies using a rat model of chronic cerebral hypoperfusion showed reduced cerebral blood flow to significantly increase the levels of BACE1 and Aβ compared to sham operated controls (Zhiyou et al., 2009).

Tau processing is also adversely affected by oxidative stress, with increased levels of tau phosphorylation detected in an *in vitro* model of chronic oxidative stress involving the inhibition of glutathione synthesis (Su et al., 2010). *In vivo*, induction of transient cerebral hypoperfusion in the triple transgenic AD mice has been shown to increase tau phosphorylation at serine^{212} and threonine^{214}, a tau epitope associated with paired helical filaments in AD patients.

Despite the growing focus on vascular disorders and CATCH in relation to AD, the underlying biological mechanisms relating chronic cerebral hypoperfusion to impaired mitochondrial function and neurodegeneration remain unknown.

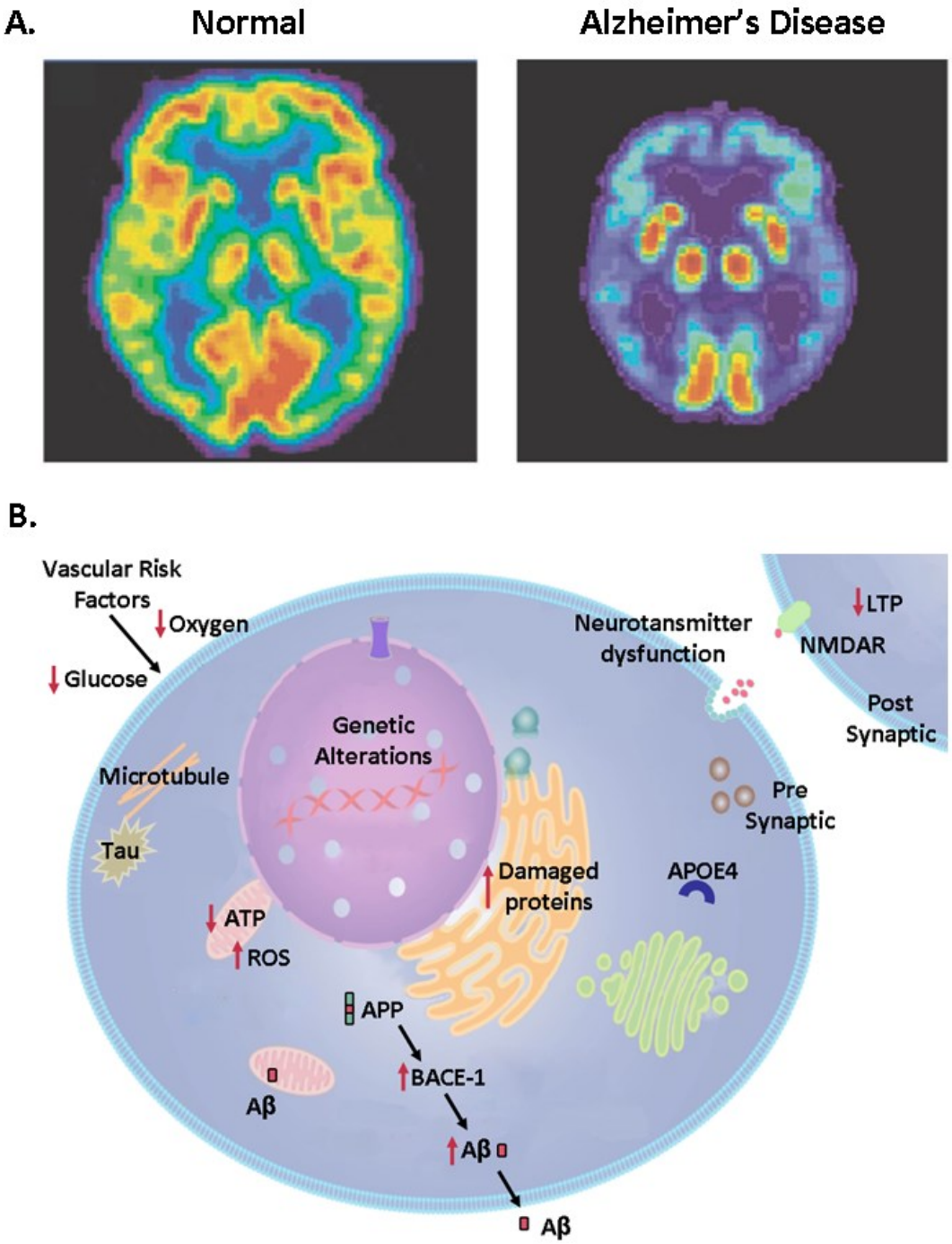

Figure 1.4 The vascular theory of Alzheimer's Disease. A. Positron emission tomography images showing the glucose uptake in healthy brains and AD brains in living subjects (reds and yellows indicate high glucose uptake). Glucose uptake is massively decreased in AD brains. Adapted from (Mattson, 2004). **B.** Vascular risk factors reduce oxygen and glucose delivery to cells, leading to ATP depletion, reactive oxygen species (ROS) production, dysfunctions in synaptic transmission, accumulation of damaged proteins in the endoplasmic reticulum, BACE1 up-regulation and Aβ overproduction, and increased tau phosphorylation. Adapted from (de la Torre, 2008).

1.3.3 Alternative Hypotheses associated with Alzheimer's disease

Alternative hypotheses associated with AD exist that either precede or build upon the amyloid and vascular hypotheses discussed above. The cholinergic hypothesis, first proposed in 1982, suggests that the loss of cholinergic activity in the brains of AD patients might account for the disruptions in learning and memory associated with this disease (Bartus et al., 1982). This cholinergic hypothesis gave rise to the only drugs that are currently available in the management of mild to moderate AD (discussed in more detail below). However, the failure of these drugs to fully arrest the progression of AD somewhat undermines a causative role for the cholinergic hypothesis in AD.

Another early theory of AD was the Prion hypothesis, based on observations that the protein accumulations and neurodegenerative processes in AD are similar to those seen in human prion diseases (Jarrett and Lansbury, 1993). Recent experiments showing that intra-cerebral injection of Aβ containing extracts from AD patients into mice induces amyloidosis and pathology has provided support for the seeding capabilities Aβ (Meyer-Luehmann et al., 2006). Further work in this field confirming the potential for Aβ transmissibility would have huge consequences for the future management and treatment of AD.

There are many hypotheses of AD, however a truly causative trigger for this disease remains elusive. It is well established that the single biggest risk factor for AD age. This fact has led to the proposal of an age based hypothesis of AD, which states that aberrant cognitive decline is driven in three key stages: an initiating injury, followed by a chronic neuroinflammatory response, and finally, a discontinuous cellular change (Herrup, 2010). This final step marks the onset of neurodegeneration, and the subsequent synaptic and neuronal loss that is so strongly associated with AD.

1.4 Prognosis and Treatments for Alzheimer's disease Patients

Despite an abundance of different hypotheses surrounding AD, there is still no effective treatment strategy for this devastating disease. However, two main classes of drugs have been developed that can improve the cognitive symptoms of AD patients: acetylcholinesterase inhibitors and *N*-methyl-D-aspartate (NMDA) receptor antagonists.

The development of acetylcholinesterase inhibitors for the treatment of AD is based on the findings that cholinergic signalling pathways in the cerebral cortex of AD patients are compromised (Perry et al., 1978). Acetylcholinesterase inhibitors aim to reduce the breakdown of acetylcholine by acetylcholinesterase, thus increasing the concentration of acetylcholine available for cholinergic neurotransmission (McGleenon et al., 1999). Donepezil, rivastigmine, and galantamine are the three cholinesterase inhibitors that are most frequently used to treat AD patients. These drugs have been shown to have small beneficial effects on cognition, function, and behavioral outcomes, however only when administered to patients with mild cognitive symptoms. Although stabilization of AD symptoms occurs with these drug treatments, the effects are not sustained. There are also significant side effects, including nausea, dizziness, headache and weight loss (Doody, 2003).

In contrast to the disruption of cholinergic neurotransmission, overstimulation of NMDA receptors by glutamate has also been implicated in AD. Glutamate is the main excitatory neurotransmitter in the brain, and is centrally involved in learning and memory processes (Riedel et al., 2003). However, under pathological conditions, persistent depolarisation of neurons releases the magnesium block of the NMDA receptor, causing increased levels of intracellular calcium, and inducing cell death by excitotoxicity. Cell death by excitotoxicity is implicated in AD, and led to the development of memantine, a NMDA receptor antagonist, for the treatment of AD (Hynd et al., 2004).

Memantine is used in moderate to severe AD cases, however its clinical efficacy is still debated (Tampi and van Dyck, 2007).

Other potential avenues for AD treatments include reducing the production of Aβ through inhibition of β- and γ-secretases, reducing Aβ aggregation, promoting the removal of Aβ from the brain with immunotherapy and reducing tau aggregation and phosphorylation(Mangialasche et al., 2010). There have been many failures of clinical trials investigating chemical compounds for the treatment of AD. In the summer 2012, Johnson & Johnson and Pfizer failed to show any benefit of bapineuzumab, a new antibody drug targeting the amyloid plaques with a view to stimulating the immune system to clear them. Soon after, Eli Lilly announced that solanezumab, a drug that targets amyloid-β peptides with a view to blocking their aggregation to plaques, had not successfully slowed the memory decline associated with AD (Callaway, 2012). The failure of these clinical trials has raised questions as to the validity of Aβ as a target for AD drug development and highlights the urgent need for the development of novel biomarkers and treatment strategies for AD.

1.5 Mitochondria, Oxidative Stress and Alzheimer's disease

1.5.1 Mitochondria: Essential Organelles in Aerobic Respiration

Mitochondria are membrane bound organelles often colloquially described as the "powerhouses" of the cell due to their role in converting organic material into ATP, the cellular energy currency. Mitochondria are composed of an inner matrix containing a complex mixture of enzymes and chemical species, an impermeable inner membrane which requires protein transporters to translocate molecules across it and a permeable outer membrane.

There are three stages of aerobic respiration: glycolysis, the Krebs cycle and the electron transport chain. Glycolysis, occurring in the cytoplasm, involves the breakdown of glucose to pyruvate via nine distinct enzymatic reactions. Glycolysis produces a total of 4ATP molecules, however uses 2ATP within the glycolytic process, therefore the net ATP production is just 2ATP (Pelicano et al., 2006). Glycolysis itself is an anaerobic process. Once pyruvate is formed, cells continue respiration in either an aerobic or anaerobic manner, depending on the cell type and the cellular environment.

In the presence of oxygen, cells with aerobic capabilities proceed to the Krebs cycle, the second respiratory process, occurring in the mitochondrial matrix. The Krebs cycle (also known as the citric acid or tricarboxylic acid cycle) begins with the transfer of pyruvate across the mitochondrial membranes into the matrix, where it is converted into acetyl-coenzyme A (acetyl-CoA) by the pyruvate dehydrogenase multienzyme complex:

$$2\ \text{Pyruvate} + 2\ \text{coenzyme A} + 2NAD^{+} \rightarrow 2\ \text{acetyl-CoA} + 2CO_2 + 2\ \text{NADH}$$

Production of acetyl-CoA allows the Krebs cycle to proceed with the reaction between acetyl-CoA and oxaloacetate to form citric acid, a reaction mediated by the enzyme citrate synthase. The Krebs cycle then proceeds via seven further enzymatic reactions, producing three NADH, one FADH2 and one ATP per acetyl-CoA molecule (Munnich, 2008) (Figure 1.5).

The final stage of aerobic respiration involves the production of the bulk of cellular ATP via the electron transport chain (ETC). The ETC is a system of protein complexes located on the inner mitochondrial membrane including:

- Complex I - NADH coenzyme Q reductase
- Complex II - succinate dehydrogenase
- Complex III - cytochrome bc1 complex
- Complex IV - cytochrome c oxidase
- Complex V - ATP synthase

Energy for ATP synthesis is derived from oxidation of the NADH and FADH2 produced during the earlier processes of glycolysis and the Krebs cycle. The ETC begins at complex I, where NADH is oxidised to NAD, with the released electron being passed into the ETC. The protein complexes of the ETC act as electron carriers. Each complex is at a successively lower energy level, therefore as electrons are passed from one complex to another, energy is released. Coenzyme-Q10 acts an electron carrier, transferring electrons from complex I and complex II, to complex III (Murphy et al., 1999). Cytochrome C is responsible for the movement of electrons between complex III and complex IV (Mehta and Li, 2009). The energy generated from electron transfer between complexes is then used to move hydrogen ions, released following the oxidation of NADH and FADH2, across the inner mitochondrial membrane into the intermembrane space (Figure 1.5).

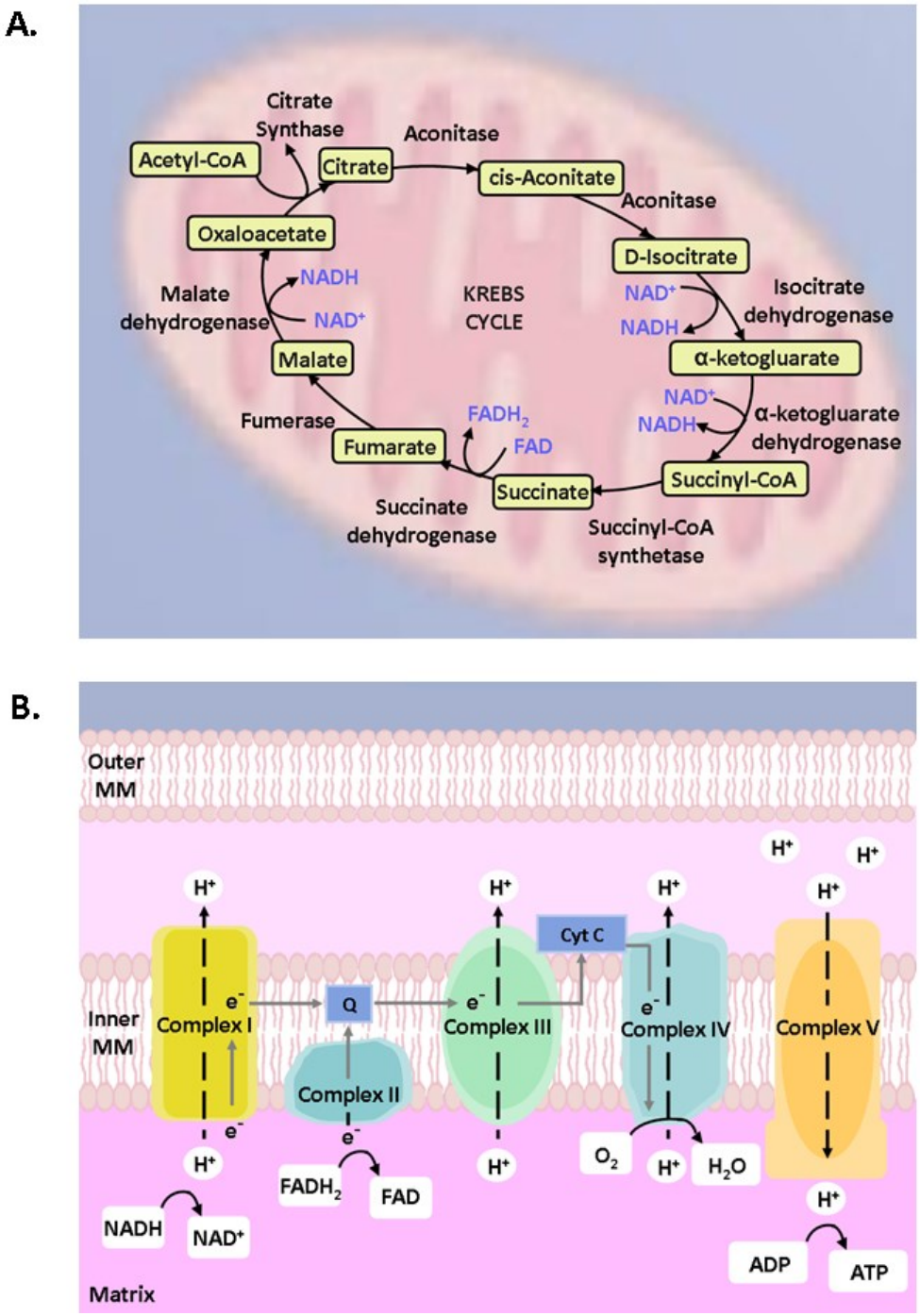

Figure 1.5 The Krebs cycle and the electron transport chain. **A.** Diagrammatic overview of the enzymatic reactions involved in the Krebs cycle. Metabolic intermediates are shown in boxes. **B.** Mitochondrial electron transport occurs via a series of protein complexes, which use the energy generated from electron transfer to pass hydrogen ions into the intermembrane space. The resulting electrochemical gradient is used by complex V (ATP synthase) to generate ATP.

The increasing concentration of hydrogen ions in the intermembrane space forms a concentration gradient, giving the ions electrical potential energy. This potential energy is released when hydrogen ions pass back across the inner mitochondrial membrane via ATP synthase (Complex V), and is used to produce ATP (Mehta and Li, 2009). Oxygen acts as the final electron acceptor, and together with the hydrogen ions, water is formed. The ETC consumes approximately 85% of cellular oxygen, with about 5% of this oxygen converted to ROS, discussed below.

Neurons need exceptionally high ATP levels in order to sustain their many functional processes, including axonal transport, maintenance of ion gradients and membrane potentials and the loading, release and recycling of vesicles in synaptic transmission. Neurons have only limited glycolytic capacity, with the majority of neuronal ATP produced by oxidative phosphorylation (Santos et al.). Healthy mitochondria, along with a steady supply of oxygen and glucose are therefore critically important to maintain normal neuronal function.

1.5.2 Mitochondria and Reactive Oxygen Species: a paradoxical relationship

Reactive oxygen species are molecules and free radicals (species with an unpaired electron) derived from molecular oxygen. Under normal conditions the brain has a solid defence against ROS, including dietary free radical scavengers and enzymatic antioxidants such as glutathione peroxidase, superoxide dismutase, catalase and thioredoxin reductase (Mates, 2000).

In the mitochondria, the electron transport chain constantly channels electrons through the series of protein complexes in the generation of ATP. Occasionally this process leaks single electrons which can reduce oxygen to form the superoxide anion ($O_2-\bullet$). Under normal conditions, superoxide dismutase (SOD) can eliminate $O_2-\bullet$ by converting it to hydrogen peroxide (H_2O_2). The hydrogen peroxide can then be converted to oxygen (O_2) and water (H_2O) by catalase (Warner et al., 2004) (Figure 1.6). If partial reduction of H_2O_2 occurs, the hydroxyl radical (OH•) is formed, which is an extremely powerful oxidant that can cause extensive cellular damage (Turrens, 2003).

Under conditions of cell stress, the ETC can become dysfunctional and ROS homeostasis is disrupted. Paradoxically, damaged mitochondria produce more ROS, which can overwhelm the antioxidant defence system, leading to a vicious cycle of further mitochondrial dysfunction and further ROS production. The oxidative stress caused by disrupted redox balance can induce dysfunction in membrane receptors, DNA damage, membrane lipid peroxidation and cytochrome C release from mitochondria, which induces apoptotic cell death (Lin and Beal, 2006).

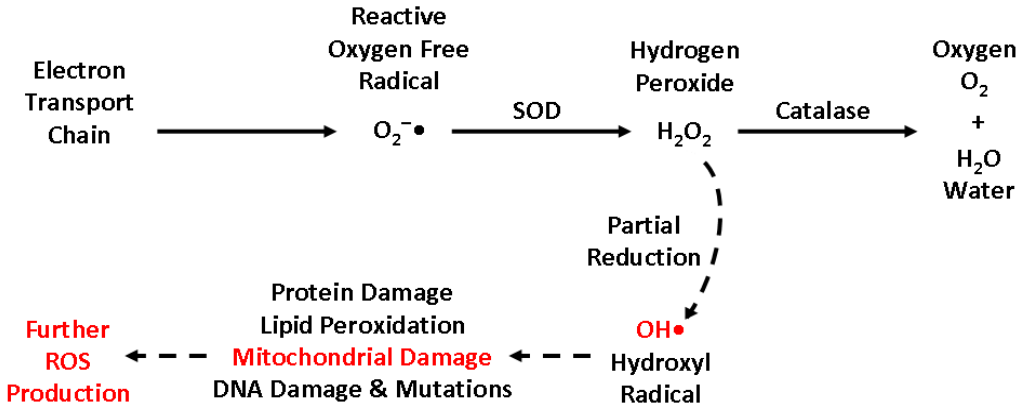

Figure 1.6 Common cellular antioxidant pathways and the vicious relationship between reactive oxygen species and mitochondrial damage.

Peroxiredoxins (Prxs) are another family of antioxidant enzymes which have reductase activity towards hydrogen peroxide. Prxs exist in 6 different isoforms, and the location of these varies within the human brain. Prx I is mainly located within astrocytes, whereas PrxII is expressed in neurons across many regions, including the cerebral cortex and hippocampus (Lee et al., 2011). In addition to antioxidant defence, PrxII has recently been shown to be significantly increased in the brains of AD patients (Krapfenbauer et al., 2003). An increase in antioxidant protein PrxII in AD brains may be indicative of increased oxidative stress in the affected tissue, thus providing support for the CATCH hypothesis of AD. Further work will need to be undertaken in order to determine the mechanism and function of this PrxII up-regulation.

1.5.3 Mitochondria, Ageing and Alzheimer's disease

The most consistent risk factor for AD is ageing itself, with mitochondria thought to contribute to the ageing process. The "free radical theory of ageing", posits that oxidative damage accrues in cells and tissues over time, contributing to age-dependent physiological decline in neuronal function (Harman, 1956). As discussed above, the mitochondria are a major source of ROS production, and are therefore a prime target for ROS damage, resulting in a compounding effect whereby damaged mitochondria produce more ROS, increasing cellular oxidative damage and inducing further mitochondrial damage (Van Remmen and Richardson, 2001).

A correlate of the free radical theory of ageing is the mitochondrial theory of ageing, which focuses on the accumulation of mitochondrial DNA (mtDNA) mutations with advancing age (Linnane et al., 1989). Mitochondrial DNA encodes 13 essential polypeptides of the oxidative phosphorylation system, including subunits of complexes I, III, IV and V, as well as the necessary RNA machinery (2 rRNAs and 22 tRNAs) for their translation within the

mitochondria (Taylor and Turnbull, 2005). Quantitative evidence for the mitochondrial theory of ageing was shown by Lin et al. who found a larger number of mtDNA mutations in the brains of elderly subjects than young subjects, with the activity of cytochrome c oxidase negatively correlating with increasing mutational burden (Lin et al., 2002). There may well be significant overlap between the mitochondrial and free radical theories of ageing, given that mtDNA itself is highly susceptible to oxidative damage (Van Remmen and Richardson, 2001).

Functional investigations corroborate with the mitochondrial and free radical theories of ageing, with numerous groups showing evolving mitochondrial dysfunction with advancing age. In aged mice, mitochondrial complexes I, III and IV show significant decreases in function compared to younger controls (Navarro et al., 2002). A similar result was found in the cortex of rhesus monkeys, where complex I and complex IV activity was significantly decreased with advancing age (Bowling et al., 1993).

In addition to the accumulation of mtDNA mutations and oxidative damage with advancing age, mitochondrial dysfunction is also directly implicated in human AD. The brains of AD patients show decreased cytochrome c oxidase activity, oxidative damage and reduced metabolism. Intriguingly, these mitochondrial disturbances are seen in advance of amyloid plaque formation (Celsi et al., 2009). Electron microscopy studies have also shown gross morphological changes in mitochondria of AD patients. A significant number of these mitochondria from AD patients show disrupted cristae, the surface of which contain the apparatus of the ETC for ATP production, potentially leading to the energy crisis observed in AD (Baloyannis, 2006).

Mitochondria are also important regulators of apoptosis and cytosolic calcium concentration, both of which are implicated in neurodegeneration. Several proteins are involved in mitochondrial control of calcium homeostasis including the mitochondrial calcium uniporter (MCU) (which rapidly moves Ca^{2+} into the matrix, driven by the negative charge of the mitochondrial membrane potential established by the electron transport chain) (Patron et al., 2013); the voltage dependent anion channel (VDAC) protein (which mediates the movement of calcium ions across the outer mitochondrial membrane) (Shoshan-Barmatz et al., 2010); and the permeability transition pore (PTP) (known for its key role in the induction of apoptosis and release of cytochrome c, the PTP also acts to release calcium and maintain homeostasis) (Celsi et al., 2009).

Calcium levels within the mitochondria can be controlled by a specialised membrane region between the mitochondria and the endoplasmic reticulum known as the "mitochondria associated membrane" (MAM). Pyruvate dehydrogenase, α-ketoglutarate and isocitrate dehydrogenases are key members of the Krebs cycle that are activated by calcium, therefore close links between the mitochondria and the endoplasmic reticulum, widely considered to be an intracellular Ca^{2+} store (Verkhratsky, 2005) seem reasonable.

Mitofusin 2 (MFN2) is present at the MAM and is involved in ER–mitochondria tethering, by both homotypic interactions and heterotypic interactions with MFN1 (Rizzuto et al., 2012). The MAM also contains high levels of Ca^{2+}-binding chaperones, including calnexin, calreticulin and BiP. These proteins enable the MAM to serve as a high capacity Ca^{2+} binding store, ensuring ample Ca^{2+} is present at the MAM, ready for transfer to the mitochondria. Inositol 1,4,5-trisphosphate receptor (IP3R) is the MAM protein responsible for mediating the release of Ca^{2+} from the ER to the mitochondria on stimulation by inositol 1,4,5-trisphosphate (Hayashi et al., 2009).

Endoplasmic reticulum sigma 1 receptor (Sig1R) is also enriched at the MAM and forms a complex with BiP. Following Ca^{2+} release from the ER, Sig1R dissociates from BiP and binds to the activated IP3R, preventing damage and degradation of the receptor and allowing sustained calcium release (Rizzuto et al., 2012). Glucose regulated protein 75 (GRP75) is also present at the MAM and functions as a link between IP3R and voltage dependent anion channels (VDACs) in the outer mitochondrial membrane. The close proximity of IP3R and VDAC allow Ca^{2+} released from endoplasmic reticulum to be readily taken up into the mitochondria (Figure 1.7). For a detailed review see (Hayashi et al., 2009).

Importantly for AD research, presenilin proteins (components of the γ-secretase complex involved in APP processing) have been located at the MAM (Area-Gomez et al., 2009). This enrichment of presenilins at the MAM, as well as its role in mitochondrial calcium uptake and cholesterol metabolism, suggests that the MAM may well be involved in the pathogenesis of AD. It is therefore important to consider changes in this dynamic membrane region in studies investigating the cellular changes relating to AD.

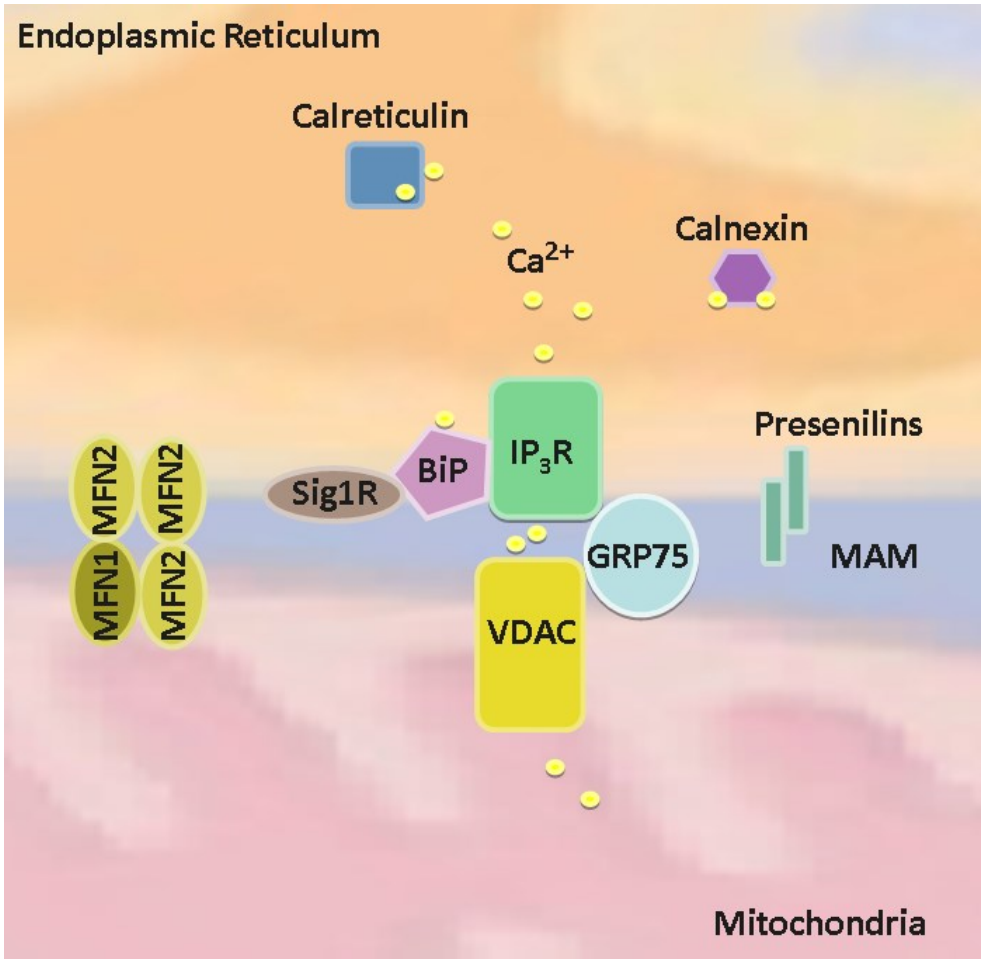

Figure 1.7 Simplified representation of the Mitochondrial Associated Membrane (MAM). Ca^{2+}binding chaperones such as calnexin, calreticulin and BiP are enriched at the MAM. The MAM therefore functions as a high capacity Ca^{2+} pool for subsequent signalling to the mitochondria. IP_3R mediates the release of Ca^{2+} from the ER, which can then be taken up into the mitochondria via the VDAC channels.

1.5.4 ABAD Protein: Bridging the gap between Aβ, mitochondrial dysfunction and Alzheimer's disease?

Aβ is best known for its aggregation into the extracellular cerebral plaques that are so famously associated with AD. However, research suggests that intracellular Aβ may also have an important role to play in the pathophysiology of AD. Intracellular Aβ has been detected in the brains of AD patients, and this intracellular Aβ appears to accrue before the appearance of NFTs and extracellular amyloid plaques. The identification of possible targets for this intracellular Aβ is therefore important to advance understanding of cellular dysfunction in AD.

In a seminal study, Yan et al. used the yeast two-hybrid system to identify a direct interaction between Aβ and a member of the 17β-hydroxysteroid dehydrogenasereductase family, which they later named "amyloid binding alcohol dehydrogenase" (ABAD) (Yan et al., 1997). ABAD, also known as endoplasmic reticulum associated amyloid-β binding protein (ERAB) or 17β-hydroxysteroid dehydrogenase type 10 (HSD17B10), is an NAD-dependent enzyme involved in the oxidation and reduction of alcohol groups from substrates such as steroids, alcohols and fatty acids. This wide range of ABAD substrate specificity is indicative of its role in numerous metabolic processes, including beta-oxidation fatty acids and sex steroid metabolism (Marques et al., 2008).

X-ray crystallography has been used to elucidate the structure of ABAD protein in the presence of co-factor NAD and an excess of $A\beta_{1-40}$ (Lustbader et al., 2004). ABAD consists of a six stranded β sheet surrounded by α-helices, forming a typical Rossman fold site associated with enzymatic activity (Figure 1.8). Interestingly, NAD was not found to be interacting with ABAD in the crystal

structure, a finding attributed to the distortion of ABAD structure in the presence of Aβ. (Figure 1.8) (Lustbader et al., 2004).

In addition to crystal structure , subcellular localisation can provide insight into potential functions of novel proteins. Colocalisation studies have shown ABAD to be localised to the endoplasmic reticulum and mitochondria, as well as showing a more diffuse distribution across the cell membrane, cytosol and nucleus, as identified in ABAD-overexpressing neuroblastoma cells (Yan et al., 1999). Importantly, this research showed ABAD to change subcellular locations under different environmental conditions. Specifically, on addition of Aβ to the cell culture system, ABAD appears to move away from the ER and accumulate close to the cell membrane, a result confirmed by subcellular fractionation (Yan et al., 1997, Yan et al., 1999). This finding introduces an important concept, namely that ABAD may change its subcellular location, and therefore its function, under different environmental conditions.

The mitochondrial location of ABAD has resulted in experiments investigating the effect of the novel Aβ – ABAD interaction on mitochondrial function. Application of Aβ to ABAD overexpressing COS cells induced suppression of mitochondrial function, when compared to non-overexpressing cells. Similarly, in experiments using neuroblastoma cells (which constitutively express ABAD), the Aβ induced mitochondrial dysfunction was ameliorated through blockade of ABAD with an anti-ABAD antibody (Yan et al., 1997). The interaction of ABAD and Aβ, and the negative effects this relationship has on mitochondrial function, suggests ABAD may be an important player in AD. Investigations using human AD brain tissue show significantly increased levels of ABAD compared to age-matched controls (Yan et al., 1997). In addition to the *in vitro* findings, the Aβ – ABAD interaction is also found in human AD tissue, with confocal and immunogold electron microscopy showing these proteins to colocalise within the mitochondria of AD patients (Figure 1.8) (Lustbader et al., 2004).

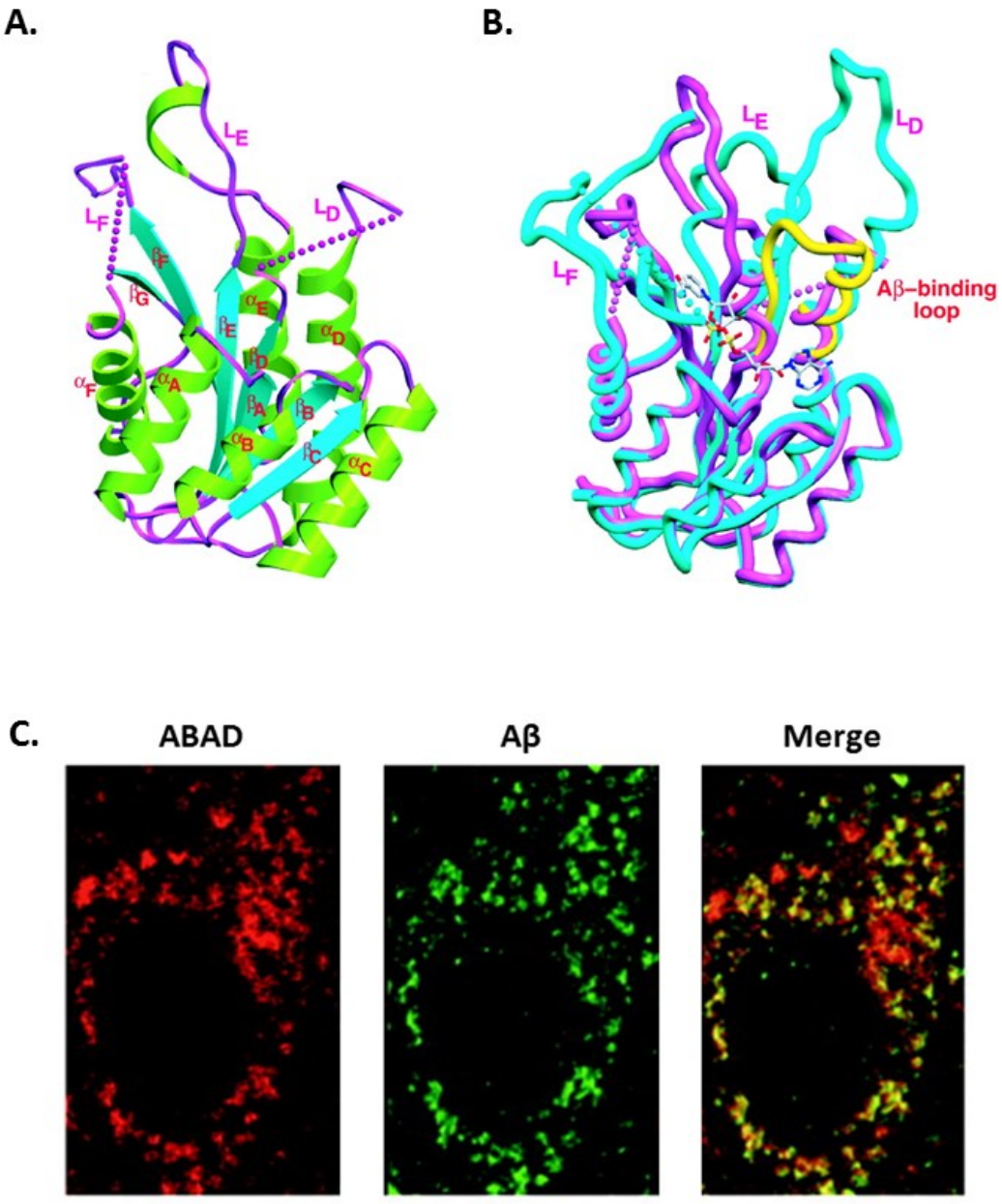

Figure 1.8 The structure of ABAD protein and evidence of its colocalisation with Aβ. A. A ribbon diagram showing the alpha-heices (green) and beta-sheets (blue) contained within an ABAD monomer. The L_D. L_E and L_F loops are also shown. **B.** Superimposed image showing the distortion of the NAD binding site in human ABAD bound with Aβ (pink) compared to rat ABAD bound with the cofactor NAD (blue). The predicted Aβ-binding loop is shown in yellow, NAD is shown as a stick model. **C.** ABAD and Aβ colocalise in the cerebral cortex of Alzheimer's disease patients (200x). Adapted from (Lustbader et al., 2004)

In contrast to the previously discussed mitochondrial dysfunction associated with increased ABAD expression, research suggests that in metabolically challenging conditions, increased levels of ABAD can be protective. This was demonstrated in an *in vitro* study where COS cells overexpressing ABAD had significantly better viability when placed in hypoglycaemic medium than control vector transfected cells (Du Yan et al., 2000). It may therefore be hypothesised that the increase in ABAD found in the brains of AD patients may be due to the metabolically challenging conditions associated with the previously described critically attained threshold of cerebral hypoperfusion (CATCH) hypothesis. In order to determine whether ABAD is a possible target for amelioration of mitochondrial dysfunction, further work needs to be carried out in order to determine both 'how' and 'why' ABAD is increased in AD tissue.

The evidence of increased ABAD protein in AD brains, the negative effect of ABAD overexpression on mitochondrial function in the presence of Aβ, and the evidence of ABAD and Aβ both colocalising to the mitochondria in the brains of AD patients suggests that this protein is an important target for further research in the field of AD. The cause and function of increased ABAD expression in AD tissue remains undetermined.

1.5.5 The Biochemical Links between Vascular Risk Factors, Mitochondrial Dysfunction and Alzheimer's disease Remain Elusive

Mitochondrial involvement in the production of ROS, the susceptibility of mtDNA damage with age, the role of mitochondria in calcium homeostasis, the presence of presenilins at the MAM and the direct interaction Aβ with mitochondrial protein ABAD, all indicate that this complex organelle is an attractive mediator of cellular dysfunction and neurodegeneration. However, the driving force behind the described mitochondrial dysfunctions associated with ageing and AD remains elusive. The previously described CATCH hypothesis suggests that advancing age, alongside co-morbid vascular disorders, induce suboptimal delivery of energy substrates to neurons. A main outcome of CATCH is mitochondrial dysfunction, with knock on effects of ROS production, oxidative stress, protein damage and aggregation, cell ionic pump deficiencies, signal transduction failure and ultimately neurodegeneration (de la Torre, 2002a).

This vascular theory of mitochondrial dysfunction in AD is attractive given that the chronic reduction in blood flow and resulting oxidative damage occurs over many years, thus potentially accounting for the late onset of sporadic AD symptoms. Developing appropriate model systems for the characterisation of the biochemical changes occurring under conditions of cerebral hypoperfusion and metabolic stress will provide insight as to the possible molecular pathways which underpin the mitochondrial dysfunction associated with ageing and AD.

1.6 Experimental Models of Cerebral Metabolic Stress

As previously discussed, neurons require a constant supply of oxygen, glucose and other nutrients in order to meet their exceptionally high ATP demands. Disturbances in cerebral blood flow disrupt the delivery of these substrates that are vital for ATP production, thus inducing a state of metabolic stress and

cellular dysfunction. The extent of the neuronal dysfunction and damage in response to metabolic stress depends on the severity and duration of hypoperfusion episode. An acute, intense cerebral metabolic challenge during conditions such as ischemic stroke can induce irreversible neuronal damage and infarction (van der Worp and van Gijn, 2007). In contrast, age-related vascular disorders resulting in sub-lethal cerebral hypoperfusion induce a more mild but chronic metabolic impairment that is thought to contribute to the evolution of neurodegenerative disease (Beal et al., 1993). Numerous experimental models have been developed in order to investigate the neurochemical cascades initiated by both acute and chronic metabolic challenges. An assessment of the various models appropriate for investigations of chronic metabolic challenge in relation to AD is provided below.

1.6.1 *In vivo* Models of Mild Metabolic Stress

In humans, blood is supplied to the brain through the two internal carotid arteries and the two vertebral arteries. The internal carotid arteries principally supply the cerebrum, whereas the vertebral arteries join to form the basilar artery which runs along the midline of the brain and connects with the Circle of Willis. The Circle of Willis gives rise to three pairs of arteries, the anterior, middle, and posterior cerebral arteries. These arteries divide into progressively smaller arteries and arterioles which penetrate the brain tissue supplying blood to the corresponding regions of the cerebral cortex (Bear et al., 2007). The complete Circle of Willis, as well as the extensive branching of the posterior, anterior, and middle cerebral arteries allows blood flow to circumvent any blockages, thus maintaining a steady supply of oxygen, glucose and nutrients to neurons.

Rodent models of reduced blood flow (rather than the full occlusion models used in stroke research) have been developed in order to examine the effects of CCH on neuronal function as it occurs in human ageing and AD. Bilateral common carotid artery occlusion (BCCAO) in the rat is a widely used model of CCH. The rat has a complete Circle of Willis, therefore stenosis, or ligation, of the common carotid arteries affords incessant, but reduced, cerebral blood flow (Farkas et al., 2007).

The BCCAO model has successfully been used to investigate the effect of CCH on learning and memory processes, an important area of research in relation to the cognitive decline associated with AD. A significant number of studies have shown BCCAO rats to cover longer swim paths and longer escape latencies in the Morris water maze task, indicative of compromised spatial learning (Farkas and Luiten, 2001). Biochemical analysis of the brains of these rats also show memory disturbances to correlate with down-regulation of proteins associated with neuronal signalling, learning and memory (Liu et al., 2005). In addition, the levels of BACE1 and Aβ are significantly increased in BCCAO rats compared to sham operated controls (Zhiyou et al., 2009), a result which demonstrates the utility of this animal model in investigating the links between CCH, amyloid processing and AD.

The BCCAO model of cerebral hypoperfusion has generated a large amount of data, however there are drawbacks associated with this model. Firstly, damage to the visual pathway in BCCAO rats has hampered interpretation of behavioural assessment (Davidson et al., 2000). Furthermore, despite recent advances in the development of conditional genetic manipulations in the rat brain (Schonig et al., 2012), the availability of successful transgenic rat models is severely limited. Thus, the ability to carry out informative genetics research in the BCCAO rat model is limited. Induction of BCCAO in the many genetically modified mouse strains would overcome this limitation. However, underdevelopment of the posterior communicating arteries of the Circle of

Willis of these animals means BCCAO induces severe ischemia rather than the desired CCH (Farkas et al., 2007).

To overcome the lack of complete Circle of Willis, and therefore the limitation of BCCAO use in mice, the bilateral common carotid artery stenosis (BCAS) technique for CCH induction was developed. In this model, small wire microcoils are wound around the common carotid arteries, inducing stenosis rather than occlusion of the vessels. The degree of hypoperfusion is adjustable according to the tightness of the microcoil winding (Shibata et al., 2004). Behavioural testing in these BCAS mice after 1 month of hypoperfusion showed significant impairment in performance on the 8-arm radial maze task, indicative of spatial working memory dysfunction (Shibata et al., 2007). Studies extending this research suggest that the impairment of spatial working memory may be induced by disruption of white matter components (Coltman et al., 2011).

The success of the BCAS microcoil technique has allowed this procedure to be carried out in transgenic mice models of AD, providing a platform for more detailed analysis of the interplay between CCH, cognitive decline and amyloid processing. For example, BCAS has been used in combination with the C57BL/6-Tg(Thy1-APPSwDutIowa) (Tg-SwDI) mouse model of AD, where a build-up of amyloid occurs on the walls of cerebral blood vessels as well as the cortex and hippocampus. Induction of CCH in these animals causes microinfarcts which were not found in the Tg-SwDI mice without BCAS or WT mice with BCAS (Okamoto et al., 2012). This combinatorial approach of CCH and transgenic modelling of AD promises to be an exciting research avenue in determining the biological processes relating vascular risk factors associated with ageing to the onset and progression of AD.

1.6.2 *In vitro* Models of Mild Metabolic Stress

There are obvious limitations in the modelling of chronic neurodegenerative disorders *in vitro.* Most pertinently in the case of AD as a vascular disorder, is the lack of blood vessels in the cell culture set up. In addition, unless co-culturing is undertaken, the lack of glial cells might also prove important as research uncovers further roles for these cells in early AD dysfunction (Farfara et al., 2008).

However, for the purpose of gaining a mechanistic insight into the cellular events pertinent to the early stages of AD, there are numerous advantages to *in vitro* modelling. Firstly, the cellular microenvironment can be closely controlled, with manipulations easily and precisely made within an experimental setting. Secondly, detailed morphological changes can be observed and recorded in a time-dependent manner throughout experimental protocols. Thirdly, secreted factors that are lost in *in vivo* cell sampling are easily obtainable from surrounding cell culture media, adding a further dimension to the material available for analysis. Finally, cultured cells are more accessible and amenable to informative research techniques such as electrophysiology, confocal and electron microscopy, which can be used in the pursuit of gaining mechanistic insight into cellular functions.

2-Deoxyglucose (2-DG) is a glucose analog which is used as a competitive inhibitor of glycolysis, restricting the availability of glucose at the cellular level, and inducing energy depletion and metabolic stress (Guo and Mattson, 2000). 2-DG is often used in investigations into cancer treatment strategies, where inhibition of glycolysis is beneficial (Ben Sahra et al., 2010). 2-DG has also been employed in neurodegenerative research investigating the cellular changes following energy depletion (Maus et al., 2006, Vornov et al., 1994).

Oxygen-glucose deprivation (OGD) is another technique used to model metabolic challenge *in vitro*. OGD is induced *in vitro* through the replacement of cell culture media with a suitable glucose-free alternative solution and incubation of this cell preparation in an anaerobic chamber (Goldberg and Choi, 1993). The duration of OGD can be controlled to model mild, moderate or severe metabolic challenges, with the extent of cell damage dependent on both the period of OGD and the re-oxygenation interval (Lushnikova et al., 2004). OGD has been successfully utilised in investigations of metabolic challenge across a range of *in vitro* set ups, including immortalised neuronal cell lines (Dohm et al., 2006), individual and mixed neuronal – glial cultures (Katchanov et al., 2001, Bell et al., 2011) and organotypic slice cultures (Cimarosti et al., 2005).

The severity of metabolic insult and the cell death processes induced in response to the 2-DG and the OGD metabolic challenges was recently characterised. 2-DG plus oxygen deprivation induced acute ischemia in primary neuronal cultures, whereas classic OGD using glucose-free culture medium plus oxygen deprivation induced delayed ischemia. Both *in vitro* models showed markers of necrosis, apoptosis, and autophagy in a dose dependent manner according to the duration of the challenge. (Meloni et al., 2011). This data shows the OGD challenge to induce a slowly evolving cellular dysfunction that may be more relevant to research concerned with the cellular dysfunction associated with ageing and neurodegeneration.

1.6.3 The SH-SY5Y Cell Line and its use in Modelling Neurodegenerative Disease

In order to model neurodegenerative disease in *in vitro* systems, the neuronal cell culture need to morphologically mature, preferably with the presence of extended neurites and the ability to form synapses with other neurons. Biochemically, the cells should express the human genome / proteome, with capabilities of detecting normal and pathological proteins under various experimental and control conditions.

SH-SY5Y cells are human in origin, from a neuroblastoma cell source (Borland et al., 2008), and possess many of the proteomic and functional properties of neurons, including neuronal marker activity, expression of neurofilament proteins and also nerve growth factor receptors (Xie et al.). Indeed, previous hypoxia experiments using SH-SY5Y cells successfully showed decreased sAPPα secretion with significantly decreased expression of ADAM10, the protein widely accepted to be α-secretase in the APP cleavage pathway (Webster et al., 2002).

SH-SY5Y cells can be differentiated in order to produce a culture system that more closely resembles mature neurons with extensive neurite outgrowths and increased expression of neuronal markers such as synaptophysin and NeuN, a postmitotic neuronal marker (Figure 1.9). Not only are these neuronal proteins increased in expression following differentiation, they also change location, moving from the cytoplasm to soma and neurites, potentially indicative of altered function in differentiated SH-SY5Y cells (Cheung et al., 2009). These factors suggest some utility in the differentiation of SH-SY5Y cells when they are to be used in neuroscientific research.

However, cellular differentiation is associated with a number of issues that might impact on the interpretation of experimental results, especially in a study concerning the global proteomic changes within the SH-SY5Y cell culture system. Differentiation affects the regulation of survival signalling pathways, with increased phosphorylation of Akt, a protein with central importance in processes including glucose metabolism, cell proliferation, apoptosis and transcription. Similarly, the phosphorylation of JNK proteins is found to be significantly changed following RA differentiation of SH-SY5Y cells (Cheung et al., 2009). JNK proteins are stress activated, therefore potentially play an important role in the cellular response to experimental changes in the environment. In studies investigating the protein responses to cell stress, including oxidative and metabolic stress, differentiation may therefore be undesirable, due to the potential for artefacts in the proteomic data from the differentiation process.

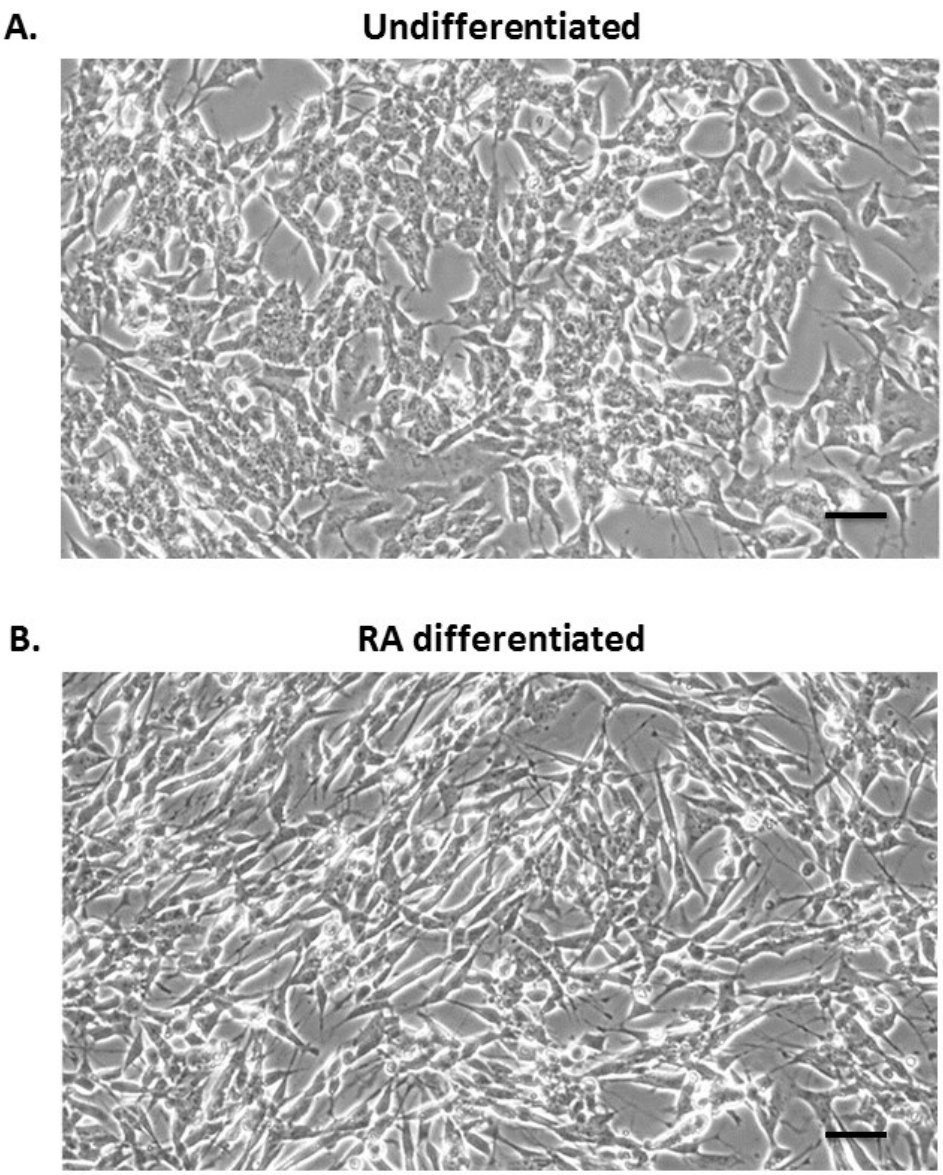

Figure 1.9 Differentiation of SH-SY5Y cells with retinoic acid (RA). A. Undifferentiated SH-SY5Y cells growing at approximately 80% confluency. Neurite outgrowths are evident between cells, with some characteristic clustering of neuroblastoma cell growth present. **B.** Differentiated SH-SY5Y cells show more extensive neurite outgrowths, however the gross morphology is not dissimilar to undifferentiated cells. Scale Bar = 50um. Adapted from (Brilot et al., 2011).

SH-SY5Y cells have been used in a range of studies to characterise the different neuronal cell death mechanisms in response to different stimuli. Short et al. employed mass spectrometry with SH-SY5Y cells to assess the proteomic basis of apoptosis in these cells in response to staurosporine exposure (Short et al., 2007). Another study investigating cell death mechanisms used SH-SY5Y cells and OGD to demonstrate necrosis to be induced following a severe ischemic insult of 32-hours of OGD (Fordel et al., 2007). OGD and SH-SY5Y cells have also been used in experiments seeking to characterise the role of calcium homeostatic disruptions in cellular dysfunction and neuronal cell death following ischemic challenges. For example, Dantrolene, a drug known to block the release of calcium ions from their stores in the endoplasmic reticulum, was shown to partially protect cells from neurotoxicity and cell death following OGD exposure (Wang et al., 2002).

These studies demonstrate the utility of SH-SY5Y cells, in combination with a range of experimental interventions, and proteomic technology, to uncover the biochemical processes underlying cellular dysfunction. In particular, the plethora of recent studies utilising OGD and SH-SY5Y cells to model mild, moderate and severe metabolic challenges, demonstrates the great utility of this cell line in interrogating the underlying dysfunctions following ischemic insults (Webster et al., 2002), (Iwata et al., 1998), (Guzy et al., 2005). A clear gap in the current literature however, is a large scale, comprehensive analysis of the proteomic response following different metabolic challenges induced by OGD in SH-SY5Y cells.

1.7 Quantitative Proteomics in Alzheimer's disease Research

1.7.1 The Evolution of Proteomics Research

Proteomics is described as "*the study of protein properties (expression level, post-translational modification, interactions etc.) on a large scale to obtain a global, integrated view of disease processes, cellular processes and networks at the protein level*" (Blackstock and Weir, 1999). At a basic level, proteomic studies are based on protein separation from complex samples, protein identification, and finally protein quantification and analysis.

Early proteomics research was primarily concerned with the isolation and identification of proteins present within a complex mixture. This era of research was defined by the development of gel-based protein separation techniques in the 70's, known as two-dimensional electrophoresis (2-DE) (O'Farrell, 1975). 2-DE involves the separation of proteins in the first dimension by their isoelectric point, and in the second dimension according to their molecular weight. Proteins are then recognized as individual spots separated across a polyacrylamide gel and can be isolated for identification.

The protein identification method conventionally used following 2-DE was Edman degradation, which involves the sequential removal of amino acid groups from the N-terminal of the protein , followed by amino acid identification by chromatography (Edman, 1949). However, Edman degradation is a time consuming, low throughput approach to protein identification, requiring multiple steps of proteolytic digestion, peptide fractionation, and peptide sequencing (Bandeira et al., 2008). This technique has now been largely superseded by mass spectrometry, which provides a high-throughput platform for protein identification and quantitation.

Knowledge of named proteins present in a biological sample is important in developing our understanding of biological processes. However, this information provides limited insight into the dynamic nature of the proteomic response to experimental conditions and disease states. To address this, the field has now evolved to "2nd generation proteomics", characterised by the use of quantitative MS-based methods to measure changes in protein abundance in response to experimental intervention or disease states (Lamond et al., 2012).

A large proportion of the current 2nd generation proteomic research uses 2-DE for protein separation. The development of gel scanners and analysis software has allowed for highly reproducible assessment of protein spot intensity, and therefore protein abundance, across different conditions. The significantly altered protein spots can then be selected, extracted from the gel, and processed for identification by mass spectrometry (Morris et al., 2010). This 2-DE, coupled to mass spectrometry, has significantly advanced our understanding of the proteomic basis of neuronal cell function and dysfunction across a range of model systems. These include *in vitro* investigations of the proteomic basis of apoptotic cell death (Short et al., 2007), characterisation of the proteomic changes underpinning spinal cord injury in the rat (Kang et al., 2006), extending to the detection of specific protein changes occurring in the white matter of schizophrenic patients compared to controls (Clark et al., 2007).

However, despite the important insights into the proteomics of neuronal function provided by these studies, there are significant limitations associated with this 2-DE coupled to mass spectrometry proteomic technique. 2DE-based proteomics fails to detect low abundance proteins, such as regulatory proteins and receptors, which are crucial to cell function. In addition, small proteins and hydrophobic proteins are notoriously difficult to detect and analyse with 2-DE. Importantly, membrane proteins are also not readily amenable to 2-DE analysis, due to their poor solubility in protein extraction buffers (Beranova-Giorgianni,

2003). Finally, and not insignificantly, 2-DE methods are very labour-intensive and often unrewarding due to the variability in gel quality affecting the reproducibility of protein abundance detection. 2-DE is relatively low throughput which is inadequate when large numbers of highly variable clinical samples are needed to adequately power the investigation.

In an effort to overcome the limitations of 2-DE, proteomics research is now moving away from gel-based protein separation and pursuing liquid-chromatography as an alternative separation technique (Patterson, 2003). This process, coupled to mass spectrometry-based protein identification, is known as tandem liquid chromatography – mass spectrometry, or LC-MS/MS. In LC-MS/MS, proteins in biological samples are converted to peptides by enzyme digestion. Liquid chromatography (LC) is then used to separate the peptides. In the LC stage, peptides are passed through a column packed with a hydrocarbon support resin. Peptides interact with the hydrocarbons in the resin, with polar peptides binding weakly and less polar peptides binding strongly. Peptide separation occurs through the sequential elution of peptides from the column using an increasingly polar solution.

The separated peptides are ionized by electrospray (electrospray ionization – ESI) before being further sorted in the linear ion trap (based on mass and charge), stored in the c-trap and finally being released into the orbitrap for detection. To gain more detailed data from the peptide spectra, parent peptides can then be fragmented into further smaller parts in the collision chamber, followed by a second round of mass / charge ratio measurement. The information gained from peptide fragment spectra provides insight into the peptide sequences, which can be accurately used to search protein sequence databases for matching peptides (Figure 1.10). A protein can then be identified by the multiple independently sequenced peptides present in a sample (Xie et al., 2011, Dancik et al., 1999).

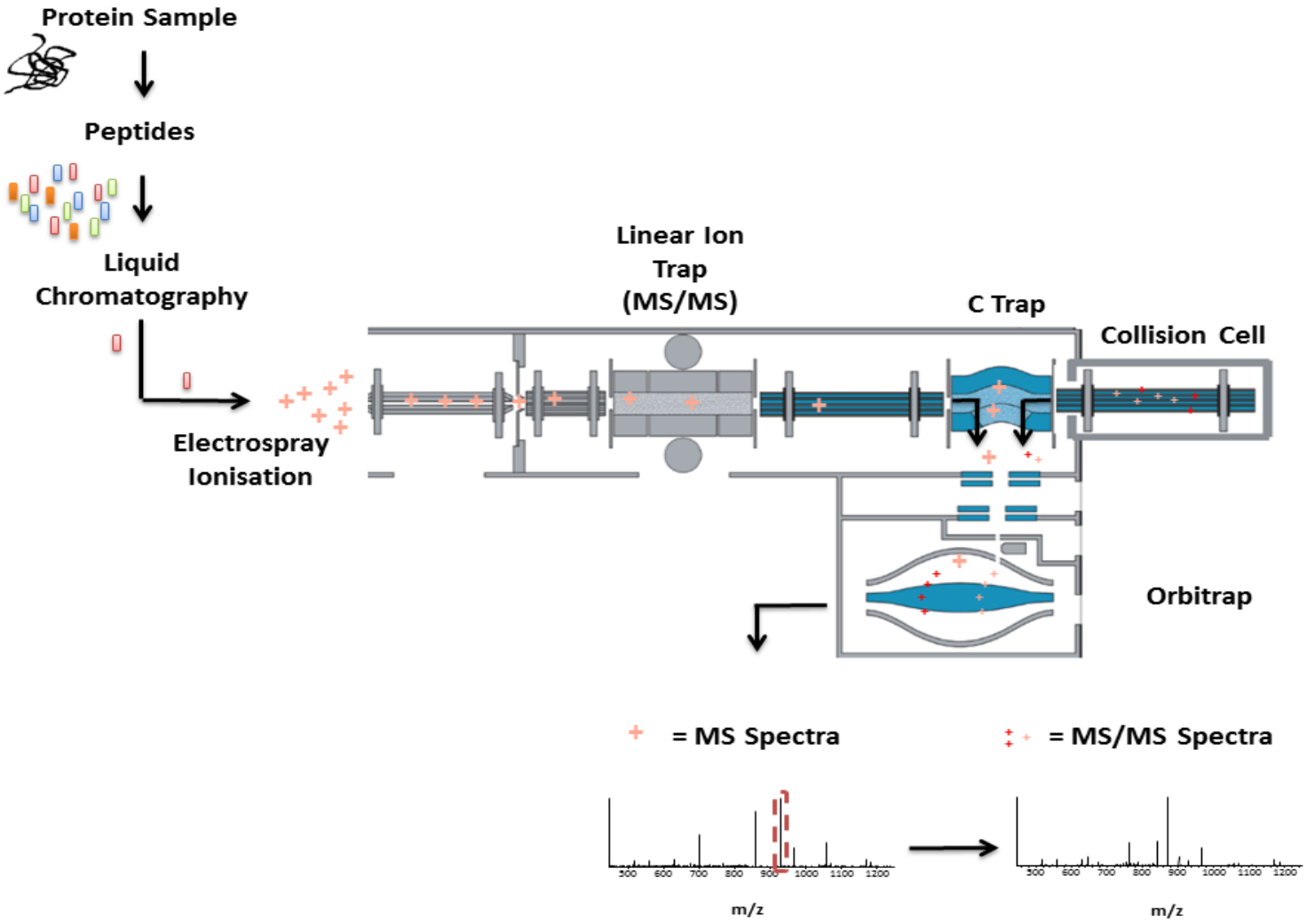

Figure 1.10 Diagrammatic representation of the tandem Liquid Chromatography – Mass Spectrometry System.

1.7.2 Quantitative LC-MS/MS Proteomics: to label or not to label?

In addition to providing wide coverage of the proteins present in complex samples, LC-MS/MS can also be used to gain information as to the expression levels of proteins. Numerous approaches exist to label proteins in advance of LC-MS/MS, facilitating quantitative comparisons of relative protein abundance between samples. Examples of commonly used protein labelling techniques include: stable isotope labelling by amino acids in cell culture (SILAC); isotope-coded affinity tags (ICAT); and isobaric tags for relative and absolute quantification (iTRAQ). These protein labelling techniques in LC-MS/MS are associated with numerous shortcomings, including complex sample preparation, requirement for high sample concentration and reduced coverage due to incomplete labelling (Patel et al., 2009).

Quantitative label-free LC-MS/MS has recently been developed in order to overcome the limitations associated with the protein labelling techniques. Label free LC-MS/MS allows peptides present in a complex protein digest mixture to be measured and the abundance of proteins identified across different samples. Label-free protein quantification is often carried out in relative terms, whereby protein abundance is expressed relative to a reference / control sample. There are two widely used techniques for label-free quantification, either (a) counting the number of fragment spectra identifying peptides from a specific protein, or (b) measuring and comparing the signal peak intensities of peptide ions from a particular protein (Matzke et al., 2013).

Spectral counting involves counting the number of fragment ion spectra that map to a particular protein across multiple LC-MS/MS analyses. This method of protein quantification is based on the premise that proteins present at high levels will produce more MS spectra from their constitutive peptides.

Therefore, relative quantification is accomplished through direct comparisons of spectral counts between samples (Bantscheff et al., 2007). Although this spectral count method of label-free protein quantification seems intuitive, the method assumes that the linearity of protein abundance and peptide spectrum count is the same for every protein. The reality is that spectrum counts are different for every peptide, and therefore acceptable quantification using this method requires observation of many spectra for each individual protein (Bantscheff et al., 2007).

In the peak intensity method, the ion chromatograms for every peptide are taken from the LC-MS/MS run and their mass spectrometric peaks are combined. The height of the peptide spike is used as an indication of protein abundance. These peak intensity values can then be compared to their respective signals in other samples, thus generating relative, quantitative data (Bantscheff et al., 2007). Matzke et al. provide a comprehensive examination of the merits and challenges associated with the two quantification approaches, and the computational tools that can be used with each (Matzke et al., 2013).

1.7.3 Proteomics in Alzheimer's disease Research

Proteomic technology in its many guises has been widely applied to the field of AD research (Butterfield et al., 2003). A popular strategy in the pursuit of biomarkers of AD is to interrogate the proteomic profile of various brain regions in post-mortem human AD tissue. A recent study used LC-MS/MS to investigate the proteomic changes occurring in the hippocampus in AD brains compared to controls. The biological processes assigned to the significantly altered proteins included "cellular metabolic processes" and "oxidative phosphorylation", indicative of the significant metabolic alterations occurring in AD (Begcevic et al., 2013). Similarly, proteomics has been used to investigate the protein changes in the cortex of AD patients, where mitochondrial protein changes were detected, including an increase in ABAD protein (Andreev et al., 2012).

The cerebral spinal fluid (CSF) of AD patients, due to its direct contact with the brain, has also been used in proteomic investigations to uncover potential biomarkers of AD. 2DE-MS/MS analysis of CSF from ante-mortem AD-patients and controls identified significant changes in proteins involved with Aβ transport and inflammation to be significantly affected by AD (Finehout et al., 2007).

However, there are significant barriers faced by researchers searching to identify novel biomarkers for AD. Firstly, proteomic analysis of post-mortem AD brain tissue and ante-mortem CSF from AD patients presenting cognitive symptoms represent late stages of disease development. At these points in disease progression, extensive neurodegeneration has probably already occurred, and thus proteomics will primarily be investigating either dead or dying tissue. Secondly, a conclusive diagnosis of AD can only be made post-mortem when a comprehensive assessment of amyloid plaque and tau-tangle burden can be made. It is therefore difficult to test biomarkers and drug targets in clinical trials as the AD patient group is likely to be a homogenous mix of different dementia subtypes. Finally, identification of healthy controls is integral to the successful pursuit of clinical biomarkers. The evolving nature of AD neurodegeneration over time presents a major challenge in the search for control subjects as there is no test to rule out the potential for future neurodegeneration in these individuals.

When all of these factors are considered alongside the low n numbers associated with human studies, and the high variability of human samples, it is clear that proteomic analysis of models of the early stages of AD would be more appropriate in the search for early disease biomarkers and strategies for intervention.

Proteomic technology has been used in conjunction with the many transgenic mice models of AD in an attempt to uncover the complex cerebral alterations occurring in AD (Chang et al., 2013, Sizova et al., 2007) Interestingly, iTRAQ proteomics using the triple transgenic AD mouse model (containing mutations in presenilin-1, amyloid precursor protein and tau) has shown many of the dysregulated proteins in the brains of these mice to be involved with the control of energy metabolism (Martin et al., 2008). This finding is consistent with the human proteomic data, which also indicates proteins involved in energy processes to be disrupted in AD (Andreev et al., 2012). .

The logical progression of the research theme of metabolic disruption in AD would be the large-scale proteomic analysis of the animal models of chronic cerebral hypoperfusion. However, only limited proteomic studies have been carried out in these models. The promising microcoil BCAS mouse model of chronic cerebral hypoperfusion has been used in a microarray study investigating the genomic changes in white matter (Reimer et al., 2011), however these BCAS mice are yet to receive full attention through large-scale proteomics research. In the rat BCCAO model, the response of individual proteins important to AD have been assessed by enzyme linked immunosorbent assay (ELISA) and western blotting (Zhiyou et al., 2009), however no proteomic - mass-spectrometry study has been carried out to characterise the global proteomic response to this stimulus.

Large-scale proteomic analyses of *in vitro* models of hypoperfusion would be similarly useful in identifying the key processes underpinning early cellular dysfunction in relation to metabolic stress. A recent study investigated the changes in small ubiquitin-like modifier protein (SUMO) interacting proteins following OGD using SILAC-based proteomics. This study identified SUMO3 to interact with numerous transcription factors, which were themselves modified by OGD (Yang et al., 2012). This study is clearly important in extending our

specific understanding of post-translational modification mediated by SUMOylation following metabolic stress. However the power of proteomics lies in its role as a hypothesis generator, allowing cellular processes to be examined in an investigative, un-biased manner, providing opportunity for discovery of novel protein changes and biomarkers of disease states.

The field of AD research is at something of a crossroads. The extensively investigated amyloid cascade hypothesis has failed to produce effective treatments for this devastating disease. Researchers have thus been forced to look elsewhere for novel theories as to the biochemical basis for the cognitive decline and neurodegeneration associated with AD. The vascular hypothesis of AD is promising, but much research still needs to be undertaken in order to establish the primary events that link metabolic challenge with the associated mitochondrial and cellular dysfunctions. The role of proteomics as a hypothesis generator ideally positions this technology at the forefront of future AD research.

1.8 Summary, Aims and Hypotheses

Vascular disorders inducing a state of chronic cerebral hypoperfusion are associated with Alzheimer's disease, as described in the C*ritically Attained Threshold of Cerebral Hypoperfusion* (CATCH) hypothesis of neurodegeneration. The cellular changes and biochemical pathways underpinning the metabolic stress induced by CATCH, in relation to the onset and progression of Alzheimer's disease, remain to be determined. Using established *in vitro* cell culture techniques, this thesis will characterise the cellular response to mild and moderate metabolic stress, and investigate the proteomic changes that underpin cellular dysfunction in relation to Alzheimer's disease.

Aim 1: To characterise the response of human SH-SY5Y cells to oxygen – glucose deprivation, an *in vitro* model of metabolic stress. Using a combination of functional assays, subcellular morphological analyses and large – scale LC-MS proteomics, this research will offer insight into the adaptive cellular response to metabolic stress. The descriptive proteomic data will provide a platform for novel hypothesis generation as to the vascular contributions to cellular dysfunction in AD, a relatively understudied area of AD research.

Aim 2: To characterise the protein interactome of amyloid binding alcohol dehydrogenase (ABAD) under control conditions and conditions of metabolic stress through the use of immunoprecipitation coupled to LC-MS (IP-MS). ABAD is the protein of choice for this interactome analysis due to its significant up-regulation in response to metabolic stress, a result obtained following the completion of Aim 1. The results of this proteomic investigation will expose the protein processes in which ABAD is involved, thus providing insight as to possible points of intervention that might avert the course of ABAD induced mitochondrial dysfunction in AD.

Aim 3: To build on the ABAD proteomic data gained through the completion of Aims 1 and 2, and test the novel hypothesis that increased ABAD expression may affect the expression levels and processing of APP. This hypothesis will be tested through transfection of ABAD into SH-SY5Y cells, and subsequent investigation of the effect of increases in ABAD protein on APP expression.

Chapter 2: Experimental Procedures

2.1 Cell Culture

Unless otherwise stated, all standard growth media used was obtained from Invitrogen (Paisley, UK) and was pre-warmed to 37°C before contact with cells. SH-SY5Y cells were routinely maintained in standard 75cm^2 cell culture treated flasks (Greiner Bio One, Stonehouse, UK) within a continuous flow incubator at 37°C, 5% CO_2. Cell growth and adhesion was monitored under the Leica DM IL inverted microscope. Growth medium was replaced bi-weekly.

2.1.1 Standard Cell Culture Procedures

SH-SY5Y cells, supplied at passage 29 from American Type Culture Collection (ATCC, Manassas, USA) were stored in liquid nitrogen until required. On defrosting, cells were grown and routinely cultured in Dulbecco's Modified Eagle Medium (DMEM) supplemented with 2mM L-Glutamine, 100 U/ml Penicillin, 100mg/ml Streptomycin and Fetal Bovine Serum (FBS) (referred to as complete media).

2.1.2 Passaging of Cells

On reaching 80% confluency, cells were passaged using the standard trypsinisation method. Flasks were washed with 10ml un-supplemented DMEM to remove any residual FBS followed by incubation for 3 – 4mins with trypsin / ethylenediaminetetraacetic acid, until all cells dispersed into solution. 10ml of complete media was added to the flasks, and the cell suspension centrifuged at 200 *g* for 7mins. The pellet was re-suspended in 5ml complete media, and 1ml added to 24ml complete media for seeding into new 75cm^2 flasks.

2.1.3 Liquid Nitrogen Cell Storage and Retrieval

2.1.3 Liquid Nitrogen Cell Storage and Retrieval

Cells not immediately required for experimental procedures were trypsinised as described in Section 2.1.2 and centrifuged down to a pellet (200 *g*, 7mins). Cells were gently vortexed into 5ml complete medium and 1ml 5% dimethyl sulfoxide (DMSO) solution (per 75cm^2 flask stripped). 1ml aliquots of cell solutions were then snap frozen in cryogenic storage vials and placed in liquid nitrogen for long term storage. Cells were revived by warming in a 37°C water-bath until thawed, and then diluted in 10ml complete medium. This new cell suspension was then washed of residual DMSO through a centrifugal step (200 *g*, 7mins), and the pellet resuspended in 5ml of complete medium. New 75cm^2 culture flasks were set up with 1ml cell suspension seeded in 24ml complete media.

2.1.4 Oxygen – Glucose Deprivation (OGD)

On reaching passage 35, 80% confluent flasks were stripped of cells using the trypsinisation method (Section 2.1.2) and cells centrifuged out of solution to pellet (200 *g*, 7mins). Cells were then resuspended in 6ml complete growth media and vortexed gently to ensure complete re-suspension. The number of cells was determined using a haemocytometer. The cells were seeded onto poly-D-lysine coated flat bottomed 96 well plates (Thermo-Fisher Scientific, Loughborough, UK) at a density of 125, 000 cells per well in 200µl complete medium. The plates were incubated overnight (37°C, 5% CO_2).

After overnight seeding, complete media was replaced in all wells with glucose free DMEM solution and the plate gently shaken. Cells were then incubated in either glucose-containing or glucose-free DMEM under either normoxic (37°C, 5% CO_2) or hypoxic (37°C, 95% N_2, 5% CO_2) conditions. The solutions used for the hypoxic condition were pre-equilibrated overnight in the hypoxic chamber before application to cells. The cells remained under control (normoxic) and experimental (hypoxic) conditions for 1hr, 3hr, 6hr, 9hr or 18hr durations.

2.1.5 MTS Assay: Assessment of Mitochondrial Function

The MTS assay is a colour change reaction whereby the tetrazolium salt (3-(4,5-dimethylthiazol-2-yl)-5-(3-carboxymethoxyphenyl)-2-(4-sulfophenyl)-2H-tetrazolium inner salt (MTS) is reduced to formazan, a soluble product forming a dark purple solution. The more viable cells that remain after OGD, the more dehydrogenase activity occurs, thus producing a more intense colour change (higher optical density (OD) reading). Therefore, measuring the OD of wells following MTS assay gives a good indication of mitochondrial function.

Following OGD treatments, all media in all wells was replaced with 200µl fresh complete media, and 20µl of CellTiter 96 AQueous One Solution Cell Proliferation Assay (MTS) (Promega, Madison, USA) was added to each well. The plates were then incubated for 1hr in normoxic conditions (37°C, 5% CO_2), followed by optical density readings taken at 490λ using an Dynex MRX plate reader (Dynex Technologies Ltd., Worthing, UK). The presence of any cells in the eluted solution following OGD was assessed using a Leica DM IL inverted microscope.

2.1.6 Trypan Blue: Cell Death Assessment

During harvesting of OGD cells for proteomics (Section 2.4.1), the total number of dead cells was assessed using a trypan blue stain (Invitrogen, Paisley, UK). Once cells were collected and resuspended in HBSS, 100µL of this solution was removed and added to a 1.5ml eppendorf tube. 20µL of trypan blue solution was added to the cell solution and left to equilibrate for 5mins at room temperature. Using a haemocytometer, the number of dead cells (stained blue) was counted and the amount of cell death was calculated as a percent of time-matched controls.

2.1.7 Oxygen Depletion Recordings: Internal Controls

In order to begin biochemical analysis on the OGD treated cells, the experiments carried out in 96 well plates needed to be scaled up to a 75cm^2 culture flask set up. This allowed larger numbers of cells to be treated and subsequently collected for proteomic analysis. Oxygen depletion curves from media in 96 well plates and in 75cm^2 culture flasks were recorded and compared.

96 well plates were seeded as previously described for the MTS assay study (Section 2.1.5). The reduction in pO_2 of the glucose free solution above the cells was measured using a fiberoptic dual oxygen-temperature sensing probe (OxyLite 2000 E Series, Oxford Optronix, Oxford, UK). The OxyLite system is based upon the principle that light emitted by the fluorescent probe will be quenched in the presence of local oxygen. The amount of quenching recorded is proportional to the pO_2 in the vicinity of the fluorescent compound (from User Manual for the Oxylite 2000 E series, Revision 1.2 2006). PO_2 measurements are temperature dependent, therefore all measurements were automatically compensated for temperature by the OxyLite instrument. Recordings were taken every 10 seconds over a 3.5hr period, representing the initial phase of OGD when O_2 is moving out of solution. The O_2 optimisation was repeated in 70 - 80% confluent 75cm^2 flasks (as will be used for collection of cells for the proteomics study) (Figure 2.1).

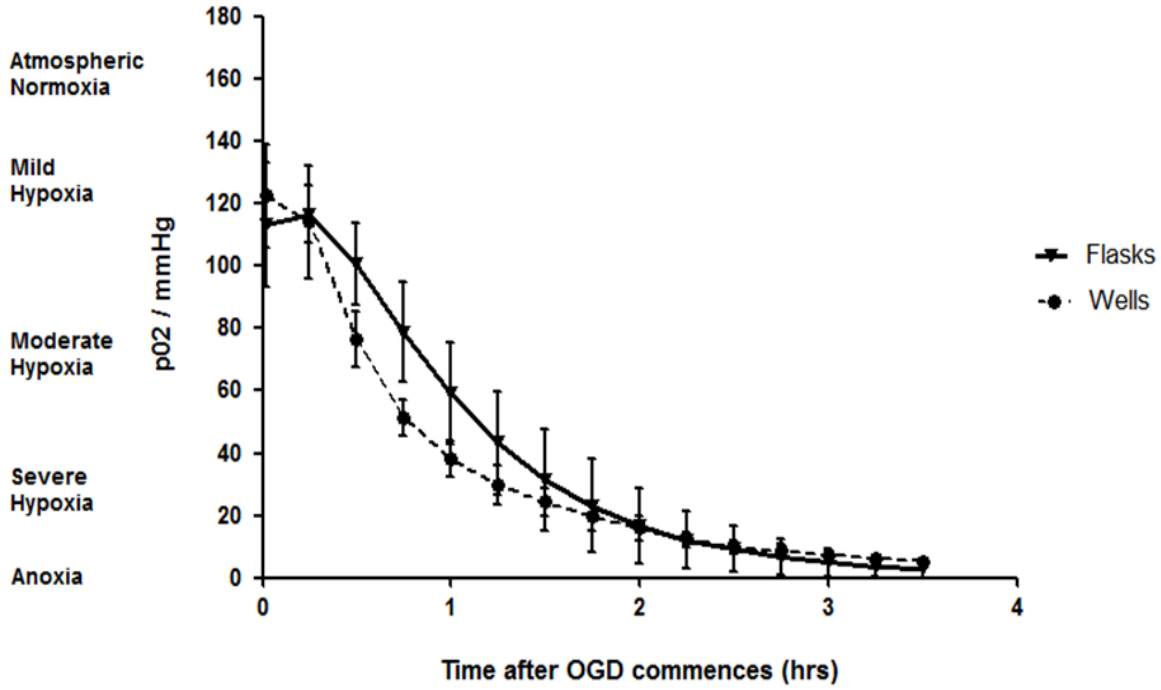

Figure 2.1 pO2 depletion profiles are comparable between 96 well plates and 75cm² flasks. Over the first 2 hours following OGD onset, oxygen depletion occurs marginally faster in the 96 well plate set up than 75cm² flasks. After 2 hours of OGD, pO2 levels decrease at the same rate from wells and flasks, and by 3h post OGD onset, pO2 is reduced in both experimental set ups to severely hypoxic levels, and remain at this level for the duration of the OGD exposure. (n = 5, means + / - SD)

2.2 Biochemistry

2.2.1 Protein Assay

The amount of protein present in samples was determined using a BCA (bicinchoninic acid) Protein Assay Reagent kit (Thermo Fisher Scientific, Loughborough, UK). A serial dilution of 2mg/ml bovine serum albumin (BSA) was carried out to produce a set of protein standards of the following concentrations: 2mg/ml, 1.5 mg/ml, 1 mg/ml, 0.5 mg/ml, 0.25 mg/ml, 0.125 mg/ml and 0mg/ml. These standards, along with protein samples (diluted to either 1 in 10 or 1 in 25), were loaded in triplicate onto a 96-well plate. 200µL of the working reagent was added and the plate was incubated at 37°C for 30mins. The absorbance of the solutions was measured at 562nm on a Dynex MRX plate reader (Dynex Technologies Ltd., Worthing, UK). Values obtained from protein standards were used to generate a standard curve from which the protein concentration of the samples was calculated.

2.2.2 Western Blotting

Protein assay results were used to prepare samples in 15µL aliquots containing 10µg of protein, with 0.5µL of 2x Laemelli buffer per µL of sample solution. Proteins were denatured from their globular structure to a linear formation on a hot-block (10mins, 70°C) to promote clean migration down through the gel. 14.5µL of samples were loaded onto NuPAGE 4-12% Bis-Tris precast polyacrylamide 15 well gels (Invitrogen, Paisley, UK) along with molecular weight marker (Li-Cor, Cambridge, UK) using a 25µL Hamilton Syringe. The gels were mounted in XCell SureLock™ Mini-Cells (Invitrogen, Paisley, UK) and proteins separated by sodium dodecyl sulfate polyacrylamide gel electrophoresis (SDS-PAGE) in NuPAGE morpholineethanesulfonic acid (MES) running buffer (Invitrogen, Paisley, UK). The electrophoresis step was run at 60V for 3h. Proteins were electro-transferred to nitrocellulose membrane (Bio-Rad, Hemel Hempstead, UK) at 30V for 1hr using the XCell II™ Blot Module system (Invitrogen, Paisley, UK) in tris-glycine transfer buffer.

Proteins were visualised on the nitrocellulose membrane using Ponceau S solution. Any membranes with evidence of unsuccessful transfer or uneven protein loading were discarded and the samples re-run. Membranes were incubated in 20ml Odyssey blocking buffer (Li-Cor, Cambridge, UK) diluted 1:1 with Phosphate Buffered Saline (PBS) for 1hr. Membranes were then incubated with primary antibody solutions containing the optimised dilution of primary antibody in 10ml blocking buffer diluted 1:1 with PBS: 0.1% tween-20. An appropriate loading control antibody of either GAPDH or α-tubulin was also added to the primary antibody solution, a choice made based on the avoidance of cross reactivity between antibody host-species . The membranes were incubated overnight at room temperature whilst being gently agitated on a shaker.

Primary antibodies were removed and the membranes washed 6 times for 5mins in PBS: 0.1% tween-20 solution. Appropriate fluorescent secondary antibodies (Li-Cor, Cambridge, UK) were diluted 1:5000 in blocking buffer and incubated with the nitrocellulose membranes at room temperature for 1hr. The secondary antibody solution was then removed and the membrane wash steps repeated, with the final wash in PBS only. The membranes were dried between blotting paper pads and imaged using the Odyssey infrared scanning system (Li-Cor, Cambridge, UK).

2.2.3 Immunocytochemistry

25mm coverslips (VWR, Leicester, UK) were coated with poly-d-lysine and placed in 6 well plates (Greiner Bio One, Stonehouse, UK). 150 000 SH-SY5Y cells suspended in complete media were seeded onto the coverslips. After a 3hr adherence phase, 3ml of complete media was added to the wells, and the cells were left to fully adhere overnight.

Coverslips were washed in glucose free DMEM and cells were exposed to control or OGD conditions as described in Section 2.1.4. Following OGD, coverslips were rinsed in pre-warmed PBS and fixed in 4% paraformaldehyde, pH 6.9, for 10mins at room temperature. The paraformaldehyde was removed and the coverslips were stored in PBS at 4°C until all samples were collected and ready for immunocytochemistry.

Immunocytochemistry was carried out at room temperature, with all wash steps carried out using PBS. Cells were quenched in 50mM ammonium chloride – PBS solution for 10mins, washed three times, and permeabilised in 0.1% tritonX. Cells were then washed again and incubated for 1hr in blocking solution: 0.1% PBS tween, 0.3M glycine, 2% bovine serum albumin. Cells were then washed and incubated in 50µL primary antibodies for 1hr. Coverslips were washed 5 times to remove excess primary antibody, and then incubated with secondary antibodies for 1hr. Coverslips were then incubated with DAPI (Invitrogen, Paisley, UK) for 10mins. Finally, cells were washed a further five times, rinsed in water, dried and mounted onto glass slides using ProLong Gold (Invitrogen, Paisley, UK) and left to dry overnight at room temperature before confocal imaging.

2.3 Molecular Biology

2.3.1 Bacterial Transformation

Myc-DDK tagged human HSD17B10 (ABAD) cDNA clone was purchased from Origene as pCMV-Entry vector along with the equivalent empty pCMV6-Entry vector (Figure 2.2) (Origene Technologies, Rockville, USA). The lyophilised vector was rehydrated in 10µL sterile distilled water. 1ng of DNA was added to 30µL of chemically competent Top10 cells and left to incubate on ice for 30mins. Transformation of the DNA into the Top10 cells was then carried out using the

heat shock method: 39℃, 45 seconds. Following heat shock treatment, the transformed cells were incubated on ice for a further 2mins, then added to 200µL Luria-Bertani (LB) media, and incubated for 1hr at 37℃ with vigorous shaking (200rpm).

Transformed cells were then spread onto LB agar plates containing 25µg/ml kanamycin. After overnight cultivation at 37°C, individual colonies were selected for plasmid propagation. Colonies were incubated for 8h in 5ml LB media, supplemented with kanamycin, at 37*°C* with vigorous shaking (200rpm). This starter culture was diluted 1:1000 into LB medium and grown overnight at 37℃ with vigorous shaking (200rpm).

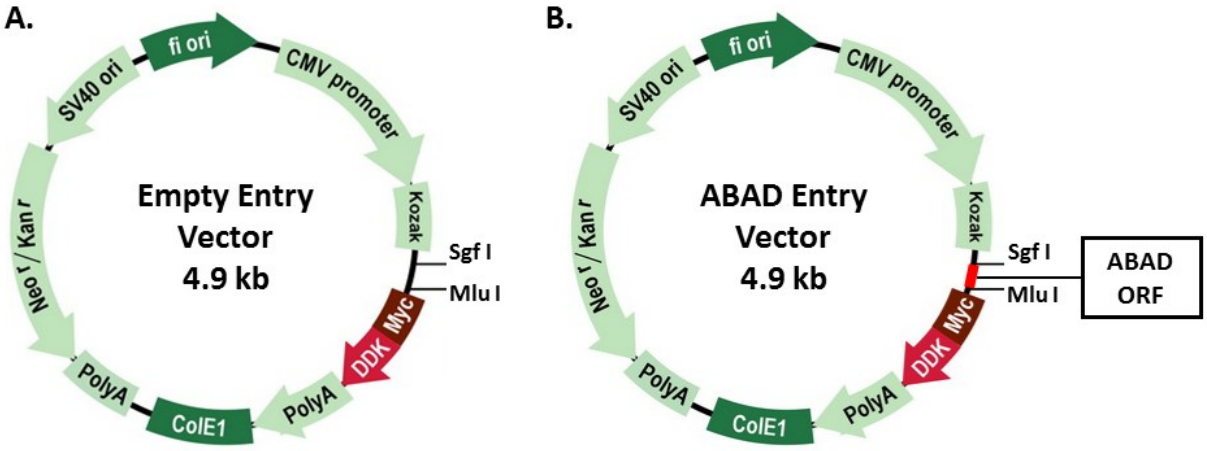

Figure 2.2 Vectors used in the ABAD overexpression study. A. Empty pCMV6-entry vector used for mock transfections in the main study. **B.** Myc-DDK tagged human HSD17B10 (ABAD) vector used for ABAD transfection and overexpression (Origene Technologies, Rockville, USA).

2.3.2 Maxi Prep: Qiagen HiSpeed® Plasmid Purification

Bacterial cells were harvested by centrifugation at 6000 *g* for 15mins at 4℃ . The bacterial pellet was resuspended in 10ml buffer P1 supplemented with RNAase A and LyseBlue reagent. 10ml of lysis buffer P2 was added to the bacterial solution and mixed thoroughly. 10ml of protein precipitation buffer P3 was added to the bacterial cell lysate and mixed thoroughly. The lysate was incubated for 10mins at room temperature in a capped QIA filter cartridge to allow bacterial protein, genomic DNA and detergent to precipitate out of solution. The cell lysate was filtered through the QIA filter cartridge into a HiSpeed Maxi Tip pre-equilibrated with 10ml QBT allowing the cleared cell lysate to enter the Maxi Tip resin by gravity flow. The HiSpeed Maxi Tip was then washed with 60ml Buffer QC by gravity flow. The ABAD DNA was then eluted from the Maxi Tip using 15ml buffer QF.

The eluent was incubated with 10.5ml isopropanol for 5mins at room temperature to precipitate the DNA. The eluate / isopropanol mixture was filtered in the QIAprecipitator and the DNA was washed in 70% ethanol. Using the plunger, air was passed through the filter in order to try out the suspended ABAD DNA. The concentrated DNA was eluted from the QIAprecipitator using TE buffer directly into a 2.5ml eppendorf tube, and DNA content was determined using a nanodrop.

2.3.3 Transfecting ABAD DNA into SH-SY5Y cells

Transfections were carried out according to the Lipofectamine 2000 DNA Transfection Reagent Protocol (Invitrogen, Paisley, UK). SH-SY5Y cells were seeded at 70% confluency in 6 well plates (Greiner Bio One, Stonehouse, UK) and left to adhere overnight. For the control transfection, 2 tubes were set up: tube A containing 900µL Opti-MEM medium (Invitrogen, Paisley, UK) and 18µg of control DNA and tube B containing 900µL Opti-MEM and 18µL Lipofectamine reagent (Invitrogen, Pailey UK). Tubes A and B were added together and incubated at room temperature for 5mins. 300µL of the DNA – lipid complex was added to each well of the 6 well plate, which was then incubated for 24 or 48h under standard growth conditions (37°C, 5% CO_2 in a humidified incubator). The same procedure was carried out for the ABAD DNA transfections.

Following 24 or 48hr transfection, media was removed from the cells and replaced with 1.5ml fresh complete media. Cells were then collected using the cell scraper method, and the cell solutions from each well transferred to individual 1.5ml eppendorfs and centrifuged for 3mins at 6000*g*. The supernatant was discarded and cells homogenised in 50µL RIPA buffer (50mM Tris-HCL, 150mM NaCl, 1% NP-40, 0.5% sodium deoxycholate and 0.1% SDS, supplemented with 1x protease inhibitor cocktail (Promega, Southampton, UK) and PMSF) using a cordless motor pestle (Sigma-Aldrich, Dorset, UK). Samples were then centrifuged at 14,000 *g* for 15mins at 4°C and the supernatant recovered. Protein concentrations of the samples were determined using the Pierce BCA Protein Assay Kit (Section 2.2.1).

2.4 Proteomics: Liquid Chromatography – Mass Spectrometry (LC-MS)

2.4.1 Sample Collection and Homogenisation

15 million cells were seeded in 75cm^2 cell culture in complete media, and left to adhere overnight. Prior to OGD, complete media was removed from the flasks and replaced with glucose free DMEM solution as a wash step to remove any residual glucose. Flasks were then incubated in 20ml DMEM + Glucose or DMEM – Glucose, both of which were supplemented with fetal bovine serum. The flasks were incubated in either normoxic (37°C, 5% CO_2) or hypoxic (37°C, 95% N_2, 5% CO_2) conditions (for controls and OGD samples, respectively) for 6 or 18h. The + / - Glucose DMEM solutions were pre-equilibrated overnight in normoxic or hypoxic conditions.

Following OGD and control incubations, cells were immediately scraped and centrifuged at 200 *g* for 7mins. The cell pellets were resuspended in HBSS and centrifuged again. The pellet was resuspended in 1ml HBSS and transferred to a 1.5ml eppendorf tube for final centrifugation wash step and pellet collection at 6000*g* for 3mins. The supernatant was removed and pellet snap frozen for storage until homogenisation.

Protein pellets were defrosted on ice. 100µL 8M urea (Sigma-Aldrich, Dorset, UK) was added to each sample and homogenised using a cordless motor pestle (Sigma-Aldrich, Dorset, UK). Samples were then centrifuged at 14,000 *g* for 15mins at 4°C and the supernatant recovered. Protein concentrations of the samples were determined using the Pierce BCA Protein Assay Kit (Section 2.2.1).

2.4.2 Sample Preparation for LC-MS

Protein samples (140µg) were made up to 100µL in 8M urea. Samples were diluted with 235µL water, 20µL ammonium bicarbonate (1M), and 20µL dithiothreithol (200mM). This sample solution was incubated for 30mins at room temperature allowing the proteins to be reduced. Cysteine residues were alkylated with 20µL iodoacetamide (500mM), and finally 5µg trypsin (Promega (Southampton, UK) was added to the samples. The sample – trypsin mixture was incubated overnight at 37°C to allow the proteins to be enzymatically digested to peptides.

After trypsin digestion, peptides were washed in a reverse phase column. 1ml buffer B (90% acetonitrile (Thermo-Fisher Scientific, Loughborough, UK), 10% water, 0.25% Tri-fluoro acetic acid (Sigma-Aldrich, Dorset, UK), 0.1% formic acid (Merck, Darmstadt, Germany) was run through the column followed by 2ml buffer A (97.5% water, 2.5% acetonitrile, 0.1% formic acid). 400µL sample was added to the column. 1ml buffer A was passed through the column, with final elution and collection of peptides in 1ml buffer B. Filtered peptides were dried overnight by Speed Vac and stored at −20 °C.

2.4.3 LC-MS Proteomic Data Collection

Proteomic data was collected on an automated micro-LC–MS/MS system, using a 1200 series micro-WPS autosampler and a binary micro-pump (Agilent Technologies, Palo Alto, CA) coupled to an LTQ-Orbitrap hybrid mass spectrometer (Thermo-Fisher, San Jose, CA). Peptides were reconstituted in 20µL of buffer A (97.5% H_2O, 2.5% acetonitrile, 0.1% formic acid) and sonicated for 15mins. 8µl of peptide mixture was loaded onto a 75µm (internal diameter) × 10 cm capillary Picotip column (New Objective, Cambridge, MA), in-house-packed with C18 reverse-phase resin (Pursuit C18; 5 µm particles; 200-Å pore size; Varian, UK) at flow rate of 5µl/min. After sample loading, the flow

rate was reduced to ~100–200 nl/min using a vented column - precolumn arrangement.

The high performance – liquid chromatography (HPLC) separation was provided by a gradient between buffer A and buffer B (90% acetonitrile, 10% H_2O, 0.025% trifluoroacetic acid, 0.1% formic acid). The peptide mixtures were separated on a 140min gradient from 0% to 65% Buffer B.

The mass spectrometer was operated in data-dependant mode, with a single MS scan (400–2000 m/z) followed by MS/MS scans in the linear ion trap on the 5 most abundant ions and dynamic excluded for 120 s.

The mass spectrometer was operated by Dr Thierry Le Bihan, University of Edinburgh

2.4.4 Global Proteomic Data Analysis

All LC-MS data were analyzed using a label-free intensity-based approach with Progenesis (version 4.0 Nonlinear Dynamics, Newcastle, UK), under randomized conditions. The MS/MS data were searched using MASCOT versions 2.3 (Matrix Science Ltd, London, UK) against a human subset of the NCBI database (downloaded on 12 January 2011) with 34,281 sequences using a maximum missed-cut of 2. Variable methionine oxidation, STY phosphorylation, protein N-terminal acetylation, and fixed cysteine carbamidomethylation were used in all searches.

Protein conflict (peptides shared between different proteins) was solved as follows: conflict resulting from multiple sequence assignment to the same peak - only the sequence having the highest score was kept. Conflict resulting from same peptide sequences assigned to different proteins - the assignment was singly attributed to the protein that had the highest number of peptides.

Regarding the label-free quantitation, the total number of features (i.e., intensity signal at a given retention time and m/z) was reduced to MSMS peaks with charge of 2, 3, or 4+ and only the five most intense MSMS spectra per 'Feature' were kept. The subset of multicharged ions (2+, 3+, and 4+) was extracted from each LC-MS run and the ions intensities summed for normalization. Protein quantitation was performed as follows: for a specific protein, the associated unique peptide ions were summed to generate an abundance value. The measured protein abundances were transformed using an ArcSinH function (as the method of detection can generate a significant amount of near zero measurement for which a log transform is not ideal). The within-group means were calculated to determine the fold change. Significant changes in protein expression (P<0.01) between control and OGD experimental groups were determined for each time point (6 and 18h) using Student's T-test.

2.4.5 Analysis of Protein Subcellular Localisation

All 958 proteins identified by LC-MS/MS by at least two or more peptides were uploaded to the Database for Annotation, Visualization and Integrated Discovery (DAVID) (http://david.abcc.ncifcrf.gov[15]) to determine subcellular localization based on gene ontology (GO). Protein clusters founded on subcellular localization with DAVID scores >2 were used. Proteins significantly altered (P<0.01) after 18h OGD were also assessed by DAVID according to subcellular localization.

2.4.6 Ingenuity Pathway Analysis (IPA)

Ingenuity Pathway Analysis (IPA) is a web-based software programme that enables analysis and integration of large proteomic datasets, providing detailed information on putative signalling pathways and biological processes associated with detected protein changes (http://www.ingenuity.com). IPA algorithmically generates protein interactomes based on direct (physical interactions and associations) and indirect (no physical interaction between proteins, however the change in expression of one protein effects the expression of another protein) interactions between proteins. Proteins within an IPA network are represented as symbols, with the shape of the symbol indicative of the protein classification. The protein symbols are colour coded depending on the direction of protein regulation: up-regulated proteins are red, down-regulated proteins are green, with the depth of shading of the protein symbol positively correlating to the magnitude of the fold change (Figure 2.3). IPA generates a score for each interactome, which is a putative measure of probability (see Deighton *et al*[16] for critical analysis).

In the present study, protein identifiers of all the proteins significantly altered after 18h OGD ($P<0.01$) were uploaded with their corresponding fold change values to IPA (http://www.ingenuity.com). Protein interactomes were generated based on direct relationships between eligible proteins.

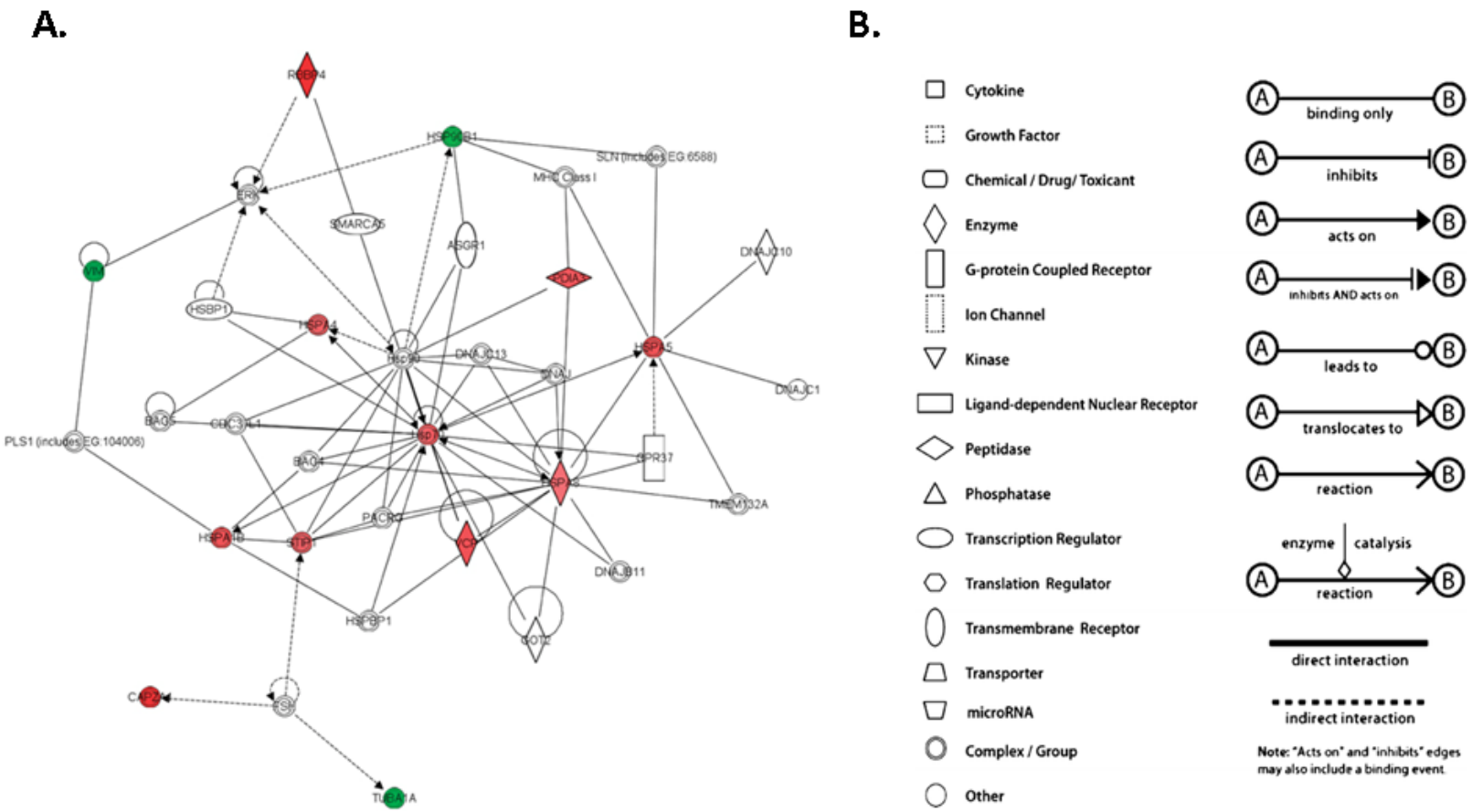

Figure 2.3 Proteomic interactome generation using Ingenuity Pathway Analysis (IPA) A. Example IPA interactome generated from the significantly altered proteins in SH-SY5Y cells following staurosporine treatment (Deighton et al., 2010). Red nodes indicate significantly increased proteins, green nodes indicate significantly decreased proteins, colorless nodes are proteins inserted by IPA to improve coherence of network. **B.** Figure legend for the shapes of protein nodes and relationships between proteins (http://www.ingenuity.com)

2.5 Proteomics: Immunoprecipitation - Mass Spectrometry (IP-MS)

2.5.1 Sample Collection & Homogenisation

15 million SH-SY5Y cells were seeded overnight in standard 75cm^2 cell culture treated flasks (Greiner Bio One, Stonehouse, UK). Cells were exposed to 18h OGD or control conditions, and harvested as described in Section 2.4.1. Cells from two equivalent 75cm^2 flasks were combined for each IP. The sample collection process was repeated until 3 OGD samples, 3 control samples and a negative control sample for both control and OGD conditions had been collected. Cell pellets were snap frozen for storage until homogenisation and protein assay.

Cell samples were homogenised in 400µL RIPA buffer (50mM Tris-HCL, 150mM NaCl, 1% NP-40, 0.5% sodium deoxycholate and 0.1% SDS, supplemented 1x protease inhibitor cocktail (Promega, Southampton, UK) and PMSF using a cordless motor pestle (Sigma-Aldrich, Dorset, UK). Samples were centrifuged at 14,000 *g* for 15mins at 4°C and the supernatant recovered. Total protein content of each sample was determined as described in Section 2.2.1. Based on the protein assay results, all samples were normalised to the sample with the lowest total protein content (2060µg) and made up to a final volume of 400µL. 1mg/ml BSA was added to each sample.

2.5.2 Immunoprecipitation & In-gel Trypsin Digestion

40µL ABAD antibody (Santa Cruz Biotechnology, Heidelberg, Germany) was added to each sample. 40µL RIPA buffer was added to the two negative control samples. Samples were incubated on a mechanical tube roller overnight at 4°C.

Illustra MicroSpin G-50 columns (GE Healthcare, Little Chalfont, UK) were thoroughly rinsed with distilled water and flushed with ice-cold PBS using centrifugation. 140µL sepharose bead suspension (Sigma-Aldrich, Dorset, UK) was added to each spin column and centrifuged. Ice-cold, filter sterilised PBS was added to the columns and centrifuged to thoroughly wash the beads, a process repeated 5 times. Beads were incubated with 500µL RIPA buffer for 1hr at 4°C. Following this blocking step, spin columns were centrifuged and the RIPA buffer flow through discarded. The 400µL of protein – ABAD antibody solution (or the 400µl protein-no antibody negative control solution) was added to the beads and incubated for 3h at 4°C.

Beads were washed twice in ice-cold RIPA buffer, followed by a wash in RIPA buffer supplemented with 500mM NaCl. The final washes were carried out in RIPA buffer followed by 20mM Tris. To elute, 75µl of 1x SDS sample buffer was added to the beads, gently vortexed, and boiled for 5mins. IP proteins were collected by centrifugation at 2800rpm for 1min.

The immunoprecipitated protein samples were loaded onto a precast polyacrylamide gel and exposed to pulse electrophoresis (60 volts, 15mins) to remove any impurities. The gel was washed in distilled water for 5 mins with orbital shaking. This wash was repeated two more times before removing the water and adding 30ml SimplyBlue SafeStain (Invitrogen, Paisley, UK). The gel was incubated with the stain for 1hr at room temperature with orbital shaking. The gel was removed from the stain solution and placed in 2% w/v NaCl destain solution overnight at room

temperature with orbital shaking. The destain solution was removed and replaced with distilled water for 1hr at room temperature on the orbital shaker.

The gel was placed on a clean glass plate and the gel bands containing the immunoprecipitated proteins were excised using a sterile scalpel. Each gel piece was cut into further smaller gel pieces and transferred to sterile 1.5ml eppendorf tube. Gel pieces were shrunk by incubation with 200µL methanol for 10mins. The methanol was removed and replaced with 200µL 50mM ammonium bicarbonate for 10mins. The ammonium bicarbonate was removed and the methanol – ammonium bicarbonate incubation cycle was repeated twice more. The final ammonium bicarbonate solution was removed and 100µL 20mM DTT in 50mM ammonium bicarbonate was added to the gel pieces. This protein reduction step was carried out at 60°C for 30mins. The DTT solution was replaced with 200µL methanol and incubated for 10mins. To alkylate the cysteines of the proteins, the methanol was removed and 100µL of 50mM iodoacetamide diluted in 50mM ammonium bicarbonate was added to the gel pieces. Incubation occurred for 1hr in the dark. The alkylating solution was replaced with 200µL methanol until all off the gel pieces had shrunk and turned white. The methanol was removed and the gel pieces were left to air dry.

A sterile syringe and needle (Thermo-Fisher Scientific, Loughborough, UK) were used to add 0.5ml 50mM ammonium bicarbonate to a 25µg trypsin vial (Promega, Southampton, UK). The trypsin solution was transferred to a sterile 1.5ml eppendorf tube and an additional 0.5ml 50mM ammonium bicarbonate was added. 30µL of the trypsin solution was added to the gel pieces and incubated for 30mins at 4°C. Enough 50mM ammonium bicarbonate was then added to fully cover the gel pieces and the trypsin digestion was left overnight at room temperature.

Gel digest solutions were transferred to a new, sterile 1.5ml eppendorf. 50µL of 1% w/v formic acid was added to the solution and incubated for 10mins. The solution was then transferred back to the previous tube and 50µL of 1% w/v formic acid in 1:1 dH_20: methanol was added. The solutions were incubated for 15mins. This process was repeated once more. Samples were loaded into a speedvac and spun at 45°C until all fluids were removed. The resulting extracts were kept at -80°C until LC-MS analysis.

2.5.3 IP-MS Proteomic Data Collection

Proteomic data was collected on a nano-HPLC-MS/MS using an on-line system consisting of a nano-pump (Dionex Ultimate 3000, Thermo-Fisher Scientific, Loughborough, UK) coupled to a QExactive instrument (Thermo-Fisher Scientific, Loughborough, UK) with a pre-column of 300 µm x 5 mm (Acclaim Pepmap, 5 µm particle size) connected to a column of 75 µm x 50 cm (Acclaim Pepmap, 3 µm particle size). Peptides were reconstituted in 5µl of Buffer A (97.5% H_2O, 2.5% acetonitrile, 0.1% formic acid) to give final concentration of 1 µg/µl. The samples were filtered with Millex filter before subjecting to HPLC-MS analysis.

Samples were analysed on a 2hr gradient in data dependent analysis (1 survey scan at 70k resolution followed by the top 5 MS/MS). The HPLC separation was provided by a gradient between buffer A and buffer B (90% acetonitrile, 10% H_2O, 0.025% trifluoroacetic acid, 0.1% formic acid). Peptide mixture was separated on a 140min gradient from 0% to 65% Buffer B. The mass spectrometer was operated in data-dependant mode, with a single MS scan (400–2000 m/z) followed by MS/MS scans in the linear ion trap on the 5 most abundant ions and dynamic excluded for 120 s. Protein identification and label-free quantification was as previously described in Section 2.5.3.

2.5.4 IP-MS Protein Enrichment Analysis

An enrichment ratio was calculated for every protein in each independent IP sample compared to the associated negative control. The frequency distribution of log enrichment scores was calculated, and a Z score > 1 was used as the inclusion criterion for protein enrichment in samples compared to negative controls (Appendix A).

The protein frequency library (PFL) database was used to reduce the chance of false discovery through non – specific protein - protein interactions. The PFL objectively evaluates whether proteins identified in an IP study are genuine protein interactor rather than binding non-specifically (www.proteinfrequencylibrary.com). Searching the database for proteins known to be immunoprecipitated under our specific experimental conditions (human derived cell line, whole cell fraction and sepharose bead support) resulted in detection frequency values being assigned to all of the immnoprecipitated proteins in the present study. A detection frequency of ≤25% set as the inclusion criteria for consideration in the final dataset.

2.6 Imaging

2.6.1 Light Microscopy: SH-SY5Y Gross Morphological Assessment

The temporal profile of gross morphological changes following each OGD exposure in wells and flasks was recorded with a Leica DM IL inverted microscope. Images were taken before and immediately after each OGD exposure at x10 and x20 magnification. Images of the eluted solutions were also recorded to determine the number of cells lost at each solution change step.

2.6.2 Confocal Microscopy

Confocal images were acquired with a Nikon A1R confocal laser scanning microscope (Nikon UK, Kingston Upon Thames, Surrey, UK) using a x60/1.4 NA oil immersion plan-apopchromat. For multicolour images a channel series protocol was used to minimise bleed through, the same high voltage gain settings were applied to control and treated samples. DAPI was excited with a 401 nm laser and signal collected from 425-475 nm; Alexafluor 488 was excited with a 488 nm laser and signal collected from 500-550 nm; Alexafluor 568 was excited with a 561nm laser and signal collected from 570-620 nm. Z-stacks were acquired with a resolution of 0.3 x 0.3 x 0.27µm in x, y and z respectively from 10 cells for each coverslip (n = 3 controls; n = 3 OGD plus negative controls from separate experiments for each condition).

Images were viewed and analysed with Image J (National Institutes of Health open software). A custom-written ImageJ macro that utilised the colocalisation threshold plugin was employed to generate a pseudocoloured image stack in which colocalised pixels were identified in cyan. These image stacks were then projected using a Z-projection and thresholded using the Otsu method to determine real staining from background (Otsu, 1979). For protein colocalization analysis, cells were manually outlined (excluding the nucleus) to determine the percent colocalisation of proteins of interest in the cell bodies. For analysis of the change in protein localisation in the nucleus, images were thresholded as described, and the image within the Z-stack containing the most complete nuclear cross section was selected. Nuclei were manually outlined and the percentage of the area stained with the protein of interest was calculated. Morphological changes in the colocalization patterns key proteins were analysed with a semi-quantitative scale. Cell images were coded and graded by 3 blinded observers as colocalized pixels appearing "lacy", having “few puncta”, or being “very punctate”.

2.6.3 Electron Microscopy

SH-SY5Y cells for electron microscopy were harvested using the trypsinisation method (Section 2.1.2) and fixed with 4% paraformaldehyde and 5% glutaradehyde in 0.08 M sodium cacodylate buffer, pH 7.2. Once fixed, cells were centrifuged, supernatant removed and replaced with a 3% agar solution. The gels were set at 4°C for 5 minutes before being cut into 1 mm^3 blocks, which were subsequently embedded and cut into 70 nm sections. Sections were collected on 300 mesh copper grids, stained with Reynold's lead citrate and contrasted with uranyl acetate.

The sections were evaluated on a JEOL CX -100 II transmission electron microscope at 40000x magnification. Cells were chosen from grid squares in a predetermined pattern until the organelles from a total of 50 cells had been assessed for each OGD and time-matched control sample. Mitochondria and endoplasmic reticulum were graded as "normal", "swollen" or "abnormal", whereas the nuclear envelope was graded as "normal", "swollen" or "blebbing". The presence of autophagic vacuoles, lipid droplets and any evidence of mitochondrial – endoplasmic reticulum interactions were also noted. The evaluator was blinded to the treatment condition of all samples.

EM samples were processed and evaluated by evaluated by M. McCulloch, University of Glasgow.

Chapter 3: Investigating the Proteomics of Metabolic Stress and Mitochondrial Dysfunction in an *in vitro* model of the Vascular Contribution to Alzheimer's disease

Chapter 3: Investigating the proteomics of metabolic stress and mitochondrial dysfunction

3.1 Background and Aims of the Chapter

Energy is required for almost all cellular reactions that occur within the body. The neurons of the brain are highly metabolically active cells, and rely on ATP produced by the mitochondria to meet these high energy demands (Fiskum et al., 1999). Energy production in the brain is maintained through the constant supply of oxygen and glucose delivered to the neurons via the cerebral vasculature. It is this glucose, together with oxygen, which forms the basis of ATP production in the mitochondria (de la Torre, 2000). Acute cerebral ischemia (i.e. a reduction of oxygen and glucose availability) is known to induce irreversible damage to neurons through disruption of the metabolic pathways vital for cell function. The effects of chronic cerebral hypoperfusion are less well understood, however it is thought that many neurodegenerative diseases, including AD, might be caused by a disruption of mitochondrial function linked to a persistent reduction in cerebral blood flow (Fiskum et al., 1999). The underlying biological mechanisms relating this chronic hypoperfusion to impaired mitochondrial function and neurodegenerative diseases remain unknown. This chapter will therefore aim to:

- Determine the effect of oxygen – glucose deprivation (OGD) on human SH-SY5Y cells, and to specifically explore the effect of varying degrees of OGD severity on mitochondrial function
- Investigate the proteomic changes underpinning moderate and severe mitochondrial and cellular dysfunction
- Utilise bioinformatics to interrogate the protein pathways integral to mitochondrial dysfunction in response to varying metabolic challenges

3.2 Methods

3.2.1 Oxygen - Glucose Deprivation (OGD)

SH-SY5Y cells were seeded in 96 well plates and exposed to a range of oxygen glucose deprivation (OGD) intensities, (notably 3hr, 6hr, 9hr, 12hr or 18hr OGD durations) as described in Section 2.1. Control cells underwent the same handling and experimental protocols, however were incubated in an equivalent glucose-containing media under normoxic conditions for the stated time course.

3.2.2 Light Microscopy: SH-SY5Y Gross Morphological Assessment

Gross morphological changes to cells following the different OGD durations were examined using light microscopy as outlined in Section 2.6.1. Multiple images were captured of cells at each time point in 96 well plates (taken before MTS assay) and 75cm^2 flasks (taken before sample collection for proteomics).

3.2.3 MTS Assay: Assessment of Mitochondrial Function

For the assessment of mitochondrial function following OGD, MTS assays were carried out as described in Section 2.1.5. The MTS assay is a colour change reaction whereby a tetrazolium salt (3-(4, 5-dimethylthiazol-2-yl)-5-(3-carboxymethoxyphenyl)-2-(4-sulfophenyl)-2H-tetrazolium, inner salt (MTS) is reduced to formazan, a soluble product forming a darker, more purple solution. The reduction of the tetrazolium salt is dependent upon the oxidation on NADH by a fully functioning complex I on the mitochondrial electron transport chain. If mitochondrial dysfunction occurs, the colour change reaction is less intense, and recorded as such via optical density readings taken using a Dynex MRX plate reader (Dynex Technologies Ltd., Worthing, UK) at 490λ. The design and timing of the MTS mitochondrial function assay is illustrated in Figure 3.1.

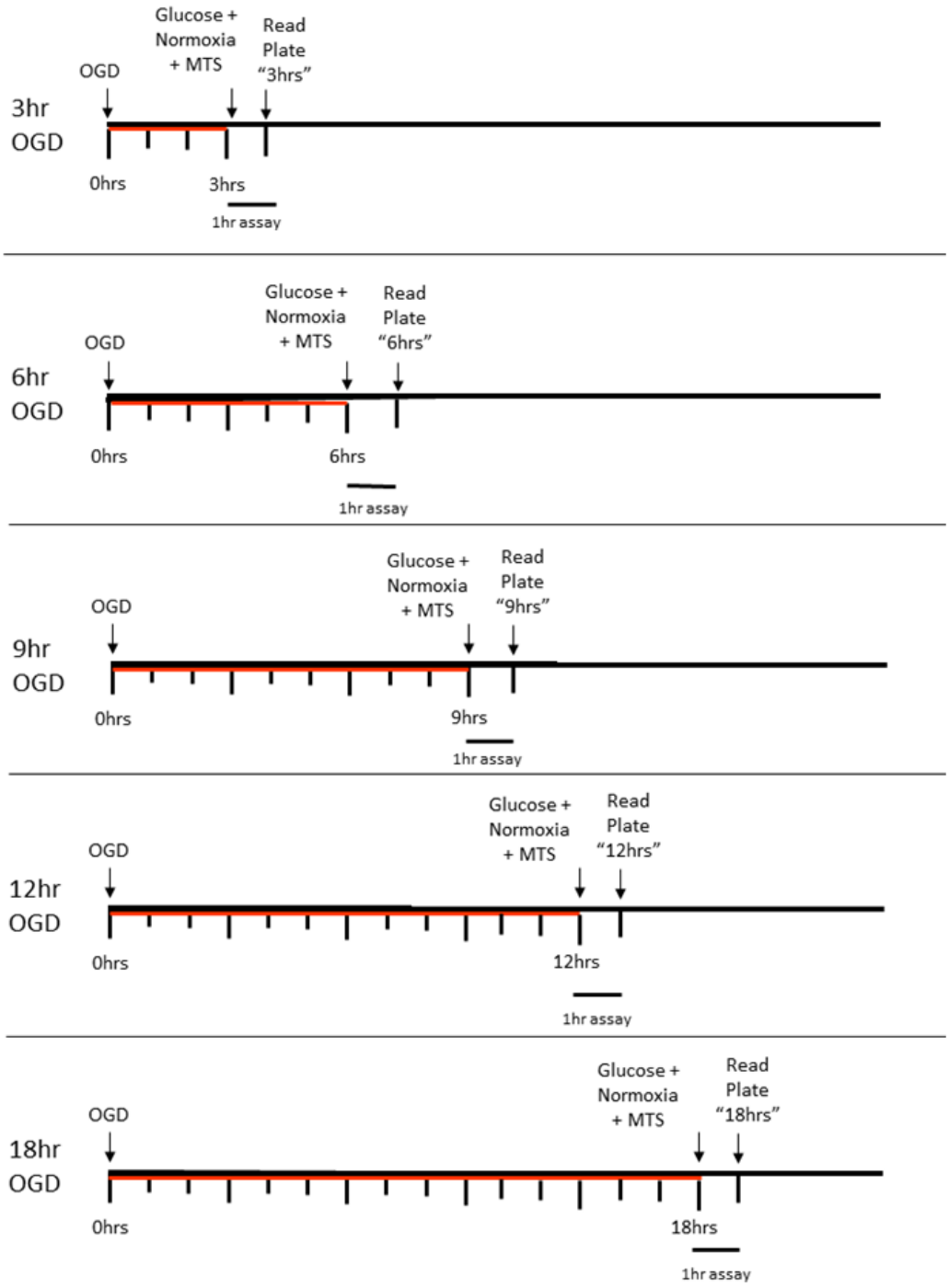

Figure 3.1 Time course of mitochondrial function assay. OGD was induced at time '0h' and maintained for 3, 6, 9, 12, and 18h. The MTS assay was incubated for 1hr, after which the optical densities of formazan product were measured.

3.2.4 Electron Microscopy: Ultra structural Morphological Assessment

SH-SY5Y cells were exposed to OGD using the same paradigm as the LC-MS study (Section 2.4.1). Samples were collected immediately after 3, 9 and 18h of OGD and fixed with 4% paraformaldehyde and 5% glutaradehyde in 0.08 M sodium cacodylate buffer, pH 7.2. Once fixed, cells were centrifuged, supernatant removed and replaced with a 3% solution of agar. Gels were cut into $1mm^3$ blocks and processed for EM.

EM images were acquired on a JEOL CX -100 II transmission electron microscope. The evaluator was blinded to the treatment condition of all samples. Cells were chosen from grid squares in a predetermined pattern. 50 cells were assessed from each treatment. For each cell the condition of mitochondria and rough endoplasmic reticulum (ER) was assessed. The presence / absence of autophagosomes and lipid droplets were also recorded. A Chi-Squared 3 x 2 matrix was used to test the null hypothesis that OGD would have no effect on the ultrastructure of organelles.

3.2.5 Trypan Blue: Cell Death Assessment

Trypan blue staining was carried out to assess the extent of cell death occurring after each OGD time point (Section 2.1.6). A haemocytometer was used to calculate the percentage of stained and unstained cells for each OGD and time matched control sample.

3.2.6 Liquid Chromatography - Mass Spectrometry (LC-MS)

Based on the OGD characterisation, SH-SY5Y cells treated with 6hr OGD (n = 6) and 18hr OGD (n = 6) as well as time matched control samples (n = 6 for each control time point) were collected as described in Section 2.4.2. Each sample was homogenised in 8M urea and protein assayed using the Pierce BCA Protein Assay Kit (Thermo Scientific, UK) as per the methods outlined in Section 2.2.1.

Samples were further processed and purified prior to LC/MS protein detection as described in Section 2.4.2. Quantitative proteomic data for each OGD and control sample was collected using high throughput liquid chromatography coupled to mass spectrometry. Protein identification and analysis of different protein intensities was carried out using the Progenesis software package (Nonlinear, Newcastle, UK).

3.2.7 Western Blotting

Western blotting was performed on the original control and OGD samples used in the LC-MS study to confirm that the changes in peptide levels detected by the mass spectrometer are reflected in the changes in total protein levels. 5μg of total protein was loaded onto the gels and standard western blotting procedures were then carried out as detailed in Section 2.2.2. The specific antibodies used in this study are listed in Table 3.1. The fluorescence intensity of the protein bands was detected using Odyssey application software (version 3.0; Li-Cor, Cambridge, UK).

Protein Identifier	LC-MS Detected Fold Change	Antibody	Concentration
UQCRC1	0.46	Invitrogen, 459140	1 : 5000
UQCRC2	0.31	Abcam, ab14745	1 : 5000
VDAC1	0.26	Abcam, ab14734	1 : 2000
TOM22	0.46	Abcam, ab57523	1 : 5000
GRP78	1.53	Cell Signalling, 3183	1 : 1000
GRP84	1.49	Cell Signalling, 2104	1 : 1000

Table 3.1 Details and specifics of the antibodies used in validating LC-MS data

3.2.8 Statistical Analysis

MTS & Trypan Blue Assay: MTS results of mitochondrial function and trypan blue data addressing cell viability following OGD treatments were expressed as a percentage of contemporaneous time matched controls. Statistically significant changes in mitochondrial function and cell viability between control and experimental groups were detected using a two-tailed Students t-test using GraphPad Prism, version 5.

Electron Microscopy: Following blind assessment of organelle morphology, a Chi-Squared 3 × 2 matrix was used to test the null hypothesis that OGD would have no effect on the ultrastructure of organelles. The Chi-Squared analysis was done using GraphPad Prism, version 5.

LC-MS Proteomics: Students t-tests were carried out in Microsoft Excel version 2010 to determine significant differences in protein expression between control and OGD experimental groups. A stringent probability of $p < 0.01$ was considered as statistically significant in order to reduce the detection rate of false positives. Proteins found to be significantly changed at $p < 0.01$ were uploaded to Ingenuity Pathway Analysis (IPA) software, where functional protein networks were generated. Statistics carried out in Microsoft Excel were validated in GraphPad Prism, version 5.

Western Blotting: Significant changes in protein abundance as detected by western blotting and densitometry analysis were determined with a two-tailed Students t-test using GraphPad Prism, version 5.

3.3 Results

3.3.1 Mitochondrial Function, Cell Viability and Morphology after OGD

Normal mitochondrial function was significantly reduced in SH-SY5Y cells following OGD relative to time-matched control cells ($p<0.0001$, at each time point analysed), with longer durations of OGD inducing more severe mitochondrial dysfunction (Figure 3.2). Viability of SH-SY5Y cells treated with OGD was quantified using Trypan Blue staining (Figure 3.2). Minimal cell death was detected after OGD, with 91% of cells remaining viable following 18h OGD.

Consistent with the trypan blue analysis, gross morphological assessment shows at no time point is global cell death seen across a cell population (Figure 3.3). After 3- and 6 hours OGD, cell bodies remain elongated and adhered, with evidence of neurite outgrowth and interconnections present between cells. At 9h OGD cell bodies appear shrunken, with fewer neurites and inter cellular connections formed. This phenotype is then consistently observed at 12 and 18-hours. At 9, 12 and 18-hours of OGD, the cellular response is heterogeneous, with a mixture of healthy and damaged cells in each condition.

Ultra-structural morphological changes in subcellular organelles were analysed relative to time-matched controls by electron microscopy following OGD. With increasing OGD duration, the number of cells displaying abnormal endoplasmic reticulum was significantly increased (Chi-Square, $p<0.01$) (Figure 3.4). SH-SY5Y cells also showed changes in mitochondrial morphology with increasing OGD duration (Figure 3.4). It should be noted that even after 18h OGD exposure, only 26% of cells displayed abnormal ER, and only 34% had abnormal mitochondria. Analysis of the EM samples for the presence / absence of autophagy and lipid droplets showed evidence of both of these features. However, there was no detectable change in the presence of autophagic vacuoles or lipid droplets following OGD treatment when compared to time-matched controls (Figure 3.5).

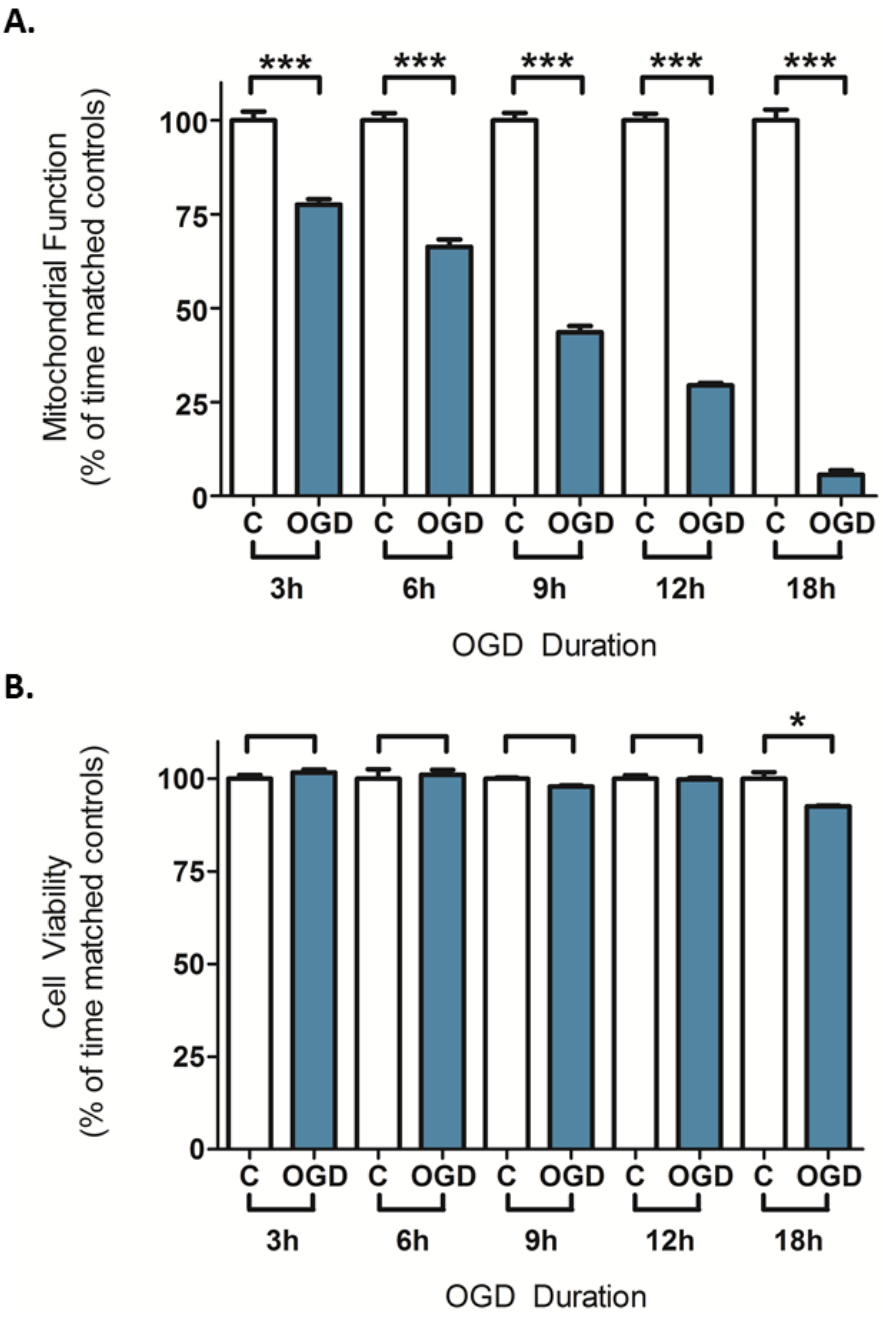

Figure 3.2 The effect of increasing duration of OGD on mitochondrial function and cell death. **A.** MTS assays following OGD exposure reveal mitochondrial function to be significantly reduced as a function of OGD duration, $p<0.0001$, $n = 8$. Results are expressed as mean percentage of controls, +/- SEM. **B.** Cell viability is maintained up to 12h OGD, with an increase in cell death detected by trypan blue after 18h OGD. Data are presented as mean +/- SEM, $n = 3$ for each time point. All data are expressed as a percentage of contemporaneous time matched controls (* $p<0.05$, *** $p < 0.0001$, T-test)

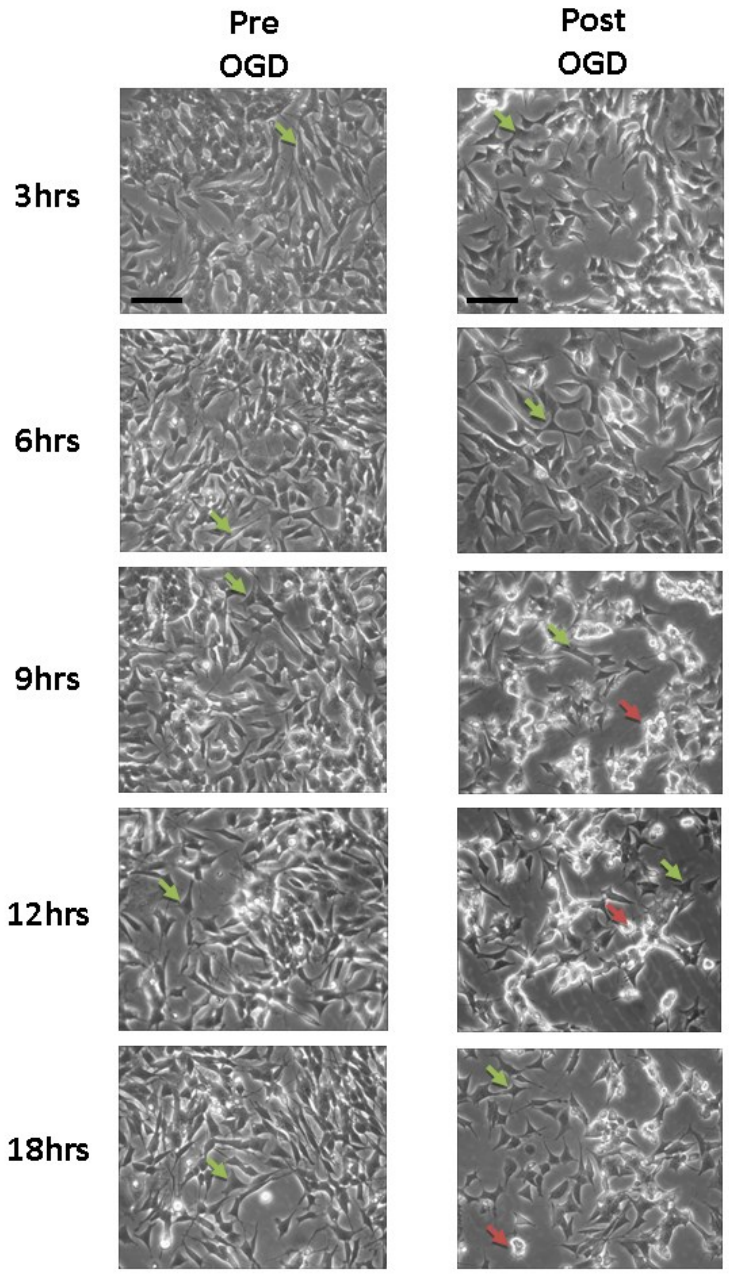

Figure 3.3 Temporal profile of morphological changes assessed visually using light microscopy. Before OGD induction, cells are healthy, with stretched cell bodies and neurite outgrowths (green arrows). There is little difference in SH-SY5Y morphology following 3 and 6-hours OGD. With increasing OGD duration, cell morphology becomes progressively irregular, with shrunken cell bodies and retracted neurites (red arrows). The cell populations following longer time points are heterogeneous, with a mixture of healthy and damaged cells. Scale Bar = 100um

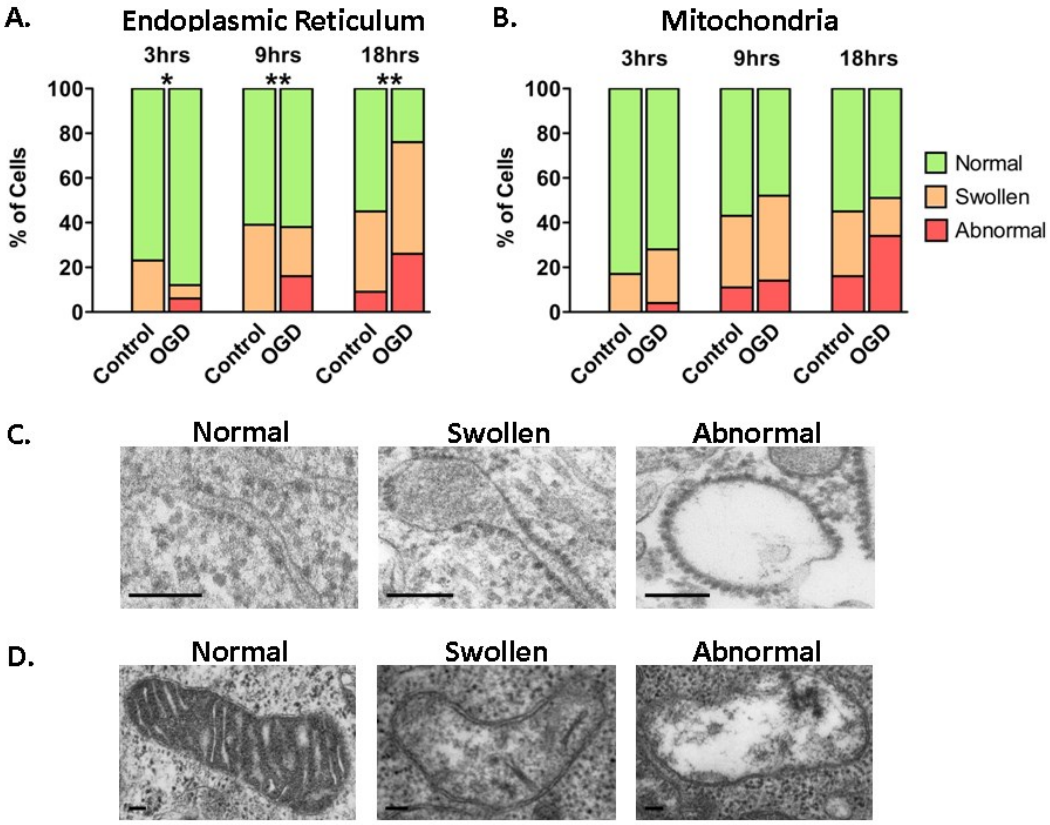

Figure 3.4 The endoplasmic reticulum (ER) and mitochondria display progressive morphological changes following oxygen glucose deprivation (OGD). **A.** OGD induced increases in the number of cells containing swollen and abnormal ER. Significant changes in the distribution of "normal", "swollen" and "abnormal" ER within cells was seen after 3, 9, and 18h OGD compared to the time matched controls (* $p<0.05$ ** $p<0.01$, X^2, n = 50 cells for each condition) **B.** The occurrence of mitochondrial morphological abnormality increases following longer OGD durations (n = 50 cells for each condition) C**.** Representative electron micrographs of the three grades of ER morphology. Scale bar = 0.1µm. **D.** Representative electron micrographs of the three grades of mitochondrial morphology. Scale bar = 0.1µm.

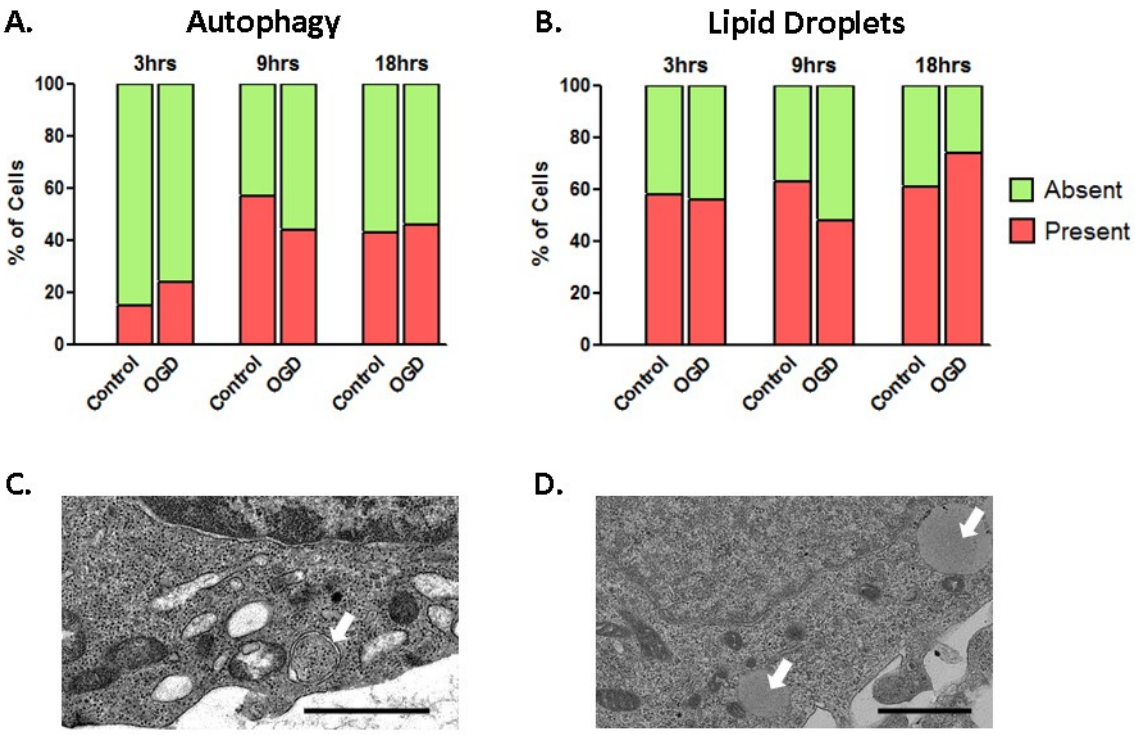

Figure 3.5 Evidence of autophagy and lipid droplets are detected across all control and OGD cells. **A.** 9 and 18h of OGD increases the number of cells containing autophagic vacuoles, however there is little difference between control and OGD cells (n = 50 cells for each condition) **B.** The presence of lipid droplets is observed consistently in all cells after each OGD exposure (n = 50 cells for each condition) **C.** Representative electron micrograph of an autophagic vacuole (white arrow). Scale bar = 1µm. **D.** Representative electron micrograph of the appearance of lipid droplets (white arrows). Scale bar = 1µm.

3.3.2 Overview of the LC-MS Proteomic Data

A total of 958 proteins were identified across all samples with two or more peptides by LC-MS (Appendix B). Minimal protein changes were observed following 6h OGD, with only 14 proteins significantly altered in expression level ($p<0.01$) (Table 3.2). Following 18h OGD, 193 proteins were significantly altered in expression level ($p<0.01$), with 130 proteins increased and 63 proteins decreased. For 765 proteins, no significant differences were observed between control and OGD samples after 18h OGD. The significantly increased and decreased proteins following 18h OGD are listed by subcellular location in Table 3.3 and Table 3.4 respectively.

The subcellular distributions of all 958 proteins identified by LC-MS were examined using DAVID software. Proteins were detected from across many subcellular compartments, including the nuclear lumen, cytoskeleton, mitochondria, endoplasmic reticulum, Golgi apparatus, ribosomes and vesicles (Figure 3.6). Similar assessment of the 193 significantly altered proteins following 18h OGD indicates that organelles are not uniformly affected by the metabolic challenge. None of the 197 detected nuclear lumen proteins were significantly altered after 18h OGD, whilst 41% of the 56 detected endoplasmic reticulum proteins and 32% of the 118 detected mitochondrial proteins were significantly altered (Figure 3.6).

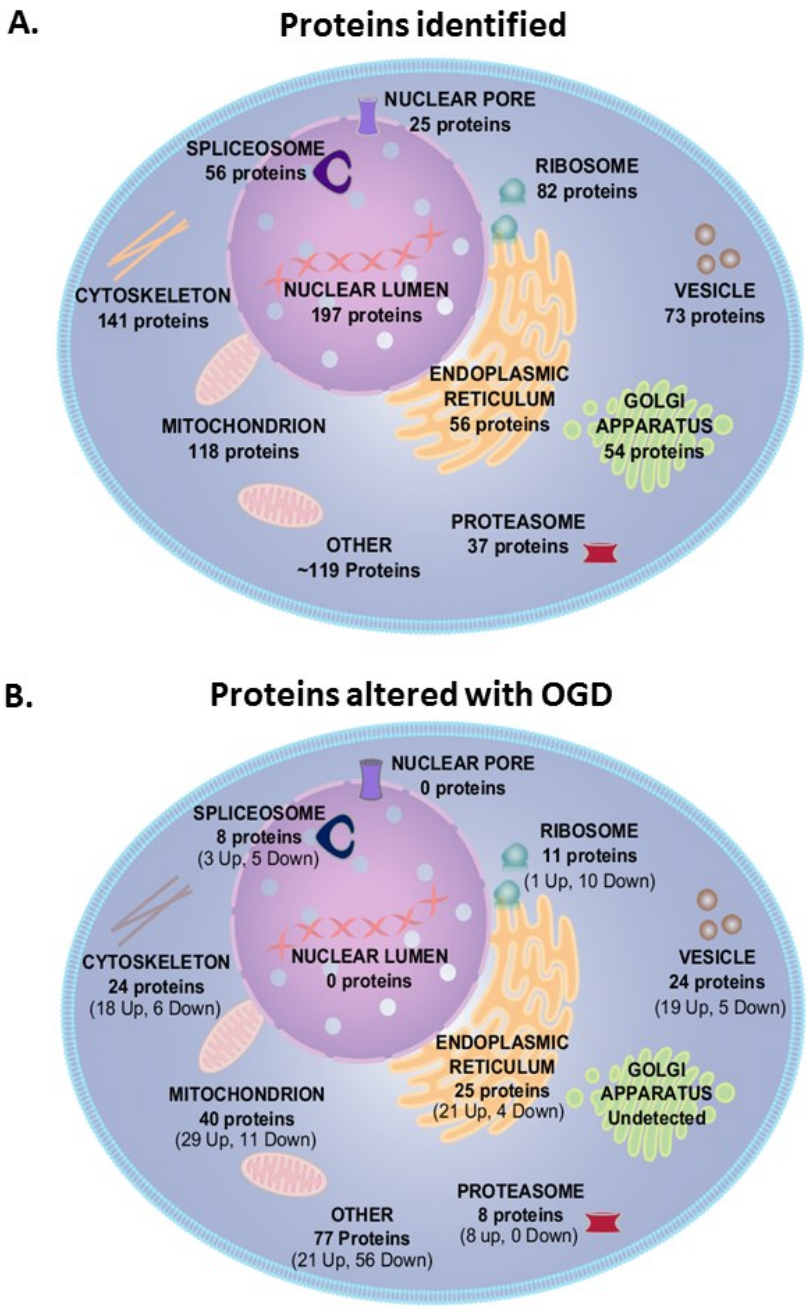

Figure 3.6 Subcellular distribution of all detected proteins contrasted with subcellular distribution of proteins significantly altered after 18h oxygen glucose deprivation (OGD) relative to their original levels in time matched control samples ($p<0.01$). **A.** Liquid chromatography mass spectrometry (LC-MS) detected 958 proteins from across many subcellular compartments, demonstrating the utility of LC-MS in providing a global overview of cellular proteomics. **B.** Organelles are differentially affected by 18h OGD. The 193 significant altered proteins were not distributed evenly across subcellular compartments: the endoplasmic reticulum and the mitochondria contained the largest proportion of significantly altered proteins, whereas no significant protein changes were detected in the Golgi apparatus or nuclear pore.

3.3.3 Translation Initiation Factors are Significantly Down-regulated following 6h OGD

Only 14 proteins were found to be significantly altered in expression level following 6h OGD (Table 3.2). This small number of significantly altered proteins needs to be treated with caution: with 958 proteins detected in the study, and at a significance threshold set at $p<0.01$, approximately 10 proteins would be expected to be "significantly altered" by chance alone. Therefore the reliability of this small dataset is limited.

However, a cautious inspection of the 14 changed proteins appears to show a functional response of proteins involved in protein synthesis pathways. Eukaryotic initiation factors EIF1, EIF4A1 and EIF3I are all significantly down-regulated following 6h OGD, and remain down-regulated following 18h OGD to a similar or greater extent (Figure 3.7). Other proteins involved in processes related to protein synthesis are detected as significantly down-regulated following 6h OGD, including BTF3, SF3B4, RPS15, EEF2 and PCBP1.

Table 3.2: Proteins Significantly Altered by 6h OGD

Uniprot Accn No.	Gene Name	Protein Name	p-value	Fold change	Protein Function
P41567	EIF1	eukaryotic translation initiation factor 1	0.0035	0.72	Protein biosynthesis
Q9Y678	COPG1	coatomer subunit gamma	0.0038	0.75	ER – Golgi transport
A6NKG5	RTL1	retrotransposon-like protein 1	0.0016	0.75	Organism development
Q8IV08	PLD2	phospholipase D3	0.0010	0.76	Lipid metabolism
P20290	BTF3	transcription factor BTF3 isoform B	0.0013	0.77	Transcription
P60842	EIF4A1	eukaryotic initiation factor 4A-I	0.00003	0.77	Protein biosynthesis
Q15427	SF3B4	splicing factor 3B subunit 4	0.0099	0.81	mRNA processing
P62841	RPS15	40S ribosomal protein S15	0.0019	0.83	Translation initiation
Q9Y696	CLIC4	chloride intracellular channel protein 4	0.0079	0.84	Ion transport
P31689	DNAJA1	dnaJ homolog subfamily A member 1	0.0062	0.85	Protein folding
Q13347	EIF3I	eukaryotic translation initiation factor 3	0.0025	0.85	Protein biosynthesis
P13639	EEF2	elongation factor 2	0.0067	0.88	Protein biosynthesis
Q15365	PCBP1	poly(rC)-binding protein 1	0.0033	0.92	RNA splicing
P21266	GSTM3	glutathione S-transferase Mu 3	0.0092	1.08	Cellular detoxification

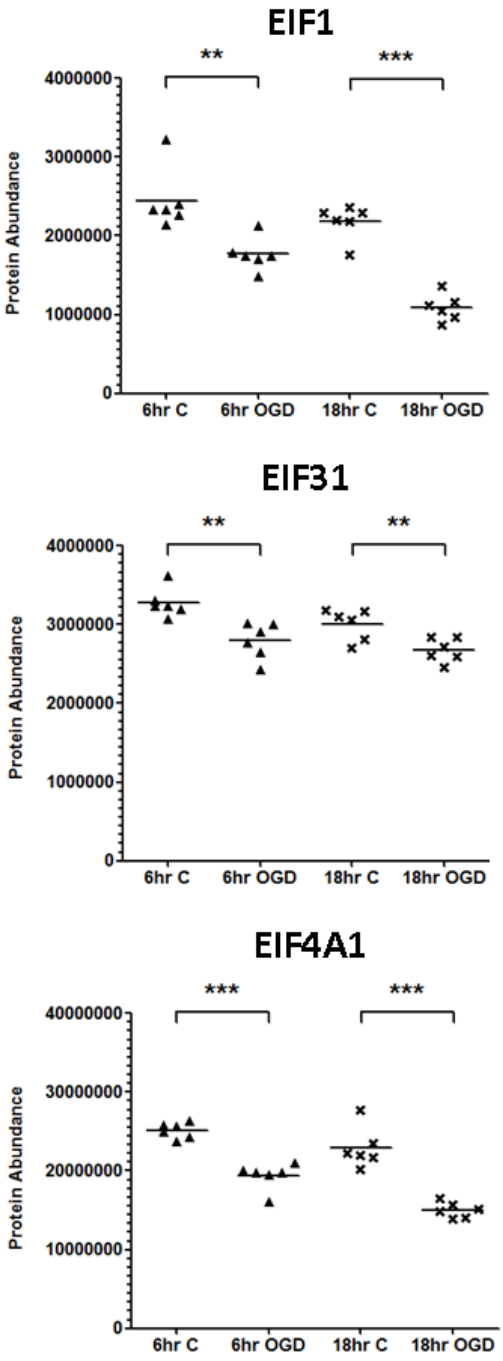

Figure 3.7 Significant regulation of proteins involved in protein synthesis following 6h and 18h OGD. 6h OGD induces significant decreases in abundance of eukaryotic translation initiation factors EIF1, EIF31 and EIF4A1. These decreases remain following 18h OGD. (** $p < 0.01$ *** $p < 0.0001$, T-test, n = 6 in each condition)

Table 3.3: Proteins Significantly Increased with 18h OGD

Uniprot Accn No.	Gene Name	Protein Name	p-value	Fold change	Protein Function
MITOCHONDRIA:					
P30048	PRDX3	Peroxiredoxin III	0.0006	1.57	Cell redox homeostasis
P61604	HSPE1	10kDa Heat Shock Protein	6.1E-06	1.51	Stress response
P18859	ATP5J	ATP synthase-coupling factor 6	0.0016	1.44	ETC complex V
O75489	NDUFS3	NADH-ubiquinone oxidoreductase 30kDa subunit	0.0030	1.38	ETC complex I
P24752	ACAT1	Acetyl-CoA acetyltransferase	9.1E-05	1.38	Ketone body metabolism
P09622	DLD	Dihydrolipoyl dehydrogenase	0.0051	1.36	Gycine cleavage
Q9UJZ1	STOML2	Stomatin-like protein 2	0.0052	1.36	Receptor binding
P09972	ALDOC	Fructose-bisphosphare aldolase C	0.0061	1.34	Glycolysis
P38606	ATP6V1A	V-type proton ATPase catalytic subunit A	0.0067	1.33	ATP hydrolysis transport
P13804	ETFA	Electron transfer flavoprotein subunit alpha	0.0005	1.33	Respiratory ETC
P30084	ECHS1	Enoyl-CoA hydratase	0.0043	1.33	Fatty acid metabolism
P40926	MDH2	Malate dehydrogenase	0.0009	1.32	Citric acid cycle
P10809	HSPD1	60kDa Heat Shock Protein	0.0012	1.31	Protein folding
P62258	YWHAE	14-3-3 protein epsilon	0.0056	1.30	Apoptosis
P04181	OAT	Orthinine aminotransferase	0.0012	1.30	Amino acid biosynthesis
Q13011	ECH1	Delta (3,5)-delta(2,4)-dienoyl-CoA isomerase	0.0048	1.28	Lipid metabolism
Q99714	HSD17B10	3-hydroxyacyl-CoA dehydrogenase type 2	0.0037	1.27	Lipid metabolism
P07954	FH	Fumarate hydratase	0.0038	1.27	Citric acid cycle
P30044	PRDX5	Peroxiredoxin 5	0.0014	1.26	Redox homeostasis
P42765	ACAA2	3-ketoacyl-CoA thiolase	0.0067	1.26	Lipid metabolism
P25325	MPST	3-mercaptopyruvate sulfurtransferase	0.0012	1.25	Response to Toxins
P30086	PEBP1	Phosphatidylethanolamine binding protein 1	0.0067	1.24	Protease inhibition
P25705	ATP5A1	ATP synthase subunit alpha	0.0019	1.21	ETC complex V
Q06830	PRDX1	Peroxiredoxin 1	0.0009	1.20	Redox Homeostasis
P43686	PSMC4	26S protease regulatory subunit 6B	0.0007	1.20	Protein degradation
Q16718	NDUFA5	NADH-ubiquinone oxidoreductase 13kDa subunit	0.0022	1.20	ETC complex I
O00154	ACOT7	Cytosolic acyl-coenzyme A thioester hydrolase	0.0009	1.19	Acyl-CoA hydrolysis
Q00610	CLTC	Clathrin heavy chain 1	4.9E-05	1.16	Endocytosis
P12277	CKB	Creatine Kinase B type	0.0027	1.16	Creatine metabolism
ENDOPLASMIC RETICULUM:					
O60568	PLOD3	Procollagen-lysine 2-oxoglutarate 5-dioxygenase 3	7.7E-05	1.87	Lysyl hydroxylation
P27797	CALR	Calreticulin	1.0E-07	1.56	Protein folding
P11021	GRP78	Glucose regulated protein 78	3.9E-05	1.53	Protein complex assembly
P14625	GRP94	Glucose regulated protein 94	5.5E-05	1.49	Protein transport
P30101	PDIA3	Protein disulphide isomerase A3	2.7E-05	1.45	Protein folding
Q16799	RTN1	Reticulon 1	0.0055	1.41	Neuron differentiation
Q8NBS9	TXNDC5	Thioredoxin-domain containing protein 5	0.0017	1.40	Cell redox homeostasis
P13667	PDIA4	Protein disulphide isomerase A4	1.4E-05	1.38	Cell redox homeostasis
Q9Y2B0	CNPY2	Protein canopy homolog 2	0.0051	1.38	Protein binding
Q15084	PDIA6	Protein disulfide isomerase A6	6.1E-06	1.37	Chaperone
P54920	NAPA	Alpha soluble NSF attachment protein	0.0003	1.35	ER-golgi vesicle transport
P14314	PRKCSH	Glucosidase 2 subunit beta	0.0016	1.33	Glycoprotein formation
Q9NQC3	RTN4	Reticulon 4	0.0033	1.32	Neurogenesis / apoptosis
Q14697	GANAB	Neutral alpha-glucosidase AB/GNAB protein	0.0018	1.27	Glycoprotein cleavage
P07237	P4HB	Protein disulfide-isomerase	0.0073	1.25	Redox homeostasis
Q9BS26	ERP44	Endoplasmic reticulum resident protein 44	0.0007	1.23	ER stress response
Q9NYU2	UGGT1	UDP-glucose:glycoprotein glucosyltransferase 1	0.0074	1.23	ER protein folding

P30040	ERP29	Endoplasmic reticulum resident protein 29	0.0003	1.23	ER protein folding
P55072	VCP	Valosin-containing protein	0.0069	1.15	ER stress response
RIBOSOMES:					
P69905	HBA1	Haemoglobin subunit alpha	0.0003	1.97	O_2 transport
VESICLE:					
O15240	VGF	Neurosecretory protein VGF	0.0035	1.39	Cell-cell interactions
P08133	ANXA6	Annexin 6	0.0075	1.18	Ca2+ binding
P21281	ATP6V1B2	V-type proton ATPase subunit B	0.0098	1.16	H+ ion transport
P07900	HSP90AA1	Heat Shock Protein HSP90-alpha	0.0030	1.11	Stress response
Q9BTT0	ANP32E	Acidic leucine-rich nuclear phosphoprotein 32E	0.0034	1.08	Phosphatase inhibitor
CYTOSKELETON:					
P52907	CAPZA1	F-actin capping protein subunit alpha 1	0.0039	1.35	Protein complex assembly
P16949	STMN1	Stathmin	0.0029	1.32	Microtubule disassembly
Q9Y230	RUVBL2	RuvB like 2	0.0037	1.31	Transcription
P47756	CAPZB	F-actin-capping protein subunit beta	3.2E-05	1.25	Protein complex assembly
Q03252	LMNB2	Lamin B2	0.0076	1.24	Cytoskeleton regulation
Q16352	INA	Alpha-internexin	4.9E-05	1.24	Neurogenesis
P07437	TUBB	Tubulin beta chain	0.0016	1.23	Microtubule constituent
P36405	ARL3	ADP-ribosylation factor-like protein 3	0.0071	1.23	Cell Division
P61163	ACTR1A	Alpha centractin	0.0029	1.23	Vesicle mediated transport
Q9UJU6	DBNL	Debrin-like protein	0.0095	1.18	Endocytosis
Q16658	FSCN1	Fascin	0.0018	1.18	Cytoskeleton organisation
P62158	CALM	Calmodulin	0.0059	1.17	Calcium modulation
Q9BZK7	TBL1XR1	F-box like/WD repeat containing protein TBL1XR1	0.0046	1.17	Protein degradation
P49773	HINT1	Histidine triad nucleotide-binding protein 1	0.0002	1.15	Signal transduction
P43487	RANBP1	Ran-specific GTPase-activating protein	0.0029	1.15	Signal transduction
SPLICEOSOME:					
Q07955	SRSF1	Serine/Arginine rich splicing factor 1	1.1E-05	1.42	mRNA splicing
Q01081	U2AF1	Splicing factor U2AF 35kDa subunit	0.0062	1.23	mRNA splicing
Q15029	EFTUD2	116kDa U5 small nuclear ribonucleoprotein	0.0069	1.19	mRNA splicing
PROTEOSOME:					
Q15008	PSMD6	26s proteasome non ATPase regulatory subunit 6	0.0053	1.61	Protein degradation
P17980	PSMC3	26S protease regulatory subunit 6A	0.0071	1.27	Protein degradation
Q13200	PSMD2	26S proteasome non-ATPase regulatory subunit 2	0.0005	1.22	Protein degradation
P54727	RAD23B	UV excision protein RAD23 homolog B	0.0009	1.22	Protein degradation
Q99460	PSMD1	26S proteasome non-ATPase regulatory subunit 1	0.0002	1.18	Protein degradation
O00231	PSMD11	26S proteasome non-ATPase regulatory subunit 11	0.0008	1.18	Protein degradation
P28066	PSMA5	Proteasome subunit alpha type 5	0.0036	1.16	Protein degradation

Table 3.4: Proteins Significantly Decreased with 18h OGD

Uniprot Accn No.	Gene Name	Protein Name	p-value	Fold change	Protein Function
MITOCHONDRIA:					
P21796	VDAC1	Voltage-dependent anion selective channel protein 1	0.0079	0.26	Ion transport
P22695	UQCRC2	Cytochrome b-c1 complex subunit 2	0.0017	0.31	ETC complex III
P31930	UQCRC1	Cytochrome b-c1 complex subunit 1	0.0097	0.46	ETC complex III
Q9NS69	TOM22	Translocase of outer membrane 22kDa subunit	0.0027	0.46	Protein transport
Q9Y3E5	BIT1	Peptidyl-tRNA hydrolase 2	0.0038	0.51	Apoptosis
P02786	TFRC	Transferrin receptor protein 1	0.0002	0.58	Endocytosis
O75534	CSDE1	Cold shock domain containing protein E1	1.0E-06	0.62	Transcription
Q9Y6H1	CHCHD2	Coiled-coil helix–coiled-coil helix domain protein 2	0.0099	0.70	*Unknown*
P11310	ACADM	Medium chain specific acyl-CoA dehydrogenase	0.0084	0.79	Lipid metabolism
ENDOPLASMIC RETICULUM:					
Q81V08	PLD3	Phospholipase D3	0.0016	0.61	Lipid degradation
Q96AG4	LRRC59	Leucine rich repeat-containing protein 59	0.0048	0.64	ER membrane interactions
P13637	ATP1A3	Na+/K+ ATPase alpha (III) subunit	0.0008	0.67	ATP hydrolysis catalyst
P04843	RPN1	Ribophorin 1	0.0094	0.68	Glycosyltransferase activity
RIBOSOMES:					
P63173	RPL38	60s ribosomal protein L38	0.0001	0.65	Protein biosynthesis
P62249	RPS16	40S ribosomal protein S16	7.9E-05	0.70	Protein biosynthesis
P35544	FAU	Ubiquitin-like protein FUB 1	0.0012	0.70	Ubiquitination modulation
P62263	RPS14	40S ribosomal protein S14	0.0004	0.74	Protein biosynthesis
P62829	RPL23	60S ribosomal protein L23	5.3E-05	0.74	Protein biosynthesis
P62266	RPS23	40S ribosomal protein S23	0.0004	0.76	Protein biosynthesis
P46781	RPS9	40S ribosomal protein S9	0.0002	0.78	Protein biosynthesis
P08708	RPS17	40S ribosomal protein S17	0.0004	0.80	Protein biosynthesis
P42766	RPL35	60S ribosomal protein L35	0.0018	0.82	Protein biosynthesis
P26373	RPL13	60S ribosomal protein L13	0.0004	0.84	Protein biosynthesis
VESICLE:					
P07355	ANXA2	Annexin A2	0.0038	0.49	Ca^{2+} binding
P62491	RAB11A	Ras-related protein Rab 11A	0.0026	0.76	Endocytic cycling
P07858	CTSB	Cathepsin B	0.0053	0.85	Protein degradation
CYTOSKELETON:					
P06493	CDK1	Cyclin-dependent kinase 1	0.0022	0.57	Cell cycle control
P28289	TMOD1	Tropomodulin 1	0.0005	0.64	Cytoskeleton organisation
Q01518	CAP1	Adenylyl cyclase-associated protein 1	4.7E-06	0.70	Signal transduction
Q9UQE7	SMC3	Structural maintenance of chromosomes protein 3	0.0084	0.71	Cell cycle
P18206	VCL	Viniculin	0.0067	0.78	Cell adhesion
Q01082	SPTBN1	Spectrin beta chain brain 1	0.0092	0.81	Cytoskeleton movement
SPLICEOSOME:					
P17844	DDX5	Probable ATP-dependent RNA helicase DDX5	2.9E-06	0.58	mRNA processing
Q9UKM9	RALY	RNA-binding protein Raly	0.0014	0.66	mRNA splicing
Q86V81	THOC4	THO complex subunit 4	0.0007	0.75	mRNA splicing
O43143	DHX15	Pre-mRNA splicing factor ATP-dep. RNA helicase	5.5E-06	0.78	mRNA splicing
P07910	HNRNPC	Heterogeneous nuclear ribonucleoproteins C/C2	0.0005	0.81	mRNA splicing

3.3.4 Key Mitochondrial Energy Metabolism Proteins are Significantly Altered following 18h OGD

193 proteins showed significant changes in abundance between control samples and samples treated with 18h OGD. The large number of significantly altered proteins allows functional protein-protein interactions to be defined using IPA software. IPA generated 10 protein interactomes (Appendix C). Three high-scoring interactomes (IPA scores > 40) highlight a shift in mitochondrial energy production, enhanced endoplasmic reticulum stress and ribosomal dysfunction which are discussed in more detail below.

38 mitochondrial proteins (out of 118 detected; assigned using the GO term *mitochondrion* GO:0005739) were significantly altered following OGD (18h): 29 were increased and 9 were decreased. VDAC1 and TOM22, proteins involved in mediating the movement of metabolites across the mitochondrial membrane, were significantly reduced after OGD. UQCRC1 and UQCRC2, integral components of complex III of the electron transport chain (ETC), were also significantly reduced. Coordinated changes in other regions of the ETC were observed after 18h OGD treatment: ETC complex V proteins ATP5J and ATP5A1, and ETC complex I proteins NDUFS3 and NDUFA5 were all significantly increased ($p<0.01$, Figure 3.8). Western blotting of the original samples sent to LC-MS confirmed these detected energy metabolism protein changes (Figure 3.9).

The highest scoring protein interactome generated by IPA features some of the alterations in energy production described above, namely increases in Complex V proteins (including ATP5J and ATP5A1) and decreases in Complex III proteins (UQCRC1 and UQCRC2) (Figure 3.10). This *Energy Production Interactome* also highlights interactions between altered components of the ETC and other cellular machinery. UQCRC1 and UQCRC2 both interact with RTN4, a protein predominantly associated with regulating ER function that is significantly up-

regulated following OGD. UQCRC2 is also shown to interact with up-regulated RUVBL2, a cytoskeletal protein involved in numerous cellular activities including transcription and cellular transformation. The *Energy Production Interactome* also contains a cluster of ribosomal proteins that are distinct but intersect with the ribosomal interactome described below.

Concurrent with the dysregulation of the oxidative phosphorylation pathway outlined above, 18h OGD also induces alterations in mitochondrial proteins involved in lipid and ketone metabolism. Acetyl-CoA acetyltransferase 1 (ACAT1) and 3-hydroxybutyrate dehydrogenase type 2 (BDH), key proteins involved in ketone metabolism, are significantly up-regulated following 18h OGD ($P<0.01$ and $p<0.05$, respectively) (Figure 3.11). The 4 proteins involved in mitochondrial beta-oxidation of fatty acids also showed altered expression profiles following 18h OGD. Acyl-CoA dehydrogenase (ACAD), the enzyme involved in the first step of fatty acid beta-oxidation, was significantly down-regulated , whereas Enoyl CoA hydratase (ECHS1), Hydroxyacyl CoA Dehydrogenase (HSD17B10), and 3-ketoacyl-CoA thiolase (ACAA2) were all significantly increased (Figure 3.11).

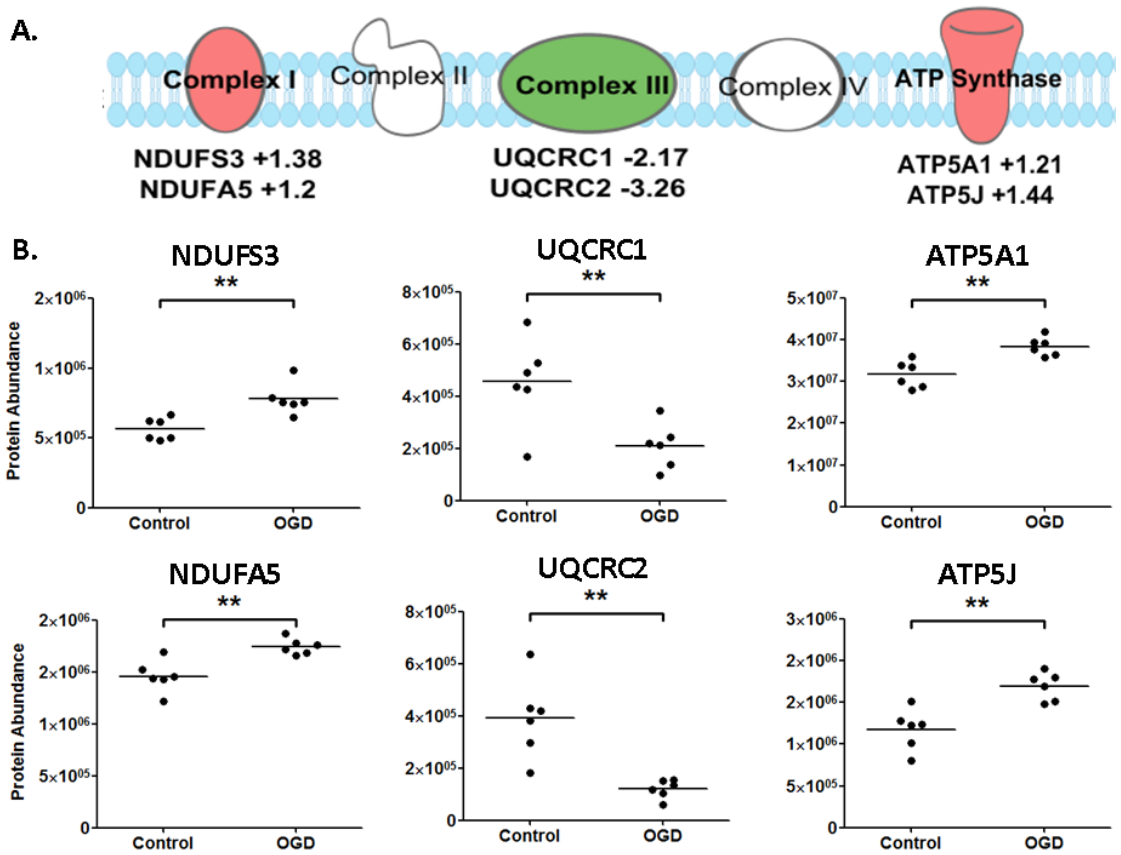

Figure 3.8 Bidirectional changes in the proteins of the electron transport chain (ETC). **A.** 18h OGD causes significant increases in complex 1 (NDUFS3 and NDUFA5) and complex 5 (ATP5A1 and ATP5J) proteins, with concurrent decreases in complex III proteins UQCRC1 and UQCRC2. **B.** Scatter plots of the protein changes detected by LC-MS between control and OGD (18h). Each data point represents an independent sample with the mean abundance line shown. (** $p<0.01$, T-test, n = 6 in each condition)

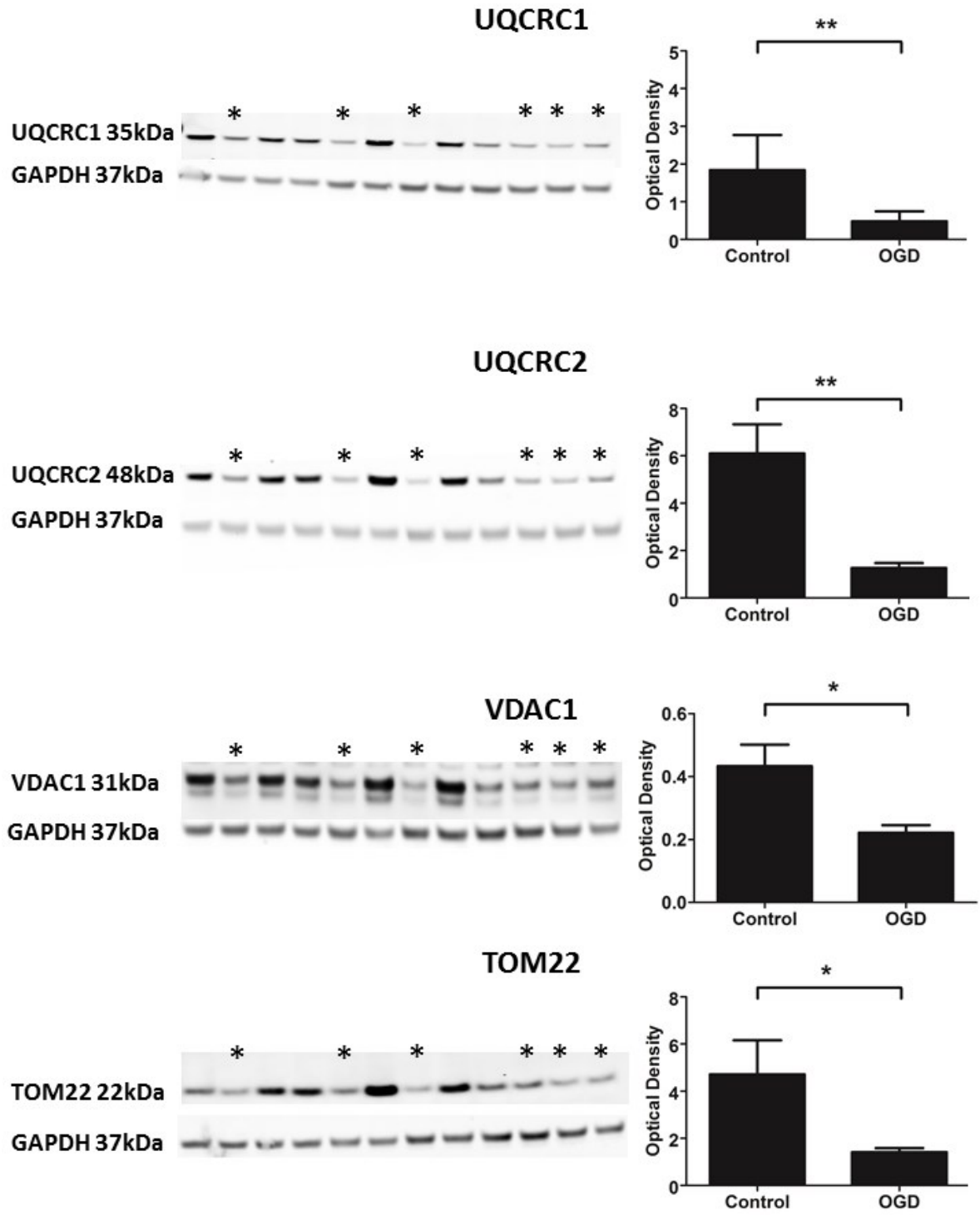

Figure 3.9 Western Blot confirmation of selected LC-MS detected protein changes associated with energy production and metabolic stress. UQCRC1, UQCRC2, VDAC1 and TOM22 are all detected by LC-MS as significantly down-regulated following 18h OGD. Western blotting of the original samples sent for LC-MS analysis confirms these results with an independent experimental technique. (* above western blots indicate OGD samples. On the bar graphs, * $p<0.05$, ** = $p<0.01$, T-test, n = 6 in each condition).

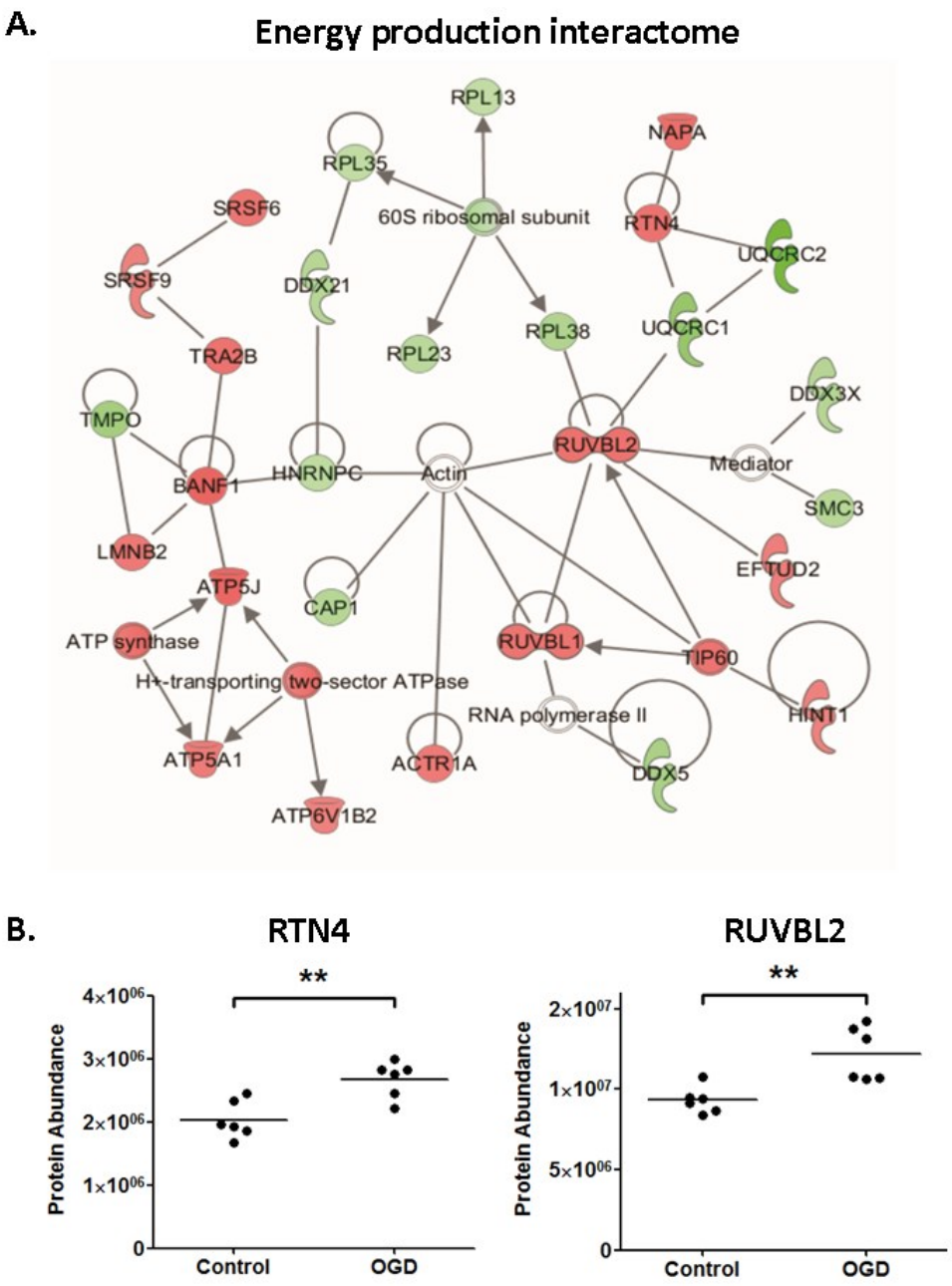

Figure 3.10 Energy Production Interactome. A. One of the highest scoring Ingenuity Pathway Analysis (IPA) networks gained from the 18hr OGD proteomic data set is presented. The network contains numerous proteins involved in mitochondrial energy production. The coloured nodes indicate proteins detected in our study as significantly altered by OGD. Red nodes are up-regulated proteins, green nodes are down-regulated. Un-shaded nodes were manually inserted by IPA to augment functional coherence. Only direct protein – protein interactions were included in the analysis. **B.** Complex III subunits 1 and 2 (UQCRC1 / UQCRC2) interact with RTN4 and RUVBL2, both are significantly up-regulated with OGD (18h). (** = $p<0.01$, T-test, n = 6 in each condition)

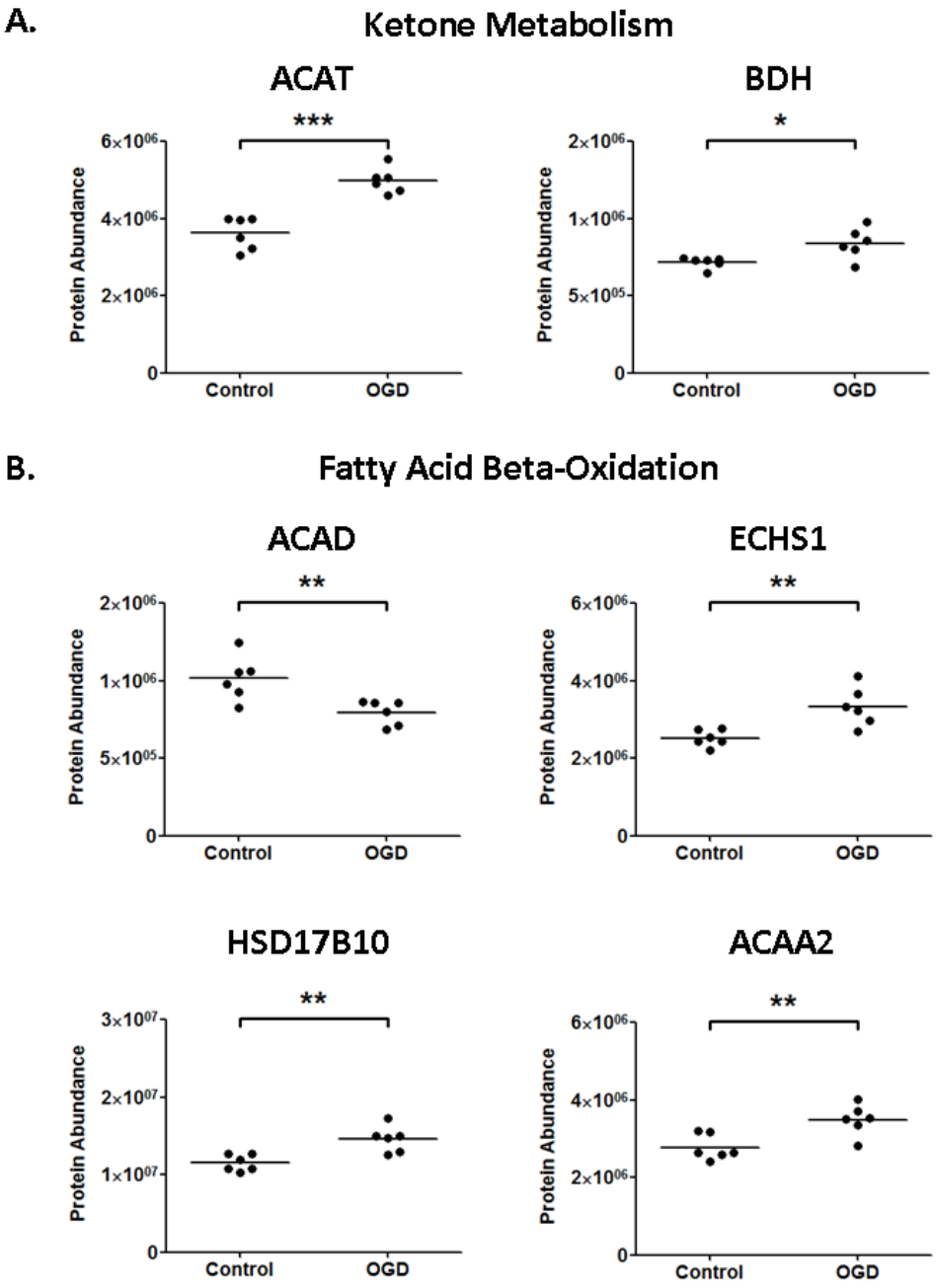

Figure 3.11 Ketone metabolism and fatty acid beta-oxidation proteins are significantly altered by OGD. A. Key proteins involved in ketone metabolism (ACAT and BDH) are significantly up-regulated in SH-SY5Y cells challenged with OGD (18h). **B.** ACAD, the first protein in the process of beta-oxidation of fatty acids, is significantly decreased following OGD (18h). The subsequent three proteins (ECHS1, HSD17B10 & ACAA2) are all increased. (*** $p<0.0001$, ** $p<0.01$, * $p<0.05$, T-test, n = 6 in each condition)

3.3.5 Protein Homeostasis Pathways are Significantly Altered following 18h OGD

23 ER proteins (out of 56 detected; assigned using the GO term *Endoplasmic reticulum* GO:0005783) were significantly altered following 18h OGD: 19 were increased and 4 were decreased. A number of proteins centrally involved in the UPR were significantly increased, including, GRP78 (aka BiP / HSPA5), GRP94 (aka HSP90B1), PDIA3 and PDIA4 ($p<0.01$) (Figure 3.12). Western blotting confirmed the significant up-regulation of GRP78 and GRP94 (Figure 3.13). Other proteins including CALR, UGGT1, ERP29, ERP44 and VCP that are integral to ER stress response and protein folding were significantly increased.

Multiple proteins that play a role in protein degradation were significantly altered following OGD (18h). Protein subunits of the 20S and 19S core structures of the 26S proteasome (PSMA5, PSMC3, PSMC4, PSMD1, PSMD2, PSMD6 and PSMD11) were increased. These proteasomal proteins, along with proteins involved in the UPR and heat shock response following OGD dominate the high scoring, *Protein Folding and Degradation Interactome* generated by IPA (Figure 3.12).

3.3.6 Ribosomal Protein Alterations are Detected following 18h OGD

11 ribosomal proteins (out of 82 detected; assigned using the GO term *Ribosome* GO:0005840) were significantly altered following 18h OGD: 1 was increased and 10 were decreased. The decreased ribosomal proteins were associated with both the 60S (RPL38, RPL23, RPL35 and RPL13) and 40S (RPS1, RPS14, RPS23, RPS9 and RPS17) ribosomal subunits (Figure 3.14). These down-regulated ribosomal proteins feature prominently in another of the high scoring energy production protein interactome generated by IPA (Figure 3.10). An additionally important feature of this *Ribosomal Interactome* is the cluster of up-regulated peroxidases (PRDX1, PRDX2 and PRDX5) (Figure 3.14) involved in redox homeostasis and protecting neurons from oxidative insults. For a review see (Bell and Hardingham, 2011).

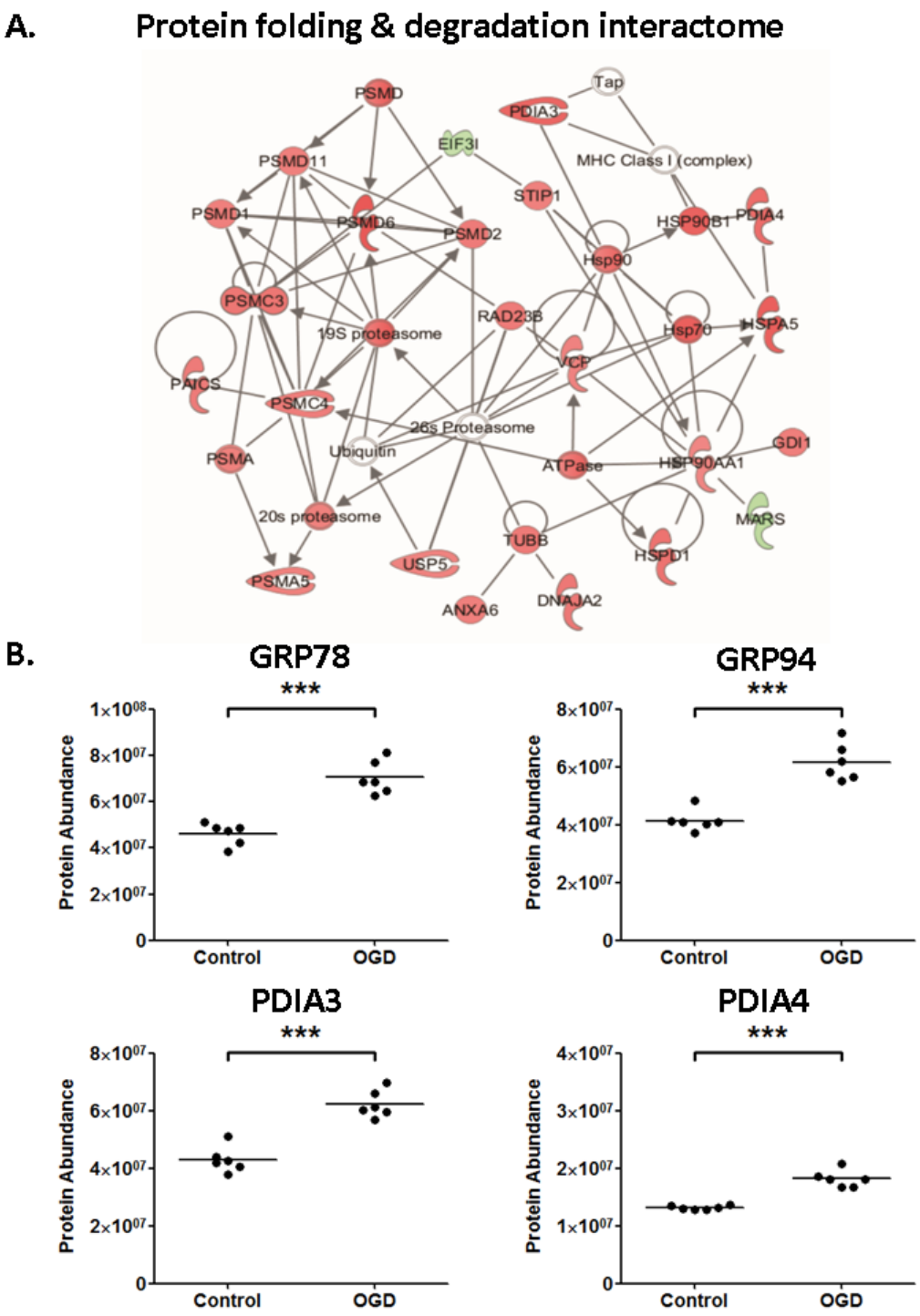

Figure 3.12 Protein folding and degradation interactome. **A.** A high scoring Ingenuity Pathway Analysis (IPA) network generated from the 18hr OGD proteomic data contained proteins involved in protein folding and degradation. **B.** Key proteins involved in protein folding and the endoplasmic reticulum stress response (GRP78 / GRP94 / PDIA3 / PDIA4) are significantly altered by OGD (18h). Each data point represents an independent sample (*** $p<0.0001$, T-test, n = 6 in each condition)

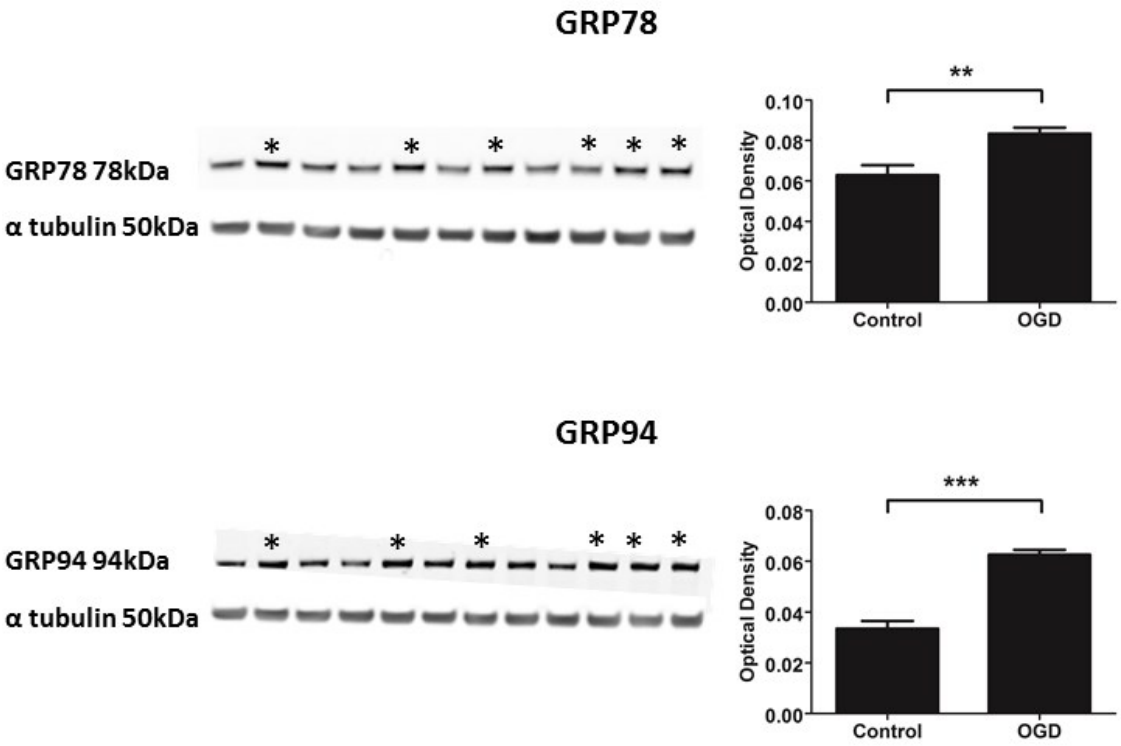

Figure 3.13 Western Blot Confirmation of selected LC-MS detected protein changes associated with protein folding and ER stress. GRP78 and GRP94 are detected by LC-MS as significantly up-regulated following 18h OGD. Western blotting of the original samples sent for LC-MS analysis confirms these results with an independent experimental technique (* above western blots indicate OGD samples. On the bar graphs, ** $p<0.01$, *** $p<0.0001$, T-test, n = 6 in each condition).

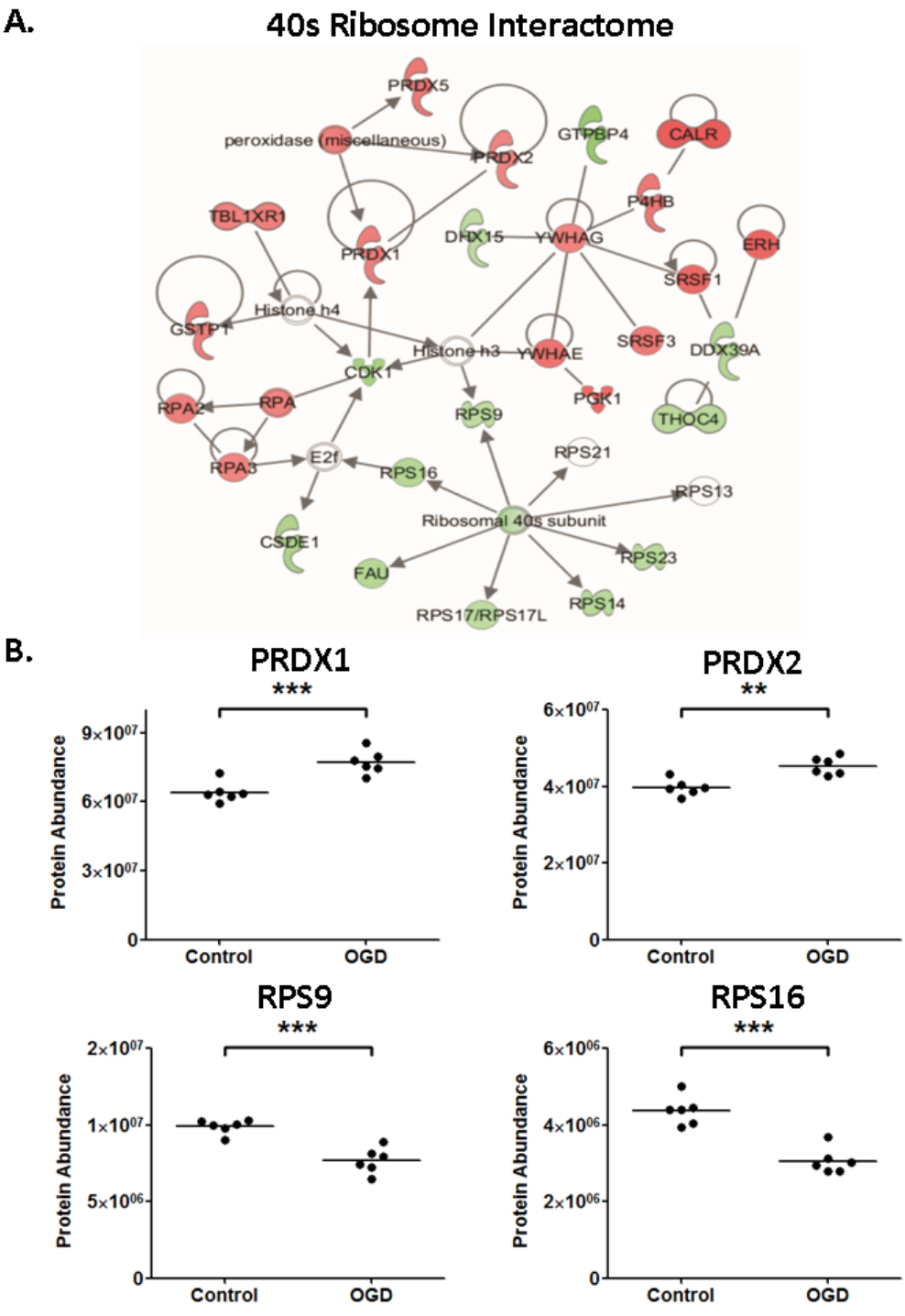

Figure 3.14 40S Ribosome Interactome. A. A further high scoring IPA network was dominated by the down-regulation of 40S ribosomal proteins and cell stress response proteins. **B.** Representative ribosomal proteins (RPS9 / RPS16) and the cellular stress response proteins (PRDX1 / PRDX2) are significantly altered by OGD (18h). Each data point represents an independent sample (** $p<0.01$, *** $p<0.0001$, T-test, n = 6 in each condition)

3.4 Discussion

In the present study, undifferentiated SH-SY5Y cells were exposed to OGD and the proteomic changes underpinning mitochondrial dysfunction were examined. The absence of pilot data, and thus the unknown coefficient of variance associated with the proteomic set up, limited the utility of *a priori* power analysis in determining an appropriate detectable fold change cut-off for this study. A stringent p-value of $p<0.01$ was therefore chosen to reduce the risk of detection of false positives within the proteomic data. At present there is no accepted standard for identifying and reporting significant changes within the proteomic literature, with a range of p-value and fold change cut-offs employed to detect important and relevant protein responses (Andreev et al., 2012, James et al., 2012b, Wishart et al., 2012, Liao et al., 2004). The need for careful experimental design in proteomic research is discussed in more detail in Section 6.

The present study showed SH-SY5Y cells to be exceptionally robust under conditions of metabolic stress. The light microscopy and trypan blue assays show that despite significant reductions in mitochondrial function, there was little evidence of a global cell death response. This robust nature of SH-SY5Y cells demonstrated in the initial characterisation phase allowed the evolving proteomic changes occurring in response to OGD induced metabolic stress to be defined, in the absence of cell death. Further work, including the inclusion of positive control experiments, as well as additional characterisation of the cellular response to OGD (for example, recording changes in mitochondrial membrane potential, or measuring the rate of reactive oxygen species production) would provide a more complete insight as to the cellular response to metabolic stress.

Protein synthesis machinery is regulated following a moderate metabolic challenge (6h OGD)

6h OGD exposure induced moderate mitochondrial dysfunction in the SH-SY5Y cells compared to time matched controls. However, despite the significant reduction in mitochondrial function, LC-MS proteomics detected only minimal protein changes, with only 14 proteins significantly altered in expression level ($p<0.01$). Within the list of nearly 1000 detected proteins, approximately 10 proteins would be expected to be altered by chance alone at a significance level of $p<0.01$. However, cautious inspection of the 14 significantly altered proteins identified eukaryotic initiation factors EIF1, EIF4A1 and EIF3I all to be significantly down-regulated following 6h OGD. These proteins remain down – regulated to a similar or greater extent at 18h OGD treatment, suggesting a functional relevance at 6h OGD.

Eukaryotic translation initiation factors (EIFs) are involved in the assembly of ribosomal complexes. EIF1 has been shown to promote an open conformation of the ribosomal complex that then scans the mRNA sequence in search of the start codon. Once the start codon has been recognised, EIF1 is released, and the ribosome stabilises around the mRNA, allowing translation to begin (Passmore et al., 2007). The significant down regulation of the EIFs following 6h OGD may be an initial attempt by the cell to conserve energy through disruption of the protein synthesis processes.

However, following 18h OGD, of the 193 significantly altered proteins, 130 of these were significantly up-regulated. This data suggests that key proteins needed to respond to metabolic stress are still being translated, despite the decreased levels of EIFs in the earlier stages of OGD. Significant decreases in the ribosomal machinery itself are detected following 18h OGD (discussed later in this section). It is therefore possible that these early decreases in EIFs might be

indicative of later ribosomal and cellular dysfunction. Further work using EIF overexpression and knockdown would be useful in determining the full effect of EIF dysregulation on cellular function.

Significant mitochondrial protein changes accompany the decrease in mitochondrial function under conditions of severe metabolic stress (18h OGD)

Concurrent with the large reduction in mitochondrial function and the mitochondrial swelling observed with EM, the proteomic data showed many significant changes in mitochondrial proteins following at 18h OGD. Two of the most markedly decreased proteins following 18h OGD were subunits 1 and 2 (UQCRC1 and UQCRC2) of ETC complex III, a result confirmed by western blot analysis. Complex III is the third component of the ETC located within the inner mitochondrial membrane. Complex III mediates the transfer of electrons from ubiquinone to cytochrome C, and in doing so translocates a proton into the inner-membrane space and contributes to the generation of the electrochemical gradient used for the production of ATP (Iwata et al., 1998). Down-regulation of the complex III subunits might therefore be a proteomic correlate of the mitochondrial dysfunction recorded with the MTS assay.

Complex III is also intrinsically involved in the generation of reactive oxygen species (ROS) from the mitochondria during hypoxia, which can be highly damaging to the cellular architecture if antioxidant systems become overwhelmed (Guzy et al., 2005). A significant decrease in UQCRC1 and UQCRC2 might therefore be an attempt by the cells to reduce the production of ROS from the mitochondria under these metabolically stressful conditions. Interestingly, UQCRC1 has also been recorded as significantly decreased in the brains of AD patients (Kim et al., 2000). The similar decrease in UQCRC1 expression observed in AD patients and cells *in vitro* following OGD may provide a link between chronic oxidative challenge and the onset and progression of AD.

The *Energy Production Interactome* (Figure 3.10) also highlights putative functional protein-protein interactions between UQCRC1, UQCRC2 and reticulon 4 (RTN4, a protein increased following 18h OGD). RTN4 is increased in hippocampal neurons of AD patients(Gil et al., 2006) and is known to interact with BACE1, reducing Aβ40 and Aβ42 levels(Murayama et al., 2006). The dysregulation of RTN4 following a metabolic challenge (18h OGD), its interaction with complex III proteins, and its potential role in APP processing, highlights RTN4 as a compelling target for future investigation.

Mitochondrial complex I and V proteins were significantly increased in expression after OGD in sharp contrast to the reduction in complex III proteins. Complex I is the first protein complex of the ETC, and initiates the transfer of electrons through the ETC, generating the energy required for oxidative phosphorylation. The process is initiated through binding and oxidation of NADH, with the concurrent transfer of 2 electrons from NADH to ubiquinone, and the translocation of 4 protons into the intermembrane space (Janssen et al., 2006). An increase in Complex I proteins following OGD may reflect a compensatory mechanism to counteract the impact of decreased complex III proteins on energy production. Similarly, the increase in Complex V proteins may reflect a compensation for down-regulated Complex III proteins or a general remodelling of the ETC, as has previously been shown in studies investigating ischemic preconditioning (Arrell et al., 2006). Functional assays of the five complexes that constitute the ETC, in ischemic conditions will need to be carried out to confirm whether such remodelling occurs. Furthermore, determining the regulatory mechanisms of these protein changes could provide valuable insight that would allow therapeutic intervention to alter the course of mitochondrial dysfunction following OGD and metabolic challenges *in vivo*.

Changes in lipid and ketone metabolism proteins indicate a possible shift in energy processes under conditions of severe metabolic stress (18h OGD)

In addition to the proteomic changes occurring in the mitochondrial electron transport chain, the metabolic challenge of 18h OGD induced changes in abundance of mitochondrial proteins associated with lipid and ketone metabolism. The changes in these proteins (ACAT1 in ketone metabolism, and ACADM, ECH1, HSD17B10 and ACAA2 in lipid metabolism) indicate a shift towards utilising lipid and ketone bodies as alternative sources of energy for SH-SY5Y cells faced with glucose restriction.

The availability of alternative cerebral energy sources is likely to be important in preventing cells hitting the point where energy provision is insufficient for cell survival, described by De la Torre as the *Critically Attained Threshold of Cerebral Hypoperfusion,* (CATCH) (de la Torre, 2000). CATCH is the point at which brain circulation is impaired to an extent where oxygen, glucose and other nutrients are delivered sub-optimally to neurons, leading to a downward spiral of metabolic and cognitive decline, with the accompanying pathology associated with AD. If alternative energy sources such as ketones could be utilised by neurons, it is feasible that CATCH could be avoided, and that restoration of neuronal metabolism to a level which meets the energy requirements of these cells might be achieved.

The potential therapeutic role for ketones in neurodegenerative diseases is beginning to be investigated. In AD, accumulation of amyloid fragment AB_{1-42} is toxic to neurons, especially to those associated with learning and memory formation within the hippocampus. *In vitro* work has shown ketone body d-B-hydroxybutyrate to be neuroprotective to hippocampal neurons exposed to Aβ42 in culture (Kashiwaya et al., 2000). The basis of this protection is unclear, however, it may be linked to the finding that Aβ 1-42 induces phosphorylation

of pyruvate dehydrogenase (PDH), causing PDH inhibition and a block in the early stages of the citric acid cycle (Hoshi et al., 1997). Ketones have the ability to bypass blocks in the citric acid cycle, ensuring a continuation of NADH production for oxidative phosphorylation.

In addition, recent studies using the triple transgenic mouse model of AD demonstrated that induction of ketogenesis through use of a 2-deoxy-D-glucose diet increased levels of ketone metabolizing enzymes, activated non-amyloidogenic APP processing pathways, reduced Aβ pathology and reduced oxidative stress (Yao et al., 2011). Our results show that under metabolic challenge cells up regulate proteins associated with ketone metabolism, potentially in an attempt to source alternative energy supplies when faced with long term OGD. When taken with the other ketone related experimental findings discussed here, it is clear that ketones and ketone metabolism provide an attractive avenue for further work in efforts to overcome the neuronal energy crisis in AD, both as an alternative energy source when glucose delivery is impeded by CCH, and also as a potential novel neuroprotectant.

To utilise ketones as an alternative energy source in the brain, acetoacetate and b-hydroxybutyrate (the main ketone bodies used for energy) need to be synthesised from acetyl-coA. Acetyl-coA is released following beta-oxidation of fatty acids, a four step process within the mitochondrial matrix requiring beta-oxidation enzymes at each stage (namely, ACAD, ECH1, HSD17B10 and ACAA2). Each of these beta-oxidation enzymes, as noted above, was significantly altered following 18h OGD. What is observed in the beta-oxidation protein changes is that Acyl CoA Dehydrogenase (ACAD, the first protein in the enzyme chain) is down-regulated following 18h OGD. The 3 following proteins are up-regulated, in what may be construed as a compensatory up-regulation profile. Why the cells might benefit from a down-regulation of ACAD at the front end of the beta-oxidation pathway, when production of acetyl coA for ketogenesis would appear to be a good option for an alternative energy source, remains to be elucidated.

Of note, the third beta-oxidative enzyme HSD17B10 (also known as amyloid binding alcohol dehydrogenase, ABAD), was significantly up-regulated following OGD. ABAD is emerging as an important player in AD, shown to directly interact with Aβ in the mitochondria of AD patients and AD transgenic mouse models. Inhibition of the ABAD-Aβ interaction suppresses induced apoptosis by increasing levels of Aβ, and conversely overexpression of ABAD in transgenic mice with high levels of Aβ has been shown to cause heightened neuronal oxidative stress and memory impairments (Lustbader et al., 2004). The direct involvement of ABAD in AD pathophysiology makes ABAD a very interesting candidate to investigate further in terms of its up-regulation upon metabolic challenge.

Beta-oxidation of fatty acids is a process traditionally recognised to occur in the liver, with subsequent delivery of these ketone bodies to the brain. Here it is demonstrated that the SH-SY5Y neuroblastoma cell line express the enzymes needed for beta-oxidation, indicating a capability of these neuronal cells to bypass the liver and carry out beta-oxidation of fatty acids to produce ketones themselves. If this were to be the case, the source of fatty acids for beta-oxidation from within the cell line needs to be established.

Fatty acids are stored in dynamic organelles called lipid droplets within cells. Lipid droplets rapidly form when there are increased levels of free fatty acids, in a process involving budding from the endoplasmic reticulum membrane (Martin and Parton, 2006). During nutrient shortages it is known that cellular lipids stored within lipid droplets are hydrolysed to fatty acids for energy supply. EM analysis showed lipid droplets to be present in SH-SY5Y cells under both control and OGD conditions, suggesting lipid droplets to potentially serve as an alternative energy source in this cell line.

Lipid droplets are also a main site of cholesterol storage, and are involved in the regulation of the amount of free cholesterol within the cell (Martin and Parton, 2006). Cholesterol has been shown to influence the processing of APP. *In vivo* work showed that rabbits fed with 1% cholesterol have increased BACE1 levels (Ghribi et al., 2006). It might therefore be hypothesised that lipid droplets, and their role in cholesterol homeostasis, might influence Aβ generation in AD. Indeed, ultra-structural examination of AD tissue identified the number of lipid droplets to be higher in neurons positive for Aβ than in neurons with little Aβ immunoreactivity (Gomez-Ramos and Asuncion Moran, 2007). The specific role of the lipid droplets within the SH-SY5Y cells examined in this study remains to be elucidated. However, the storage of lipids within these droplet structures, and their role in cholesterol homeostasis may provide important insight into part of the cellular changes in AD.

Another cellular tactic to obtain energy substrates during an energy crisis is to induce autophagy, where proteins and organelles are broken down in lysosomes to obtain free energy (Zechner and Madeo, 2009). Recent work investigating both lipid droplets and autophagy showed a complex interplay between the two components, termed macrolipophagy. Inhibition of autophagy in *in vitro* hepatocyte cells caused increased fat storage in lipid droplets, and lipid droplet structural proteins were demonstrated to be co-localised with autophagic compartments (Singh et al., 2009).

If SH-SY5Y cells are capable of beta-oxidation of fatty acids to produce the excess acetyl coA needed for ketogenesis, it is possible that macrolipophagy might be the source of fatty acids to drive this process. The case for the prediction of an involvement of autophagy in lipid metabolism being involved in the response of cells to OGD is strengthened by the fact that endoplasmic reticulum stress triggers autophagy (Yorimitsu et al., 2006), discussed in more detail below. Electron microscopy images reveal the presence of lipid droplets and autophagosomes in the majority of SH-SY5Y cells. Coupled to the

compelling proteomic changes associated with lipid and fatty acid metabolism, there is evidence for a switch to alternative energy metabolism in SH-SY5Y cells in response to oxygen – glucose deprivation.

Key mitochondrial pore forming proteins are significantly decreased under conditions of severe metabolic stress (18h OGD)

Key pore forming proteins VDAC1 and TOM22 were significantly down-regulated following OGD, a result confirmed by western blot analysis. VDAC proteins are located in the outer mitochondrial membrane and form a pore for the movement of substances in and out of the mitochondria. Studies using liposomes carrying the VDAC channel proteins show VDAC channels to be targeted by pro-apoptotic Bax and Bak, causing the channel to open and allowing the passage of pro-apoptotic cytochrome c (Shimizu et al., 1999). It may therefore be hypothesised that the significant down-regulation of VDAC1 following 18h OGD may be an apoptosis aversion mechanism, reducing the availability of VDAC to bind Bax and Bak, and averting the release of cytochrome c.

TOM22 is another mitochondrial pore forming proteins that is significantly decreased following 18h OGD treatment. A recent study utilising a bacterial two-hybrid assay identified TOM22 to be a mitochondrial receptor of pro-apoptotic BAX. Moreover, antisense knock-down of TOM22 expression inhibited the BAX – mitochondrion association and prevented apoptosis (Bellot et al., 2007). It might therefore be hypothesised that the significant down-regulation on TOM22 in the 18hr OGD model is an attempt by the cells to avoid the initiation of BAX mediated apoptosis. This hypothesis is supported by the lack of cell death observed by the trypan blue assay following 18h OGD. However, further work investigating the specific associations of BAX and TOM22 under both control and OGD conditions, as well as specific measure of apoptosis induction would need to be carried out in order to fully test this hypothesis.

ER stress response proteins are central to the response of SH-SY5Y cells to severe metabolic stress (18h OGD)

A major proteomic response in the endoplasmic reticulum was identified following OGD. The ER stress response (also known as the unfolded protein response, UPR) is a cellular reaction activated to clear misfolded proteins that accumulate in the ER under conditions of cell stress, thus returning the cell to a state of proteostasis(Scheper et al., 2011). Two central molecular chaperones, GRP78 and GRP94, involved in the early and late stages of the UPR respectively were up-regulated following OGD in SH-SY5Y cells (as well as numerous other UPR proteins and ER stress proteins) (Figure 3.12 – 3.13). These data are consistent with recent results from OGD in mixed primary cortical cultures where increases in both GRP78 and GRP94 were also detected (Badiola et al., 2011).

The induction of the UPR in response to OGD was also implied in the electron microscopic data. The ER demonstrated a progressive morphologic swelling that significantly increased after longer durations of OGD exposure compared to time-matched controls. An expanded ER forms an important part of the UPR as it enables larger numbers of misfolded proteins to be incorporated within the ER membrane, thus increasing cellular capacity to deal with abundant protein damage (Schuck et al., 2009). A larger ER volume also reduces the concentration of protein intermediates, therefore reducing the risk of protein aggregate formation(Apetri and Horwich, 2008). The morphological observation of enlarged ER, along with the significant increase in UPR proteins GRP78 and GRP94 detected in this proteomic data provide telling insights into how the human neuronal cells respond to the metabolic challenge of OGD.

There is emerging evidence that levels of the proteins centrally involved in the UPR are adversely affected with increasing age. In the cerebral cortex of aged C57 / B6 mice, a 30% decrease in GRP78 was recorded when compared to young (3 month) old mice (Naidoo et al., 2008). The present study demonstrates increases in UPR proteins to be centrally involved in the cellular response to a metabolic challenge. It is therefore feasible to hypothesise that if the levels of these UPR proteins are declining with age, then neurons will be less capable of coping with a metabolic challenge such as the decrease in oxygen and glucose delivery to the brain, as experienced during chronic cerebral hypoperfusion. This may therefore lead to suboptimal activation of the UPR process, resulting in the accumulation of misfolded proteins, as seen in neurodegenerative diseases such as AD.

In addition to the protein folding and repair function of GRP78 (aka BiP) discussed here, this protein also plays a role at the mitochondrial associated membrane (MAM). The MAM is a specialised membrane region between the mitochondria and the endoplasmic reticulum, thought to mediate ER – mitochondrial calcium signalling (Rizzuto et al., 2012). GRP78, along with calreticulin (another ER chaperone), are both found enriched at the MAM, and are also both significantly up-regulated following 18h OGD. The role for these proteins at the MAM, due to their ability to bind Ca^{2+}, is to serve as a high capacity Ca^{2+} binding store. This ensures ample Ca^{2+} is present in pools at the MAM, ready for transfer to the mitochondria (Hayashi et al., 2009).

The significant increase in GRP78 and calreticulin following OGD may therefore be indicative of increased Ca^{2+} release from the ER to the mitochondria under conditions of metabolic stress. The increased release of Ca^{2+} would deplete the Ca^{2+} pools, therefore more GRP78 and calreticulin is needed to restore the high Ca^{2+} concentrations at the MAM. Interestingly, VDAC1, the MAM protein responsible for Ca^{2+} uptake to the mitochondria, is significantly down-regulated with 18h OGD. Conversely, GRP75, the MAM protein tethering IP3R and VDAC1

is unchanged with OGD treatment. Further work needs to be carried out in order to reconcile the apparently inconsistent protein changes occurring at the MAM under conditions of metabolic stress. Despite the apparently incongruent protein changes detected at the MAM, the present study clearly shows that this specialised membrane region between the ER and the mitochondria may play an important role in the cellular response to metabolic stress.

The importance of the described protein changes at the MAM in relation to metabolic stress, and possibly AD, is enhanced by the recent identification of presenilin proteins at this specialised membrane region. Experimental evidence shows that mutations in presenilin genes, akin to those seen in early onset AD, cause presenilin to interact with IP3R, stimulating excess calcium release from the ER (Cheung et al., 2008).

In accord with activation of the UPR, an up-regulation of numerous proteins involved in proteasomal degradation was highlighted by the *Protein Folding and Degradation Interactome*. Proteins of the 20S and 19S (core and regulatory) subunits that constitute the 26S proteasome were increased, suggesting 26S proteasomal degradation to be a fundamental mechanism for degrading the misfolded proteins that accumulate in response to metabolic challenge. There is a long-standing hypothesis that protein aggregates in the diseased brain impair the protein degradation function of the 26S proteasome (Taylor et al., 2002, Ciechanover and Brundin, 2003, Valera et al., 2005). The proteomic data presented here demonstrates proteasomal proteins to be up-regulated following a metabolic challenge. It is therefore possible to hypothesize that any proteasomal response to metabolic challenge might be adversely affected in the presence of protein aggregates associated with neurodegenerative diseases, such as AD. In this situation, the cellular capacity to cope with metabolic stress would be impaired, potentially leading to deterioration in cellular function.

Decreases in ribosomal proteins suggest a decrease in protein translation under conditions of severe metabolic stress (18h OGD)

A coordinated response following 18h OGD was also observed in the ribosomal proteome. Numerous ribosomal proteins that constitute the core ribosomal machinery were down-regulated, and in line with this, several eukaryotic initiation factors central to protein synthesis were also decreased. It is well established that cells undergoing severe metabolic stress experience a down-regulation of protein translation, which can be reversible in more resistant brain areas, and irreversible in vulnerable regions (Paschen et al., 2003). Further work involving a recovery phase would need to be undertaken in order to understand whether the decrease in protein synthesis machinery is a survival mechanism to conserve energy, or whether it ultimately pushes the cells down a cell death route. The proteomic data does suggest that activation of the UPR correlates with a decrease in global protein synthesis, perhaps to deal with the accumulation of misfolded proteins (Zhang and Kaufman, 2006).

The proteomic data contained within the ribosomal interactome revealed a significant up-regulation of peroxiredoxins 1, 2 and 5 (PRDX1, PRDX2 and PRDX5). Peroxiredoxins play a key role in the cellular antioxidant defence system, converting hydrogen peroxide into oxygen, and averting the formation of hydroxyl radicals (Bell and Hardingham, 2011). Thus the increases in Prdx proteins may have a protective role in the cellular response to chronic metabolic stress. Indeed previous studies have shown PrxII to suppress the generation of ROS in the PC12 neuronal cell line (Simzar et al., 2000).

PrdxII has also been found significantly increased in frontal cortex tissue from human AD brains (Krapfenbauer et al., 2003). In the opening chapter it was hypothesised that this increase in PrdxII may serve as an indicator of oxidative stress in the brains of these patients. The corroborative increase in PrxII in this OGD study of metabolic stress provides further evidence for this theory.

Moreover, recent research into PrxII expression found that increases in this protein can be mediated by an interaction between ABAD and Aβ. This work used transgenic mice expressing solely mAPP (Tg mAPP), ABAD (Tg ABAD), both mAPP and ABAD (Tg mAPP/ABAD) or non-transgenic littermate controls (non-Tg) to investigate the effect of these genetic combinations on PrxII expression. PrxII was found consistently up-regulated in the Tg mAPP and Tg mAPP/ABAD mice compared to the PrxII expression in the Tg ABAD transgenic animals or the non-Tg littermates. Further experiments showed that PrxII overexpression provides a level of protection to neuronal cells in culture from the neurotoxic Aβ peptide (Yao et al., 2007).

The present study provides the first comprehensive analysis of the proteomic and morphological response of human SH-SY5Y cells to prolonged metabolic challenge. The LC-MS proteomics results show alterations and interactions in mitochondrial, endoplasmic reticulum, and ribosomal proteins under conditions of metabolic stress. Electron transport chain (ETC) proteins displayed bidirectional changes (Complex I and V proteins increased and Complex III proteins decreased) in response to OGD. Other mitochondrial proteins involved in lipid and ketone metabolism were also increased suggesting the potential of these cells to utilise alternative energy sources in hypoglycaemic conditions. ER stress response proteins along with proteins involved in proteasomal/ubiquitination degradation formed an important part of the up-regulated proteomic response to the metabolic challenge of OGD. The significant increase in ABAD protein, alongside its known interactions with Aβ and their effects on mitochondrial function and PrxII levels indicate this protein to be an important target for future research into AD.

These interesting protein changes detected by LC-MS were validated using western blotting, with relative protein abundance calculated through densitometry analysis and normalisation to a loading control (either GAPDH or alpha-tubulin). A possible limitation of this validation technique is that these common loading control proteins have been shown to be altered across a range of models of neurodegeneration. Future studies might therefore use the alternative approach of normalisation using total protein analysis to avoid possible skewing of the data (Eaton et al., 2013).

The discussed protein changes provide insight into the complex molecular alterations underpinning cellular adaptation to metabolic stress. The lack of acute ischemic cell death in our *in vitro* model of neuronal metabolic stress makes the proteomic results particularly pertinent to non-fatal, sustained ischemic challenges and the compromised energy metabolism associated with slowly evolving neurodegenerative disorders such as AD (de la Torre, 2010).

However, caution must be exercised in the extrapolation of the present data to cerebral ischemia *in vivo*. The SH-SY5Y cells used in this research are from a neuroblastoma cell line with significant glycolytic capabilities, which may well affect the cellular response to the metabolic challenge of OGD. Further validation experiments therefore need to be carried out in order to determine the physiological relevance of the protein changes recorded in this model following OGD. Differentiation of SH-SY5Y cells into a more neuronal phenotype has been shown to induce a sixfold increase in cellular oxygen consumption, indicative of a shift to oxidative phosphorylation as their energy production process rather than glycolysis (Xun et al., 2012). Differentiation might therefore help to overcome the limitation of the neuroblastoma origins of SH-SY5Y cells in future studies of metabolic stress. However, as previously discussed in Section 1.6.3, there are also limitations of differentiation that might have negatively impacted on the present proteomic study.

It is important to remember that no single cell culture system can fully model the complexity of cerebral tissue and its response to substrate deprivation. Additional proteomic and biochemical analyses across a range of different cell types and model systems would enhance our understanding of the proteomic response to metabolic stress described here.

Data from this chapter are published in the Journal of Cerebral Blood Flow and Metabolism (Herrmann et al., 2013a).

Chapter 4: Examining ABAD Interacting Proteins and their Response to Metabolic Stress

Chapter 4: Examining ABAD Interacting Proteins and their Response to Metabolic Stress

4.1 Background and Aims of the Chapter

The use of LC-MS proteomics to investigate the global proteomic changes underpinning mitochondrial dysfunction in an *in vitro* model of metabolic stress was described in Chapter 3. A key finding from this study was the significant up-regulation of amyloid binding alcohol dehydrogenase (ABAD) protein under conditions of metabolic stress. ABAD is emerging as a key player in AD and is known to interact with amyloid beta (Aβ), resulting in significant mitochondrial dysfunction (Lustbader et al., 2004). The 3×Tg-AD mouse model of AD shows that ABAD and Aβ levels are increased in the mitochondria before the appearance of the classic amyloid plaque pathology typically associated with AD (Yao et al., 2009). ABAD is an attractive target for the amelioration of mitochondrial dysfunction and altering the course of AD progression, however the detailed biochemical pathways in which this protein is involved remain elusive. This chapter will therefore aim to:

- Investigate the protein – protein interactions of ABAD under control conditions and in response to OGD induced metabolic stress
- Confirm key ABAD protein interactions in independent samples and in human AD tissue
- Generate novel hypotheses as to the role of ABAD in normal cell function and in response to metabolic stress

4.2 Methods

4.2.1 Preliminary Study: ABAD Immunoprecipitation

15 million SH-SY5Y cells were seeded overnight in standard 75cm^2 cell culture treated flasks (Greiner Bio One, Stonehouse, UK). Without any treatment, cells were scraped and collected using the protocol described in Section 2.4.1. The cell sample was homogenised in 400µl RIPA buffer (50mM Tris-HCL, 150mM NaCl, 1% NP-40, 0.5% sodium deoxycholate and 0.1% SDS, supplemented with protease inhibitors and PMSF). Samples were centrifuged at 12000RPM for 15mins at 4°C and the supernatant recovered. Total protein content of each sample was determined using the Pierce BCA Protein Assay Kit (Thermo Scientific, UK), as described in Section 2.2.1. 1mg/ml BSA was added to the sample.

3 separate IPs were carried out to determine whether ABAD protein was being immunoprecipitated by the ABAD antibody suspended on the bead support:

- IP a: 200µg protein, 10µl ABAD antibody (Santa Cruz, sc-7689) (Normal)
- IP b: 200µg protein, 10µl RIPA buffer (no antibody control)
- IP c: No protein, 150µl RIPA buffer, 10µl antibody (no sample control)

Immunoprecipitation of ABAD was carried out as described in Section 2.5. The immunoprecipitated samples, along with the protein extracts from the original, flow through and wash steps of the immunoprecipitation were analysed by western blot according to the protocol described in Section 2.2.2. The successful immunoprecipitation of ABAD protein was tested using ABAD antibody (ab10260). To conclusively determine whether ABAD was being successfully immunoprecipitated in the experimental set up, the original and immunoprecipitated samples were fully separated on a precast polyacrylamide gel using electrophoresis, as described in Section 2.2.2. The proteins were

stained for 1hr in SimplyBlue SafeStain (Invitrogen, Paisley, UK) followed by incubation 2% w/v NaCl destain solution overnight at room temperature with orbital shaking.

The gel band at 27kDa (molecular weight of ABAD) in each lane was carefully excised and transferred to a sterile 1.5ml eppendorf tube. Proteins were then exposed to the in-gel digestion protocol described in Section 2.5.2. The final digested protein samples were dried in a speedvac, and sent to LC-MS for confirmation of ABAD immunoprecipitation.

4.2.2 Main Study: Sample Preparation for Immunoprecipitation – Mass Spectrometry (IP-MS)

15 million SH-SY5Y cells were seeded overnight in standard 75cm^2 cell culture treated flasks as previously described. Cells were exposed to 18h OGD or control conditions and harvested as described in Section 2.4.1. After centrifugation, cells from two 75cm^2 flasks were harvested and combined for each IP. The sample collection process was repeated until 3 control samples, 3 OGD samples and a negative control sample for both conditions had been collected (Figure 4.1). Cell pellets were snap frozen for storage until homogenisation and protein assay.

Sample pellets were homogenised and protein assayed. Based on protein assay results, all samples were normalised to the sample with the lowest total protein content (2060µg) and made up to a final volume of 400ul. 40µl ABAD antibody (Santa Cruz Biotechnology, Heidelberg, Germany) was added to each sample. 40µl RIPA buffer was added to the two negative control samples. Samples were incubated on a mechanical tube roller overnight at 4°C. Immunoprecipitations and in-gel protein digestions were carried out as described in Section 2.5. The final digested protein samples were dried in a speedvac, and stored at -80°C until ready for LC-MS analysis.

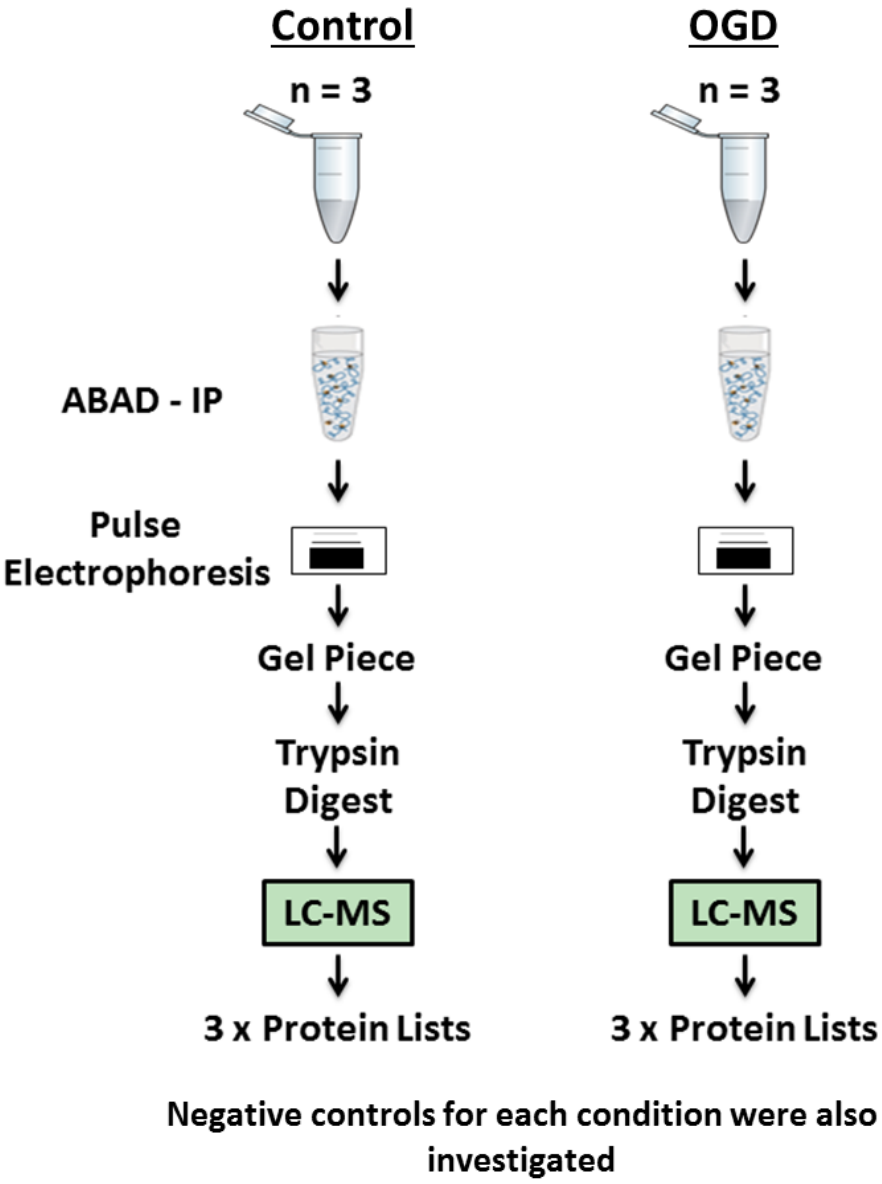

Figure 4.1 IP-MS study design. 3 control samples (normoxic, with glucose) and 3 OGD samples (no oxygen, no glucose) underwent immunoprecipitation. Eluted samples were cleaned by "pulse electrophoresis" into a polyacrylamide gel, and the proteins then trypsin digested ready for LC-MS detection.

4.2.3 Main Study: Investigating ABAD Interacting Partners with IP-MS

Peptides were reconstituted in 5µl of Buffer A (97.5% H_2O, 2.5% acetonitrile, 0.1% formic acid) to give final concentration of 1µg/µl. The peptide mixtures were filtered before proteomic data collection on a nano-HPLC-MS/MS as described in Section 2.5.3. The MS/MS peptide data were searched using MASCOT versions 2.4 (Matrix Science Ltd, London, UK) against a human subset of the NCBI database.

4.2.4 IP-MS Quantification, Analysis and Inclusion Criteria

LC-MS label-free quantification was performed using Progenesis 4.0 (Nonlinear Dynamics, Newcastle, UK). For each protein, the associated unique peptide ions were summed to generate a protein abundance value in each sample. This abundance value was then transformed using an ArcSinH function to give the final protein abundance value that is comparable across samples.

An enrichment ratio was calculated for every protein in each independent IP sample compared to the associated negative control. The frequency distribution of log enrichment scores was calculated, and a Z score > 1 was used as the inclusion criterion for protein enrichment in samples compared to negative controls (Appendix A).

The protein frequency library (PFL) database was used to reduce the chance of false discovery through non – specific protein - protein interactions. The PFL objectively evaluates whether proteins identified in an IP study are genuine protein interactor rather than binding non-specifically (www.proteinfrequencylibrary.com). Searching the database for proteins known to be immunoprecipitated under our specific experimental conditions (human derived cell line, whole cell fraction and sepharose bead support) resulted in detection frequency values being assigned to all of the

immunoprecipitated proteins in the present study. A detection frequency of ≤25% set as the inclusion criteria for consideration in the final dataset.

4.2.5 Confirmatory Immunoprecipitations: Independent Control, OGD and Human Samples

Several ABAD interacting proteins identified by IP-MS were chosen for verification in independent control and OGD samples. The OGD protocol was repeated, with 3 control and 3 OGD samples being collected and processed for IP. The IP protocol was repeated as per the original study, with negative control samples containing goat anti-MAG primary antibody (Santa Cruz Biotechnology, Heidelberg, Germany). ABAD immunoprecipiated samples were probed with the antibodies shown in Table 4.1.

ABAD immunoprecipitations were repeated using brain tissue from the frontal cortex of subjects with either an AD diagnosis or no cognitive impairment obtained from the Alzheimer Disease Research Center at Massachusetts General Hospital. Tissue was homogenised in RIPA buffer and protein assayed to determine total protein content of samples as previously described in Section 2.2.1. All human tissue was handled in agreement with local and national IRB guidelines. Four AD cases and four cognitively normal controls were included in this study, with a negative control containing goat anti-MAG primary antibody (Santa Cruz Biotechnology, Heidelberg, Germany) run for the control and AD samples (Table 4.2).

Protein Identifier	Log Enrichment Factor	Confidence Score	Antibody	Concentration
Proteins Interacting only in Control Samples				
CALR	2.98	2	Abcam ab9484	1 : 1000
CDK5RAP2	5.86	3	Millipore 06-1398	1 : 1000
Proteins Interacting only in OGD Samples				
GRP75	3.88	3	Abcam ab75158	1 : 500
VDAC2	3.43	2	Abcam ab37985	1 : 1000

Table 4.1 Details of the antibodies used in the validation of the IP-MS study.

Case No.	Gender	Age	APOE Genotype	Braak Score	Clinical Diagnosis
Control					
911	M	82	3.3	I	Non-demented
989	F	76	3.3	I	Non-demented
1136	M	86	3.3	I	Non-demented
1301	M	85	3.3	II	Non-demented
Alzheimer's disease					
602	M	90	3.4	V	Demented
612	M	95	3.3	VI	Demented
614	F	69	2.4	VI	Demented
618	M	84	4.4	V	Demented

Table 4.2 Details of the human control and AD cases used in the validation of the ABAD – GRP75 interaction.

4.2.6 Electron Microscopy

SH-SY5Y cells were exposed to OGD using the same paradigm as the original LC-MS study, detailed in Section 2.4.1. Samples were collected immediately after 3, 9 and 18h of OGD and fixed with 4% paraformaldehyde and 5% glutaradehyde in 0.08 M sodium cacodylate buffer, pH 7.2. Once fixed, cells were centrifuged, supernatant removed and replaced with a 3% solution of agar. Gels were cut into $1mm^3$ blocks and processed for EM.

EM sections were evaluated on a JEOL CX -100 II transmission electron microscope. The evaluator was blinded to the treatment condition of all samples. Cells were chosen from grid squares in a predetermined pattern. 50 cells were assessed from each treatment. For each cell the condition of the nuclear membrane was assessed. A Chi-Squared 3 x 2 matrix was used to test the null hypothesis that OGD would have no effect on the structure of the nuclear membrane.

4.2.7 Immunocytochemistry, Confocal Microscopy & Colocalisation Analysis

SH-SY5Y cells were seeded onto 25mm coverslips (VWR, Leicester, UK) overnight and treated with 18h OGD or control conditions the following day. For immunocytochemistry, SH-SY5Y cells were fixed with 4% paraformaldehyde for 10mins at room temperature. Cells were then quenched in 50mM ammonium chloride – PBS solution for 10mins, washed three times in PBS, and permeabilised in 0.1% tritonX. Cells were washed again and incubated for1hr in blocking solution: 0.1% PBS tween, 0.3M glycine, 2% bovine serum albumin. Cells were then washed and incubated in 50µL primary antibodies for 1hr: ABAD (ab10260, abcam, 1:500) and GRP75 (ab53098, abcam, 1:500). Coverslips were washed 5 times to remove excess primary antibody, and then incubated with secondary antibodies for 1hr: goat anti mouse 488 (1:500) and donkey anti rabbit 594 (1:1000). Coverslips were then incubated with DAPI

(Invitrogen, 1:1000) for 10mins. Finally, cells were washed a further five times, rinsed in water, dried and mounted onto glass slides using ProLong Gold (Invitrogen, Paisley, UK) and left to dry overnight at room temperature. Confocal images were acquired with a Nikon A1R confocal laser scanning microscope (Nikon UK, Kingston Upon Thames, Surrey, UK) and analysed using Image J (National Institutes of Health open software) as described in Section 2.6.2. For nuclear protein localisation analysis, confocal Z-stacks were examined and the section containing the most complete nuclear cross section was selected. Using Image J, nuclei were manually outlined and the percentage of the area containing ABAD staining was calculated. For the analysis of changes in the colocalization patterns of key proteins associated with the mitochondrial – associated membrane, confocal images were analysed with a semi-quantitative scale. Cell images were coded and graded by 3 blinded observers as colocalizaed pixels appearing "lacy", having “few puncta”, or being “very punctate”.

4.2.8 Statistical Analysis

IP-MS Enrichment Ratios: For each IP sample, the number of proteins identified with 2 or more peptides was determined. The protein enrichment ratio for each protein was calculated (abundance of protein in the IP sample divided by the abundance of that protein in the negative control). The frequency distribution of log enrichment ratios was plotted using GraphPad Prism, version 5, and proteins with a Z-score > 1 were included as potential ABAD interactors (Appendix A).

Confirmatory Immunoprecipitations: Enrichment ratios were calculated for IP’d samples compared to the negative control sample. Significant changes in enrichment ratios between control vs OGD IP samples and control vs AD tissue were determined with a two-tailed Students t-test, using GraphPad Prism, version 5.

Western Blotting: Significant changes in protein abundance as detected by western blotting and densitometry analysis were determined with a two-tailed Students t-test, using GraphPad Prism, version 5.

Electron Microscopy: Following blind assessment of nuclear envelope morphology, a Chi-Squared 3 × 2 matrix was used to test the null hypothesis that OGD would have no effect on the ultrastructure of this membrane.

Confocal Microscopy: Significant changes in ABAD localisation to the nucleus following OGD was tested using a two-tailed Students t-test. Following blind assessment of staining appearance, a Chi-Squared 3 × 2 matrix was used to test the null hypothesis that OGD would have no effect on the ABAD and GRP75 colocalisation pattern observed in control cells .

4.3 Results

4.3.1 Preliminary Data: LC-MS Confirms Successful ABAD Immunoprecipitation

To confirm the successful immunoprecipitation of ABAD in advance of the full IP-MS study, a sample of whole cell lysate (original), the IP flow through eluents, the IP samples (IPa, IPb and IPc), and eluents from the two wash stages in the IP protocol were run out on a western blot gel. ABAD was probed using the ab10260 (abcam) antibody (Figure 4.2). However, ABAD is detected at 27kDa, which coincides with the molecular weight of the immunoglobulin heavy chain of the antibody used to precipitate ABAD in the IP. The western blot data is therefore inconclusive as to the successful immunoprecipitations of ABAD in this experimental set up.

Validation of successful ABAD immunoprecipitations was achieved by excising the predicted ABAD bands and sending them for mass spectrometry analysis. ABAD protein (3-hydroxyacyl co-A dehydrogenase type-2) was identified only in IPa sample, and not in either of IPb or IPc negative control samples (Figure 4.2). This data confirms successful ABAD immunoprecipitation under the proposed experimental conditions.

A.

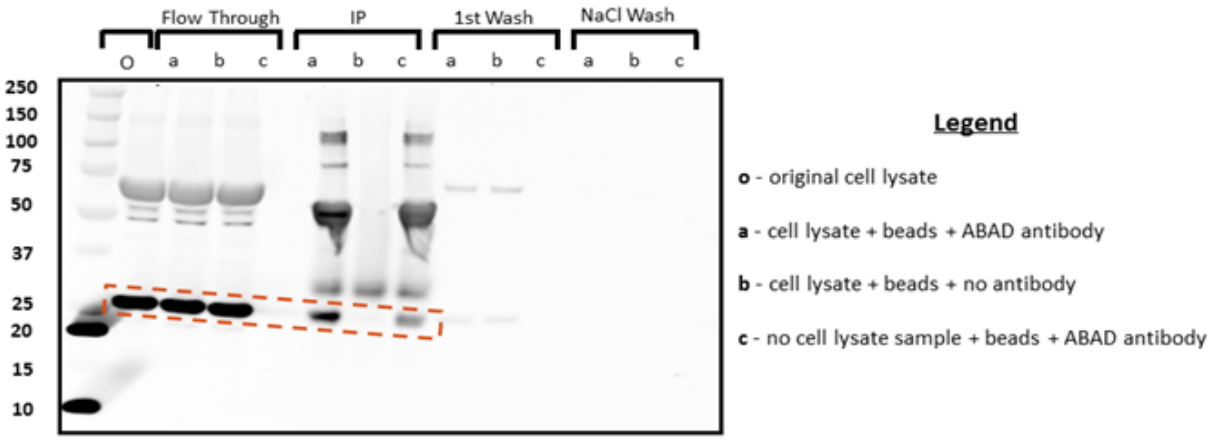

B.

IP a	IP b	IP c
Protein Name	**Protein Name**	**Protein Name**
keratin, type I cytoskeletal 9	keratin, type I cytoskeletal 10	keratin, type I cytoskeletal 9
keratin, type I cytoskeletal 10	keratin, type I cytoskeletal 9	serum albumin preproprotein
3-hydroxyacyl-CoA dehydrogenase type-2	keratin, type II cytoskeletal 2 epidermal	keratin, type I cytoskeletal 10
keratin, type II cytoskeletal 1	keratin, type II cytoskeletal 1	keratin, type II cytoskeletal 1
14-3-3 protein gamma	serum albumin preproprotein	keratin, type II cytoskeletal 2 epidermal
PREDICTED: immunoglobulin kappa	dermcidin preproprotein	PREDICTED: immunoglobulin kappa
keratin, type II cytoskeletal 6A		cysteine-rich secretory protein 3 isoform
spectrin beta chain, brain 3		spectrin beta chain, brain 3
hypothetical protein LOC283987		nesprin-2 isoform 2
leucine-rich repeat-containing protein 37A3		

Figure 4.2 Preliminary Data: LC-MS Confirms the successful ABAD immunoprecipitation under the proposed IP experimental conditions. A. Whole cell lysate (original), IP flow through eluents, IP samples and wash step eluents are probed with ABAD antibody. ABAD is detected at 27kDa (red box) in the original and flow through A and B samples. However, the ABAD band coincides with the IgG antibody light chain in the IP samples, therefore successful ABAD IP cannot be conclusively determined. **B.** ABAD (3-hydroxyabyl-CoA dehydrogenase type-2) is present only in sample IPa (containing cell lysate, beads and ABAD antibody). ABAD protein is not immunoprecipitated in the control samples IPb (containing cell lysate, beads, no antibody) or IPc (containing no cell lysate, beads, and ABAD antibody).

4.3.2 The ABAD Interactome under Normoxic – Normoglycaemic Conditions

67 proteins were identified as potential ABAD interactors under normoxic – normoglycaemic control conditions following enrichment analysis compared to negative controls and inclusion based on a detection frequency cut off of ≤25% (Boulon et al., 2010) (Table 4.3). Of these, 18 proteins were considered "likely" interactions (immunoprecipitating with ABAD in all 3 experimental replicates, confidence score = 3); 36 proteins were considered "probable" interactions (immunoprecipitating with ABAD in 2 of the replicates, confidence score = 2); and 13 proteins were considered "possible" interactions (immunoprecipitating with ABAD in 1 replicate, confidence score = 1) (Figure 4.3).

These "likely" and "probable" ABAD interacting partners were clustered into functional groups using DAVID software. Glucose metabolic process (n = 7), Cell Redox Homeostasis (n=3), Regulation of Neurogenesis (n = 4) and Oxidation – reduction (n = 6) were all identified as significant functional clusters (DAVID score >1.3, $p<0.05$) (Figure 4.4).

Analysis of the subcellular distribution of the "likely" and "probable" ABAD interacting proteins under control conditions shows ABAD to be interacting with proteins across many subcellular locations, including the plasma membrane, nucleus, mitochondria, vesicles and endoplasmic reticulum (Figure 4.5). Gross assessment of ABAD subcellular location by confocal microscopy concurs with the proteomic data, showing ABAD to be located throughout the cells, with the outline of the cells discernible, potentially suggesting ABAD presence at the plasma membrane (Figure 4.6).

4.3.3 The ABAD Interactome in Response to Oxygen – Glucose Deprivation

69 proteins were identified as potential ABAD interacting proteins under OGD conditions following enrichment analysis as previously described (Table 4.4). Of these, 23 proteins were considered "likely" interactions; 28 proteins were considered "probable" interactions; and 18 proteins were considered "possible" interactions (Figure 4.3).

The "likely" and "probable" ABAD interacting partners under OGD conditions were clustered into functional groups using DAVID software. Under metabolic stress, "glucose metabolic process" (n = 4, score 2.06) remained the top functional cluster for ABAD interactions. The other significant functional cluster was identified as "RNA processing" (n = 8, score 1.36) (Figure 4.4). Subcellular location analysis of the "likely" and "probable" ABAD interacting proteins following OGD treatment shows ABAD continuing to interact with proteins from across many organelles. However, OGD treatment induces large increases in the number of ABAD interactions in the nucleus and the mitochondria, and a reduction in the number of interactions occurring in the cytosol (Figure 4.5).

Direct comparisons of all of the interacting proteins in control and OGD samples showed 28 proteins to be stably interacting with ABAD under both conditions (Figure 4.7). Chi-squared analysis shows the control and OGD interactomes to be significantly similar before and after OGD, $\chi^2 = 56.4$, $p<0.0001$ (Figure 4.7). Proteins commonly interacting with ABAD under both control and OGD conditions are identified in italics in Tables 4.3 and 4.4. This significant commonality between ABAD interactions pre- and post-OGD is reflected in the protein subcellular analysis, where in each organelle there are proteins which stably interact with ABAD under both experimental conditions (Figure 4.5).

A. Control

Protein Pulled Out	ABAD Interaction	Number of Proteins
In 3 Samples	Likely	18
In 2 Samples	Probable	36
In 1 Sample	Possible	13

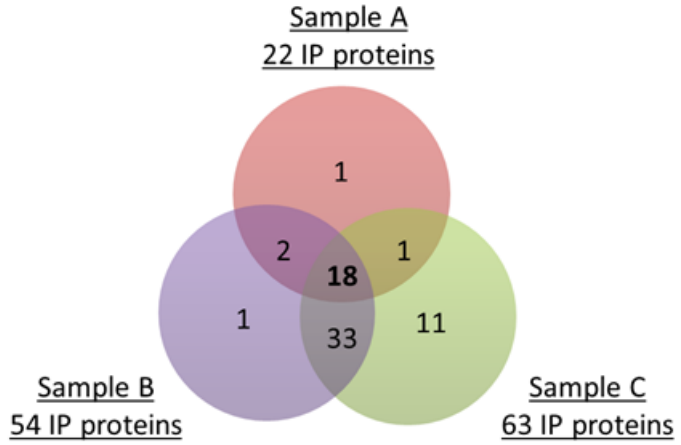

B. OGD

Protein Pulled Out	ABAD Interaction	Number of Proteins
In 3 Samples	Likely	23
In 2 Samples	Probable	28
In 1 Sample	Possible	18

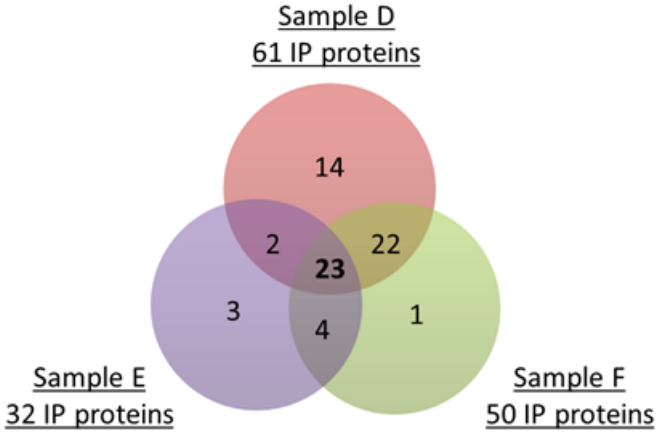

Figure 4.3 Summary of the ABAD interactions found in each of the control and OGD samples. The confidence of the ABAD protein interactions was determined by the number of samples the interaction was detected in. **A.** Under control conditions 18 "likely" ABAD protein interactions were detected in all 3 independent IP samples; 36 "probable" ABAD interactions were detected in 2 IP samples; and 13 "possible" ABAD interactions were identified in only 1 IP sample. **B.** Under OGD conditions, 23 ABAD protein interactions were deemed "likely, 28 were found to be "probable" interactions and 18 "possible" ABAD interactions were detected.

Table 4.3 ABAD interacting partners under control conditions ranked according to detection frequency. Proteins in *italics* are found commonly interacting with ABAD between control and OGD conditions.

Gene name	Protein Name	Log Enrichment Factor	Detection Frequency
ABAD interacting proteins found in 3 Control Samples			
PGAM1	*phosphoglycerate mutase 1*	*1.91*	*0*
OTUB1	*ubiquitin thioesterase OTUB1*	*1.35*	*0*
PCK2	*phosphoenolpyruvate carboxykinase [GTP], mitochondrial*	*1.04*	*0*
OXSR1	*serine/threonine-protein kinase OSR1*	*0.89*	*0*
CDK5RAP2	CDK5 regulatory subunit-associated protein 2	0.77	0
AGL	glycogen debranching enzyme	0.40	0
CYB5R3	*NADH-cytochrome B5 Reductase*	*0.25*	*0*
STAT1	*signal transducer and activator of transcription 1-alpha/beta*	*0.68*	*4*
TMOD2	tropomodulin-2	0.37	4
PPP2CA	*serine/threonine-protein phosphatase 2A catalytic subunit alpha*	*1.09*	*7*
RAB5C	ras-related protein Rab-5C	0.28	7
GNAI3	*guanine nucleotide-binding protein G(k) subunit alpha*	*0.47*	*11*
IPO4	*importin-4*	*2.25*	*14*
GDIA1	*rho GDP-dissociation inhibitor 1*	*0.66*	*18*
ARPC5L	*actin-related protein 2/3 complex subunit 5-like protein*	*0.43*	*21*
ELAVL4	*ELAV-like protein 4*	*0.21*	*21*
ACTR3	*actin-related protein 3*	*0.20*	*21*
GSTP1	*glutathione S-transferase P*	*3.12*	*25*
ABAD interacting proteins found in 2 Control Samples			
CALR	calreticulin	0.47	0
UCHL1	ubiquitin carboxyl-terminal hydrolase isozyme L1	0.46	0
MAPRE1	microtubule-associated protein RP/EB family member 1	0.41	0
CS	*citrate synthase*	*0.32*	*0*
HMGB2	high mobility group protein B2	0.22	0
DDX42	ATP-dependent RNA helicase DDX42	0.20	0
PDI	*protein disulfide-isomerase*	*0.19*	*0*
TMPO	thymopoietin isoform gamma	0.16	0
DPYSL2	dihydropyrimidinase-related protein 2	0.12	0
MDN1	*midasin*	*0.11*	*0*
CACYBP	calcyclin-binding protein	0.10	0
PDIA6	protein disulfide-isomerase A6	0.09	0
MDH2	malate dehydrogenase	0.69	4
OLA1	obg-like ATPase 1	0.17	4
PRDX6	peroxiredoxin-6	0.11	4
CORO7	*coronin-7*	*0.11*	*4*
CBR1	carbonyl reductase [NADPH] 1	0.10	4
CPN3	copine-3	0.10	4
PA2G4	proliferation-associated protein 2G4	0.49	7
TPI1	triosephosphate isomerase	0.15	7
PAICS	multifunctional protein ADE2	0.25	11
HMG1	*high mobility group protein B1*	*0.22*	*11*
ABCF1	ATP-binding cassette sub-family F member 1	0.21	11
GNB1	guanine nucleotide-binding protein G(I)/G(S)/G(T) subunit beta-1	0.11	11
PGK1	*phosphoglycerate kinase 1*	*0.76*	*18*
GAPDH	glyceraldehyde-3-phosphate dehydrogenase	0.53	18
GARS	glycyl-tRNA synthetase	0.22	18

RAB1A	*ras-related protein Rab-1A*	*0.08*	*18*
U2AF2	*splicing factor U2AF 65 kDa subunit*	*0.16*	*21*
NAP1L1	*nucleosome assembly protein 1-like 1*	*0.55*	*25*
UBA1	ubiquitin-like modifier-activating enzyme 1	0.48	25
EWSR1	*RNA-binding protein EWS*	*0.37*	*25*
EZR	ezrin	0.26	25
UBAP2L	ubiquitin-associated protein 2-like	0.21	25
RBBP4	*histone-binding protein RBBP4*	*0.12*	*25*
ARF1	*ADP-ribosylation factor 1*	*0.11*	*25*
ABAD interacting proteins found in 1 Control Sample			
CEP250	centrosome-associated protein CEP250	1.04	0
ACOT7	cytosolic acyl coenzyme A thioester hydrolase isoform hBACHb	0.08	0
FLOT1	flotillin-1	0.11	0
CEP128	hypothetical protein LOC145508	0.56	0
ACADM	*medium-chain specific acyl-CoA dehydrogenase, mitochondrial*	*0.30*	*0*
MARCKS	myristoylated alanine-rich C-kinase substrate	0.16	0
LYN	*tyrosine-protein kinase Lyn*	*0.15*	*4*
VDAC1	voltage-dependent anion-selective channel protein 1	0.10	4
ALDOB	fructose-bisphosphate aldolase A	0.20	7
STOML3	stomatin-like protein 2	0.13	7
OST4	dolichyl-diphosphooligosaccharide--protein glycosyltransferase	0.19	11
ARPC1B	actin-related protein 2/3 complex subunit 1B	0.24	18
FSCN2	fascin	0.19	21

Table 4.4 ABAD interacting partners under OGD conditions ranked according to detection frequency. Proteins in *italics* are found commonly interacting with ABAD between control and OGD conditions.

Gene name	Protein Name	Log Enrichment Factor	Detection Frequency
ABAD interacting proteins found in 3 OGD Samples			
CKB	creatine kinase B-type	1.51	0
ACADM	*medium-chain specific acyl-CoA dehydrogenase, mitochondrial*	0.73	0
MMSDH	methylmalonate-semialdehyde dehydrogenase [acylating]	1.02	0
MDN1	*midasin*	0.77	0
CYB5R3	*NADH-cytochrome b5 reductase*	0.54	0
OSBPL8	oxysterol-binding protein-related protein 8	6.12	0
PCK2	*phosphoenolpyruvate carboxykinase [GTP], mitochondrial*	1.27	0
PGAM1	*phosphoglycerate mutase 1*	1.25	0
PC	pyruvate carboxylase, mitochondrial	0.73	0
OTUB1	*ubiquitin thioesterase OTUB1*	1.19	0
MTHFD1L	monofunctional C1-tetrahydrofolate synthase, mitochondrial	0.73	4
STAT1	*signal transducer and activator of transcription 1-alpha/beta*	1.84	4
GRP75	heat shock protein 75 kDa, mitochondrial	0.59	7
PPP2CA	*serine/threonine-protein phosphatase 2A catalytic subunit*	3.24	7
IPO4	*importin-4*	3.22	14
GDIA1	*rho GDP-dissociation inhibitor 1*	0.60	18
CHD4	chromodomain-helicase-DNA-binding protein 4	0.70	18

ARPC5L	*actin-related protein 2/3 complex subunit 5-like protein*	0.84	21
ELAVL4	*ELAV-like protein 4*	0.61	21
GSTP1	*glutathione S-transferase P*	6.65	25
HNRNPA0	heterogeneous nuclear ribonucleoprotein A0	1.26	25
NAP1L1	*nucleosome assembly protein 1-like 1*	1.17	25
SMARCC2	SWI/SNF complex subunit SMARCC2	2.29	25
ABAD interacting proteins found in 2 OGD Samples			
NT5DC2	5'-nucleotidase domain-containing protein 2	0.59	0
AARS2	alanyl-tRNA synthetase, mitochondrial	0.70	0
AGPS	alkyldihydroxyacetonephosphate synthase	0.47	0
DARS2	aspartyl-tRNA synthetase, mitochondrial	0.52	0
CDK1	cell division protein kinase 1	0.75	0
CPSF3	cleavage and polyadenylation specificity factor subunit 3	0.64	0
MRPP1	mitochondrial ribonuclease P protein 1	0.62	0
TBRG4	protein TBRG4	0.58	0
SAP30BP	SAP30-binding protein	0.46	0
TRIP13	thyroid receptor-interacting protein 13	0.79	0
CS	*citrate synthase*	0.60	0
CORO7	*coronin-7*	0.65	0
OXSR1	*serine/threonine-protein kinase OSR1*	0.92	0
CLPX	ATP-dependent Clp protease ATP-binding subunit clpX-like	0.91	4
COPB1	coatomer subunit beta	0.75	4
SEPT2	septin-2	0.75	4
GNAI3	*guanine nucleotide-binding protein G(k) subunit alpha*	0.60	11
AP2B1	AP-2 complex subunit beta	0.98	18
PPP1R9B	neurabin-2	1.23	18
PGK1	*phosphoglycerate kinase 1*	0.51	18
PDI	*protein disulfide-isomerase*	0.58	18
PSMC3	26S protease regulatory subunit 6A	0.87	21
HSP105	heat shock protein 105 kDa	0.49	21
KPNA2	importin subunit alpha-2	0.74	21
EIF2AK2	interferon-induced, double-stranded RNA-activated kinase	0.76	21
VDAC2	voltage-dependent anion-selective channel protein 2	0.54	21
DPM1	dolichol-phosphate mannosyltransferase	0.46	25
ARF1	*ADP-ribosylation factor 1*	0.76	25
ABAD interacting proteins found in 1 OGD Sample			
ENPF	centromere protein F	0.70	0
DDX41	probable ATP-dependent RNA helicase DDX41	0.52	0
Nup107	nuclear pore complex protein Nup107	0.51	4
DPF2	zinc finger protein ubi-d4	0.50	4
LYN	*tyrosine-protein kinase Lyn*	0.62	4
EIF3L	eukaryotic translation initiation factor 3 subunit L	0.55	7
PFKM	6-phosphofructokinase, muscle type	0.52	11
NSUN2	tRNA (cytosine-5-)-methyltransferase NSUN2	0.47	11
VPS35	vacuolar protein sorting-associated protein 35	0.48	11
HMG1	*high mobility group protein B1*	0.46	11
ACTR1A	alpha-centractin	0.48	18
ALB	serum albumin preproprotein	1.04	18
UBE2O	ubiquitin-conjugating enzyme E2 O	0.51	18
RAB1A	*ras-related protein Rab-1A*	0.47	18
U2AF2	*splicing factor U2AF 65 kDa subunit*	0.68	21
THOC4	THO complex subunit 4	0.92	25
RBBP4	*histone-binding protein RBBP4*	0.52	25
EWSR1	*RNA-binding protein EWS*	0.65	25

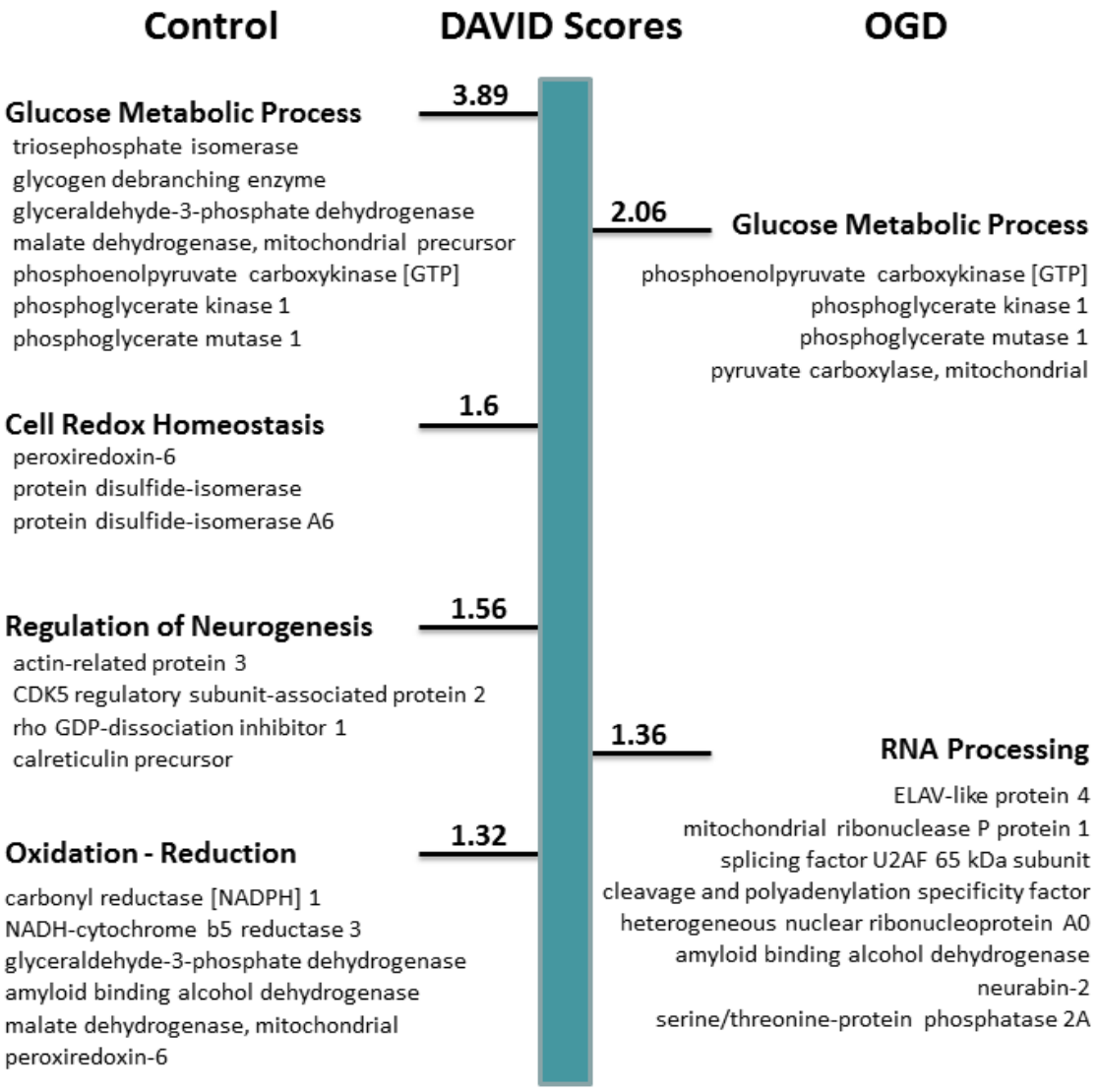

Figure 4.4 Functional clustering of the ABAD interacting proteins under control and OGD conditions. "Likely" and "Probable" ABAD interacting proteins were uploaded to DAVID software and analysed for functionality. Clusters with a score > 1.3 are shown as these are equivalent to a significance of $p<0.05$ (the DAVID score is calculated as the minus log transform of the p value).

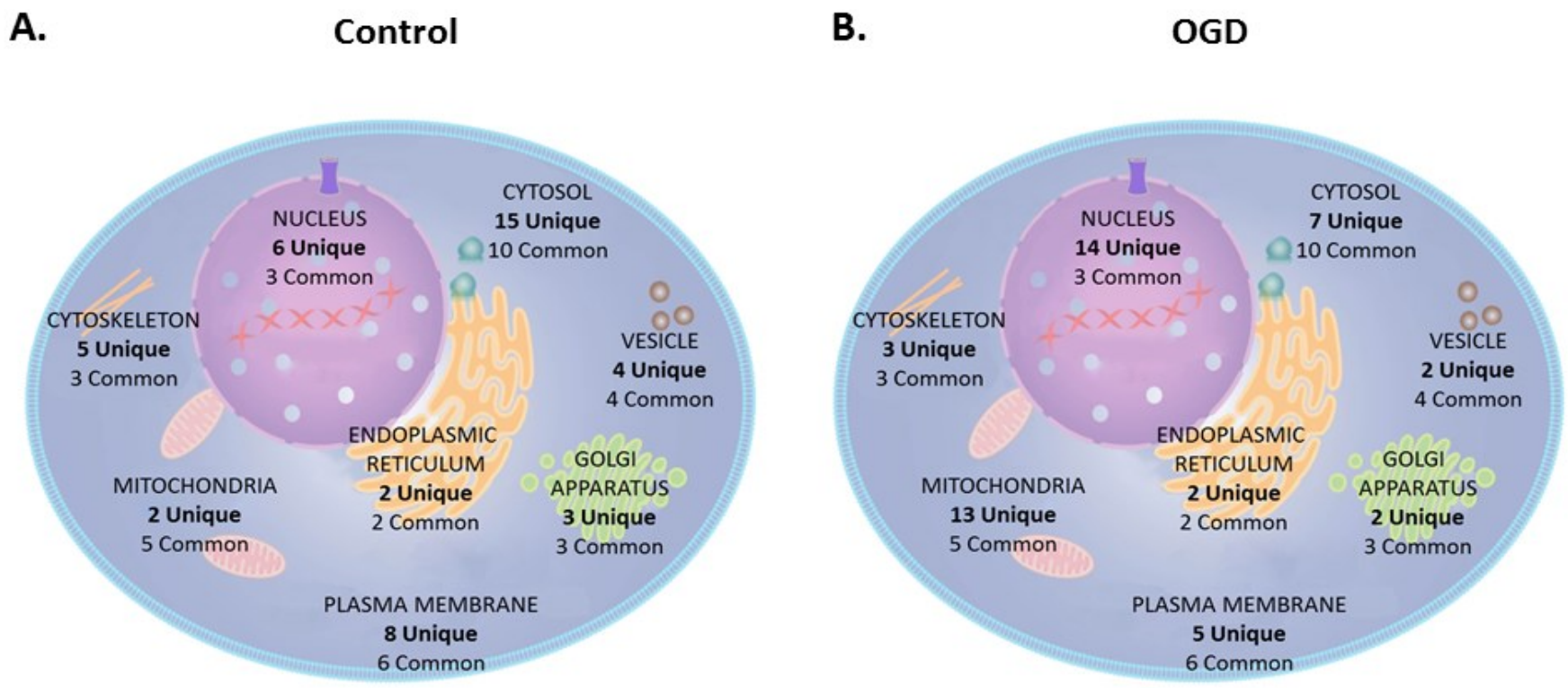

Figure 4.5 ABAD protein – protein interactions are found across many subcellular organelles. "Likely and "Probable" ABAD interacting proteins were uploaded to DAVID and analysed by subcellular compartment. **A.** Under control conditions ABAD interacts with proteins originating in many subcellular organelles. **B.** Following OGD treatment, ABAD continues to interact with proteins from many subcellular organelles, however there are large increases in the number of ABAD interactions occurring in the mitochondria and the nucleus. Unique: protein interactions only occurring in either control or OGD conditions. Common: protein interactions are found under control and OGD conditions.

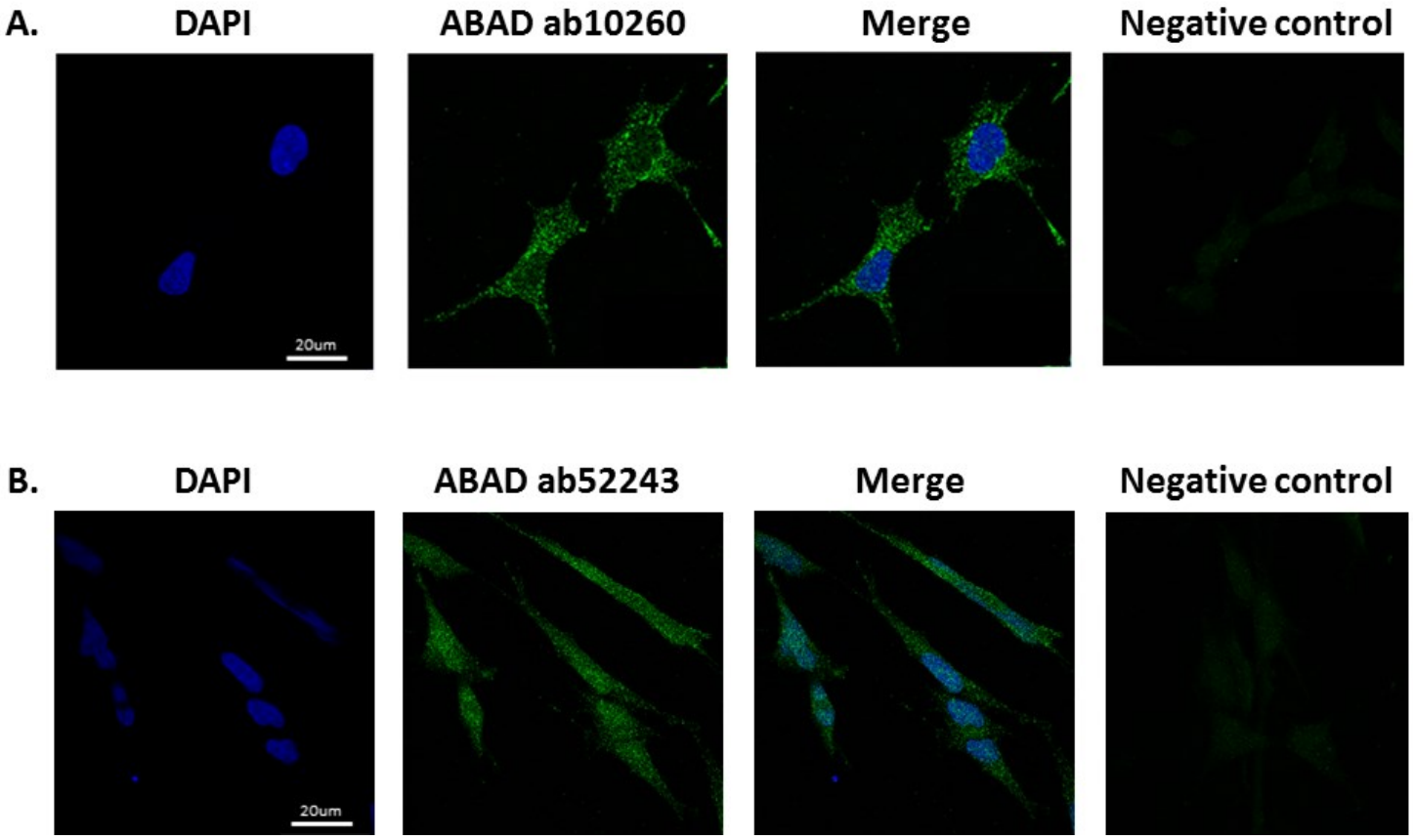

Figure 4.6 Diffuse ABAD staining shown by immunocytochemistry. A. SH-SY5Y cells were nuclear stained with DAPI and co-stained with ABAD antibody ab10260. A diffuse distribution of ABAD is seen that is absent in the no primary antibody negative control **B.** The ABAD immunostain with ABAD antibody ab52243 showed a similar diffuse ABAD distribution that was absent from the negative control.

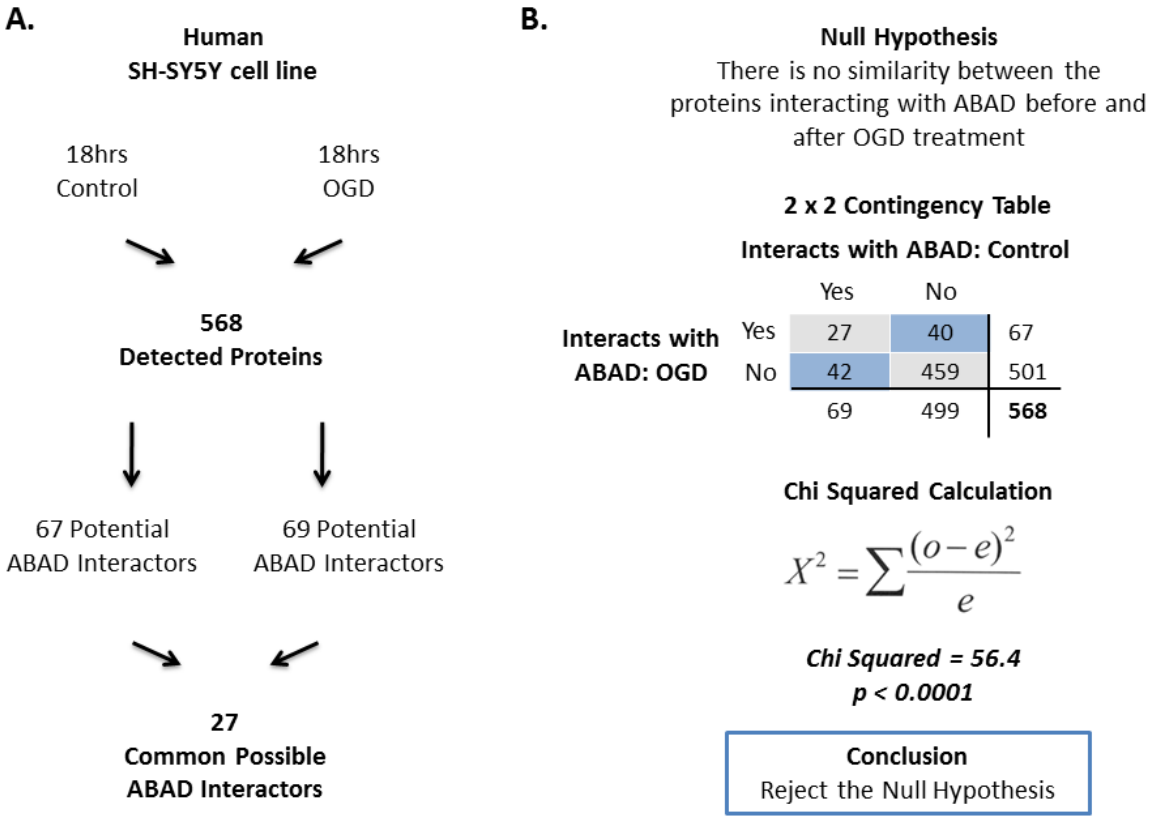

Figure 4.7 The ABAD protein interactome is significantly similar pre- and post-OGD: a chi-squared analysis. A. 27 proteins are commonly detected as interacting with ABAD under both control and OGD conditions. **B.** Using a 2 x 2 contingency table a Chi-squared analysis can be carried out. The result is a Chi-squared value of 56.4, $p<0.0001$. The null hypothesis is rejected, therefore it can be stated that there is significant similarity between the ABAD interactome under control and OGD conditions.

4.3.4 Nuclei and Mitochondria contain the Largest Changes in ABAD Interacting Proteins following OGD

The largest number of OGD induced changes in ABAD interacting proteins are found in the nuclei and mitochondria of SH-SY5Y cells. In the nucleus, 3 proteins stably interact with ABAD under control and OGD conditions: glutathione S-transferase P (GSTP1), signal transducer and activator of transcription 1 (STAT1) and midasin (MDN1). 6 nuclear proteins uniquely interact with ABAD under control conditions: ATP-dependent RNA helicase DDX42 (DDX42), glyceraldehyde-3-phosphate dehydrogenase (GAPDH), high mobility group protein B2 (HMGB2), obg-like ATPase 1 (OLA1), proliferation-associated protein 2G4 (PA2G4) and ubiquitin carboxyl-terminal hydrolase (UCHL1).

Following OGD, 14 new nuclear proteins were found to interact with ABAD: chromodomain-helicase-DNA-binding protein 4 (CHD4), heterogeneous nuclear ribonucleoprotein A0 (HNRNPA0), SWI/SNF complex subunit SMARCC2 (SMARCC2), 26S protease regulatory subunit 6A (PSMC3), cell division protein kinase 1 (CDK1), cleavage and polyadenylation specificity factor subunit 3 (CPSF3), importin subunit alpha-2 (KPNA2), neurabin-2 (PPP1R9B), SAP30-binding protein (SAP30BP), septin-2 (SEPT2), thyroid receptor-interacting protein 13 (TRIP13), high mobility group protein B1 (HMG1), histone-binding protein RBBP4 (RBBP4) and splicing factor U2AF 65 kDa (U2AF2) (Figure 4.8). Using biological functions ascribed by DAVID and Uniprot, these ABAD interacting proteins can be broadly categorised into 4 groups: transcription & translation; regulation of apoptosis; protein transport and protein processing; and cell cycle / other (Figure 4.8). Confocal microscopy analysis confirms ABAD localisation in the nucleus, and also shows the amount of ABAD in the nucleus to be markedly increased following OGD treatment (Figure 4.9).

To investigate whether the large increase in nuclear ABAD protein interactions was due to damage to the nuclear membrane, ultra-structural morphological analysis was undertaken using electron microscopy. With increasing OGD duration, the number of cells displaying abnormal nuclear membranes was significantly increased compared to the equivalent time matched controls (Chi-Square, *$p<0.05$, **$p<0.01$, Figure 4.10). However, despite this increase in nuclear membrane swelling and blebbing, it should be noted that even after 18h OGD exposure, 49% of cells maintained a "normal" nuclear membrane structure.

In the mitochondria, 5 proteins stably interact with ABAD under control and OGD conditions: glutathione-S-transferase P (GSTP1), NADH-cytochrome b5 reductase 3 (CYB5R3), phosphoenolpyruvate carboxykinase [GTP] (PCK2), serine/threonine-protein phosphatase 2A catalytic subunit (PPP2CA), and medium-chain specific acyl-CoA dehydrogenase (ACADM). 2 mitochondrial proteins uniquely interact with ABAD under control conditions: glycyl-tRNA synthetase (GARS) and malate dehydrogenase (MDH2).

Following OGD, 13 new mitochondrial proteins were found to interact with ABAD: creatine kinase B-type (CKB), heat shock protein 75 (HSP75 / GRP75), methylmalonate-semialdehyde dehydrogenase [acylating] (MMSDH), monofunctional C1-tetrahydrofolate synthase (MTHFD1L), pyruvate carboxylase (PC), alanyl-tRNA synthetase (AARS2), alkyldihydroxyacetonephosphate synthase (AGPS), aspartyl-tRNA synthetase (DARS2), ATP-dependent Clp protease ATP-binding subunit clpX-like (CLPX), mitochondrial ribonuclease P protein 1 (MRPP1), protein TBRG4 (TBRG4) and voltage-dependent anion-selective channel protein 2 (VDAC2). Using biological functions ascribed by Uniprot, these ABAD interacting proteins can be broadly categorised into 4 groups: fatty acid oxidation & lipid metabolism; Krebs cycle & gluconeogenesis; protein biosynthesis & protein folding; and induction of apoptosis / other (Figure 4.11).

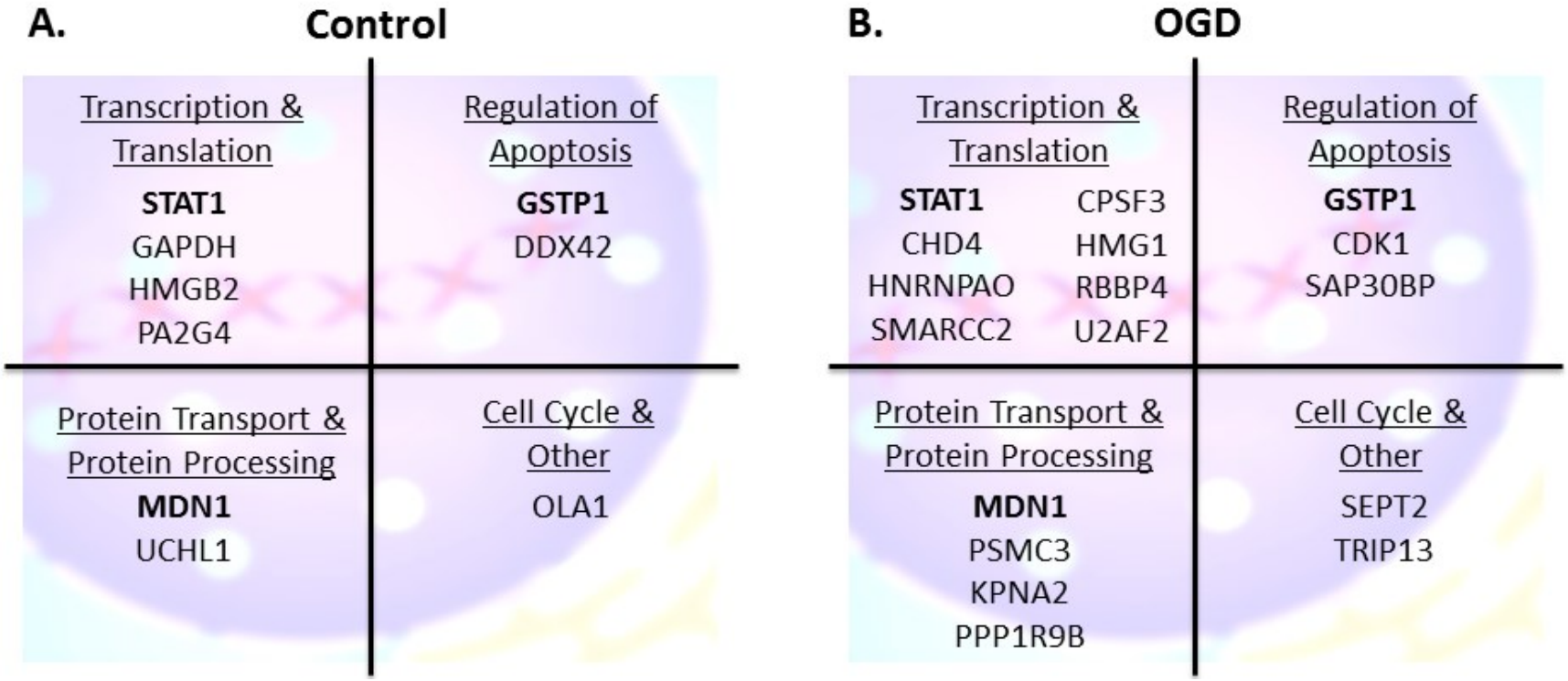

Figure 4.8 Nuclear ABAD protein – protein interactions. **A.** Under control conditions, the ABAD interactions occurring in the nucleus can be broadly categorised as involved with "Transcription & Translation", "Regulation of Apoptosis", "Protein Transport & Protein Processing" and "Cell Cycle & Other". **B.** Under OGD conditions the same broad categories apply to the ABAD interacting proteins. Many more ABAD protein interactions are found in the nucleus under conditions of metabolic stress. Proteins shown in bold are found interacting with ABAD under both control and OGD conditions. The full protein names corresponding to their gene names shown here can be seen in Tables 4.3 and 4.4.

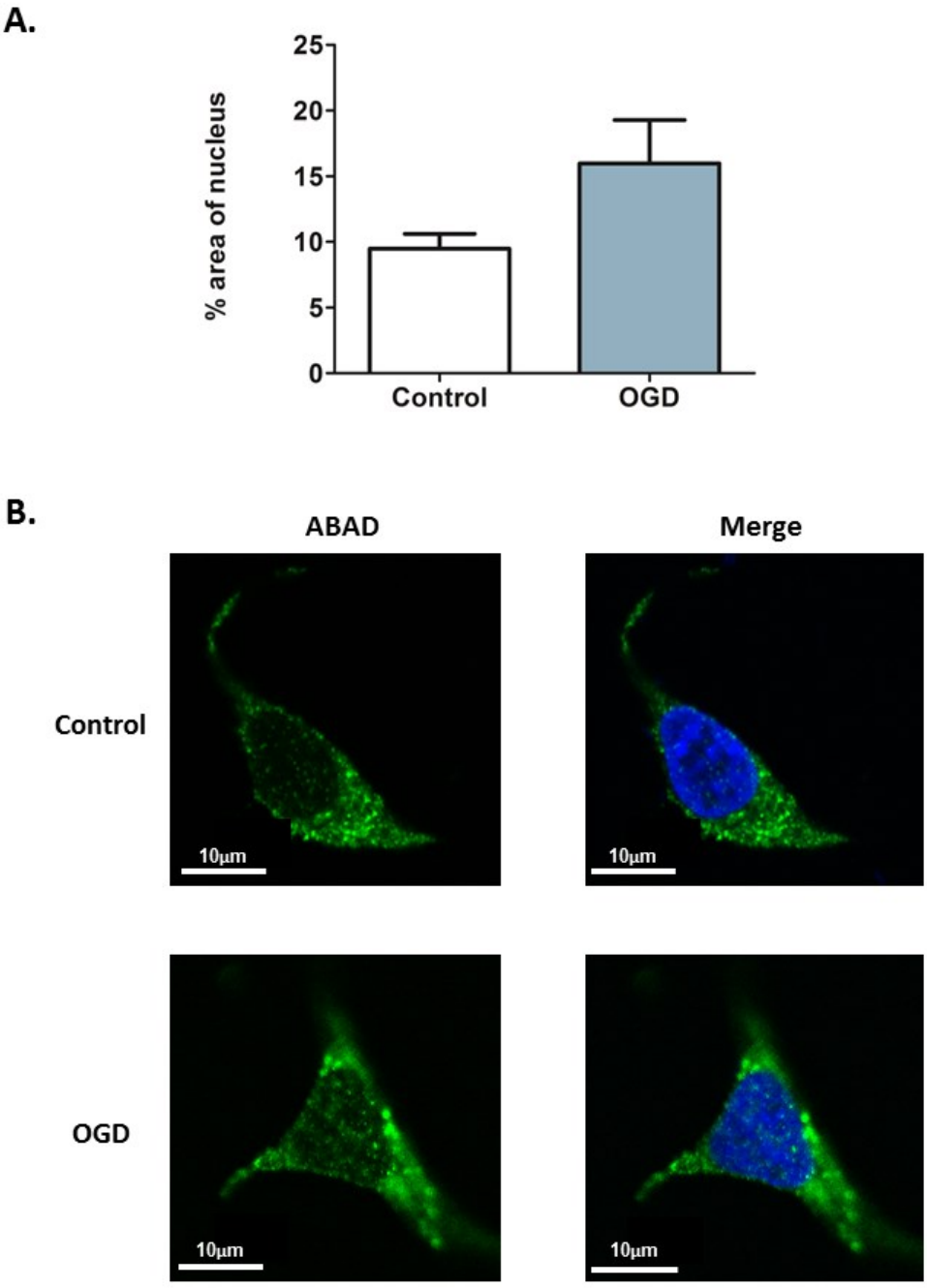

Figure 4.9 ABAD protein is found at increased levels in the nucleus following OGD. A. Consistent with the increased numbers of ABAD protein interactions occurring in the nucleus following OGD, the immunostaining of ABAD within the nucleus was markedly increased following OGD treatment compared to controls. n = 20 cells in each condition. **B.** Representative images of increased ABAD immunostaining in the nucleus of SH-SY5Y cells post-OGD treatment.

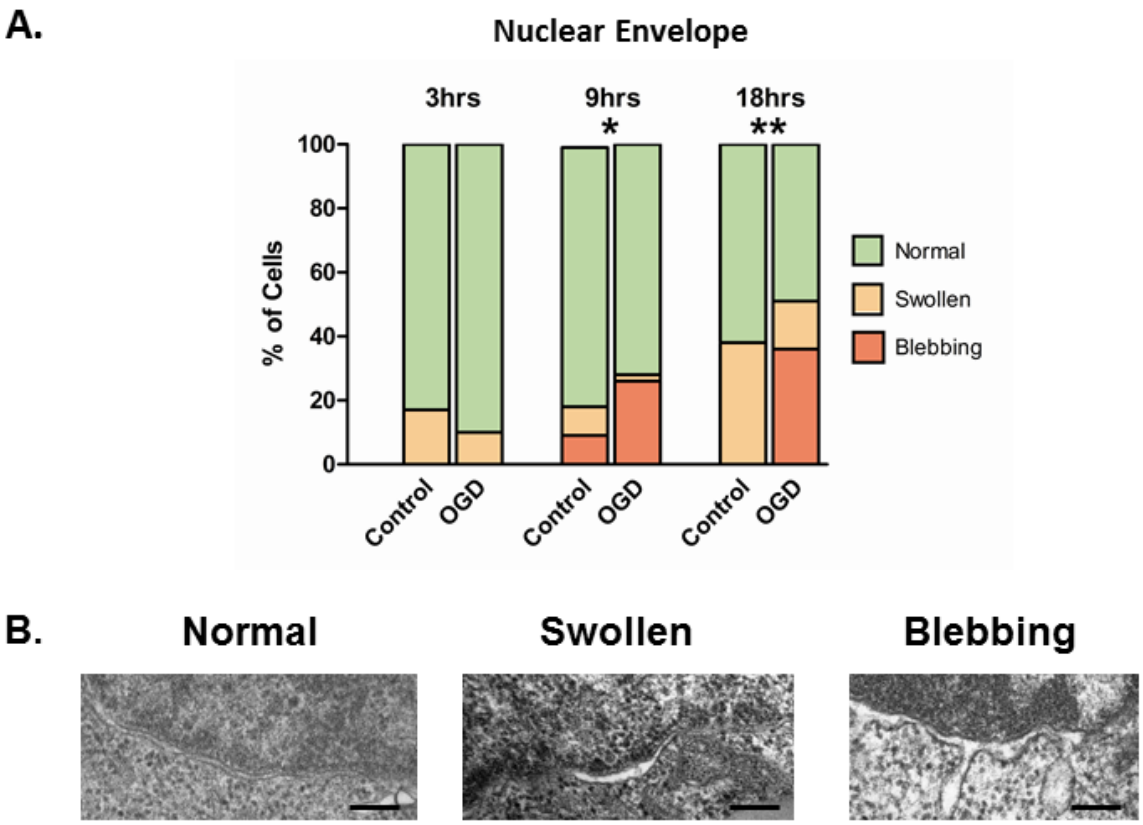

Figure 4.10 The nuclear membrane displays progressive morphological changes following oxygen glucose deprivation (OGD). **A.** OGD induced increases in the number of cells containing swollen and blebbing nuclear membranes. Significant changes in the distribution of "normal", "swollen" and "blebbing" nuclear membranes within cells was seen after 3, 9, and 18h OGD compared to the time matched controls (* $p<0.05$ ** $p<0.01$, X^2, n = 50 cells in each condition*)* **B.** Representative electron micrographs of the three grades of nuclear membrane morphology. Scale bar = 0.1µm.

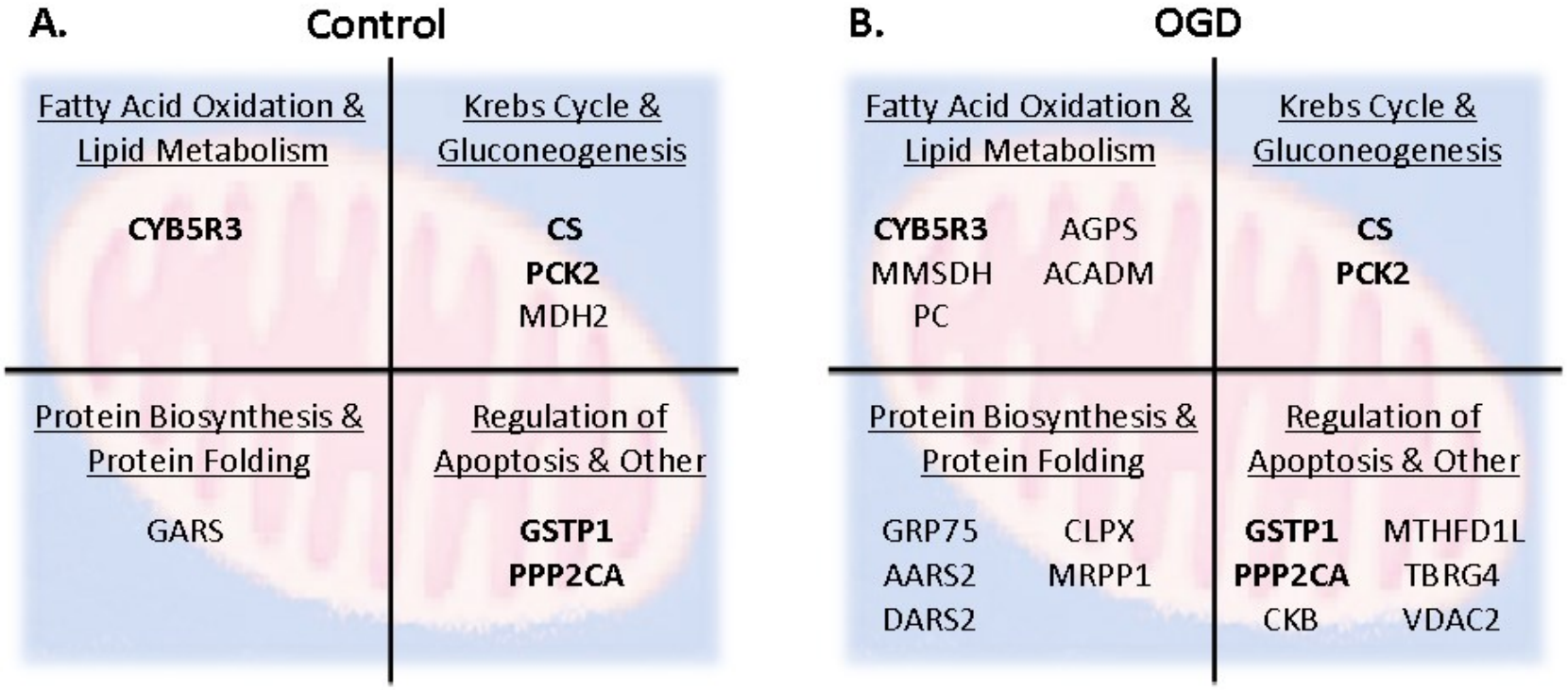

Figure 4.11 Mitochondrial ABAD protein – protein interactions. **A.** Under control conditions, the ABAD interactions occurring in the mitochondria can be broadly categorised as involved with "Fatty Acid Oxidation & Lipid Metabolism", "Krebs Cycle and Gluconeogenesis", "Protein Biosynthesis & Protein Folding" and "Regulation of Apoptosis & Other". **B.** Under OGD conditions the same broad categories apply to the mitochondrial ABAD interacting proteins. Many more ABAD protein interactions are found in the mitochondria under conditions of metabolic stress. Proteins shown in bold are found interacting with ABAD under both control and OGD conditions. The full protein names corresponding to their gene names shown here can be seen in Tables 4.3 and 4.4.

4.3.5 ABAD Interacts with Proteins Involved in Trafficking and Transport

"Protein Transport" and "Vesicle Mediated Transport" are two other functional groups ascribed to DAVID interacting proteins under control and OGD conditions, respectively. Under control and OGD conditions, ABAD stably interacts with proteins associated with coronin-7 (CORO7), importin-4 (IPO4), NADH-cytochrome b5 reductase 3 (CYB5R3), ADP-ribosylation factor 1 (ARF1) and ras-related protein Rab-1A (RAB1A). Under control conditions only, ABAD interacts with actin-related protein 3 (ACTR3), ras-related protein Rab-5C (RAB5C), ezrin (EZR) and thymopoietin (TMPO). Following OGD, ABAD loses these interactions, however gains interactions with AP-2 complex subunit beta (AP2B1), coatomer subunit beta (COPB1) and importin subunit alpha-2 (KPNA2). These proteins can be grouped into the following broad categories: endoplasmic reticulum – Golgi transport; vesicle mediated transport; actin networks & protein anchors; and nuclear protein import (Figure 4.12).

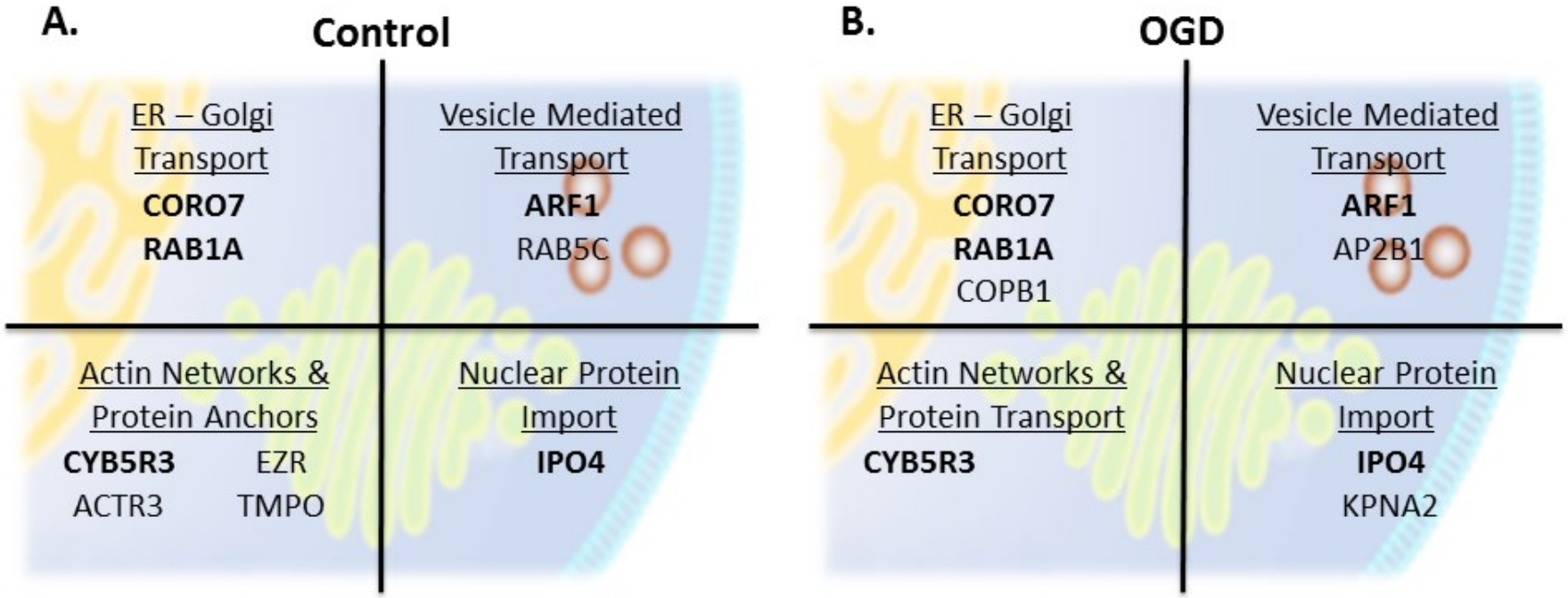

Figure 4.12 ABAD forms interactions with key proteins involved in protein trafficking. **A.** Under control conditions ABAD interacts with proteins involved in numerous aspects of protein trafficking and endocytosis, "ER-Golgi Transport", "Vesicle Mediated Transport", "Actin Networks & Protein Anchors" and "Nuclear Protein Import". **B.** Under OGD conditions the same broad categories apply to the ABAD interactions associated with protein transport., with many of the interactions remaining stable following OGD treatment. Proteins shown in bold are found interacting with ABAD under both control and OGD conditions. The full protein names corresponding to their gene names shown here can be seen in Tables 4.3 and 4.4.

4.3.6 ABAD Interacts with Alzheimer's Related Protein CDK5RAP2 under Control Conditions

Under control conditions, IP-MS shows ABAD to interact with CDK5RAP2, a protein thought to regulate the activity of cyclin dependent kinase (CDK5) (Table 4.3). Western blotting of independent control and OGD samples shows CDK5RAP2 to be significantly reduced under conditions of OGD, and the interaction with ABAD to be lost under these conditions of metabolic stress (Figure 4.13).

4.3.7 ABAD Interacts with GRP75 under OGD Conditions

The IP-MS data shows an interaction between ABAD and GRP75 following OGD treatment that is absent in control samples (Table 4.4). GRP75 is found in the mitochondria, but is also considered to be a marker of the mitochondrial associated membrane. Independent immunoprecipitations were carried out in order to validate this novel ABAD – GRP75 interaction. Western blot analysis of the samples show levels of GRP75 to be unaffected by OGD, and confirms the interaction of ABAD and GRP75 following OGD treatment (Figure 4.14).

Immunocytochemistry provided further evidence for this novel ABAD – GRP75 interaction. Colocalisation analysis shows ABAD and GRP75 to colocalise under control and OGD conditions, with a trend towards less colocalisation following OGD treatment (Figure 4.15). GRP75 is a mitochondrial protein, with the lacy green staining indicative of the typical mitochondrial morphology expected with fluorescent microscopy. Following, OGD treatment, the colocalisation pattern of ABAD to GRP75 is significantly more punctate along the mitochondria (Figure 4.15).

4.3.8 Evidence of ABAD – GRP75 interaction in Human Tissue

Immunoprecipitations were carried out using human brain samples to investigate whether the ABAD and GRP75 interaction is seen in the human brain, and to also investigate whether this interaction is affected by AD. Western blot analysis of the human samples shows the abundances of ABAD and GRP75 to be unchanged in the AD samples. The IP results show GRP75 protein to interact with ABAD in control and AD tissue, with a significant decrease in the amount of immunoprecipitated GRP75 protein in the AD samples (Figure 4.16).

4.3.9 Other ABAD Interactions Detected with LC-MS Remain Unconfirmed

In addition to GRP75 and CDK5RAP2, the interactions of other biologically important ABAD interacting proteins identified by IP-MS were tested in the independent control and OGD samples. IP-MS detected endoplasmic reticulin protein calreticulin (CALR) to interact with ABAD under control conditions, and voltage dependent anion channel 2 (VDAC2) to interact with ABAD under OGD conditions. In the independent samples, calreticulin failed to show any interaction with ABAD under control conditions but did appear to interact with ABAD under OGD conditions. However, the calreticulin also interacts with the negative control antibody MAG under OGD conditions, therefore the ABAD – CALR interaction appears to be non-specific (Figure 4.17). VDAC2 showed ABAD interaction across all samples, including the negative control (Figure 4.18). This ABAD interaction also appears to be non-specific and remains unconfirmed.

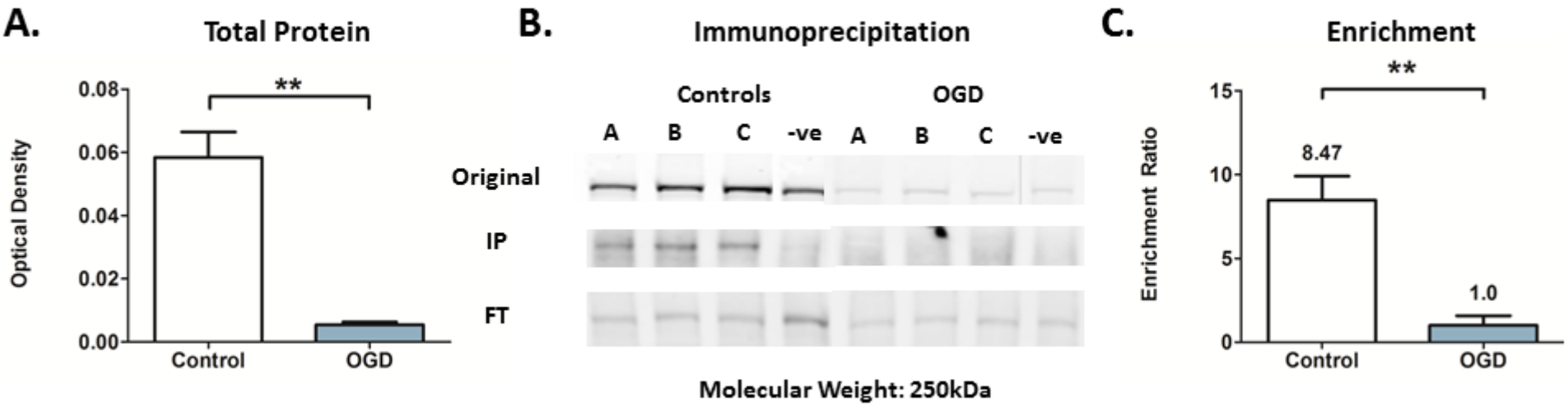

Figure 4.13 The IP-MS predicted interaction of ABAD with CDK5RAP2 under control conditions is confirmed in independent samples. A. Western Blot analysis for CDK5RAP2 (Original Samples) shows a significant decrease in this protein following OGD treatment. **B.** Immunoprecipitation confirms the ABAD – CDK5RAP2 interaction to occur only in control conditions **C.** Enrichment analysis of CDK5RAP2 levels in control IPs compared to negative controls and in OGD IPs compared to negative controls shows significantly greater enrichment of CDK5RAP2 in control samples compared to OGD samples (** $p < 0.01$ T-test, $n = 3$ in each condition).

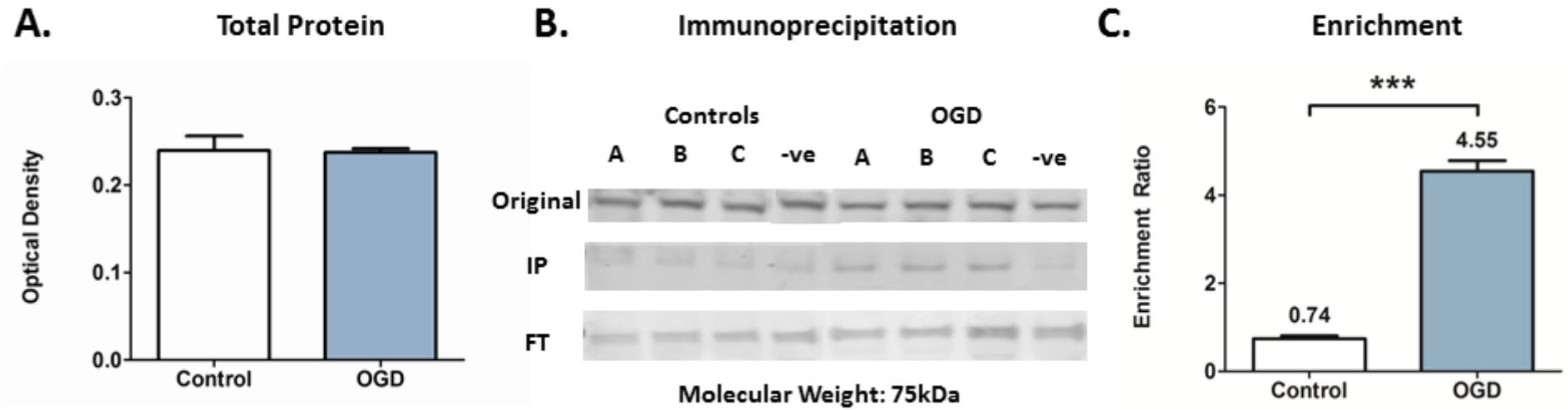

Figure 4.14 The IP-MS predicted interaction of ABAD with GRP75 under OGD conditions is confirmed in independent samples. **A.** Western Blot analysis for GRP75 (Original Samples) shows no significant change in the levels of this protein between control and OGD conditions. **B.** Immunoprecipitation confirms the ABAD – GRP75 interaction to occur only in OGD samples **C.** Enrichment analysis of GRP75 levels in OGD IPs compared to negative controls and in control IPs compared to negative controls shows significantly greater enrichment of GRP75 in OGD samples compared to control samples. (*** $p < 0.0001$, T-test, $n = 3$ in each condition)

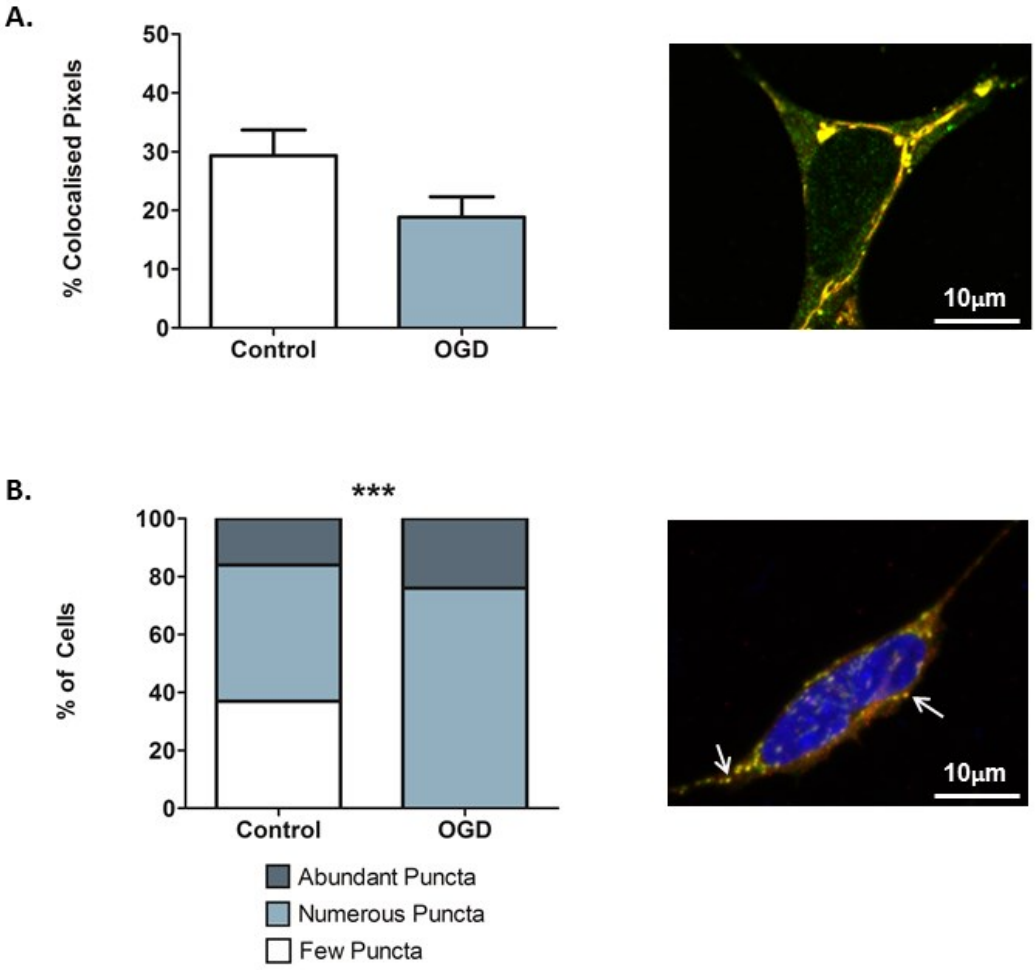

Figure 4.15 Confocal analysis of the colocalisation of ABAD and GRP75. **A.** ABAD and GRP75 proteins colocalise in SH-SY5Y cells under both control and OGD conditions. The colocalisation was unaffected by OGD, however there appears to be a trend towards less protein colocalisation under conditions of metabolic stress. **B.** Although the ABAD – GRP75 is not significantly affected by OGD, the appearance of the colocalisation pattern is changed under conditions of metabolic stress. Following OGD, the ABAD – GRP75 colocalisation staining was significantly more punctate compared to control cells (*** $p<0.0001$, X^2 , n = 20 cells in each condition.*).*

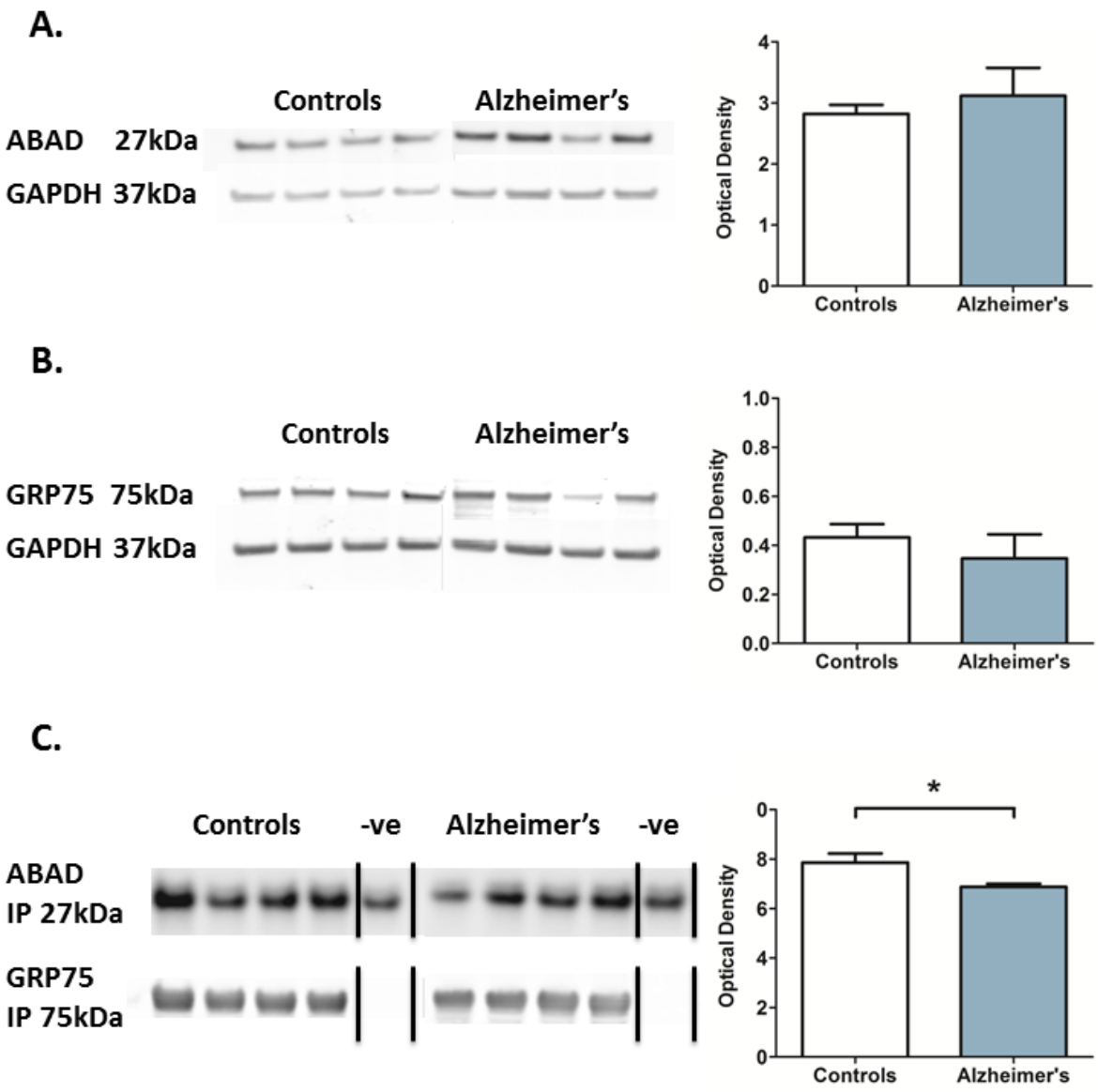

Figure 4.16 Assessing the effect of Alzheimer's disease on ABAD, GRP75 and their interaction. A. ABAD protein abundance was unchanged between human control and AD brain tissue. **B.** GRP75 protein abundance was unchanged between human control and AD brain tissue. **C.** The confirmatory ABAD IP is inconclusive due to the masking of the ABAD protein band by the heavy IgG chain. GRP75 and ABAD interact in human control and AD brain samples. The amount of GRP75 immunoprecipitated in AD samples is significantly less that in controls (* $p < 0.05$, T-test, n = 4 in each condition)

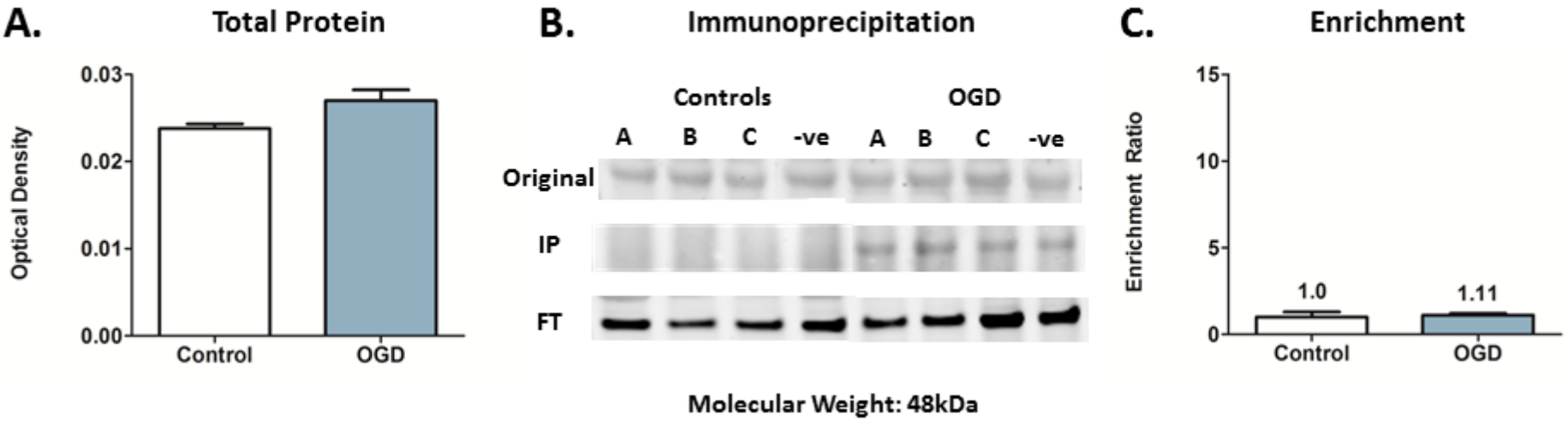

Figure 4.17 The IP-MS predicted interaction of ABAD with calreticulin is unconfirmed in independent control and OGD samples. **A.** Western Blot analysis for calreticulin (Original Samples) shows no effect of OGD on the level of this protein compared to controls. **B.** Immunoprecipitation shows calreticulin and ABAD do not interact in control samples. Under OGD conditions, ABAD and calreticulin appear to interact, however calreticulin is also seen in the negative control sample containing supposedly unrelated MAG protein, therefore **C.** there is no significant enrichment of calreticulin in either the normoxic – normoglycaemic controls or in the OGD samples. (n = 3 in each condition)

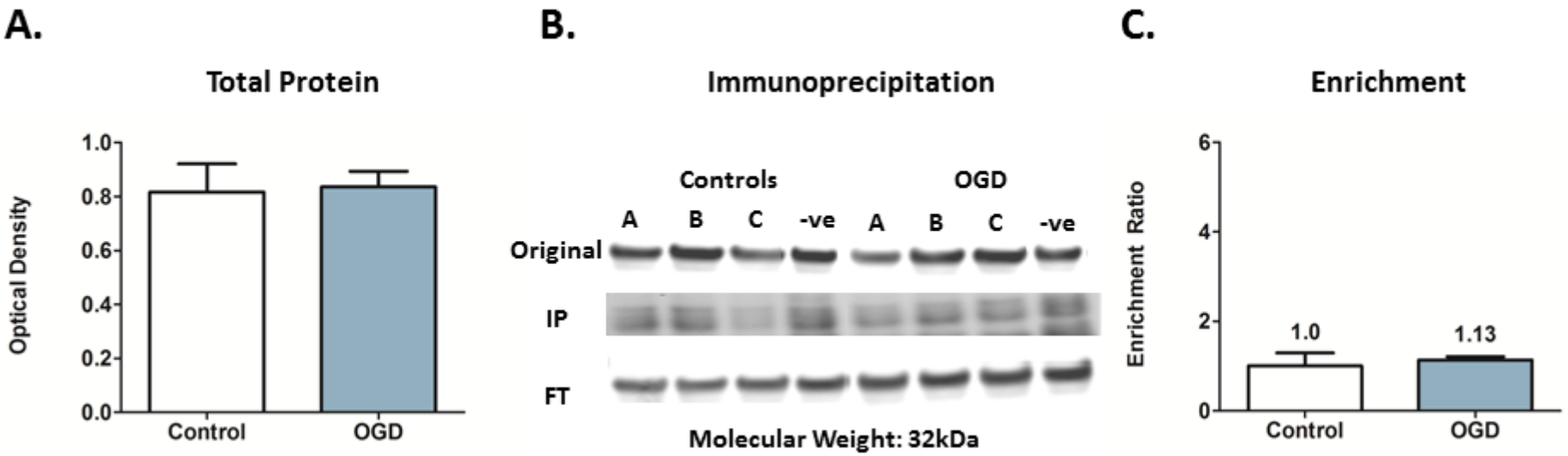

Figure 4.18 The IP-MS predicted interaction of ABAD with VDAC2 is unconfirmed in independent control and OGD samples. A. Western Blot analysis for calreticulin (Original Samples) shows no effect of OGD on the level of this protein compared to controls. **B.** Immunoprecipitation shows calreticulin and ABAD do not interact in control samples. Under OGD conditions, ABAD and calreticulin appear to interact, however calreticulin is also seen in the negative control sample containing supposedly unrelated MAG protein, therefore **C.** there is no significant enrichment of calreticulin in either the normoxic – normoglycaemic controls or in the OGD samples. (n = 3 in each condition)

4.4 Discussion

This study provides the first comprehensive analysis of the protein – protein interactions of ABAD, a protein identified as an important player in mitochondrial dysfunction and AD. The characterisation of the response of SH-SY5Y cells to OGD carried out in Chapter 3 demonstrated the robustness of SH-SY5Y cells to external stressors. This resilience has allowed the response of the ABAD interactome to be extensively examined when challenged with prolonged OGD. Following LC-MS confirmation that ABAD protein was being successfully immunoprecipitated in the experimental set up, the full scale IP-MS study was undertaken. The discovery of a complex ABAD interactome that is altered following OGD provides insight into the possible roles this protein plays under conditions of metabolic stress.

ABAD was originally identified within the endoplasmic reticulum, and consequentially named endoplasmic reticulum associated amyloid-binding protein (ERAB) (Yan et al., 1997). Using liver tissue, subcellular fractionation studies extended our understanding of ABAD distribution identifying ABAD enrichment in mitochondrial as well as ER fractions (Oppermann et al., 1999). Concurrent with this early research, the present study shows ABAD to interact with proteins located in both the mitochondria and the endoplasmic reticulum under control conditions. ABAD was also found to interact with proteins located within other organelles, including the nucleus, golgi apparatus and the plasma membrane. This wide distribution of ABAD interactions across the cell is backed up by images obtained by immunocytochemistry, which shows a disperse ABAD staining pattern, unspecific to individual organelles.

DAVID analysis identified "Glucose Metabolic Process" (GO:0006006) to be the top functional cluster ascribed to the ABAD interacting proteins under both control and OGD conditions. Proteins glyceraldehyde-3-phosphate dehydrogenase (GAPDH) and triosephosphate isomerase (TPI) are found within this top cluster. GAPDH and TPI are enzymes that catalyse two consecutive steps in the glycolytic pathway, a process resulting in the production of pyruvate for entry into the Krebs cycle. ABAD interacts with both of these proteins under control conditions, however following OGD, loses the interactions with these key glycolytic enzymes. It might therefore be hypothesised that the interaction of these proteins with ABAD might be indicative of a modulatory role for ABAD in the glycolytic pathway. For example, under control conditions, ABAD may somehow suppress the glycolytic pathway, whereas after OGD, the dissociation of ABAD from GAPDH and TPI allows these enzymes to undertake their functions in anaerobic energy metabolism. A novel role for ABAD in metabolic homeostasis is not an unrealistic hypothesis given that transgenic mice overexpressing ABAD are shown to have higher baseline levels of ATP (Du Yan et al., 2000) Further work assessing the activity of GAPDH and TPI enzymes under control and OGD conditions in the presence and absence of ABAD would need to be undertaken in order to test this hypothesis.

"Cell Redox Homeostasis" (GO:0045454) is the second functional cluster ascribed by DAVID analysis to the ABAD interacting proteins under control conditions. Reactive oxygen species are molecules derived from molecular oxygen that react with and damage DNA, lipids and proteins (Magder, 2006). If oxygen is reduced by one electron, the superoxide anion ($O_2-\bullet$) is produced, the precursor of most ROS. Reactions of $O_2-\bullet$ with the antioxidant superoxide dismutase produces hydrogen peroxide (H_2O_2) which can either be reduced to water (H_2O) or partially reduced to form the hydroxyl radical ($OH\bullet$), an extremely powerful oxidant that can cause extensive cellular damage (Turrens, 2003). The respiratory chain within the mitochondria is considered to be a

major site of ROS production, which under normal conditions is kept in homeostasis by the cells antioxidant systems. Under conditions of stress, such as cerebral hypoperfusion and ischemia, a vicious cycle of cellular injury is induced, whereby mitochondrial dysfunction causes increased reactive oxygen species production, which further impairs mitochondrial function. This cycle of events is thought to be one of the mechanisms linking cerebral hypoperfusion, mitochondrial dysfunction and neurodegeneration (Fiskum et al., 1999).

Peroxiredoxin-6 (Prx6) is an important protein identified as an ABAD interactor that falls into this "Cell Redox Homeostasis" cluster. Peroxiredoxins are a universally expressed group of proteins involved in the reduction and removal of oxidants within the cell. Prx6 is unique among the peroxiredoxin family: in addition to its peroxidase function, Prx6 also shows phospholipase A_2 (PLA_2) activity (Chen et al., 2000). PLA_2 activity results in the cleavage of fatty acids from phospholipids (Sun et al., 2004). Given the role of ABAD in beta oxidation of fatty acids, and the PLA_2 activity of Prx6, it appears logical that these two proteins would be present in each other's vicinity within the cell. A synergistic interplay between ABAD and Prx6 based around the supply and oxidation of fatty acids is logical, however the interaction is lost under conditions of metabolic stress, where utilisation of fatty acids as an alternative energy sources would be most useful. It might therefore be suggested that the function of the ABAD – Prx6 interaction (and loss of interaction under conditions of metabolic stress) is more complex than first thought.

Prx6 has recently been shown to be significantly modified by 4-hydroxynonenal (HNE) in the hippocampi of AD patients compared to controls (Perluigi et al., 2009). HNE is a highly reactive electrophilic aldehyde formed as a result of lipid peroxidation, and is thought to play a key role in oxidative protein damage. Following OGD, it may be this HNE modification of Prx6 that disrupts the interaction with ABAD after treatment with OGD. Further work needs to be carried out to determine whether Prx6 is being modified by HNE under OGD

conditions, and whether this modification has an effect of the ABAD – Prx6 interaction. The binding of Prx6 to ABAD, plus the oxidative modification of Prx6 in AD tissue indicates that this novel protein – protein interaction may play an important role in maintaining cell redox homeostasis. The loss of this interaction following OGD treatment may be indicative of the disruption in redox homeostasis under conditions of metabolic stress, providing insight into a possible mechanism linking ABAD, mitochondrial dysfunction and neurodegenerative disease.

Interestingly, ABAD protein has previously been linked to peroxiredoxins in AD research. Peroxiredoxin II (Prx2) was found at increased levels in transgenic mice expressing both mutant APP and ABAD compared to littermate controls. Intriguingly, the level of Prx2 could be normalised by blocking the ABAD-Aβ interaction (Yao et al., 2007). This result shows that the expression level of peroxiredoxins can be affected by ABAD - Aβ interaction. It would therefore be interesting to test whether the induction of metabolic stress induces interplay between Prx6 and Prx2: It could be hypothesised that the loss of ABAD – Prx6 interaction under OGD conditions allows for an ABAD – Aβ interaction to take place, inducing an increase in Prx2 protein similar to that seen in the transgenic model.

In addition to Prx6, protein disulphide isomerase (PDI) and protein disulphide isomerase A6 (PDIA6) are found to interact with ABAD, and are grouped into the "cell redox homeostasis" functional cluster. Protein disulphide isomerases caltalyse the reduction (breaking), oxidation (forming) and isomerisation (rearranging) of protein disulphide bonds, which are imperative to correct protein folding (Andreu et al., 2012). PDIA6 interacts with ABAD only in control samples, whereas PDI interacts with ABAD under both control and OGD conditions. PDI is involved in the endoplasmic reticulum stress response, a process initiated in response to an accumulation of misfolded proteins in the ER under conditions of cell stress. PDI, along with glucose regulated protein 78

(GRP78) and glucose regulated protein 94 (GRP94) are significantly up-regulated following OGD, indicative of the activation of the ER stress response (Chapter 3, (Herrmann et al., 2013a)). The stable interaction of ABAD with PDI under both control and OGD conditions suggests ABAD may also be involved in the ER stress response, providing a further link between ABAD, metabolic stress, protein misfolding and neurodegeneration. PDI has been investigated specifically in the brains of AD patients. In these patients a nitric oxide group is added to the protein (S-nitrosylation) resulting in inhibition of PDI function and accumulation of misfolded proteins (Uehara et al., 2006). The present study shows PDI to be involved in the cell response to metabolic stress, which may also involve ABAD, inferred through its stable interaction with PDI. If the function of PDI is inhibited (eg. through S-nitrosylation) then the defence mechanism against metabolic stress will also be impeded, potentially leading to neurodegenerative disease.

Linked to "Cell Redox Homeostasis", "Oxidation – Reduction" is another significant functional cluster associated with the ABAD interacting proteins under control conditions. Malate dehydrogenase (MDH2) is included in the "Oxidation – Reduction" functional cluster, and is found to interact with ABAD under control conditions. MDH2 is a Krebs cycle enzyme, responsible for the oxidation of malate to oxaloacetate and the concurrent reduction of NAD+ to NADH. Interestingly, ABAD is also found to interact with citrate synthase (CS), another Krebs cycle enzyme which catalyses the combination of oxaloacetate and acetyl-CoA to form citrate, allowing the cycle to continue. However, the ABAD interaction with CS is stable across control and OGD conditions, whereas ABAD only appears to interact with MDH2 in control samples.

The identification of ABAD interactions within the Krebs cycle led to an inspection of the original LC-MS OGD dataset described in Chapter 3, to see whether OGD affects the expression profiles of MDH2 and CS, as well as the other Krebs cycle enzymes. The data showed CS to be significantly down-

regulated following OGD; aconitase and isocitrate dehydrogenase to be unchanged; with fumerase and malate dehydrogenase being significantly up-regulated with OGD treatment. α-ketoglutarate dehydrogenase, succinyl-CoA synthetase and succinate dehydrogenase were undetected in the LC-MS study (Figure 4.19).

Combining information from the IP-MS and LC-MS studies suggests that ABAD may play a role in modulating key enzymes of the Krebs cycle under conditions of metabolic stress. When ABAD remains interacting with CS under OGD conditions, the enzyme is down-regulated, whereas when the ABAD interaction with MDH2 is lost, the enzyme is up-regulated. Further work needs to be carried out in order to establish the precise consequences of the ABAD interactions with the Krebs cycle enzymes. Interestingly, autopsy and assessment of the brains of AD patients shows the enzymes of the Krebs cycle to be significantly altered compared to controls. Concurrent with the protein changes presented here, MDH activity was significantly increased ($P<0.01$), however isocitrate dehydrogenase, an enzyme unchanged following treatment with OGD was significantly decreased in the end-stage Alzheimer's brains (Bubber et al., 2005). The biological mechanisms underlying these changes remain to be confirmed. However, the loss of the ABAD – MDH interaction under OGD conditions, and the subsequent increase in MDH expression, might provide insight into how metabolic stress influences the enzymes of the Krebs cycle, possible providing a link between chronic cerebral hypoperfuson, mitochondrial dysfunction and AD.

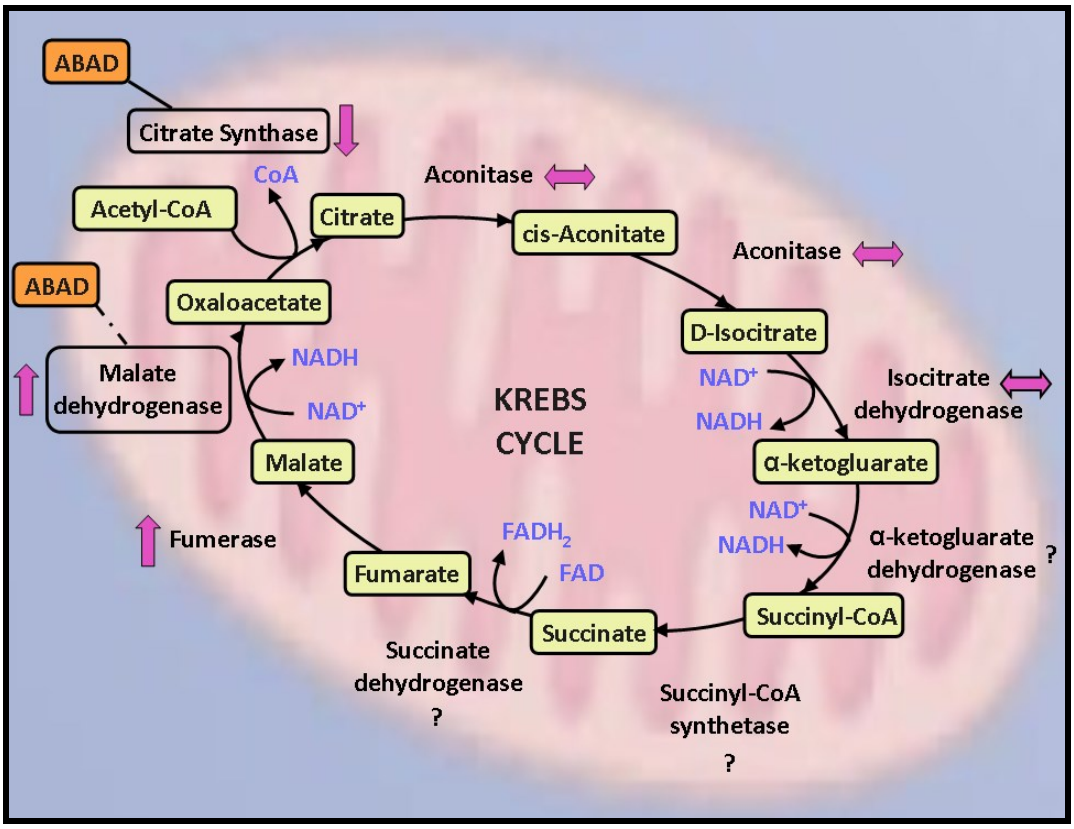

Figure 4.19 Krebs cycle proteins and their interacting partners are altered by OGD. ABAD is found to stably interact with citrate synthase under control and OGD conditions (solid line), however this protein is significantly decreased following OGD treatment (purple arrow). ABAD also interacts with malate dehydrogenase under control conditions, however this interaction is lost following OGD (dotted line). Malate dehydrogenase is significantly increased following OGD treatment. Other proteins of the Krebs cycle were either unchanged following OGD treatment (horizontal arrow), or were not detected in the protein samples by mass spectrometry (question mark).

The other significant functional cluster associated to the ABAD interacting proteins under control conditions is "Regulation of Neurogenesis" (GO:0050767). It seems counterintuitive that ABAD, a protein predominantly researched in relation to AD and neurodegeneration, might also be involved in the regulation of neurogenesis. However, research has shown that many of the key players in neurodegenerative disease, including Alzheimer's related presenilins and tau proteins, are also involved in the modulation of brain plasticity. CDK5 regulatory subunit-associated protein 2 (CDK5RAP2) is a key ABAD interacting protein found within this cluster. CDK5RAP2 can significantly affect the intracellular localisation and substrate specificity of cyclin-dependent kinase-5 (Cdk5), a key player in pathogenic tau hyperphosphorylation and aggregation (Kraemer et al., 2011, Noble et al., 2003).

Due to the high interest in linking metabolic stress and tau aggregation in AD, the ABAD-CDK5RAP2 interaction was followed up in independent control and OGD samples. Confirmatory imunoprecipitations and western blot analysis validate the ABAD - CDK5RAP2 interaction in control samples, with this interaction lost following OGD treatment. Reproducing this finding with a reverse co-IP would strengthen the evidence for this novel protein – protein interaction. The release of CDK5RAP2 from its interaction with ABAD under conditions of metabolic stress may perhaps enable CDK5RAP2 to modulate Cdk5 activity, with important implications for tau phosphorylation. Furthermore, research recently demonstrated that knocking down Cdk5 in triple-transgenic AD mice strongly reduced the number of tau neurofibrillary tangles in the hippocampi of these animals (Piedrahita et al., 2010). It is now important to follow up the discovery of a CDK5RAP2 – ABAD interaction in order to understand how this interaction might impact on tau processing under conditions of metabolic stress.

Under OGD conditions, "RNA Processing" (GO:0006396) was found to be a significant functional cluster of ABAD interacting proteins in addition to "Glucose Metabolic Process" (GO:0006006). Of particular interest, splicing factor U2AF 65kDa subunit (U2AF2) was shown to interact with ABAD in two out of the three OGD IP samples, whereas this protein only interacted with ABAD in one out of three control samples. U2AF2 is involved in the splicing of tau transcripts (Wang et al., 2004). Tau exon 10 encodes one of four microtubule-binding repeats found in tau protein. Inclusion of exon 10 results in tau proteins that contain four microtubule binding repeats (4R). Exclusion of exon 10 results in tau protein containing only 3 microtubule binding repeats (3R). Alternate splicing of the tau transcript tightly controls the ratio of 3R and 4R tau isoforms, and alterations in this ratio can lead to tau aggregation and neurodegeneration (Zhou et al., 2008, Glatz et al., 2006). Mining the original OGD LC-MS proteomic data described in Chapter 3 shows that U2AF2 is unchanged in response to both 6h and 18h OGD. However, a significant increase in ABAD protein in conjunction with the U2AF2 – ABAD interaction following OGD might be indicative of alterations in tau exon10 splicing. Changes in splicing could potentially disrupt the fine balance of 3R and 4R tau isoforms, potentially leading to tau accumulation and neurodegeneration (Figure 4.20).

Furthermore, following OGD, ABAD is shown to interact with cyclin dependent kinase 1 (CDK1), a protein intricately involved in cell cycle regulation and apoptosis (Sakurikar et al., 2012). It is known that uncontrolled activation of CDK1 can cause cells to prematurely undergo mitosis, resulting in apoptosis. Additionally, CDK1 can influence apoptotic pathways directly via modulation of the Bcl-2 proteins (Castedo et al., 2002). With regard to neurodegeneration, unregulated expression and activation of CDK1 has been seen in neurofibrillary tangle-bearing neurons from AD brains (Vincent et al., 1997). The interaction of ABAD with CDK1 under OGD conditions is therefore potentially important with regard to apoptosis and also neurodegeneration. The specific nature of the interaction needs to be further investigated in order to determine whether the interaction promotes apoptotic processes or is working to prevent them.

Of the 8 proteins contained within the "RNA processing" cluster, 4 are identified as nuclear proteins: splicing factor U2AF 65 kDa subunit (U2AF2), cleavage and polyadenylation specificity factor (CPSF3), heterogeneous nuclear ribonucleoprotein A0 (HNRNPA0) and neurabin-2 (PPP1R9B). This finding is congruent with the initial subcellular categorisation of ABAD interacting proteins which showed a large increase in the number interactions occurring in the nucleus following OGD treatment. Randomised and blind confocal microscopy analysis further confirms the presence of ABAD in the nucleus, with nuclear ABAD staining found to be markedly increased following OGD treatment.

Electron microscopy was used to assess the structural integrity of the nuclear envelope following OGD, ensuring that ABAD localisation to the nucleus was functionally relevant, rather than an artifact of aberrant protein distribution due to membrane damage. The electron microscopy results show an increase in nuclear envelope swelling and blebbing with longer OGD durations. The nucleus can be targeted during cell death processes where pro-apoptotic proteins can regulate the disassembly of nuclear structures including the nuclear membrane (Andrade et al., 2010). The significant increase in nuclear blebbing might be indicative of the induction of apoptosis in the SH-SY5Y cells following the longer exposures to metabolic stress. However, it is also important to note that despite these morphological changes, the nuclear envelope appears normal in almost 50% of the cells assessed.

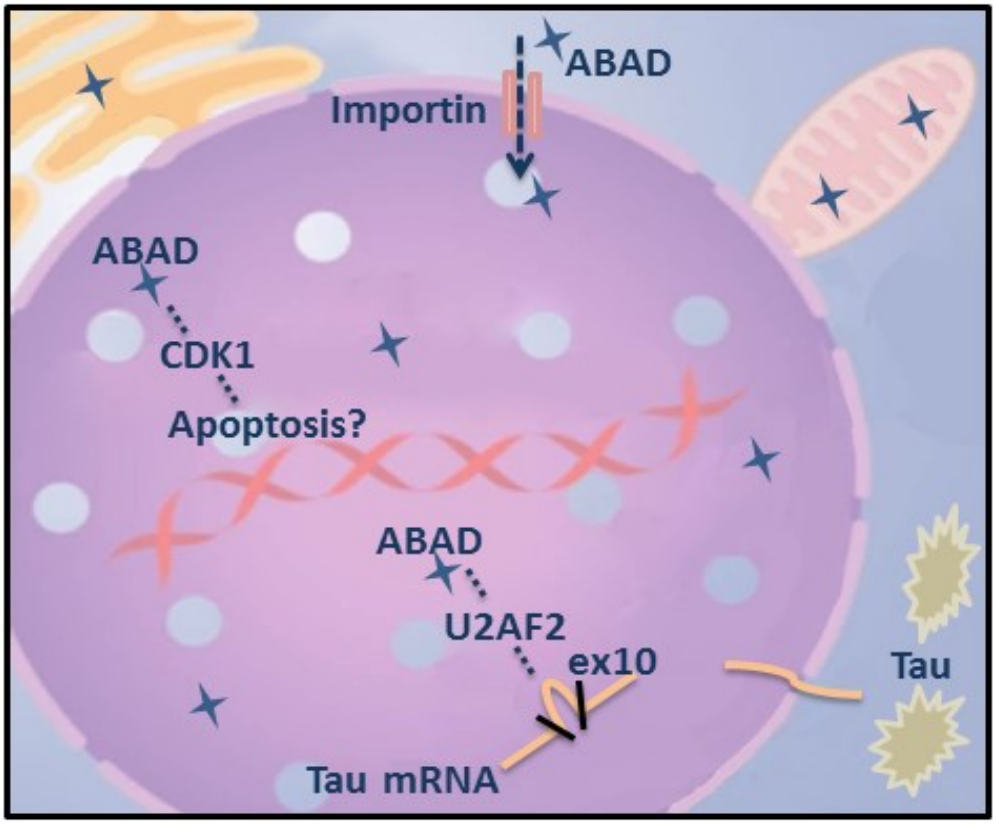

Figure 4.20 ABAD interactions within the nucleus. Under both control and OGD conditions ABAD is found to interact with importin, a protein mediating protein transport across the nuclear membrane. It might be hypothesised that ABAD is transported into the mitochondria via its interaction with importins. Once inside the nucleus ABAD can interact with CDK1 and U2AF2, proteins involved in apoptosis and tau processing, respectively. These ABAD protein interactions may be important in linking metabolic stress to neurodegenerative disease.

The intact nuclear envelope in these cells suggests that functional protein import / export machinery is still required to move proteins across the nuclear membrane. The IP-MS data shows ABAD to consistently interact with importin-4 under both control and OGD conditions (Tables 4.3 and 4.4). Importins are centrally involved in the shuttling of proteins from the cytoplasm to the nucleus (Kohler and Hurt, 2007) and the original LC-MS study demonstrates importin-4 to be unaffected by OGD (Chapter 3, (Herrmann et al., 2013a)). The stable interaction of importin-4 and ABAD suggests ABAD may move routinely from the cytoplasm to the nucleus. However, the large increase in ABAD interactions within the nucleus following OGD treatments along with the significantly increased ABAD localization to the nucleus (as confirmed with confocal microscopy) may indicate a change in ABAD function under conditions of metabolic stress.

In addition to the nucleus, the mitochondria also showed a large increase in ABAD interactions following OGD. The ABAD interactions with mitochondrial proteins can be broadly grouped into 4 categories: Fatty Acid Oxidation & Lipid Metabolism, Krebs Cycle & Gluconeogenesis, Protein Biosynthesis & Protein Folding, and Regulation of Apoptosis. The "Krebs Cycle and Gluconeogenesis" interactions have already been discussed in relation to the DAVID functional groups these proteins falls into. Within the "Fatty Acid Oxidation & Lipid Metabolism" mitochondrial sub-category, ABAD is shown to interact with Acyl-Coenzyme A Dehydrogenase (ACADM). ACADM initiates the first step in the beta-oxidation of fatty acids, a process which involves ABAD in the third stage (Houten and Wanders, 2010). An interaction between ABAD and ACADM therefore seems logical since they are closely related in function, participating in the same biochemical pathway of fatty acid oxidation. More detailed experiments would need to be carried out to ensure these proteins are directly interacting rather than indirectly being precipitated as part of a "beta – oxidation" complex.

Within the "Protein Biosynthesis & Protein Folding" mitochondrial subgroup, ABAD is found to interact with glucose regulated protein 75 (GRP75) under OGD conditions, a result confirmed in independent IP samples. Reproducing this finding with a reverse co-IP would strengthen the evidence for this novel interactiontion between ABAD and GRP75. GRP75 is a member of the heat shock 70 protein family and is traditionally thought to be located in the mitochondria, contributing to the successful translocation and folding of imported proteins (Wiedemann et al., 2004, Mizzen et al., 1991). Based on the results from the IP-MS study, the interaction of ABAD and GRP75 was investigated in human brain tissue. Western blot analysis showed GRP75 to interact with ABAD in both control and AD tissue, with a significant decrease in the amount of GRP75 immunoprecipitated in the AD tissue, despite the apparent increase in ABAD protein level in AD. The decreased levels of GRP75 IP'd in AD tissue may be due to a disruption of the ABAD – GRP75 interaction in the AD brain. Furth investigation of more samples needs to be carried out in order to confirm a change in ABAD – GRP75 interactions, and to assess the functional relevance of this finding in relation to AD.

In addition to its role in mitochondrial protein import, GRP75 has been found enriched at the mitochondrial associated membrane (MAM), an area of membrane interaction between the mitochondria and the endoplasmic reticulum (Hayashi et al., 2009). The key MAM functions are in mediating lipid transport and calcium signalling (Voelker, 2005, Patergnani et al., 2011), both of which are integral to maintaining cellular homeostasis. Analysis of the ABAD – GRP75 confocal images identifies a significant increase in the number of cells displaying a punctate pattern of ABAD – GRP75 colocalisation along the outline of the mitochondria (Figure 4.15). This punctate colocalisation may be a correlate of the ABAD – GRP75 interaction occurring at the specific MAM region following OGD treatment. Higher resolution imaging techniques, such as immune-electron microscopy would be useful in confirming this observation.

Re-inspection of the EM images taken for the analysis of nuclear membrane blebbing shows evidence of ER – mitochondrial interaction in SH-SY5Y cells following OGD. There are insufficient examples to quantify whether the presence of MAM changes in response to OGD, however representative images of the interaction are shown in Figure 4.21.

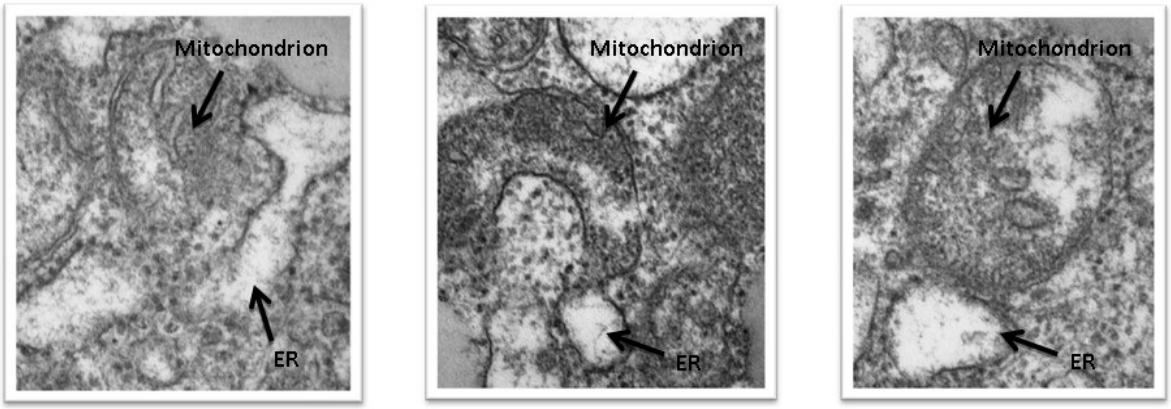

Figure 4.21 Electron micrographs show evidence of the Mitochondrial Associated Membrane (MAM) is SH-SY5Y cells following OGD treatment.

A recent and significant advance in AD research was the localisation of presenilin-1 (PS1) and presenilin-2 (PS2) to the MAM (Area-Gomez et al., 2009). The presenilins form the catalytic component of γ-secretase, a protein complex responsible for the cleavage of APP within its transmembrane domain to release the neurotoxic amyloid-beta peptide (De Strooper, 2003). The discovery of presenilins at the MAM, along with the newly identified ABAD – GRP75 interaction, leads to the proposal that the MAM might be a novel site of APP cleavage and could therefore be the initial point of contact between ABAD and Aβ. The ABAD – Aβ complex would then be in an ideal position on the outer mitochondrial membrane to move inside the mitochondria and mediate the well documented mitochondrial dysfunction characteristic of AD (Figure 4.22) (Lustbader et al., 2004).

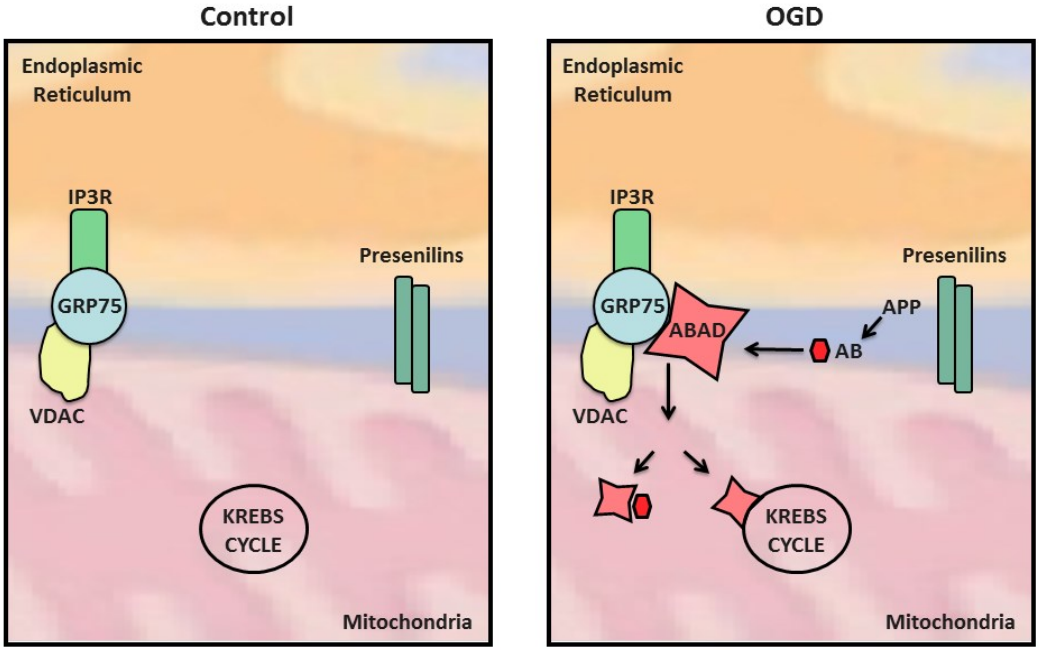

Figure 4.22 The ABAD – GRP75 – MAM hypothesis of mitochondrial dysfunction in Alzheimer's disease. GRP75 and presenilins are enriched at the MAM. Following OGD, ABAD is localised to the MAM and interacts with GRP75. The hypothesis suggests that APP may also localise to the MAM following OGD where it is cleaved by presenilins. The amyloid beta peptides produced from this APP cleavage can then interact with ABAD and be transported into the mitochondria, inducing the mitochondrial dysfunction that characteristic of both metabolic stress and Alzheimer's disease.

Further post-proteomic investigations need to be undertaken in order to validate and extend this ABAD – GRP75 - MAM hypothesis of mitochondrial dysfunction under conditions of metabolic stress. Numerous research questions need to be addressed, including:

- Is APP protein affected by OGD and / or the associated ABAD up-regulation?
- Does the presence of the MAM change under OGD conditions?
- Are ABAD & APP enriched at the MAM?

The ABAD – GRP75 - MAM hypothesis of mitochondrial dysfunction under conditions of metabolic stress suggests both ABAD and APP to be present at the MAM. APP is found at the plasma membrane and can be internalised by endocytosis. Research shows that the majority of amyloidogenic cleavage of APP occurs in endosomes, with the mildly acidic nature of these organelles providing the optimum environment for BACE1 mediated cleavage of APP (De Strooper et al., 2010). Interestingly, the present study shows ABAD to not only interact with proteins at the plasma membrane, but also with proteins involved in protein trafficking and endocytosis. Of particular pertinence is the interaction of ABAD and AP2B1, which is only detected under conditions of metabolic stress. AP2B1 is the beta subunit of the AP2 protein complex, which itself is involved in cargo selection and vesicle formation, as well as playing a role in binding clathrin to vesicle membranes.

The location of APP at the plasma membrane and the components of the γ-secretase complex being located intracellularly (including at the MAM) is part of the "spatial paradox" associated with APP processing (Cupers et al., 2001). The interaction of ABAD with trafficking proteins (including AP2B1) could provide insight into a novel endocytic mechanism by which ABAD and APP might move

intracellularly towards the MAM, thus feeding into the ABAD – GRP75 - MAM hypothesis of mitochondrial dysfunction.

Since the discovery of the ABAD – Aβ interaction and the deleterious effects of this interaction on mitochondrial function, ABAD has been a focus of much AD research. In order to fully understand the role of ABAD in AD, an appreciation of its subcellular location and interaction partners needed to be established. Using state of the art proteomic technology, the present study provides a comprehensive analysis of the ABAD protein interactome, and how these interactions change in response to prolonged metabolic stress. This large scale IP-MS proteomics study has provided an excellent platform for the generation of novel hypotheses of the biological function of ABAD proteins. The proposed ABAD– GRP75 - MAM hypothesis might be particularly important in providing the elusive link between metabolic stress, mitochondrial dysfunction and AD. This hypothesis will be investigated further in Chapter 5.

Chapter 5: Investigating a Possible Role for ABAD in APP Processing

Chapter 5: Investigating a Possible Role for ABAD in APP processing

5.1 Background and Aims of the Chapter

Amyloid binding alcohol dehydrogenase (ABAD) is a protein found at increased levels in the brains of Alzheimer's disease (AD) patients (Yan et al., 1997), and through its interaction with amyloid-beta (Aβ), mediates mitochondrial dysfunction (Lustbader et al., 2004). In Chapter 3, LC-MS revealed ABAD to be significantly up-regulated in response to a severe, but non-lethal oxygen-glucose deprivation (OGD) stimulus, concurrent with a significant decrease in mitochondrial function. In Chapter 4, ABAD was found to interact with glucose regulated protein 75 (GRP75), a protein enriched at the mitochondrial associated membrane (MAM). This interaction was confirmed in human brain tissue. Presenilin proteins are also enriched at the MAM, suggesting this region may be involved in APP processing.

APP is also processed within the endocytic pathway, where the mildly acidic environment of the endosomes provides the optimum environment for β-secretase mediated cleavage of APP (De Strooper et al., 2010). Significantly, the data presented in Chapter 4 showed ABAD to interact with numerous proteins involved in protein trafficking (Figure 4.12). The synchronised location of APP and ABAD at various sites throughout the cell led to the hypothesis that increased ABAD expression might have an effect on the expression levels and processing of APP. This chapter will therefore aim to:

- Determine the effect of ABAD protein overexpression in SH-SY5Y cells on APP expression
- Explore the response of the mitochondrial associated membrane to varying degrees of OGD severity

5.2 Methods

5.2.1 Western Blotting

Western blots were used to investigate changes in expression of APP and ABAD in independent control and OGD samples according to the protocol described in Section 2.2.2. Western blotting was also used to determine transfection efficiency in ABAD over-expressing SH-SY5Y cells. Details of the antibodies used are shown in Table 5.1. The intensity of the bands was assessed using Odyssey application software (version 3.0; Li-Cor, Cambridge, UK). APP western blotting was also performed on ABAD overexpressing SH-SY5Y cells.

Protein Identifier	Antibody	Concentration
ABAD	Abcam ab10260	1 : 500
APP	Millipore MAB348	1 : 1000
MYC	Sigma, M4439	1 : 5000
a tubulin	Abcam ab4074	1 : 50000

Table 5.1 Antibodies used to probe the effect of ABAD overexpression on amyloid precursor protein

5.2.2 APP – ABAD Immunoprecipitation

Immunoprecipitation of ABAD was carried out as described in Section 2.5.2. The immunoprecipitated samples, along with the protein extracts from the original, flow through and wash steps of the immunoprecipitation were probed for APP (1:1000 dilution, Millipore MAB348) by western blot, according to the protocol described in Section 2.2.2.

5.2.3 Bacterial Transformation & SH-SY5Y Transfection

Transformation of the both the pCMV6-empty entry vector and pCMV6-ABAD vector into competent Top10 was carried out using the heat-shock method, as described in Section 2.3.1. For transfections, SH-SY5Y cells were seeded at 70% confluency in 6-well plates, and left to adhere overnight. ABAD DNA or empty vector controls were transfected into cells using the Lipofectamine 2000 DNA Transfection Reagent Protocol (Invitrogen, Paisley, UK).

Following transfection, media was removed from cells and replaced with 1.5ml complete media. Cells were collected and cells homogenised in 50µl RIPA buffer (50mM Tris-HCL, 150mM NaCl, 1% NP-40, 0.5% sodium deoxycholate and 0.1% SDS, supplemented with protease inhibitors and PMSF). Samples were then centrifuged at 12000RPM for 15mins at 4°C and the supernatant recovered. Protein concentrations of the samples were determined using the Pierce BCA Protein Assay Kit (Section 2.2.1).

5.2.4 Electron Microscopy

Cells for electron microscopy (EM) were treated with 3-, 9- and 18h OGD as described in Section 2.5.1, with a time-matched control collected for each time point. EM sections were evaluated on a JEOL CX -100 II transmission electron microscope. The evaluator was blinded to the treatment condition of all samples. Cells were chosen from grid squares in a predetermined pattern. 50 cells were assessed from each treatment. For each cell, the extent of ER – mitochondrial interaction was assessed and graded as either absent, possibly present (where the image was inconclusive) or abundant. A Chi-Squared 3 x 2 matrix was used to test the null hypothesis that OGD would have no effect on the extent of ER – mitochondrial membrane interaction.

5.2.5 Statistical Analysis

Western Blotting: Significant changes in protein abundance as detected by western blotting and densitometry analysis were determined with a two-tailed Students t-test using GraphPad Prism, version 5.

Electron Microscopy: Following blind assessment of the extent of mitochondria and endoplasmic reticulum interaction, a Chi-Squared 3 × 2 matrix was used to test the null hypothesis that OGD would have no effect on the interaction of these organelles. This Chi-Squared analysis was carried out in GraphPad Prism, version 5.

5.3 Results

5.3.1 APP is Significantly Decreased following OGD, Concurrent with an Increase in ABAD Expression

Western blotting of independent control and OGD samples demonstrates levels of APP to be significantly decreased under conditions of metabolic stress. Densitometry analysis coupled with a student's T-test showed this decrease in APP to be highly significant ($p<0.001$) (Figure 5.1). ABAD protein appears to increase in the independent OGD samples, however this this increase fails to reach statistical significance (Figure 5.1).

5.3.2 APP and ABAD Do Not Directly Interact in SH-SY5Y cells

The IP-MS screen for candidate ABAD interactors described in Chapter 4 did not detect an ABAD – APP interaction. To verify this result, a direct investigation of a possible ABAD – APP interaction using immunoprecipitation (IP) on independent samples was conducted. The results confirmed that there is no direct interaction of ABAD and APP in either control or OGD treated samples (Figure 5.2).

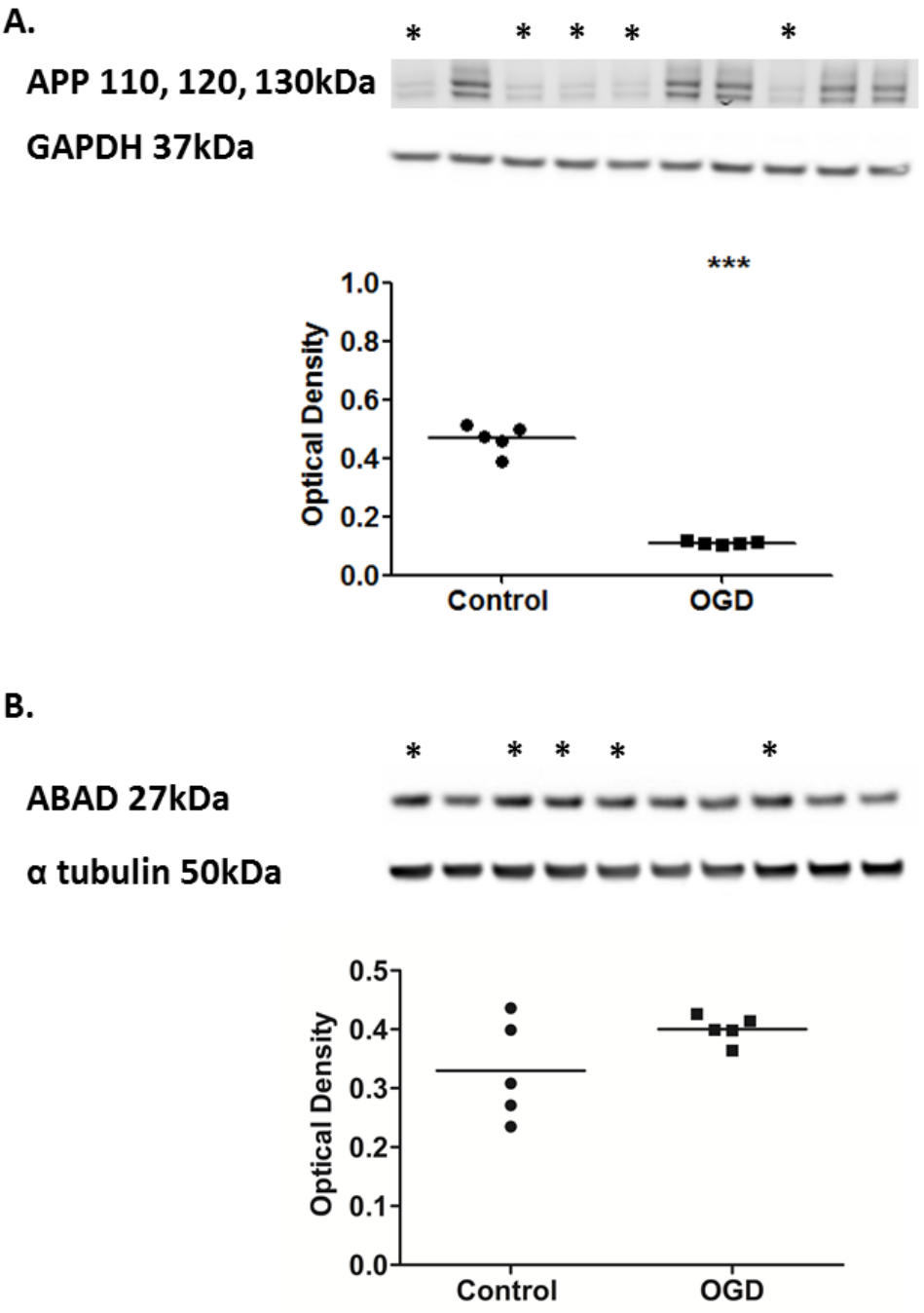

Figure 5.1: APP is significantly reduced concurrent with an increase in ABAD expression following OGD. A. Western blot analysis of independent control and 18hr OGD samples show APP to be significantly reduced, $p<0.001$. **B.** ABAD protein appears to be increased in independent samples following 18h OGD, however this increase fails to reach statistical significance. Bands marked with * represent OGD samples. (*** $p<0.0001$, T-test, $n = 5$).

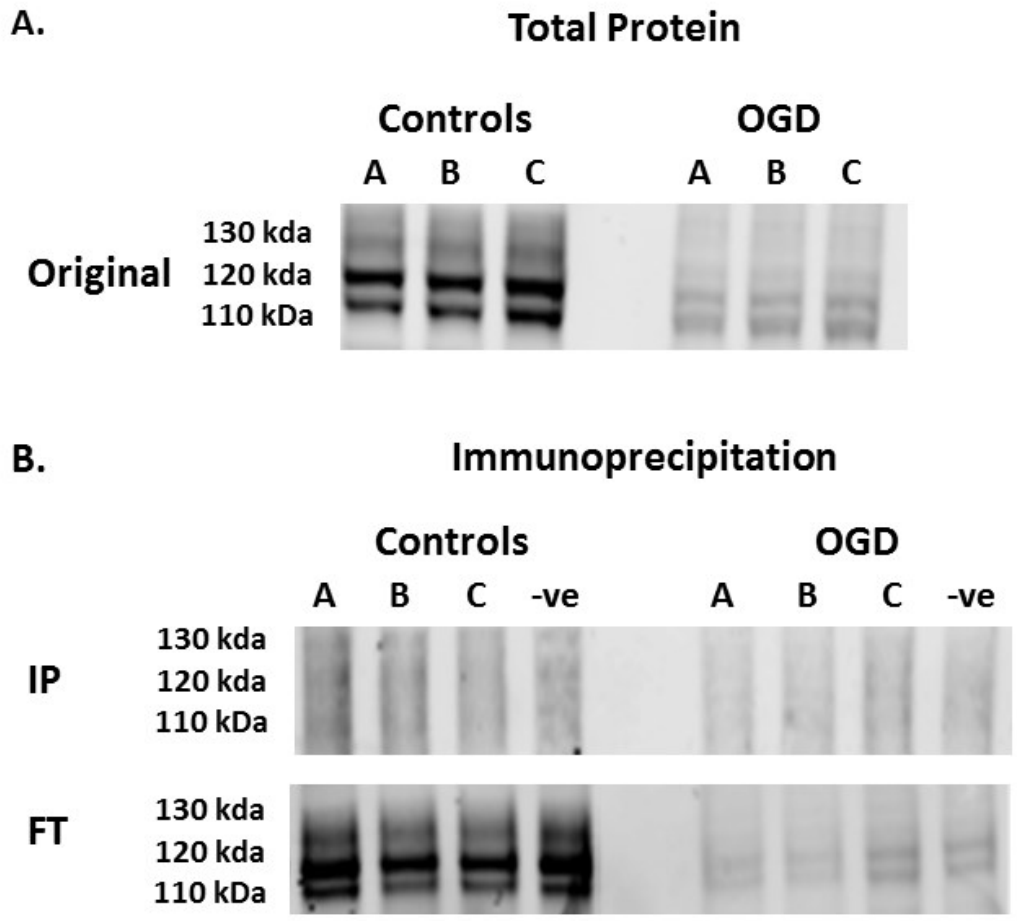

Figure 5.2: ABAD and APP do not directly interact in either control or OGD SH-SY5Y cell samples. A. Western blotting for APP in the original samples used for immunoprecipitation confirm APP down-regulation following OGD treatment. **B.** Immunoprecipitation fails to detect an interaction between ABAD and APP in either control or OGD samples. Flow through (FT) of each IP sample is also shown **(**n = 3 in each condition).

5.3.3 Pilot Data: ABAD Overexpression Affects the Expression of Mature and Soluble APP

ABAD protein was successfully overexpressed in SH-SY5Y (Figure 5.3). The band predicted to be over-expressed myc –tagged ABAD was confirmed by concurrent western blotting for the myc epitope (Figure 5.3). Calculation of transfection efficiency showed ABAD to be over-expressed by 47.2% of endogenous ABAD levels at 24h post transfection, and by 47.4% at 48h post-transfection (Figure 5.3).

Once successful ABAD overexpression was established in SH-SY5Y cells, the effect of increased ABAD on APP expression was investigated in a pilot study. Western blot analysis at 24h post ABAD transfection, showed there to be no change in APP expression compared to non-transfected controls (Figure 5.4). At 48h post ABAD transfection, the 130kDa band of mature APP appears to be lost and the 120kDa band of soluble APP (sAPP) appears to be increased in two out of three ABAD overexpressing samples (Figure 5.4).

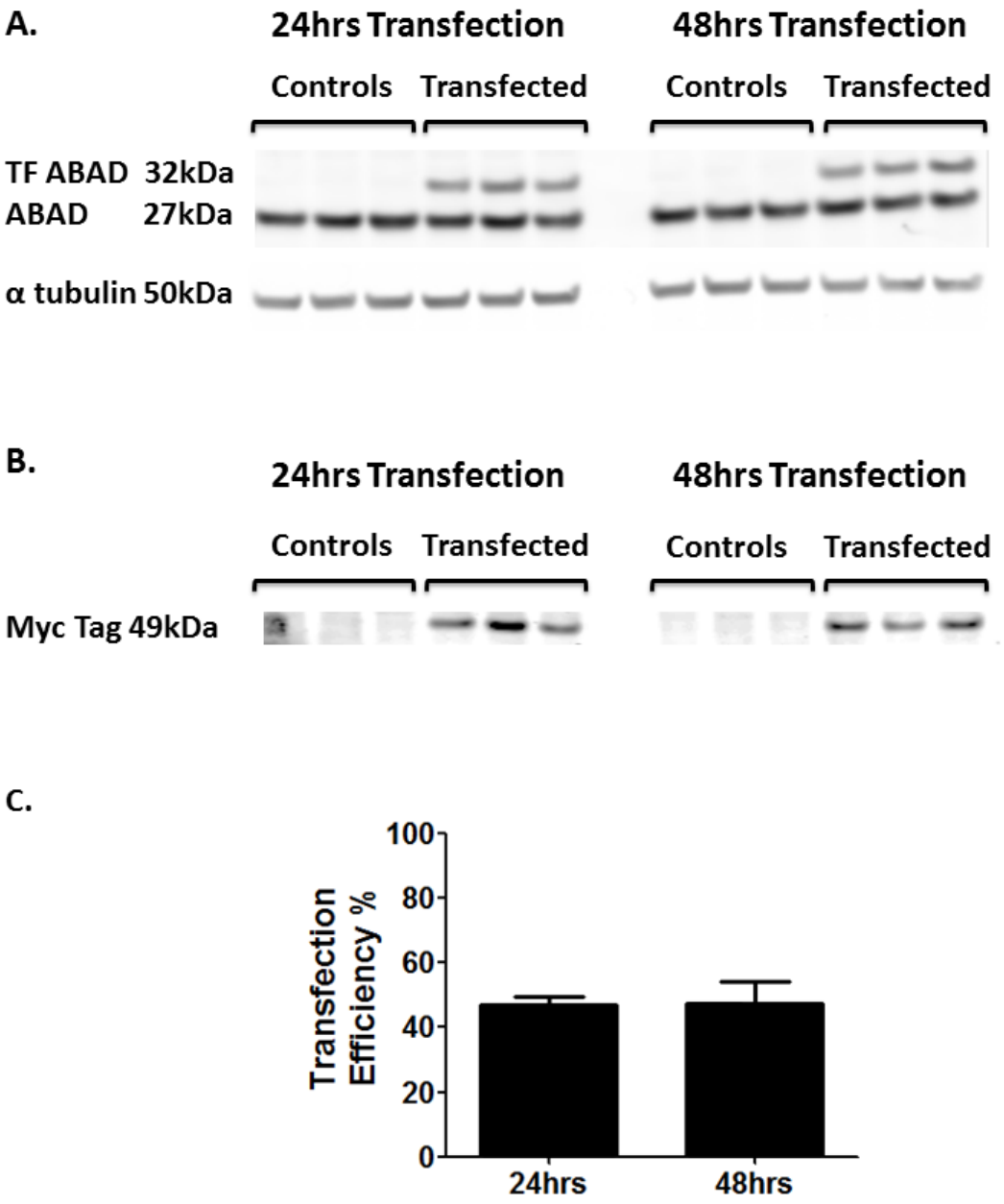

Figure 5.3: ABAD levels are successfully increased following transfection. A. Lipofectamine transfection of ABAD DNA into SH-SY5Y cells successfully overexpresses ABAD at 24 and 48h post transfection (TF = Transfected). **B.** Western blotting for the myc tag confirms the overexpression of ABAD at 24 and 48h post transfection. **C.** Calculation of transfection efficiency shows the lipofectamine - TrueOrf origene vector to stably overexpress ABAD with 47% efficiency at 24 and 48h post-transfection. **(**n = 3 in each condition).

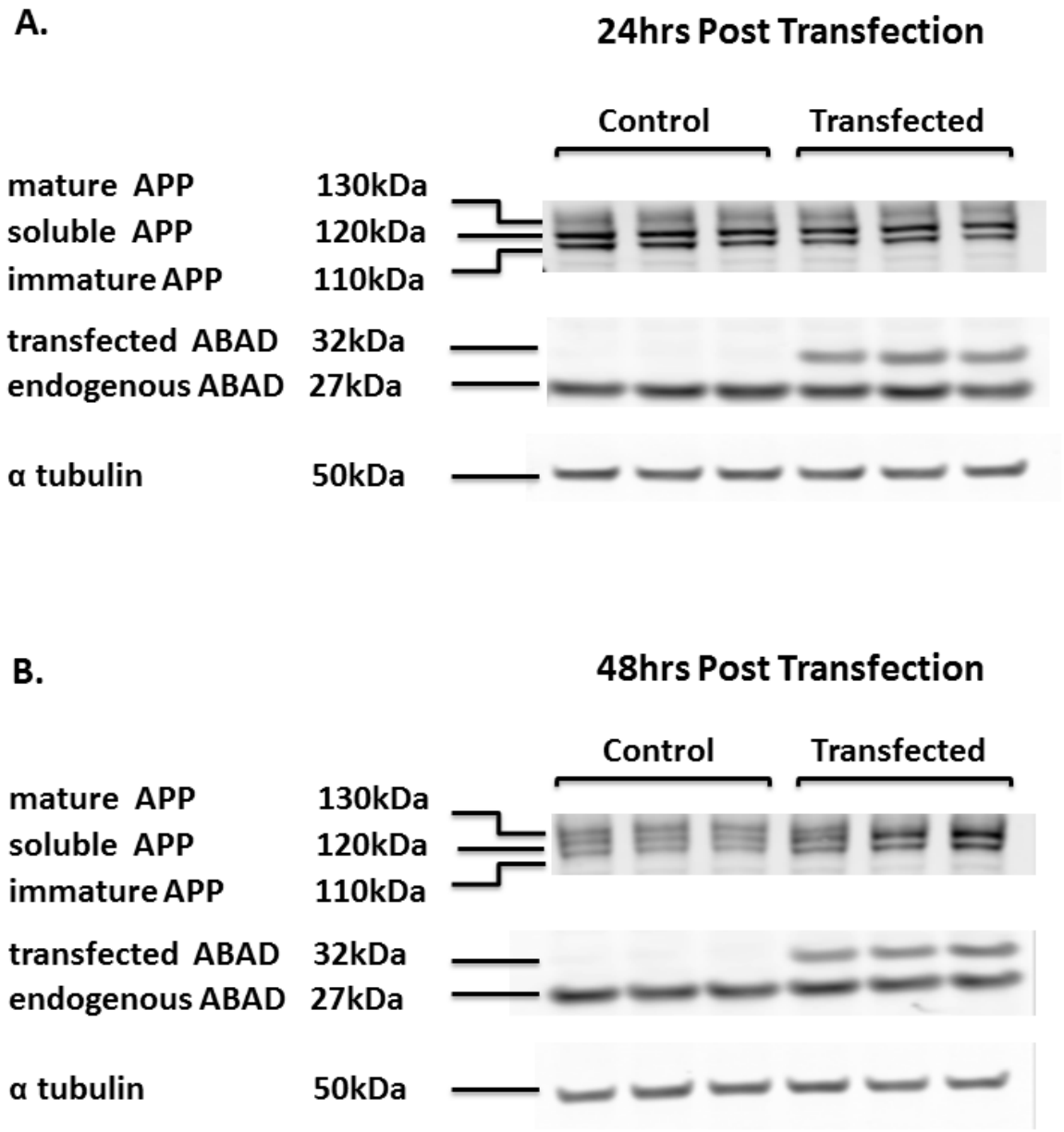

Figure 5.4: Pilot ABAD transfection data. A. At 24h post transfection there is no effect of ABAD overexpression on mature, soluble or immature APP. **B.** At 48h post ABAD transfection, the mature APP band appears to be lost, with increased levels of soluble and immature APP in two of the three transfected samples. **(**n = 3 in each condition).

5.3.4 Main Study: The Changes in APP Induced by ABAD Overexpression in the Pilot Study are not replicated in Separate ABAD Transfected Samples

The results from the pilot study of reduced mature APP and increased soluble and immature APP following 48h of ABAD overexpression failed to be reproduced in a replicate experiment using increased numbers of samples (n = 5 per group) and more rigorous controls (cells transfected with an empty pCMV6-ENTRY vector) (Figure 5.5).

5.3.5 The Mitochondrial Associated Membrane is Present in SH-SY5Y cells and is affected by Metabolic Stress

Electron microscopy analysis shows evidence of endoplasmic reticulum – mitochondrial interactions occurring in SH-SY5Y cells. Under mild and moderate metabolic stress (3- and 9h OGD, respectively), the number of cells displaying ER – mitochondrial interactions is significantly decreased (Chi-Square, $p<0.01$). Following 18h OGD, the occurrence of the ER – mitochondrial interaction increases, returning to comparable levels to those seen in control cells (Figure 5.6).

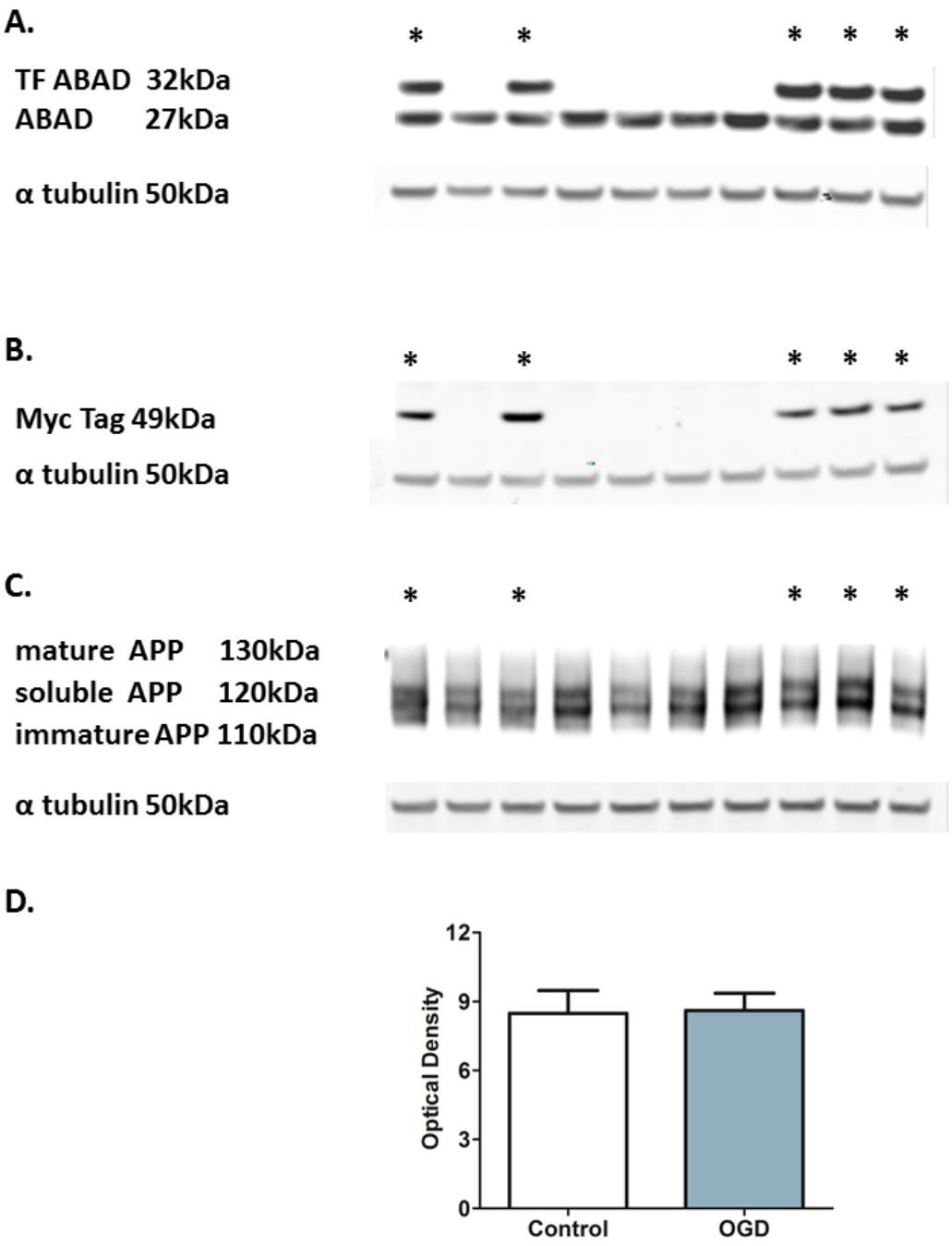

Figure 5.5: ABAD transfection data. **A.** ABAD is successfully overexpressed in the five transfected samples, with endogenous ABAD unaffected by the transefection process. **B.** The up-regulation of ABAD in confirmed by the presence of the myc tag in the ABAD overexpressing samples**. C.** Two bands of APP are detected across transfected and mock transfected samples suggesting the vector transfection affects APP levels. **D.** Densitometry analysis of total APP shows no effect of ABAD overexpression on APP, compared to mock transfected controls. **(**n = 5 in each condition).

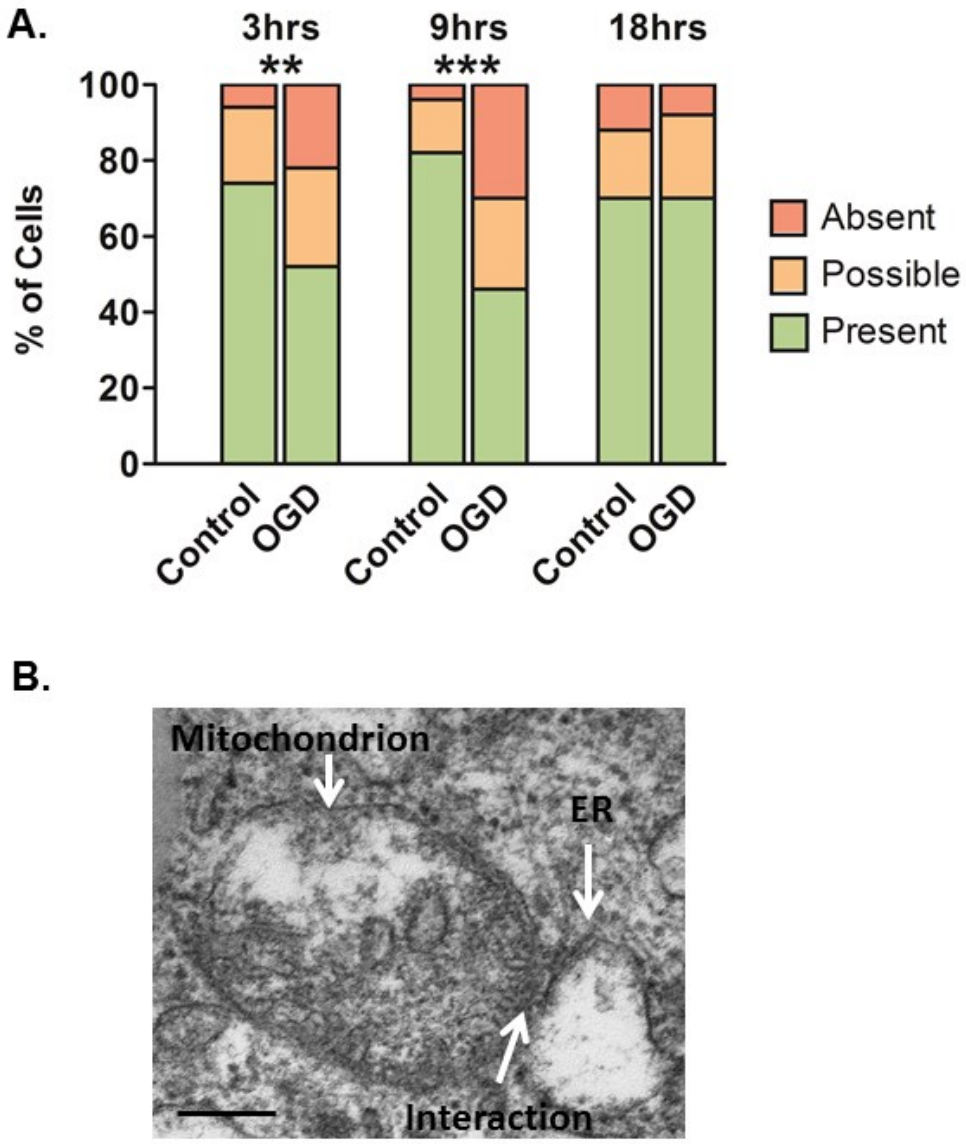

Figure 5.6: The presence of the mitochondrial associated membrane (MAM) is affected by OGD induced metabolic stress. **A.** OGD induces significant decreases in the number of cells showing presence of MAM. The presence of MAM was categorised as "absent", "possible presence" and "present". (** $p<0.01$, *** $p<0.0001$, X^2, n = 50 cells for each condition) **B.** Representative electron micrographs of the MAM in SH-SY5Y cells. Scale bar = 0.1µm.

5.4 Discussion

Chapter 3 identified ABAD to be significantly up-regulated in response to prolonged metabolic stress (18h OGD). Chapter 4 then found ABAD to interact with proteins involved with endoplasmic reticulum – Golgi transport and vesicle mediated transport. In addition to interactions with protein trafficking proteins, ABAD was also shown to interact with GRP75, a protein enriched at the MAM, following OGD. The MAM has recently been shown to contain presenilin proteins involved in the proteolytic cleavage of APP. The synchronised location of APP and ABAD at various sites throughout the cell led to the hypothesis that OGD, and the resulting increase in ABAD protein expression, might have an effect on the expression levels and processing of APP.

Consistent with the first part of the working hypothesis, a significant decrease in APP expression was detected following 18h OGD. The antibody used in this study detects three APP isoforms: immature ~110kDa, sAPP ~120kDa and mature APP ~130kDa. The abundance of all three of these APP isoforms was significantly decreased following 18h OGD.

On the basis of the significantly decreased APP expression with OGD treatment, immunoprecipitations were used to probe for a possible interaction between ABAD and APP. Exposing a direct interaction between these two proteins would provide invaluable insight into a novel mechanism underpinning the APP reduction. However, these IP experiments failed to detect a direct interaction between the APP and ABAD proteins. Repeating this experiment with a reverse co-IP would strengthen the conclusion that APP and ABAD do not directly interact. The lack of direct interaction between APP and ABAD does not rule out the possibility that increases in ABAD following OGD may lead to decreased expression of APP. ABAD is an enzyme with a broad array of substrates, including 17β-estradiol (Du Yan et al., 2000). Indeed, in a study involving the

application of physiological concentrations of 17β-estradiol to R-75-1 human breast carcinoma cell (a cell line containing a high level of oestrogn receptors), the amount of the amino-terminal cleavage product of APP (soluble APP) was significantly increased in the culture medium (Jaffe et al., 1994). This result indicates that the substrates of ABAD can have a significant effect on APP processing. Therefore, despite the lack of direct interaction of ABAD and APP, the significant increase in ABAD protein following OGD may still indirectly affect the expression level of APP.

The potential for an indirect action of ABAD on APP processing led to the study of the possible effect of increased ABAD expression on APP. The pilot data was promising, appearing to show a change in ratio between mature, soluble, and immature APP. The mature APP isoform is lost in two of the three ABAD over-expressing samples, with the sAPP and immature APP appearing to be to be darker, indicative of increased amounts of these isoforms.

Regrettably however, the pilot results failed to be reproduced in a more extensive transfection study involving increased sample numbers and more rigorous control (control cells were transfected with an empty TrueOrf origene vector Figure 2.2). In this study, only two clear APP bands were detected across all samples as opposed to the previously detected three bands. This result suggests that the transfection process produces experimental artefacts that alter the expression of endogenous APP, and highlights the importance of rigorous experimental controls to avoid false interpretations of experimental artefacts. Repeating the western blots on a lower percentage gel might separate the APP isoforms more effectively, providing further insight as to which of the isoforms has been lost as a result of the experimental intervention.

It is therefore concluded that the ABAD overexpression seen in response to 18h OGD does not directly affect the expression or processing of APP. There must therefore be other important processes that are initiated under conditions of metabolic stress that mediate the observed decrease in APP levels.

Of major importance to AD research, the decrease in APP may be attributable to an increase in proteolytic cleavage, either via the amyloidogenic or non-amyloidogenic pathway. The proteomic data collected in Chapter 3 sheds little light on whether either of these APP proteolytic processing pathways is activated following 18h OGD. However, research from other groups has shown a significant decrease in α-secretase enzume ADAM10 following 8h OGD in SH-SY5Y cells, with no change in β-secretase BACE1 enzyme activity or expression, and a significant increase in γ-secretase activity (Lee et al., 2006). Similar studies investigating the expression and activity of the APP secretase enzymes in our OGD cell culture, along with assessment of Aβ levels, would clarify the potential role of APP proteolytic processing in the observed APP down-regulation following 18h OGD.

Autophagy could be another possible process accounting for the decreased APP expression following 18h OGD. Autophagy describes the process by which cellular constituents are targeted to lysosomes for degradation. APP at the plasma membrane is endocytosed, where it is either amyloidogenically processed in the endocytic organelles, recycled back to the plasma membrane, or degraded in lysosomes (Haass et al., 2012). The electron microscope data described in Chapter 3 identified the presence of autophagosomes in the SH-SY5Y cells, however the number of autophagosomes was not altered in response to OGD, suggesting this route of APP degradation may not be the prime cause of the decreased APP expression seen here following 18h OGD. Repeating the OGD study in the presence of autophagy inhibitors would clarify this data.

Alternatively, the ubiquitin - proteasome protein degradation pathway may be another possible mediator of the APP down-regulation following 18h OGD. Ubiquitination involves a sequence of enzymatic reactions including ubiquitin-activating enzyme (E1), ubiquitin-conjugating enzyme (E2), and ubiquitin-protein ligase (E3). Research has shown that F-box and leucine rich repeat protein2 (FBL2) (part of the E3 ubiquitin complex) interacts with APP, mediating its ubiquitination and subsequent proteasomal degradation (Watanabe et al., 2012). The proteomic characterisation of SH-SY5Y cells described in Chapter 3 identified significant increases in 26s proteasome proteins, with *Protein Folding and Degradation* being a significant interactome identified by Ingenuity Pathway Analysis. It is therefore possible that the significant decreases in APP following OGD might be due to ubiquitin - proteasome protein degradation.

The lack of effect of ABAD overexpression on APP protein levels in the present study is disappointing. However, the data presented here is by no means futile. The results from the transfection experiments show SH-SY5Y cells to be capable of successful ABAD over-expression, with almost 50% transfection efficiency at 24h. This data provides a solid basis for further investigative studies into the mitochondrial and cellular dysfunction associated with ABAD overexpression in AD.

Using the proteomic data described in the previous chapters as a hypothesis generator, a logical next experiment would be to investigate whether ABAD overexpression has any effect on the significant down-regulation of CDK5RAP2 seen following 18h OGD. ABAD is shown to interact with CDK5RAP2 under control conditions, however following OGD, this interaction is lost, ABAD is significantly up-regulated, and CDK5RAP2 is significantly down-regulated (Figure 4.13,). CDK5RAP2 affects the localisation and substrate specificity of cyclin-dependent kinase-5 (Cdk5), a protein involved in tau hyperphosphorylation and aggregation (Kraemer et al., 2011, Noble et al.,

2003). Following up this line of research in the ABAD overexpressing cells might therefore provide insight into potential links between the ABAD protein and tau pathology, two important elements in cellular dysfunction related to AD.

An important finding from the previous chapter was that following OGD, ABAD interacts with GRP75, a protein enriched at the MAM (Figure 4.14). This result was confirmed in human control and AD tissue. Confocal microscopy showed the ABAD – GRP75 colocalisation to have a significantly more punctate appearance along the surface of the lacy GRP75 stained mitochondria, possibly indicative of the distinct colocalisation of these proteins at the MAM.

Based on these findings, electron microscopy was used to assess the effect of mild, moderate and severe OGD on the mitochondrial associated membrane. Following mild (3h OGD) and moderate (9h OGD) metabolic challenge, the number of cells showing evidence of MAMs was significantly decreased compared to time matched controls (Chi-Square, $p<0.01$).

The dynamic nature of the MAM suggests it is responsive to changes in the cellular environment. In addition to Ca^{2+} homeostasis, the MAM is also involved in cholesterol metabolism, with acyl-CoA:cholesterol acyltransferase (ACAT) being highly enriched in this membrane region (Hayashi et al., 2009). Cholesterol homeostasis is important for cell survival as accumulation of free cholesterol can be toxic to cells. To prevent accumulation and toxicity, ACAT converts cholesterol to cholesterol esters, are then exist within lipid droplets in cells (Chang et al., 2006). However, ACAT mediated cholesterol esterification requires ATP as a cofactor (Chang et al., 1997), therefore under conditions of low ATP availability, this process may be shut down. The reduction in presence of MAM, as evidenced by electron microscopy, may well be an ultra-structural change designed to discontinue cholesterol esterification, thus conserving ATP.

Research shows cholesterol processing to be aberrant in AD. Circulating total cholesterol and cholesterol esters in the brain are increased in AD patients, but the reasons for these changes are unknown (Schon and Area-Gomez, 2013). Further characterisation of the ACAT enriched MAM and its alterations under conditions of metabolic stress might therefore provide further insight into the cholesterol changes that are linked to AD.

The MAM also plays a key role in ER – mitochondrial Ca^{2+} crosstalk, with the close proximity of the ER – mitochondrial membranes allowing Ca^{2+} released from the ER to be directly taken up into the mitochondria. Mitochondrial Ca^{2+} levels are important in regulating many cellular functions, including ATP production and cell death (Patergnani et al., 2011). Prolonged increases in mitochondrial Ca^{2+} causes the mitochondrial permeability transition pore (PTP) to open, a crucial step in the process of apoptotic cell death (Kim et al., 2003). It might therefore be hypothesised that the recovery of MAM abundance to control levels following 18h OGD may be part of an apoptotic mechanism to initiate programmed cell death following severe metabolic challenge.

The enrichment of presenilins at the MAM, the interaction and colocalisation of ABAD to important MAM proteins, the role of the MAM in cholesterol homeostasis, and the adaptive nature of the MAM under conditions of metabolic stress all suggest that this protein enriched membrane region may have an important role to play in AD. If indeed the decrease in APP described in the present chapter is due to amyloidogenic proteolytic processing, then the ABAD – GRP75 – MAM hypothesis of mitochondrial dysfunction described in Chapter 4 may well be valid. This hypothesis suggests that following prolonged OGD, ABAD localises to the MAM via its interaction with GRP75. BACE-1 cleaved APP may also then localise to the MAM following OGD, where it is further cleaved by presenilins to form Aβ. These Aβ peptides then interact with ABAD and are transported into the mitochondria, inducing the mitochondrial dysfunction that is characteristic of both metabolic stress and AD.

The biochemical basis for the significant reduction in APP processing following OGD treatment remains to be elucidated. Furthermore, future studies involving MAM fractionation followed by western blotting for ABAD protein enrichment, both before and after OGD treatment, would help to test the proposed hypothesis. Additionally, blocking the interaction of ABAD and GRP75, and monitoring the effect this intervention has on the OGD induced mitochondrial dysfunction, would functionally validate the importance of this novel protein interaction.

Chapter 6: Discussing the Utility of the Present Studies and Future Proteomic Investigations in enhancing our Understanding of Alzheimer's disease

6.1 Reviewing the research findings and their impact on our understanding of Alzheimer's disease

Epidemiological studies have identified vascular disorders inducing a state of chronic cerebral hypoperfusion to be important risk factors for late-onset AD (Breteler, 2000), however the underlying biological mechanisms for this remain elusive. The aim of the present research was to establish the proteomic basis of cellular dysfunction under conditions of metabolic stress, and determine whether the detected protein changes can provide insight into how chronic cerebral hypoperfusion might be linked to AD.

6.1.1 Chronic metabolic stress induces mitochondrial protein changes that are also seen in post-mortem Alzheimer's disease brains

A major limitation of AD research is that biochemical investigations of the human brain are limited to post-mortem tissue analysis. Beyond the general limitations of working with human tissue (homogeneity of samples, protein degradation, and limitations of experimental controls), there is the overriding yet unavoidable drawback that this is dead tissue at the end-stage of the disease. Proteomics research on such tissue is useful in identifying end-stage biomarkers, but has limited utility in uncovering the underlying causes of cellular dysfunction. However, the value of these post-mortem AD proteomics studies is greatly enhanced when interpreted in conjunction with an investigative intervention study, such as oxygen-glucose deprivation (OGD) proteomics study presented in this thesis.

OGD is an established *in vitro* model of chronic cerebral hypoperfusion, where the experimental conditions and can be tightly controlled to produce exceptionally reproducible proteomic data. The initial study presented here identified proteins involved in mitochondrial energy production, protein folding, and protein degradation to be significantly altered in response to OGD. For example, specific protein changes were detected within the electron transport chain, consistent with the significant mitochondrial dysfunction recorded following OGD treatment. Increases in abundances were seen in proteins from complex I and complex V, and significant decreases found in complex III proteins. These bidirectional protein changes demonstrate a direct link between disrupted oxygen and glucose delivery to cells and the alterations in mitochondrial function that are common in AD.

Not only are these protein changes important in uncovering potential causes of mitochondrial dysfunction under conditions of metabolic stress, but also they extend our understanding of mitochondrial dysfunction in AD. Post-mortem analysis of AD brain tissue identifies a decrease in ETC complex III, however the causes of this reduction were, until now, unknown. The present proteomics study provides direct evidence for a reduction in cellular oxygen and glucose delivery to cause a down-regulation of complex III subunits. It is therefore feasible that the vascular disorders that are known to be risk factors for AD induce a state of chronic cerebral hypoperfusion, disrupting the delivery of oxygen and glucose to neurons, thus driving the decrease in complex III expression found in post-mortem AD brains. The present research has therefore extended our understanding of the proteomic basis of mitochondrial dysfunction in response to OGD, which is directly relevant to the mitochondrial protein changes seen in AD.

However, further work clearly needs to be undertaken in order to fully elucidate the mechanisms underpinning these mitochondrial protein changes. Individual activity of each mitochondrial complex would provide further insight as to the functional relevance of the described up- and down-regulated proteins. Furthermore, the IPA network analyses described in Chapter 3 identify many novel putative protein – protein interactions. Future work validating and interrogating the role of these interactions in the altered ETC proteins would potentially uncover novel sites of intervention to avert the mitochondrial dysfunction under conditions of metabolic stress.

6.1.2 Chronic metabolic stress induces the endoplasmic reticulum stress response: implications for proteostasis mechanisms in Alzheimer's disease

Mitochondria clearly play an important role in both normal cell function and in the dysfunction associated with AD. However, AD is primarily thought of as a disease associated with protein misfolding and aggregation, with amyloid plaques and tau tangles considered key hallmarks of the disease. Cellular proteostasis is maintained through the normal functioning endoplasmic reticulum. Understanding the proteomic basis of endoplasmic reticulum function and the response of ER proteins to reduced oxygen and glucose environments is therefore integral to understanding how vascular risk factors might be linked to AD.

The ER stress response (also known as the unfolded protein response, UPR) is an ER mediated process involved in clearing misfolded proteins and returning the cell to a state of proteostasis (Scheper et al., 2011). Two central molecular chaperones, GRP78 and GRP94, involved in the early and late stages of the UPR respectively, were significantly up-regulated following OGD, indicative of the initiation of the UPR in response to metabolic stress. Concurrent with this proteomic data, electron microscopy images show swelling of the endoplasmic reticulum lumen following OGD. Enlarged endoplasmic reticulum can accommodate more unfolded proteins, with the larger area reducing the risk of aggregation of protein intermediates (Bernales et al., 2006). Therefore, both proteomic and morphologic data show that cellular deprivation of oxygen and glucose initiates the UPR.

The described UPR activation under cellular stress conditions is not in itself novel. However, what is unique about the present system is that the cells undergo periods of chronic oxygen and glucose depletion in the absence of cell death. It would therefore be worth investigating whether the activation of the UPR is serving to avert the cellular dysfunction and ultimate cell death that would normally be associated with an accumulation of misfolded proteins under conditions of cell stress.

Once again, consideration of this UPR proteomic data alongside animal and human AD studies serves to advance our understanding of how vascular risk factors might be linked to AD. In our *in vitro* model of chronic cerebral hypoperfuson, the UPR is activated to deal with the accumulation of damaged proteins casued by metabolic stress. It is therefore hypothesised that this UPR activation plays an important part in averting cell death within our system. The same may well be true in AD. Age associated vascular risk factors can reduce cerebral blood flow, and therefore oxygen and glucose delivery to the brain, over many years. This will gradually cause a build-up of damaged and

misfolded proteins that are dealt with through a functioning UPR. Data acquired from mice studies shows evidence of decreased expression of UPR proteins with advancing age (Naidoo et al., 2008). This age associated decline in expression of UPR proteins, alongside a continued state of cerebral hypoperfusion, would lead to a build-up of damaged and aggregating proteins, causing increased cellular stress, and eventually neurodegeneration.

Clearly more work needs to be undertaken to validate this hypothesis. However, it is clear that the proteomic data gained from the present research has provided a feasible hypothesis that may significantly advance our understanding of how vascular risk factors are linked to protein aggregation and AD.

6.1.3 ABAD protein: the link between vascular risk factors and Alzheimer's disease?

Amyloid binding alcohol dehydrogenase (ABAD) was significantly increased following severe metabolic challenge. ABAD is emerging as an important player in mitochondrial dysfunction and AD. The second phase of research reported here used protein immunoprecipitation coupled to LC-MS to identify many novel ABAD protein interactions under control and OGD conditions. Functional analysis showed ABAD and its interacting partners to be involved in glucose metabolic processes, cell redox homeostasis and RNA processing. ABAD was found to interact with important proteins already linked to neurodegeneration, a result which implicates ABAD as a potentially important link between metabolic stress and AD.

A limitation of the ABAD protein interactions are studied in homogenised tissue, potentially resulting in the generation of non-physiologically relevant protein interactions. Additionally, the ABAD protein interactions are seen in isolation, without consideration of the subcellular compartments or the many competing protein interactions that occur within intact cells. Moreover, in the example of the ABAD – GRP75 interaction, colocalisation analysis only shows the proteins to be located in the same subcellular region, and is not indicative of direct protein interactions.

A more informative future study would be to use ffluorescence lifetime imaging microscopy (FLIM), a technique based on Förster resonance energy transfer (FRET). Fluorescence lifetime is the amount of time a molecule spends in an excited state before returning to ground state, with the release of a photon. FRET describes the transfer of energy from the excited state molecule to another nearby molecule, which usually occurs over distances less than ~10 nm (Sun et al., 2011). FRET therefore provides a sensitive tool for investigating protein – protein interactions in living cells that would be useful in further validation of the ABAD – GRP75 interaction. However, there are limitations associated with this technique. For example, the large size of fluorescent protein tags can interfere with the protein – protein interaction of interest, thus risking the creation of false negative data. Similarly, it is possible that the fluorescent tags might interact with each other, therefore creating false positive data (Piston and Kremers, 2007). These factors need to be carefully considered and the appropriate control experiments undertaken in any research utilizing FRET to study protein – protein interactions.

6.1.4 Assessing the utility of proteomics as a hypothesis generator in researching the vascular basis of Alzheimer's disease

In the present study, the interaction of ABAD with proteins involved in the endocytic pathways and at the mitochondrial associated membrane (MAM) (both of which have been linked to the amyloidogenic processing of APP) led to the hypothesis that metabolic stress and the overexpression of ABAD may impact on the proteolytic cleavage of APP. The experiments in the final data chapter found OGD to significantly reduce APP protein levels within SH-SY5Y cells. Unfortunately, the hypothesis that an overexpression of ABAD might be involved in this decrease in APP expression was not confirmed. It might therefore be concluded that the utility of proteomics as a hypothesis generator is limited in this case. However, the proteomic data also implicated the MAM as a possible player in the cellular response to metabolic stress. This result was confirmed in the adaptive response of the MAM detected under conditions of metabolic stress with electron microscopy, providing tangible evidence of the utility of proteomics in meaningful hypothesis generation.

In the wider research field, the utility of proteomics in enhancing our understanding of the vascular risk factors associated with AD greatly depends on the tissue and the models being investigated. Quantitative LC-MS in cortical samples of AD brains identified 197 proteins to be significantly altered in abundance compared to control brain samples. These proteins were involved in various processes including regulation of protein phosphorylation, lipid metabolism, energy production, and cell death (Andreev et al., 2012). The identification of proteins involved in energy production suggests some level of metabolic challenge, but with the high variability and co-morbidities in human brain samples it is difficult to pinpoint specific causes of individual protein changes. Moreover, proteomic data from post-mortem tissue provides little insight into the potentially modifiable disease processes occurring early in disease onset.

A further complexity in the use of proteomics to identify biomarkers of AD comes from the difficulty in identifying appropriate, healthy, aged-matched control tissue. The nature of neurodegeneration in AD is that cellular dysfunction and disease processes evolve over time. It is therefore impossible to predict whether an individual's brain tissue represents a true "healthy" control rather than simply being at an earlier stage in the neurodegenerative process.

As an alternative to the use of human tissue for research into the proteomic basis of AD, animal models can be developed to extend our understanding of the cellular changes occurring in the earlier stages of AD progression. For example, proteomic analyses of APP/PS-1 double transgenic mice at 9 months (prior to Aβ deposition) and 12 months of age (post Aβ deposition) have been used to model the earlier and later stages of AD. Many of the significantly altered proteins were involved in energy production pathways, most pertinently being the bidirectional change in ATP synthase subunits, which were decreased in the younger Tg mice and increased in the older Tg mice (Robinson et al., 2011).

In addition to the Tg mouse models of AD, numerous models of reduced cerebral blood flow exist that would allow the effect chronic cerebral hypoerfusion (CCH) on the brain to be directly analysed with proteomics. Despite the existence of these useful animal models of CCH, relatively few large scale proteomics-based studies have been conducted with them. Future proteomics studies using these animal models will certainly be complementary to the various studies completed on human tissues and in cell culture. However, it may be still challenging to draw direct parallels between the different proteomic data sets. Indeed, each cell culture, human and animal model have their strengths and weaknesses, and the most useful strategy going forward will be to use combinations of models and techniques to study the disease processes involved in AD.

6.2 The extent to which LC-MS proteomics can advance our understanding of Alzheimer's disease greatly depends on appropriate experimental design and data handling strategies

The experimental evolution of this thesis, from large-scale LC-MS research to focussed analysis of ABAD – APP processing, provides evidence that proteomics can advance our understanding of the biological processes linking vascular risk factors and AD. The success of this proteomic research is largely dependent on the level of experimental rigour upstream of LC-MS, and the down-stream data analysis strategies. In numerous other proteomic studies, fundamental weaknesses and arbitrary design decisions are present, which skew the interpretation of the proteomic data, and potentially produce misleading results. In order to assess whether LC-MS proteomics can truly provide insight into the biological mechanisms underlying AD, it is important to critically appraise the current accepted protocols of LC-MS data acquisition and analysis.

6.2.1 Assessing the reproducibility of LC-MS protein detection

If proteomic studies are to provide insight into complex biological mechanisms, the LC-MS platform itself has to be highly reproducible in the detection of protein abundance. The design of the human cell line *in vitro* study provides a unique opportunity to examine internal variability of the LC-MS system. SH-SY5Y cells were exposed to OGD for a short duration (6h) and a longer duration (18h). Linear regression analysis of the control data from this study demonstrates the high technical reproducible the LC-MS system between samples (Figure 6.1). The effect of abundance on the reproducibility of protein detection was analysed using the *in vitro* proteomic data. It is generally accepted that lower abundance proteins are less reproducibly detected than higher abundance proteins(Wang et al., 2010). Our data shows that the lowest abundance proteins do indeed show a slight increase in detection variability, however the effect is small, with the r^2 value calculated as 0.145 (Figure 6.1).

6.2.2 Considering the trade-off between reducing variance and the number of proteins remaining for analysis

The first common step in proteomic data dissection is exclusion of proteins identified with fewer than two peptides. Though seemingly arbitrary, this exclusion criterion is important for two reasons: firstly, removal of 1-peptide proteins increases the security of the LC-MS data to identify true protein levels and avoid false detections. A single peptide feature may be found in several different proteins or protein isoforms, therefore a truly definitive identification is less likely (Mallick and Kuster, 2010). Secondly, this cut-off significantly reduces the variance within the dataset, increasing the power to detect subtle protein changes, as demonstrated through the analysis of contemporaneous cell culture and mouse model LC-MS data (Figure 6.2). However, there is clearly a trade-off between reducing variance and the number of proteins remaining for analysis. Extending the inclusion criterion to identification of proteins with 3 or more peptides further reduces variance, however also drastically reduces the number of proteins available for further analysis by nearly half of those originally identified by 1 peptide.

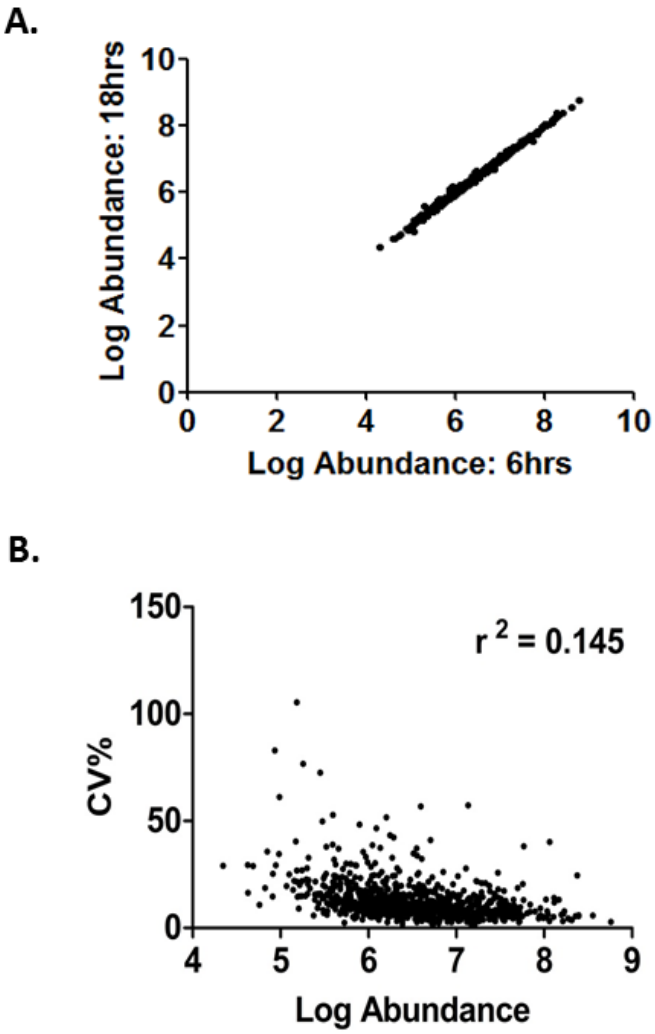

Figure 6.1 LC-MS protein detection is highly reproducible with protein abundance having minimal effect of detection. A. The mean protein abundances from control cohorts from the 6hr and 18hr OGD experiments were plotted against together to demonstrate the reproducibility of protein quantitation using LC-MS technology. **B.** Lower abundance proteins are detected with higher variability across control samples than higher abundance proteins, however the overall effect of this variability is modest, $r^2 = 0.145$.

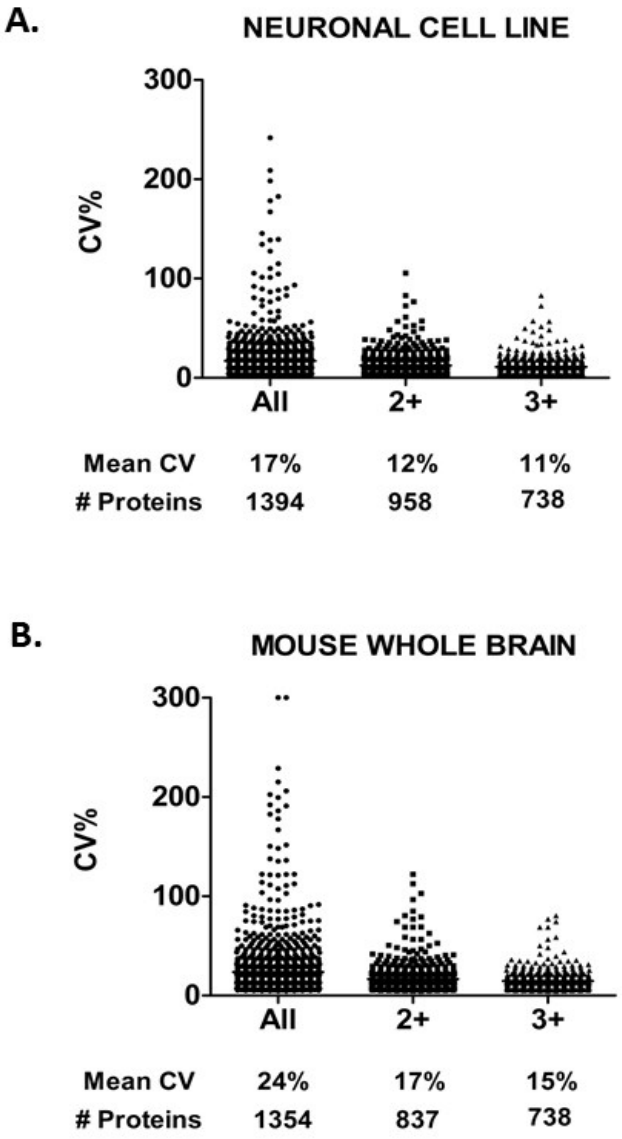

Figure 6.2: 2+ peptide identification inclusion criteria reduces variance. Increasing the number of peptides used to identify a protein increases the confidence of the identification, reduces the number of proteins available for statistical analysis and reduces variance. **A.** Using the common inclusion criteria of proteins identified with at least 2 peptides reduces the mean variance from 17% to 12% in the *in vitro* cell line model of CCH. **B.** Similarly, the same inclusion criterion applied to mouse whole brain proteomic data reduces the mean variance from 24% to 17%. More stringent inclusion criteria of proteins identified with 3 or more peptides has minimal effect on the overall variance of the data set, with a reduction of 1% and 2% in the cell line and whole brain respectively. All data shown for control groups. Mouse whole brain neuroproteomic data was generously made available for analysis by Dr JL Searcy.

6.2.3 Upstream tissue processing is associated with increases in variance structure, limiting the ability to detect subtle protein changes

Understanding the sources of variance in protein detection is important in order to allow experimental steps to be taken to limit this variance and increase the ability to detect small protein changes. Sample processing techniques including microvessel dissection (Hartz et al., 2012), mitochondrial enrichment (James et al., 2012a) or synaptosomal fractionation(Ansari and Scheff, 2010) can be used upstream of proteomic analysis to provide a more detailed proteomic profile of how individual cell types and subcellular compartments are affected by different experimental conditions. However, by increasing technicality upstream of protein detection, the variance of the final dataset is also increased, as demonstrated by the analysis of proteomic data generated after a range of brain region dissection and fractionation techniques had been employed (Figure 6.3). These data demonstrate that intricate upstream tissue handling techniques leads to larger coefficients of variance, with up to 20% increases in variance in the most technically demanding studies compared to whole brain homogenates. Adding value to biological research through upstream tissue processing is beneficial in answering specific biological questions, however the effect of the associated increases in variance structure needs to be considered: more subtle protein changes are likely to be undetectable within highly variable systems.

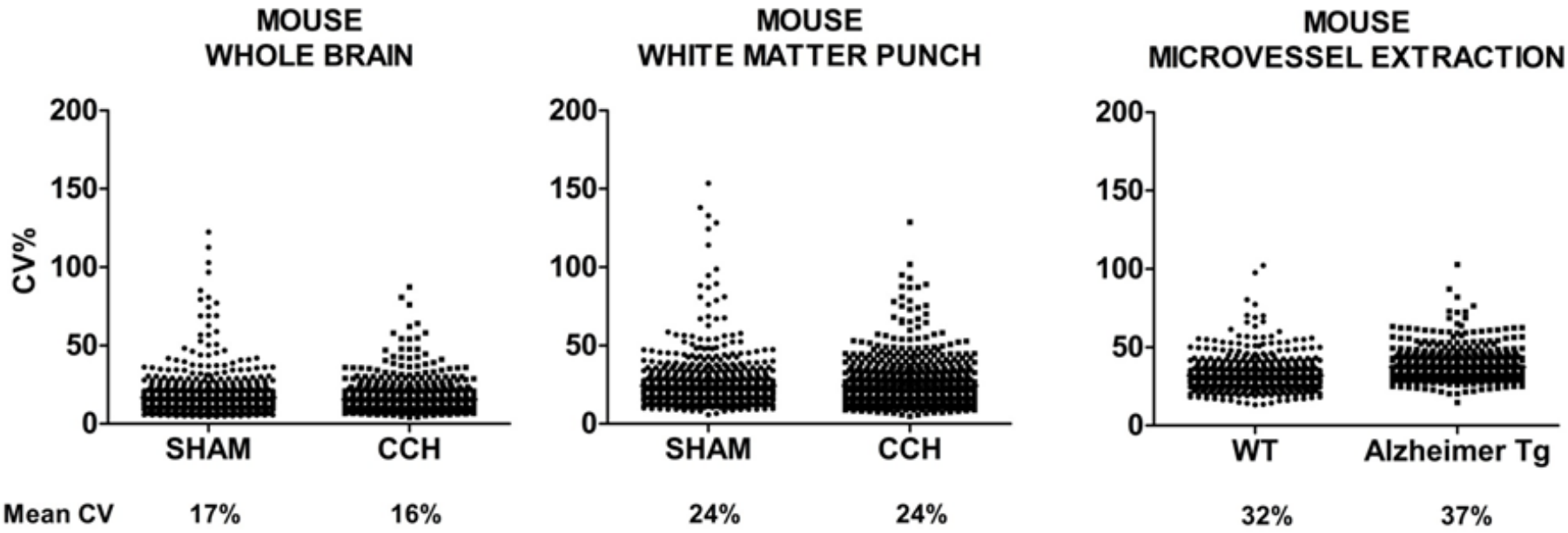

Figure 6.3. More complex tissue processing techniques increase variance. Whole brain tissue samples show practically identical coefficients of variance in both sham and CCH (14% and 13% respectively). White matter dissection introduces more variance into the system (20% and 21% for sham and CCH respectively). Technically demanding techniques such as microvessel dissection further increase variance (32% and 37% in WT and Tg mice respectively). Independent variables (surgery or transgene) had little effect on the coefficient of variance. Mouse neuroproteomic data was generously made available for analysis by Dr JL Searcy.

6.2.4 Fold change is a misleading and inappropriate inclusion criterion in proteomic studies, excluding important proteins from data analysis

In addition to the number of peptides used for identification, the magnitude of the detected change (fold change) is another popular inclusion / exclusion criteria used by researchers to dissect the huge data sets produced by LC-MS (Tiwari et al., 2012, Polisetty et al., 2012). The level of fold change that can reliably be detected within a given experiment can be deduced through simple *a priori* power calculations, based on number of replicates and an estimate of the variance. However, the nature of *a priori* power calculations means that without extensive pilot data, an estimate of variance needs to be made, which may or may not be appropriate to the specific study (where tissue type and sample processing upstream of LC-MS has a huge impact on variance structure). As a result, many published proteomic papers default to an inclusion criterion of a minimum 1.5 or 2 fold change, with no apparent explanation for the use of this value.

Analysis of the *in vitro* proteomic data shows protein fold change inclusion criteria to be misleading, inappropriate and risks the creation of many false negatives. In this *in vitro* study, the effect of global metabolic challenge on mitochondrial function and cellular proteomics was investigated. A total of 958 proteins were identified with 2 or more peptides. An a priori decision on statistical analysis dictated the use of a stringent significance threshold of $p<0.01$ for a protein change to be deemed significant, resulting in a final protein list of 193 significantly altered proteins. However, as well as a p-value threshold, many investigators also employ a fold change cut-off to rapidly identify the most "important" protein changes. Datasets with a low overall variance allow for the detection of subtle protein changes, however, employing an arbitrary fold change inclusion criterion such as the popular "minimum 1.5 fold change" on these low variance datasets excludes the subtle yet significant

protein changes. The fold change cut-off drastically reduces the number of proteins included in the final analysis and increases the risk of creating false negatives (Figure 6.4)

A similar analysis of the impact of arbitrary fold change cut-offs was carried out on the more variable microvessel extraction data (Figure 6.4). Due to the increased variability of these data (as shown in Figure 6.3), employing a stringent alpha value of $P < 0.01$ significantly reduces the number of proteins in the final list for analysis from 653 identified with two or more peptides to only 12. In this more variable system, imposing a 1.5 fold change cut-off has no further effect on protein number, due to a large fold change required to overcome the variance for inclusion at the set alpha level. It is therefore concluded that inclusion of a fold change data cut-off is either dangerous in the creation of false negatives (in studies with low overall variance) or irrelevant (in studies with high overall variance).

Alternatively, power calculations can be used to determine the magnitude of change required to detect a significant difference between two populations given the technical and biological variance (Levin, 2011). Used *a priori*, power calculations are beneficial in study design, guiding decisions regarding the number of replicates needed to obtain a set level of power (Bezeau and Graves, 2001). However, the nature of *a priori* power calculations means these calculations are based on an estimate of overall biological and technical variance. Our analysis reveals that the coefficient of variance is highly dependent upon the type of tissue being analysed and the degree of upstream tissue processing involved (Figure 6.3). Using a coefficient of variance that is not specific to the dataset to decide detectable fold change can be problematic, and could lead to an over- or underestimation of proteins found to be differentially expressed. To ensure maximum accuracy in *a priori* power calculations, extensive and specific pilot data should be obtained.

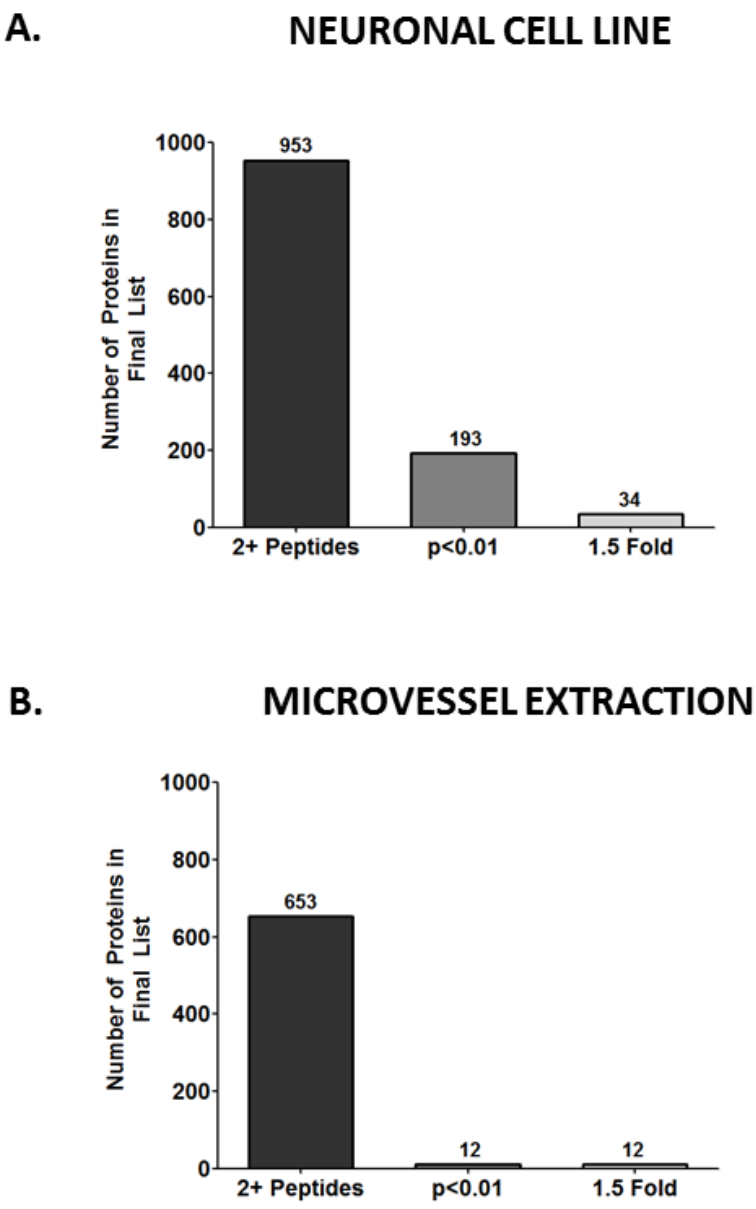

Figure 6.4: Arbitrary fold change cut-offs are associated with the increased likelihood false negatives. A. Employing the common "minimum 1.5 fold change" inclusion criterion on datasets with low overall variance drastically reduces the number of proteins available for analysis. A stringent alpha value of $p<0.01$ reduces the number of proteins in from 958 identified with 2 or more peptides to 193. Imposing an additional fold change cut-off of 1.5 on this reduced protein list results in a final list for analysis containing only 34 proteins. **B.** Analysis of the more variable microvessel enrichment data demonstrates that a stringent alpha value of $p<0.01$ reduces the number of proteins available for analysis from 653 identified with 2 or more peptides to only 12. Imposing a 1.5 fold change cut-off has no further effect on protein number, due to a large fold change required to overcome the variance for inclusion at the set alpha threshold. Mouse neuroproteomic data was generously made available for analysis by Dr JL Searcy.

The question of whether inclusion of fold change cut-offs in addition to a p-value adds any biological value to proteomic data remains. To assess this, we identified two key proteins involved in the endoplasmic reticulum stress response: glucose regulated protein 78 (GRP78) and glucose regulated protein 94 (GRP94). In our *in vitro* study, experimental intervention with the metabolic challenge of OGD saw significant up-regulation of both of these proteins ($p<0.01$). However, GRP78 underwent a fold change of 1.53, whereas GRP94 only had a fold change of 1.48 (Figure 6.5) (Herrmann et al., 2013a). The popular fold change cut-off of 2 would exclude both of these proteins from the analysis, and only GRP78 would be included if a fold change of 1.5 was used.

The interplay between these two proteins is integral to the endoplasmic reticulum stress response, however one or both of these proteins would be lost from the final dataset if an arbitrary fold change inclusion criterion was employed. Temporal evolution of protein level alterations is another important factor to be considered when elucidating complex protein pathways. Data from the *in vitro* study demonstrates that following 6h of OGD, small increases in protein levels of GRP78 and GRP94 predict larger increases following 18h OGD (Figure 6.5). These results suggest that protein fold change should not be used as threshold for inclusion, but rather as an indicator of evolving events occurring within the cell. A protein exhibiting a small fold change at an early time point can be indicative of increasing abundance that might be detected as significant at a later time.

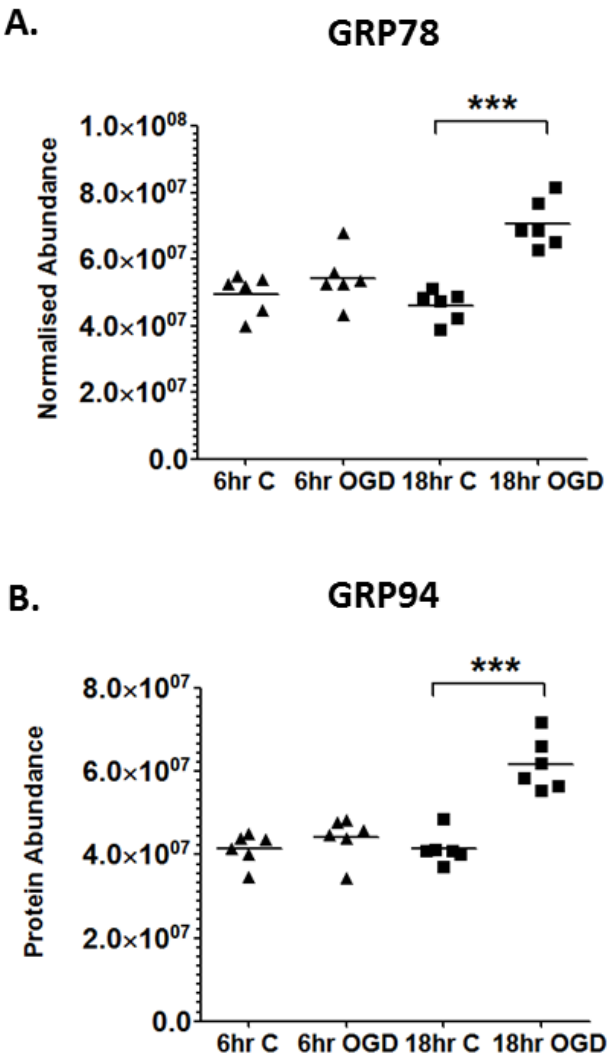

Figure 6.5: Conventional proteomic fold change inclusion criteria would exclude biological relevant proteins from further analysis. **A.** GRP78, a critically important protein in the endoplasmic reticulum stress response is significantly increased following a severe metabolic challenge (18h OGD), and undergoes a fold change increase of 1.53 from control to OGD samples. This protein would be included for further analysis in most proteomic studies **B.** Biologically related protein GRP94 is also significantly increased following a severe metabolic challenge (18h OGD) however undergoes a fold change increase of 1.48. This protein would be excluded from further analysis in most proteomic studies, demonstrating the arbitrary and irrelevant nature of fold change inclusion criteria. Each data point in **A** and B represent an independent biological replicate (n=6 for each condition, *** $p < 0.0001$, T-test).

The ability to detect a fold change at a particular level of significance is intrinsically linked to the variance of the data, and this variance is dependent on tissue source and processing techniques used. It is therefore misguided to include fold change in the initial stages of data dissection. A protein reaching the threshold set by a stringent p-value (which in its nature incorporates the variance and the magnitude of change) should be sufficient for the initial inclusion criterion, resulting in a much reduced but relevant list of protein changes (Figure 6.4).

The concept of excluding proteins based on fold change not only increases the likelihood of making type II errors, but is also fundamentally flawed, given that the biological relevance of a change in protein abundance is likely to be protein specific. For example, proteins in the Bcl-2 family are important evolutionarily conserved regulators of apoptosis. However, even within this family, certain proteins are more influential that others: PUMA (p53 up-regulated modulator of apoptosis) being one of the most potent (Yu and Zhang, 2008). Subtle changes in this protein are likely to have important cellular effects, however may be ruled out if stringent fold change cut-offs are employed when analysing data. The importance of subtle protein changes needs to be recognised in the analysis of large proteomic datasets to avoid the loss of valuable data through the use of inappropriate fold change cut-offs.

6.3 The future of proteomics in Alzheimer's disease research

The field of AD research is in desperate need of novel hypotheses as to the causes of cellular dysfunction and cognitive decline associated with this devastating disease. The research presented in this thesis demonstrates the utility of proteomics for this much needed hypothesis generation. The experiments evolved from a highly descriptive protein quantification study, through to the identification of interesting protein candidates that might link metabolic stress and AD, and finally to the development of a novel hypothesis relating ABAD protein, the MAM and APP processing.

The promise of novel proteomic based AD hypotheses is enhanced by the current evolution of proteomic research into its 3rd generation. 3rd generation proteomics will focus on investigating the spatial and temporal response of proteins, above and beyond simple protein identification and quantification. In order to achieve these aims and enhance the field of AD research, mass spectrometry based experiments will need to be carried out in combination with other experimental techniques.

Improved spatial resolution of proteomic data can be achieved through subcellular fractionation in advance of mass spectrometry. However, as discussed, fractionation methods are associated with increased variance within the final proteomic data set. Careful experimental design will therefore need to be undertaken in order to maximize the utility of such proteomic datasets in future AD studies.

Alternatively, advances in imaging techniques are making localization of proteins within cell or tissue samples highly effective. For example, the spatial resolution of light microscopy has been greatly advanced through the

development of array tomography. The ultrathin tissue sectioning used in this technique overcomes the limitations of axial resolution associated with standard confocal microscopy. Proteins of interest within these sections can be labelled with immunofluorescent antibodies and imaged at high resolution, even to the level of individual synapses (Kay et al., 2013). Employing array tomography in conjunction with hypothesis generating AD proteomic studies will increase the spatial resolution of novel protein biomarkers, greatly enhancing our understanding of specific proteins involved in AD pathogenesis.

In addition to high-resolution imaging, a host of experimental methods exist that could be used to investigate the functionality of novel protein biomarkers identified in AD proteomic studies. Electrophysiological investigations of native vs genetically manipulated cells can provide insight as to the role of proteins of interest in neuronal excitability. In addition, evolution of genetic manipulation technology, for example, by tetracycline-controlled transcriptional activation, allows the control of specific protein expression to be manipulated in living animals. This tool, in combination with discovery proteomics, would allow the function and effect of novel AD related proteins on animal phenotypes and behaviours to be examined.

In conclusion, the power of proteomics lies in its role as a hypothesis generator, and a tool for generating novel biomarkers and drug targets of disease. With the availability of a host of *in vitro* and *in vivo* AD models, and a wide range of complementary experimental technologies, proteomics is poised to make significant advances in our understanding of AD pathophysiology.

Data from this discussion are published in Proteomics
(Herrmann et al., 2013b)

REFERENCES

ALIEV, G., OBRENOVICH, M. E., SMITH, M. A. & PERRY, G. 2003. Hypoperfusion, Mitochondria Failure, Oxidative Stress, and Alzheimer Disease. *J Biomed Biotechnol,* 2003**,** 162-163.

ANDRADE, R., CRISOL, L., PRADO, R., BOYANO, M. D., ARLUZEA, J. & ARECHAGA, J. 2010. Plasma membrane and nuclear envelope integrity during the blebbing stage of apoptosis: a time-lapse study. *Biol Cell,* 102**,** 25-35.

ANDREEV, V. P., PETYUK, V. A., BREWER, H. M., KARPIEVITCH, Y. V., XIE, F., CLARKE, J., CAMP, D., SMITH, R. D., LIEBERMAN, A. P., ALBIN, R. L., NAWAZ, Z., EL HOKAYEM, J. & MYERS, A. J. 2012. Label-Free Quantitative LC–MS Proteomics of Alzheimer's Disease and Normally Aged Human Brains. *Journal of Proteome Research,* 11**,** 3053-3067.

ANDREU, C. I., WOEHLBIER, U., TORRES, M. & HETZ, C. 2012. Protein disulfide isomerases in neurodegeneration: from disease mechanisms to biomedical applications. *FEBS Lett,* 586**,** 2826-34.

ANSARI, M. A. & SCHEFF, S. W. 2010. Oxidative stress in the progression of Alzheimer disease in the frontal cortex. *J Neuropathol Exp Neurol,* 69**,** 155-67.

APETRI, A. C. & HORWICH, A. L. 2008. Chaperonin chamber accelerates protein folding through passive action of preventing aggregation. *Proceedings of the National Academy of Sciences,* 105**,** 17351-17355.

AREA-GOMEZ, E., DE GROOF, A. J., BOLDOGH, I., BIRD, T. D., GIBSON, G. E., KOEHLER, C. M., YU, W. H., DUFF, K. E., YAFFE, M. P., PON, L. A. & SCHON, E. A. 2009. Presenilins are enriched in endoplasmic reticulum membranes associated with mitochondria. *Am J Pathol,* 175**,** 1810-6.

ARRELL, D. K., ELLIOTT, S. T., KANE, L. A., GUO, Y., KO, Y. H., PEDERSEN, P. L., ROBINSON, J., MURATA, M., MURPHY, A. M., MARBÁN, E. & VAN EYK, J. E. 2006. Proteomic Analysis of Pharmacological Preconditioning. *Circulation Research,* 99**,** 706-714.

ARRIAGADA, P. V., GROWDON, J. H., HEDLEY-WHYTE, E. T. & HYMAN, B. T. 1992. Neurofibrillary tangles but not senile plaques parallel duration and severity of Alzheimer's disease. *Neurology,* 42**,** 631-9.

BADIOLA, N., PENAS, C., MINANO-MOLINA, A., BARNEDA-ZAHONERO, B., FADO, R., SANCHEZ-OPAZO, G., COMELLA, J. X., SABRIA, J., ZHU, C., BLOMGREN, K., CASAS, C. & RODRIGUEZ-ALVAREZ, J. 2011. Induction of ER stress in response to oxygen-glucose deprivation of cortical cultures involves the activation of the PERK and IRE-1 pathways and of caspase-12. *Cell Death and Dis,* 2**,** e149.

BALES, K. R., LIU, F., WU, S., LIN, S., KOGER, D., DELONG, C., HANSEN, J. C., SULLIVAN, P. M. & PAUL, S. M. 2009. Human APOE isoform-dependent effects on brain beta-amyloid levels in PDAPP transgenic mice. *J Neurosci,* 29**,** 6771-9.

BALLATORE, C., LEE, V. M. & TROJANOWSKI, J. Q. 2007. Tau-mediated neurodegeneration in Alzheimer's disease and related disorders. *Nat Rev Neurosci,* 8**,** 663-72.

BALOYANNIS, S. J. 2006. Mitochondrial alterations in Alzheimer's disease. *J Alzheimers Dis,* 9**,** 119-26.

BANDEIRA, N., PHAM, V., PEVZNER, P., ARNOTT, D. & LILL, J. R. 2008. Automated de novo protein sequencing of monoclonal antibodies. *Nat Biotechnol,* 26**,** 1336-8.

BANTSCHEFF, M., SCHIRLE, M., SWEETMAN, G., RICK, J. & KUSTER, B. 2007. Quantitative mass spectrometry in proteomics: a critical review. *Anal Bioanal Chem,* 389**,** 1017-31.

BARRON, A. M. & PIKE, C. J. 2012. Sex hormones, aging, and Alzheimer's disease. *Front Biosci (Elite Ed),* 4**,** 976-97.
BARTUS, R. T., DEAN, R. L., 3RD, BEER, B. & LIPPA, A. S. 1982. The cholinergic hypothesis of geriatric memory dysfunction. *Science,* 217**,** 408-14.
BEAL, M. F., HYMAN, B. T. & KOROSHETZ, W. 1993. Do defects in mitochondrial energy metabolism underlie the pathology of neurodegenerative diseases? *Trends Neurosci,* 16**,** 125-31.
BEAR, M., CONNORS, B. & PARADISO, M. 2007. *Neuroscience: Exploring the Brain*, Lippincott Williams & Wilkins.
BEGCEVIC, I., KOSANAM, H., MARTINEZ-MORILLO, E., DIMITROMANOLAKIS, A., DIAMANDIS, P., KUZMANOV, U., HAZRATI, L. N. & DIAMANDIS, E. P. 2013. Semiquantitative proteomic analysis of human hippocampal tissues from Alzheimer's disease and age-matched control brains. *Clin Proteomics,* 10**,** 5.
BELL, K. F., AL-MUBARAK, B., FOWLER, J. H., BAXTER, P. S., GUPTA, K., TSUJITA, T., CHOWDHRY, S., PATANI, R., CHANDRAN, S., HORSBURGH, K., HAYES, J. D. & HARDINGHAM, G. E. 2011. Mild oxidative stress activates Nrf2 in astrocytes, which contributes to neuroprotective ischemic preconditioning. *Proc Natl Acad Sci U S A,* 108**,** E1-2; author reply E3-4.
BELL, K. F. & HARDINGHAM, G. E. 2011. CNS peroxiredoxins and their regulation in health and disease. *Antioxid Redox Signal,* 14**,** 1467-77.
BELLOT, G., CARTRON, P. F., ER, E., OLIVER, L., JUIN, P., ARMSTRONG, L. C., BORNSTEIN, P., MIHARA, K., MANON, S. & VALLETTE, F. M. 2007. TOM22, a core component of the mitochondria outer membrane protein translocation pore, is a mitochondrial receptor for the proapoptotic protein Bax. *Cell Death Differ,* 14**,** 785-94.
BEN SAHRA, I., LAURENT, K., GIULIANO, S., LARBRET, F., PONZIO, G., GOUNON, P., LE MARCHAND-BRUSTEL, Y., GIORGETTI-PERALDI, S., CORMONT, M., BERTOLOTTO, C., DECKERT, M., AUBERGER, P., TANTI, J. F. & BOST, F. 2010. Targeting cancer cell metabolism: the combination of metformin and 2-deoxyglucose induces p53-dependent apoptosis in prostate cancer cells. *Cancer Res,* 70**,** 2465-75.
BERANOVA-GIORGIANNI, S. 2003. Proteome analysis by two-dimensional gel electrophoresis and mass spectrometry: strengths and limitations. *TrAC Trends in Analytical Chemistry,* 22**,** 273-281.
BERNALES, S., MCDONALD, K. L. & WALTER, P. 2006. Autophagy Counterbalances Endoplasmic Reticulum Expansion during the Unfolded Protein Response. *PLoS Biol,* 4**,** e423.
BERRIOS, G. 1990. Alzheimer's Disease: A Conceptual History. *International Journal of Geriatric Psychiatry,* 5**,** 355-365.
BERTRAM, L., MCQUEEN, M. B., MULLIN, K., BLACKER, D. & TANZI, R. E. 2007. Systematic meta-analyses of Alzheimer disease genetic association studies: the AlzGene database. *Nat Genet,* 39**,** 17-23.
BEZEAU, S. & GRAVES, R. 2001. Statistical power and effect sizes of clinical neuropsychology research. *J Clin Exp Neuropsychol,* 23**,** 399-406.
BLACKSTOCK, W. P. & WEIR, M. P. 1999. Proteomics: quantitative and physical mapping of cellular proteins. *Trends Biotechnol,* 17**,** 121-7.
BORLAND, M. K., TRIMMER, P. A., RUBINSTEIN, J. D., KEENEY, P. M., MOHANAKUMAR, K., LIU, L. & BENNETT, J. P., JR. 2008. Chronic, low-dose rotenone reproduces Lewy neurites found in early stages of Parkinson's disease, reduces mitochondrial movement and slowly kills differentiated SH-SY5Y neural cells. *Mol Neurodegener,* 3**,** 21.
BOULON, S., AHMAD, Y., TRINKLE-MULCAHY, L., VERHEGGEN, C., COBLEY, A., GREGOR, P., BERTRAND, E., WHITEHORN, M. & LAMOND, A. I. 2010.

Establishment of a protein frequency library and its application in the reliable identification of specific protein interaction partners. *Mol Cell Proteomics,* 9**,** 861-79.
BOWLING, A. C., MUTISYA, E. M., WALKER, L. C., PRICE, D. L., CORK, L. C. & BEAL, M. F. 1993. Age-dependent impairment of mitochondrial function in primate brain. *J Neurochem,* 60**,** 1964-7.
BRAAK, H. & BRAAK, E. 1995. Staging of Alzheimer's disease-related neurofibrillary changes. *Neurobiol Aging,* 16**,** 271-8; discussion 278-84.
BRAAK, H. & DEL TREDICI, K. 2011. The pathological process underlying Alzheimer's disease in individuals under thirty. *Acta Neuropathol,* 121**,** 171-81.
BRETELER, M. M. 2000. Vascular risk factors for Alzheimer's disease: an epidemiologic perspective. *Neurobiol Aging,* 21**,** 153-60.
BRILOT, F., MERHEB, V., DING, A., MURPHY, T. & DALE, R. C. 2011. Antibody binding to neuronal surface in Sydenham chorea, but not in PANDAS or Tourette syndrome. *Neurology,* 76**,** 1508-13.
BUBBER, P., HAROUTUNIAN, V., FISCH, G., BLASS, J. P. & GIBSON, G. E. 2005. Mitochondrial abnormalities in Alzheimer brain: mechanistic implications. *Ann Neurol,* 57**,** 695-703.
BURNS, A. & ILIFFE, S. 2009. Alzheimer's disease. *BMJ,* 338.
BUTTERFIELD, D. A., BOYD-KIMBALL, D. & CASTEGNA, A. 2003. Proteomics in Alzheimer's disease: insights into potential mechanisms of neurodegeneration. *Journal of Neurochemistry,* 86**,** 1313-1327.
CALLAWAY, E. 2012. Alzheimer's drugs take a new tack. *Nature,* 489**,** 13-4.
CASTEDO, M., PERFETTINI, J. L., ROUMIER, T. & KROEMER, G. 2002. Cyclin-dependent kinase-1: linking apoptosis to cell cycle and mitotic catastrophe. *Cell Death Differ,* 9**,** 1287-93.
CELSI, F., PIZZO, P., BRINI, M., LEO, S., FOTINO, C., PINTON, P. & RIZZUTO, R. 2009. Mitochondria, calcium and cell death: a deadly triad in neurodegeneration. *Biochim Biophys Acta,* 1787**,** 335-44.
CHANG, S. H., JUNG, I. S., HAN, G. Y., KIM, N. H., KIM, H. J. & KIM, C. W. 2013. Proteomic profiling of brain cortex tissues in a Tau transgenic mouse model of Alzheimer's disease. *Biochem Biophys Res Commun,* 430**,** 670-5.
CHANG, T.-Y., CHANG, C. C. Y., OHGAMI, N. & YAMAUCHI, Y. 2006. Cholesterol Sensing, Trafficking, and Esterification. *Annual Review of Cell and Developmental Biology,* 22**,** 129-157.
CHANG, T. Y., CHANG, C. C. & CHENG, D. 1997. Acyl-coenzyme A:cholesterol acyltransferase. *Annu Rev Biochem,* 66**,** 613-38.
CHEN, J. W., DODIA, C., FEINSTEIN, S. I., JAIN, M. K. & FISHER, A. B. 2000. 1-Cys peroxiredoxin, a bifunctional enzyme with glutathione peroxidase and phospholipase A2 activities. *J Biol Chem,* 275**,** 28421-7.
CHEUNG, K. H., SHINEMAN, D., MULLER, M., CARDENAS, C., MEI, L., YANG, J., TOMITA, T., IWATSUBO, T., LEE, V. M. & FOSKETT, J. K. 2008. Mechanism of Ca2+ disruption in Alzheimer's disease by presenilin regulation of InsP3 receptor channel gating. *Neuron,* 58**,** 871-83.
CHEUNG, Y. T., LAU, W. K., YU, M. S., LAI, C. S., YEUNG, S. C., SO, K. F. & CHANG, R. C. 2009. Effects of all-trans-retinoic acid on human SH-SY5Y neuroblastoma as in vitro model in neurotoxicity research. *Neurotoxicology,* 30**,** 127-35.
CIECHANOVER, A. & BRUNDIN, P. 2003. The ubiquitin proteasome system in neurodegenerative diseases: sometimes the chicken, sometimes the egg. *Neuron,* 40**,** 427-46.
CIMAROSTI, H., ZAMIN, L. L., FROZZA, R., NASSIF, M., HORN, A. P., TAVARES, A., NETTO, C. A. & SALBEGO, C. 2005. Estradiol protects against oxygen and

glucose deprivation in rat hippocampal organotypic cultures and activates Akt and inactivates GSK-3beta. *Neurochem Res,* 30**,** 191-9.
CLARK, D., DEDOVA, I., CORDWELL, S. & MATSUMOTO, I. 2007. Altered proteins of the anterior cingulate cortex white matter proteome in schizophrenia. *Proteomics Clin Appl,* 1**,** 157-66.
COLTMAN, R., SPAIN, A., TSENKINA, Y., FOWLER, J. H., SMITH, J., SCULLION, G., ALLERHAND, M., SCOTT, F., KALARIA, R. N., IHARA, M., DAUMAS, S., DEARY, I. J., WOOD, E., MCCULLOCH, J. & HORSBURGH, K. 2011. Selective white matter pathology induces a specific impairment in spatial working memory. *Neurobiol Aging,* 32**,** 2324 e7-12.
CUPERS, P., BENTAHIR, M., CRAESSAERTS, K., ORLANS, I., VANDERSTICHELE, H., SAFTIG, P., DE STROOPER, B. & ANNAERT, W. 2001. The discrepancy between presenilin subcellular localization and gamma-secretase processing of amyloid precursor protein. *J Cell Biol,* 154**,** 731-40.
DANCIK, V., ADDONA, T. A., CLAUSER, K. R., VATH, J. E. & PEVZNER, P. A. 1999. De novo peptide sequencing via tandem mass spectrometry. *J Comput Biol,* 6**,** 327-42.
DAVIDSON, C. M., PAPPAS, B. A., STEVENS, W. D., FORTIN, T. & BENNETT, S. A. 2000. Chronic cerebral hypoperfusion: loss of pupillary reflex, visual impairment and retinal neurodegeneration. *Brain Res,* 859**,** 96-103.
DAVIES, P. & MALONEY, A. J. 1976. Selective loss of central cholinergic neurons in Alzheimer's disease. *Lancet,* 2**,** 1403.
DE LA TORRE, J. C. 2000. Critically attained threshold of cerebral hypoperfusion: the CATCH hypothesis of Alzheimer's pathogenesis. *Neurobiol Aging,* 21**,** 331-42.
DE LA TORRE, J. C. 2002a. Alzheimer's disease: how does it start? *J Alzheimers Dis,* 4**,** 497-512.
DE LA TORRE, J. C. 2002b. Vascular basis of Alzheimer's pathogenesis. *Ann N Y Acad Sci,* 977**,** 196-215.
DE LA TORRE, J. C. 2008. Pathophysiology of neuronal energy crisis in Alzheimer's disease. *Neurodegener Dis,* 5**,** 126-32.
DE LA TORRE, J. C. 2010. The Vascular Hypothesis of Alzheimer's Disease: Bench to Bedside and Beyond. *Neurodegenerative Diseases,* 7**,** 116-121.
DE STROOPER, B. 2003. Aph-1, Pen-2, and Nicastrin with Presenilin generate an active gamma-Secretase complex. *Neuron,* 38**,** 9-12.
DE STROOPER, B., VASSAR, R. & GOLDE, T. 2010. The secretases: enzymes with therapeutic potential in Alzheimer disease. *Nat Rev Neurol,* 6**,** 99-107.
DEARY, I. J., GOW, A. J., TAYLOR, M. D., CORLEY, J., BRETT, C., WILSON, V., CAMPBELL, H., WHALLEY, L. J., VISSCHER, P. M., PORTEOUS, D. J. & STARR, J. M. 2007. The Lothian Birth Cohort 1936: a study to examine influences on cognitive ageing from age 11 to age 70 and beyond. *BMC Geriatr,* 7**,** 28.
DEIGHTON, R. F., KERR, L. E., SHORT, D. M., ALLERHAND, M., WHITTLE, I. R. & MCCULLOCH, J. 2010. Network generation enhances interpretation of proteomic data from induced apoptosis. *Proteomics,* 10**,** 1307-15.
DOHM, C. P., SIEDENBERG, S., LIMAN, J., ESPOSITO, A., WOUTERS, F. S., REED, J. C., BAHR, M. & KERMER, P. 2006. Bax inhibitor-1 protects neurons from oxygen-glucose deprivation. *J Mol Neurosci,* 29**,** 1-8.
DOODY, R. S. 2003. Current treatments for Alzheimer's disease: cholinesterase inhibitors. *J Clin Psychiatry,* 64 Suppl 9**,** 11-7.
DU YAN, S., ZHU, Y., STERN, E. D., HWANG, Y. C., HORI, O., OGAWA, S., FROSCH, M. P., CONNOLLY, E. S., JR., MCTAGGERT, R., PINSKY, D. J., CLARKE, S., STERN, D. M. & RAMASAMY, R. 2000. Amyloid beta -peptide-binding alcohol dehydrogenase is a component of the cellular response to nutritional stress. *J Biol Chem,* 275**,** 27100-9.

EATON, S. L., ROCHE, S. L., LLAVERO HURTADO, M., OLDKNOW, K. J., FARQUHARSON, C., GILLINGWATER, T. H. & WISHART, T. M. 2013. Total Protein Analysis as a Reliable Loading Control for Quantitative Fluorescent Western Blotting. *PLoS One,* 8**,** e72457.

EDMAN, P. 1949. A method for the determination of amino acid sequence in peptides. *Arch Biochem,* 22**,** 475.

FARFARA, D., LIFSHITZ, V. & FRENKEL, D. 2008. Neuroprotective and neurotoxic properties of glial cells in the pathogenesis of Alzheimer's disease. *J Cell Mol Med,* 12**,** 762-80.

FARKAS, E. & LUITEN, P. G. 2001. Cerebral microvascular pathology in aging and Alzheimer's disease. *Prog Neurobiol,* 64**,** 575-611.

FARKAS, E., LUITEN, P. G. & BARI, F. 2007. Permanent, bilateral common carotid artery occlusion in the rat: a model for chronic cerebral hypoperfusion-related neurodegenerative diseases. *Brain Res Rev,* 54**,** 162-80.

FINEHOUT, E. J., FRANCK, Z., CHOE, L. H., RELKIN, N. & LEE, K. H. 2007. Cerebrospinal fluid proteomic biomarkers for Alzheimer's disease. *Ann Neurol,* 61**,** 120-9.

FISKUM, G., MURPHY, A. N. & BEAL, M. F. 1999. Mitochondria in neurodegeneration: acute ischemia and chronic neurodegenerative diseases. *J Cereb Blood Flow Metab,* 19**,** 351-69.

FORDEL, E., THIJS, L., MARTINET, W., SCHRIJVERS, D., MOENS, L. & DEWILDE, S. 2007. Anoxia or oxygen and glucose deprivation in SH-SY5Y cells: a step closer to the unraveling of neuroglobin and cytoglobin functions. *Gene,* 398**,** 114-22.

FOX, N. C., WARRINGTON, E. K. & ROSSOR, M. N. 1999. Serial magnetic resonance imaging of cerebral atrophy in preclinical Alzheimer's disease. *Lancet,* 353**,** 2125.

GEORGANOPOULOU, D. G., CHANG, L., NAM, J. M., THAXTON, C. S., MUFSON, E. J., KLEIN, W. L. & MIRKIN, C. A. 2005. Nanoparticle-based detection in cerebral spinal fluid of a soluble pathogenic biomarker for Alzheimer's disease. *Proc Natl Acad Sci U S A,* 102**,** 2273-6.

GERMAN, D. C. & EISCH, A. J. 2004. Mouse models of Alzheimer's disease: insight into treatment. *Rev Neurosci,* 15**,** 353-69.

GHRIBI, O., LARSEN, B., SCHRAG, M. & HERMAN, M. M. 2006. High cholesterol content in neurons increases BACE, beta-amyloid, and phosphorylated tau levels in rabbit hippocampus. *Exp Neurol,* 200**,** 460-7.

GIANNAKOPOULOS, P., HERRMANN, F. R., BUSSIERE, T., BOURAS, C., KOVARI, E., PERL, D. P., MORRISON, J. H., GOLD, G. & HOF, P. R. 2003. Tangle and neuron numbers, but not amyloid load, predict cognitive status in Alzheimer's disease. *Neurology,* 60**,** 1495-500.

GIL, V., NICOLAS, O., MINGORANCE, A., URENA, J. M., TANG, B. L., HIRATA, T., SAEZ-VALERO, J., FERRER, I., SORIANO, E. & DEL RIO, J. A. 2006. Nogo-A expression in the human hippocampus in normal aging and in Alzheimer disease. *J Neuropathol Exp Neurol,* 65**,** 433-44.

GLATZ, D. C., RUJESCU, D., TANG, Y., BERENDT, F. J., HARTMANN, A. M., FALTRACO, F., ROSENBERG, C., HULETTE, C., JELLINGER, K., HAMPEL, H., RIEDERER, P., MOLLER, H. J., ANDREADIS, A., HENKEL, K. & STAMM, S. 2006. The alternative splicing of tau exon 10 and its regulatory proteins CLK2 and TRA2-BETA1 changes in sporadic Alzheimer's disease. *J Neurochem,* 96**,** 635-44.

GOLDBERG, M. P. & CHOI, D. W. 1993. Combined oxygen and glucose deprivation in cortical cell culture: calcium-dependent and calcium-independent mechanisms of neuronal injury. *J Neurosci,* 13**,** 3510-24.

GOMEZ-ISLA, T., HOLLISTER, R., WEST, H., MUI, S., GROWDON, J. H., PETERSEN, R. C., PARISI, J. E. & HYMAN, B. T. 1997. Neuronal loss correlates with but exceeds neurofibrillary tangles in Alzheimer's disease. *Ann Neurol,* 41**,** 17-24.

GOMEZ-RAMOS, P. & ASUNCION MORAN, M. 2007. Ultrastructural localization of intraneuronal Abeta-peptide in Alzheimer disease brains. *J Alzheimers Dis,* 11**,** 53-9.

GUO, Z. H. & MATTSON, M. P. 2000. In vivo 2-deoxyglucose administration preserves glucose and glutamate transport and mitochondrial function in cortical synaptic terminals after exposure to amyloid beta-peptide and iron: evidence for a stress response. *Exp Neurol,* 166**,** 173-9.

GUZY, R. D., HOYOS, B., ROBIN, E., CHEN, H., LIU, L., MANSFIELD, K. D., SIMON, M. C., HAMMERLING, U. & SCHUMACKER, P. T. 2005. Mitochondrial complex III is required for hypoxia-induced ROS production and cellular oxygen sensing. *Cell Metabolism,* 1**,** 401-408.

HAASS, C., KAETHER, C., THINAKARAN, G. & SISODIA, S. 2012. Trafficking and proteolytic processing of APP. *Cold Spring Harb Perspect Med,* 2**,** a006270.

HARDY, J. 1997. Amyloid, the presenilins and Alzheimer's disease. *Trends Neurosci,* 20**,** 154-9.

HARDY, J. A. & HIGGINS, G. A. 1992. Alzheimer's disease: the amyloid cascade hypothesis. *Science,* 256**,** 184-5.

HARMAN, D. 1956. Aging: a theory based on free radical and radiation chemistry. *J Gerontol,* 11**,** 298-300.

HARTZ, A. M., BAUER, B., SOLDNER, E. L., WOLF, A., BOY, S., BACKHAUS, R., MIHALJEVIC, I., BOGDAHN, U., KLUNEMANN, H. H., SCHUIERER, G. & SCHLACHETZKI, F. 2012. Amyloid-beta contributes to blood-brain barrier leakage in transgenic human amyloid precursor protein mice and in humans with cerebral amyloid angiopathy. *Stroke,* 43**,** 514-23.

HAYASHI, T., RIZZUTO, R., HAJNOCZKY, G. & SU, T.-P. 2009. MAM: more than just a housekeeper. *Trends in Cell Biology,* 19**,** 81-88.

HECKMANN, J. M., LOW, W. C., DE VILLIERS, C., RUTHERFOORD, S., VORSTER, A., RAO, H., MORRIS, C. M., RAMESAR, R. S. & KALARIA, R. N. 2004. Novel presenilin 1 mutation with profound neurofibrillary pathology in an indigenous Southern African family with early-onset Alzheimer's disease. *Brain,* 127**,** 133-42.

HERRMANN, A. G., DEIGHTON, R. F., LE BIHAN, T., MCCULLOCH, M. C., SEARCY, J. L., KERR, L. E. & MCCULLOCH, J. 2013a. Adaptive changes in the neuronal proteome: mitochondrial energy production, endoplasmic reticulum stress, and ribosomal dysfunction in the cellular response to metabolic stress. *J Cereb Blood Flow Metab*.

HERRMANN, A. G., SEARCY, J. L., LE BIHAN, T., MCCULLOCH, J. & DEIGHTON, R. F. 2013b. Total variance should drive data handling strategies in third generation proteomic studies. *Proteomics,* 13**,** 3251-5.

HERRUP, K. 2010. Reimagining Alzheimer's disease--an age-based hypothesis. *J Neurosci,* 30**,** 16755-62.

HOLTZMAN, D. M., MORRIS, J. C. & GOATE, A. M. 2011. Alzheimer's disease: the challenge of the second century. *Sci Transl Med,* 3**,** 77sr1.

HOSHI, M., TAKASHIMA, A., MURAYAMA, M., YASUTAKE, K., YOSHIDA, N., ISHIGURO, K., HOSHINO, T. & IMAHORI, K. 1997. Nontoxic Amyloid beta Peptide1-42 Suppresses Acetylcholine Synthesis. POSSIBLE ROLE IN CHOLINERGIC DYSFUNCTION IN ALZHEIMER'S DISEASE. *J. Biol. Chem.,* 272**,** 2038-2041.

HOUTEN, S. M. & WANDERS, R. J. 2010. A general introduction to the biochemistry of mitochondrial fatty acid beta-oxidation. *J Inherit Metab Dis,* 33**,** 469-77.

HYND, M. R., SCOTT, H. L. & DODD, P. R. 2004. Glutamate-mediated excitotoxicity and neurodegeneration in Alzheimer's disease. *Neurochem Int,* 45**,** 583-95.

IWATA, S., LEE, J. W., OKADA, K., LEE, J. K., IWATA, M., RASMUSSEN, B., LINK, T. A., RAMASWAMY, S. & JAP, B. K. 1998. Complete Structure of the 11-Subunit Bovine Mitochondrial Cytochrome bc1 Complex. *Science,* 281**,** 64-71.

JACK, C. R., JR., PETERSEN, R. C., XU, Y. C., WARING, S. C., O'BRIEN, P. C., TANGALOS, E. G., SMITH, G. E., IVNIK, R. J. & KOKMEN, E. 1997. Medial temporal atrophy on MRI in normal aging and very mild Alzheimer's disease. *Neurology,* 49**,** 786-94.

JAFFE, A. B., TORAN-ALLERAND, C. D., GREENGARD, P. & GANDY, S. E. 1994. Estrogen regulates metabolism of Alzheimer amyloid beta precursor protein. *J Biol Chem,* 269**,** 13065-8.

JAMES, R., SEARCY, J. L., LE BIHAN, T., MARTIN, S. F., GLIDDON, C. M., POVEY, J., DEIGHTON, R. F., KERR, L. E., MCCULLOCH, J. & HORSBURGH, K. 2012a. Proteomic analysis of mitochondria in APOE transgenic mice and in response to an ischemic challenge. *J Cereb Blood Flow Metab,* 32**,** 164-176.

JAMES, R., SEARCY, J. L., LE BIHAN, T., MARTIN, S. F., GLIDDON, C. M., POVEY, J., DEIGHTON, R. F., KERR, L. E., MCCULLOCH, J. & HORSBURGH, K. 2012b. Proteomic analysis of mitochondria in APOE transgenic mice and in response to an ischemic challenge. *J Cereb Blood Flow Metab,* 32**,** 164-76.

JANSSEN, R. J., NIJTMANS, L. G., VAN DEN HEUVEL, L. P. & SMEITINK, J. A. 2006. Mitochondrial complex I: structure, function and pathology. *J Inherit Metab Dis,* 29**,** 499-515.

JARRETT, J. T. & LANSBURY, P. T., JR. 1993. Seeding "one-dimensional crystallization" of amyloid: a pathogenic mechanism in Alzheimer's disease and scrapie? *Cell,* 73**,** 1055-8.

JIN, M., SHEPARDSON, N., YANG, T., CHEN, G., WALSH, D. & SELKOE, D. J. 2011. Soluble amyloid beta-protein dimers isolated from Alzheimer cortex directly induce Tau hyperphosphorylation and neuritic degeneration. *Proc Natl Acad Sci U S A,* 108**,** 5819-24.

KADIR, A., MARUTLE, A., GONZALEZ, D., SCHÖLL, M., ALMKVIST, O., MOUSAVI, M., MUSTAFIZ, T., DARREH-SHORI, T., NENNESMO, I. & NORDBERG, A. 2011. Positron emission tomography imaging and clinical progression in relation to molecular pathology in the first Pittsburgh Compound B positron emission tomography patient with Alzheimer's disease. *Brain,* 134**,** 301-317.

KANG, S. K., SO, H. H., MOON, Y. S. & KIM, C. H. 2006. Proteomic analysis of injured spinal cord tissue proteins using 2-DE and MALDI-TOF MS. *Proteomics,* 6**,** 2797-812.

KARANTZOULIS, S. & GALVIN, J. E. 2011. Distinguishing Alzheimer's disease from other major forms of dementia. *Expert Rev Neurother,* 11**,** 1579-91.

KASHIWAYA, Y., TAKESHIMA, T., MORI, N., NAKASHIMA, K., CLARKE, K. & VEECH, R. L. 2000. D-beta-hydroxybutyrate protects neurons in models of Alzheimer's and Parkinson's disease. *Proc Natl Acad Sci U S A,* 97**,** 5440-4.

KATCHANOV, J., HARMS, C., GERTZ, K., HAUCK, L., WAEBER, C., HIRT, L., PRILLER, J., VON HARSDORF, R., BRUCK, W., HORTNAGL, H., DIRNAGL, U., BHIDE, P. G. & ENDRES, M. 2001. Mild cerebral ischemia induces loss of cyclin-dependent kinase inhibitors and activation of cell cycle machinery before delayed neuronal cell death. *J Neurosci,* 21**,** 5045-53.

KATZMAN, R., TERRY, R., DETERESA, R., BROWN, T., DAVIES, P., FULD, P., RENBING, X. & PECK, A. 1988. Clinical, pathological, and neurochemical changes in dementia: a subgroup with preserved mental status and numerous neocortical plaques. *Ann Neurol,* 23**,** 138-44.

KAY, K. R., SMITH, C., WRIGHT, A. K., SERRANO-POZO, A., POOLER, A. M., KOFFIE, R., BASTIN, M. E., BAK, T. H., ABRAHAMS, S., KOPEIKINA, K. J., MCGUONE, D., FROSCH, M. P., GILLINGWATER, T. H., HYMAN, B. T. &

SPIRES-JONES, T. L. 2013. Studying synapses in human brain with array tomography and electron microscopy. *Nat Protoc,* 8**,** 1366-80.
KIM, J., BASAK, J. M. & HOLTZMAN, D. M. 2009. The role of apolipoprotein E in Alzheimer's disease. *Neuron,* 63**,** 287-303.
KIM, J. S., HE, L. & LEMASTERS, J. J. 2003. Mitochondrial permeability transition: a common pathway to necrosis and apoptosis. *Biochem Biophys Res Commun,* 304**,** 463-70.
KIM, S. H., VLKOLINSKY, R., CAIRNS, N. & LUBEC, G. 2000. Decreased levels of complex III core protein 1 and complex V beta chain in brains from patients with Alzheimer's disease and Down syndrome. *Cell Mol Life Sci,* 57**,** 1810-6.
KLEIN, W. L., KRAFFT, G. A. & FINCH, C. E. 2001. Targeting small Abeta oligomers: the solution to an Alzheimer's disease conundrum? *Trends Neurosci,* 24**,** 219-24.
KOFFIE, R. M., HYMAN, B. T. & SPIRES-JONES, T. L. 2011. Alzheimer's disease: synapses gone cold. *Mol Neurodegener,* 6**,** 63.
KOHLER, A. & HURT, E. 2007. Exporting RNA from the nucleus to the cytoplasm. *Nat Rev Mol Cell Biol,* 8**,** 761-73.
KRAEMER, N., ISSA, L., HAUCK, S. C., MANI, S., NINNEMANN, O. & KAINDL, A. M. 2011. What's the hype about CDK5RAP2? *Cell Mol Life Sci,* 68**,** 1719-36.
KRAPFENBAUER, K., ENGIDAWORK, E., CAIRNS, N., FOUNTOULAKIS, M. & LUBEC, G. 2003. Aberrant expression of peroxiredoxin subtypes in neurodegenerative disorders. *Brain Res,* 967**,** 152-60.
LAMOND, A. I., UHLEN, M., HORNING, S., MAKAROV, A., ROBINSON, C. V., SERRANO, L., HARTL, F. U., BAUMEISTER, W., WERENSKIOLD, A. K., ANDERSEN, J. S., VORM, O., LINIAL, M., AEBERSOLD, R. & MANN, M. 2012. Advancing Cell Biology Through Proteomics in Space and Time (PROSPECTS). *Molecular & Cellular Proteomics,* 11.
LEE, P., HWANG, E., HONG, H., BOO, J., JUNG, I. & HUH, K. 2006. Effect of Ischemic Neuronal Insults on Amyloid Precursor Protein Processing. *Neurochemical Reseach,* 31**,** 821-827.
LEE, Y. J., GOO, J. S., KIM, J. E., NAM, S. H., HWANG, I. S., CHOI, S. I., LEE, H. R., LEE, E. P., CHOI, H. W., KIM, H. S., LEE, J. H., JUNG, Y. J., KIM, H. J. & HWANG, D. Y. 2011. Peroxiredoxin I regulates the component expression of gamma-secretase complex causing the Alzheimer's disease. *Lab Anim Res,* 27**,** 293-9.
LEVIN, Y. 2011. The role of statistical power analysis in quantitative proteomics. *Proteomics,* 11**,** 2565-7.
LIAO, L., CHENG, D., WANG, J., DUONG, D. M., LOSIK, T. G., GEARING, M., REES, H. D., LAH, J. J., LEVEY, A. I. & PENG, J. 2004. Proteomic characterization of postmortem amyloid plaques isolated by laser capture microdissection. *J Biol Chem,* 279**,** 37061-8.
LIN, M. T. & BEAL, M. F. 2006. Mitochondrial dysfunction and oxidative stress in neurodegenerative diseases. *Nature,* 443**,** 787-95.
LIN, M. T., SIMON, D. K., AHN, C. H., KIM, L. M. & BEAL, M. F. 2002. High aggregate burden of somatic mtDNA point mutations in aging and Alzheimer's disease brain. *Hum Mol Genet,* 11**,** 133-45.
LINNANE, A. W., MARZUKI, S., OZAWA, T. & TANAKA, M. 1989. Mitochondrial DNA mutations as an important contributor to ageing and degenerative diseases. *Lancet,* 1**,** 642-5.
LIU, H. X., ZHANG, J. J., ZHENG, P. & ZHANG, Y. 2005. Altered expression of MAP-2, GAP-43, and synaptophysin in the hippocampus of rats with chronic cerebral hypoperfusion correlates with cognitive impairment. *Brain Res Mol Brain Res,* 139**,** 169-77.

LUCHSINGER, J. A. & MAYEUX, R. 2004. Dietary factors and Alzheimer's disease. *Lancet Neurol,* 3**,** 579-87.
LUSHNIKOVA, I. V., VORONIN, K., MALIAREVS'KYI, P., SMOZHANYK, K. H. & SKIBO, H. H. 2004. [Effect of oxygen-glucose deprivation of different duration on rat hippocampal slice cultures]. *Fiziol Zh,* 50**,** 94-100.
LUSTBADER, J. W., CIRILLI, M., LIN, C., XU, H. W., TAKUMA, K., WANG, N., CASPERSEN, C., CHEN, X., POLLAK, S., CHANEY, M., TRINCHESE, F., LIU, S., GUNN-MOORE, F., LUE, L. F., WALKER, D. G., KUPPUSAMY, P., ZEWIER, Z. L., ARANCIO, O., STERN, D., YAN, S. S. & WU, H. 2004. ABAD directly links Abeta to mitochondrial toxicity in Alzheimer's disease. *Science,* 304**,** 448-52.
MAGDER, S. 2006. Reactive oxygen species: toxic molecules or spark of life? *Crit Care,* 10**,** 208.
MALLICK, P. & KUSTER, B. 2010. Proteomics: a pragmatic perspective. *Nat Biotechnol,* 28**,** 695-709.
MANGIALASCHE, F., SOLOMON, A., WINBLAD, B., MECOCCI, P. & KIVIPELTO, M. 2010. Alzheimer's disease: clinical trials and drug development. *Lancet Neurol,* 9**,** 702-16.
MARQUES, A. T., FERNANDES, P. A. & RAMOS, M. J. 2008. Molecular dynamics simulations of the amyloid-beta binding alcohol dehydrogenase (ABAD) enzyme. *Bioorg Med Chem,* 16**,** 9511-8.
MARTIN, B., BRENNEMAN, R., BECKER, K. G., GUCEK, M., COLE, R. N. & MAUDSLEY, S. 2008. iTRAQ analysis of complex proteome alterations in 3xTgAD Alzheimer's mice: understanding the interface between physiology and disease. *PLoS One,* 3**,** e2750.
MARTIN, S. & PARTON, R. G. 2006. Lipid droplets: a unified view of a dynamic organelle. *Nat Rev Mol Cell Biol,* 7**,** 373-8.
MATES, J. M. 2000. Effects of antioxidant enzymes in the molecular control of reactive oxygen species toxicology. *Toxicology,* 153**,** 83-104.
MATTSON, M. P. 2004. Pathways towards and away from Alzheimer's disease. *Nature,* 430**,** 631-9.
MATZKE, M. M., BROWN, J. N., GRITSENKO, M. A., METZ, T. O., POUNDS, J. G., RODLAND, K. D., SHUKLA, A. K., SMITH, R. D., WATERS, K. M., MCDERMOTT, J. E. & WEBB-ROBERTSON, B. J. 2013. A comparative analysis of computational approaches to relative protein quantification using peptide peak intensities in label-free LC-MS proteomics experiments. *Proteomics,* 13**,** 493-503.
MAUS, M., TORRENS, Y., GAUCHY, C., BRETIN, S., NAIRN, A. C., GLOWINSKI, J. & PREMONT, J. 2006. 2-Deoxyglucose and NMDA inhibit protein synthesis in neurons and regulate phosphorylation of elongation factor-2 by distinct mechanisms. *Journal of Neurochemistry,* 96**,** 815-824.
MCGLEENON, B. M., DYNAN, K. B. & PASSMORE, A. P. 1999. Acetylcholinesterase inhibitors in Alzheimer's disease. *Br J Clin Pharmacol,* 48**,** 471-80.
MEHTA, S. L. & LI, P. A. 2009. Neuroprotective role of mitochondrial uncoupling protein 2 in cerebral stroke. *J Cereb Blood Flow Metab,* 29**,** 1069-78.
MELONI, B. P., MEADE, A. J., KITIKOMOLSUK, D. & KNUCKEY, N. W. 2011. Characterisation of neuronal cell death in acute and delayed in vitro ischemia (oxygen-glucose deprivation) models. *J Neurosci Methods,* 195**,** 67-74.
MEYER-LUEHMANN, M., COOMARASWAMY, J., BOLMONT, T., KAESER, S., SCHAEFER, C., KILGER, E., NEUENSCHWANDER, A., ABRAMOWSKI, D., FREY, P., JATON, A. L., VIGOURET, J. M., PAGANETTI, P., WALSH, D. M., MATHEWS, P. M., GHISO, J., STAUFENBIEL, M., WALKER, L. C. & JUCKER, M. 2006. Exogenous induction of cerebral beta-amyloidogenesis is governed by agent and host. *Science,* 313**,** 1781-4.

MIZZEN, L. A., KABILING, A. N. & WELCH, W. J. 1991. The two mammalian mitochondrial stress proteins, grp 75 and hsp 58, transiently interact with newly synthesized mitochondrial proteins. *Cell Regul,* 2**,** 165-79.
MORRIS, J. S., CLARK, B. N., WEI, W. & GUTSTEIN, H. B. 2010. Evaluating the performance of new approaches to spot quantification and differential expression in 2-dimensional gel electrophoresis studies. *J Proteome Res,* 9**,** 595-604.
MUCKE, L. 2009. Neuroscience: Alzheimer's disease. *Nature,* 461**,** 895-7.
MUIR, J. L. 1997. Acetylcholine, aging, and Alzheimer's disease. *Pharmacol Biochem Behav,* 56**,** 687-96.
MUNNICH, A. 2008. Casting an eye on the Krebs cycle. *Nat Genet,* 40**,** 1148-9.
MURAYAMA, K. S., KAMETANI, F., SAITO, S., KUME, H., AKIYAMA, H. & ARAKI, W. 2006. Reticulons RTN3 and RTN4-B/C interact with BACE1 and inhibit its ability to produce amyloid beta-protein. *Eur J Neurosci,* 24**,** 1237-44.
MURPHY, A. N., FISKUM, G. & BEAL, M. F. 1999. Mitochondria in neurodegeneration: bioenergetic function in cell life and death. *J Cereb Blood Flow Metab,* 19**,** 231-45.
NAIDOO, N., FERBER, M., MASTER, M., ZHU, Y. & PACK, A. I. 2008. Aging impairs the unfolded protein response to sleep deprivation and leads to proapoptotic signaling. *J Neurosci,* 28**,** 6539-48.
NAVARRO, A., SANCHEZ DEL PINO, M. J., GOMEZ, C., PERALTA, J. L. & BOVERIS, A. 2002. Behavioral dysfunction, brain oxidative stress, and impaired mitochondrial electron transfer in aging mice. *Am J Physiol Regul Integr Comp Physiol,* 282**,** R985-92.
NGANDU, T., VON STRAUSS, E., HELKALA, E. L., WINBLAD, B., NISSINEN, A., TUOMILEHTO, J., SOININEN, H. & KIVIPELTO, M. 2007. Education and dementia: what lies behind the association? *Neurology,* 69**,** 1442-50.
NOBLE, W., OLM, V., TAKATA, K., CASEY, E., MARY, O., MEYERSON, J., GAYNOR, K., LAFRANCOIS, J., WANG, L., KONDO, T., DAVIES, P., BURNS, M., VEERANNA, NIXON, R., DICKSON, D., MATSUOKA, Y., AHLIJANIAN, M., LAU, L. F. & DUFF, K. 2003. Cdk5 is a key factor in tau aggregation and tangle formation in vivo. *Neuron,* 38**,** 555-65.
O'FARRELL, P. H. 1975. High resolution two-dimensional electrophoresis of proteins. *J Biol Chem,* 250**,** 4007-21.
OKAMOTO, Y., YAMAMOTO, T., KALARIA, R. N., SENZAKI, H., MAKI, T., HASE, Y., KITAMURA, A., WASHIDA, K., YAMADA, M., ITO, H., TOMIMOTO, H., TAKAHASHI, R. & IHARA, M. 2012. Cerebral hypoperfusion accelerates cerebral amyloid angiopathy and promotes cortical microinfarcts. *Acta Neuropathol,* 123**,** 381-94.
OPPERMANN, U. C., SALIM, S., TJERNBERG, L. O., TERENIUS, L. & JORNVALL, H. 1999. Binding of amyloid beta-peptide to mitochondrial hydroxyacyl-CoA dehydrogenase (ERAB): regulation of an SDR enzyme activity with implications for apoptosis in Alzheimer's disease. *FEBS Lett,* 451**,** 238-42.
OTSU, N. 1979. A Threshold Selection Method from Gray-Level Histograms. *Automatica,* 9**,** 5.
PASCHEN, W., MENGESDORF, T. & AUFENBERG, C. 2003. Suppression of protein synthesis after transient cerebral ischemia. *International Congress Series,* 1252**,** 179-191.
PASSMORE, L. A., SCHMEING, T. M., MAAG, D., APPLEFIELD, D. J., ACKER, M. G., ALGIRE, M. A., LORSCH, J. R. & RAMAKRISHNAN, V. 2007. The eukaryotic translation initiation factors eIF1 and eIF1A induce an open conformation of the 40S ribosome. *Mol Cell,* 26**,** 41-50.
PATEL, V. J., THALASSINOS, K., SLADE, S. E., CONNOLLY, J. B., CROMBIE, A., MURRELL, J. C. & SCRIVENS, J. H. 2009. A comparison of labeling and label-free mass spectrometry-based proteomics approaches. *J Proteome Res,* 8**,** 3752-9.

PATERGNANI, S., SUSKI, J. M., AGNOLETTO, C., BONONI, A., BONORA, M., DE MARCHI, E., GIORGI, C., MARCHI, S., MISSIROLI, S., POLETTI, F., RIMESSI, A., DUSZYNSKI, J., WIECKOWSKI, M. R. & PINTON, P. 2011. Calcium signaling around Mitochondria Associated Membranes (MAMs). *Cell Commun Signal,* 9**,** 19.

PATRON, M., RAFFAELLO, A., GRANATIERO, V., TOSATTO, A., MERLI, G., DE STEFANI, D., WRIGHT, L., PALLAFACCHINA, G., TERRIN, A., MAMMUCARI, C. & RIZZUTO, R. 2013. The mitochondrial calcium uniporter (MCU): molecular identity and physiological roles. *J Biol Chem,* 288**,** 10750-8.

PATTERSON, S. D. 2003. Proteomics: evolution of the technology. *Biotechniques,* 35**,** 440-4.

PELICANO, H., MARTIN, D. S., XU, R. H. & HUANG, P. 2006. Glycolysis inhibition for anticancer treatment. *Oncogene,* 25**,** 4633-46.

PEREZ, R. G., SORIANO, S., HAYES, J. D., OSTASZEWSKI, B., XIA, W., SELKOE, D. J., CHEN, X., STOKIN, G. B. & KOO, E. H. 1999. Mutagenesis identifies new signals for beta-amyloid precursor protein endocytosis, turnover, and the generation of secreted fragments, including Abeta42. *J Biol Chem,* 274**,** 18851-6.

PERLUIGI, M., SULTANA, R., CENINI, G., DI DOMENICO, F., MEMO, M., PIERCE, W. M., COCCIA, R. & BUTTERFIELD, D. A. 2009. Redox proteomics identification of 4-hydroxynonenal-modified brain proteins in Alzheimer's disease: Role of lipid peroxidation in Alzheimer's disease pathogenesis. *Proteomics Clin Appl,* 3**,** 682-693.

PERRIN, R. J., FAGAN, A. M. & HOLTZMAN, D. M. 2009. Multimodal techniques for diagnosis and prognosis of Alzheimer's disease. *Nature,* 461**,** 916-22.

PERRY, E. K., TOMLINSON, B. E., BLESSED, G., BERGMANN, K., GIBSON, P. H. & PERRY, R. H. 1978. Correlation of cholinergic abnormalities with senile plaques and mental test scores in senile dementia. *Br Med J,* 2**,** 1457-9.

PIEDRAHITA, D., HERNANDEZ, I., LOPEZ-TOBON, A., FEDOROV, D., OBARA, B., MANJUNATH, B. S., BOUDREAU, R. L., DAVIDSON, B., LAFERLA, F., GALLEGO-GOMEZ, J. C., KOSIK, K. S. & CARDONA-GOMEZ, G. P. 2010. Silencing of CDK5 reduces neurofibrillary tangles in transgenic alzheimer's mice. *J Neurosci,* 30**,** 13966-76.

PISTON, D. W. & KREMERS, G. J. 2007. Fluorescent protein FRET: the good, the bad and the ugly. *Trends Biochem Sci,* 32**,** 407-14.

PLASSMAN, B. L., HAVLIK, R. J., STEFFENS, D. C., HELMS, M. J., NEWMAN, T. N., DROSDICK, D., PHILLIPS, C., GAU, B. A., WELSH-BOHMER, K. A., BURKE, J. R., GURALNIK, J. M. & BREITNER, J. C. 2000. Documented head injury in early adulthood and risk of Alzheimer's disease and other dementias. *Neurology,* 55**,** 1158-66.

POLISETTY, R. V., GAUTAM, P., SHARMA, R., HARSHA, H. C., NAIR, S. C., GUPTA, M. K., UPPIN, M. S., CHALLA, S., PULIGOPU, A. K., ANKATHI, P., PUROHIT, A. K., CHANDAK, G. R., PANDEY, A. & SIRDESHMUKH, R. 2012. LC-MS/MS analysis of differentially expressed glioblastoma membrane proteome reveals altered calcium signaling and other protein groups of regulatory functions. *Mol Cell Proteomics,* 11**,** M111 013565.

POOLER, A. M., NOBLE, W. & HANGER, D. P. 2014. A role for tau at the synapse in Alzheimer's disease pathogenesis. *Neuropharmacology,* 76, Part A**,** 1-8.

POOLER, A. M., POLYDORO, M., WEGMANN, S., NICHOLLS, S. B., SPIRES-JONES, T. L. & HYMAN, B. T. 2013. Propagation of tau pathology in Alzheimer's disease: identification of novel therapeutic targets. *Alzheimers Res Ther,* 5**,** 49.

POPE, S. K., SHUE, V. M. & BECK, C. 2003. Will a healthy lifestyle help prevent Alzheimer's disease? *Annu Rev Public Health,* 24**,** 111-32.

QIU, C., DE RONCHI, D. & FRATIGLIONI, L. 2007. The epidemiology of the dementias: an update. *Curr Opin Psychiatry,* 20**,** 380-5.
QUERFURTH, H. W. & LAFERLA, F. M. Alzheimer's disease. *N Engl J Med,* 362**,** 329-44.
REIMER, M. M., MCQUEEN, J., SEARCY, L., SCULLION, G., ZONTA, B., DESMAZIERES, A., HOLLAND, P. R., SMITH, J., GLIDDON, C., WOOD, E. R., HERZYK, P., BROPHY, P. J., MCCULLOCH, J. & HORSBURGH, K. 2011. Rapid disruption of axon-glial integrity in response to mild cerebral hypoperfusion. *J Neurosci,* 31**,** 18185-94.
RICHARDSON, J. R., ROY, A., SHALAT, S. L., VON STEIN, R. T., HOSSAIN, M. M., BUCKLEY, B., GEARING, M., LEVEY, A. I. & GERMAN, D. C. 2014. Elevated Serum Pesticide Levels and Risk for Alzheimer Disease. *JAMA Neurol*.
RIEDEL, G., PLATT, B. & MICHEAU, J. 2003. Glutamate receptor function in learning and memory. *Behav Brain Res,* 140**,** 1-47.
RIZZUTO, R., DE STEFANI, D., RAFFAELLO, A. & MAMMUCARI, C. 2012. Mitochondria as sensors and regulators of calcium signalling. *Nat Rev Mol Cell Biol,* 13**,** 566-78.
ROBINSON, R. A. S., JOSHI, G., HUANG, Q., SULTANA, R., BAKER, A. S., CAI, J., PIERCE, W., ST. CLAIR, D. K., MARKESBERY, W. R. & BUTTERFIELD, D. A. 2011. Proteomic analysis of brain proteins in APP/PS-1 human double mutant knock-in mice with increasing amyloid β-peptide deposition: Insights into the effects of in vivo treatment with N-acetylcysteine as a potential therapeutic intervention in mild cognitive impairment and Alzheimer's disease. *Proteomics,* 11**,** 4243-4256.
RON, D. & WALTER, P. 2007. Signal integration in the endoplasmic reticulum unfolded protein response. *Nat Rev Mol Cell Biol,* 8**,** 519-29.
SAKURIKAR, N., EICHHORN, J. M. & CHAMBERS, T. C. 2012. Cyclin-dependent Kinase-1 (Cdk1)/Cyclin B1 Dictates Cell Fate after Mitotic Arrest via Phosphoregulation of Antiapoptotic Bcl-2 Proteins. *Journal of Biological Chemistry,* 287**,** 39193-39204.
SANTOS, R. X., CORREIA, S. C., WANG, X., PERRY, G., SMITH, M. A., MOREIRA, P. I. & ZHU, X. Alzheimer's disease: diverse aspects of mitochondrial malfunctioning. *Int J Clin Exp Pathol,* 3**,** 570-81.
SCHEPER, W., NIJHOLT, D. A. & HOOZEMANS, J. J. 2011. The unfolded protein response and proteostasis in Alzheimer disease: preferential activation of autophagy by endoplasmic reticulum stress. *Autophagy,* 7**,** 910-1.
SCHON, E. A. & AREA-GOMEZ, E. 2013. Mitochondria-associated ER membranes in Alzheimer disease. *Mol Cell Neurosci,* 55**,** 26-36.
SCHONHEIT, B., ZARSKI, R. & OHM, T. G. 2004. Spatial and temporal relationships between plaques and tangles in Alzheimer-pathology. *Neurobiol Aging,* 25**,** 697-711.
SCHONIG, K., WEBER, T., FROMMIG, A., WENDLER, L., PESOLD, B., DJANDJI, D., BUJARD, H. & BARTSCH, D. 2012. Conditional gene expression systems in the transgenic rat brain. *BMC Biol,* 10**,** 77.
SCHUCK, S., PRINZ, W. A., THORN, K. S., VOSS, C. & WALTER, P. 2009. Membrane expansion alleviates endoplasmic reticulum stress independently of the unfolded protein response. *J Cell Biol,* 187**,** 525-36.
SELKOE, D. J. 2002. Alzheimer's Disease Is a Synaptic Failure. *Science,* 298**,** 789-791.
SHIBATA, M., OHTANI, R., IHARA, M. & TOMIMOTO, H. 2004. White matter lesions and glial activation in a novel mouse model of chronic cerebral hypoperfusion. *Stroke,* 35**,** 2598-603.
SHIBATA, M., YAMASAKI, N., MIYAKAWA, T., KALARIA, R. N., FUJITA, Y., OHTANI, R., IHARA, M., TAKAHASHI, R. & TOMIMOTO, H. 2007. Selective impairment of working memory in a mouse model of chronic cerebral hypoperfusion. *Stroke,* 38**,** 2826-32.

SHIMIZU, S., NARITA, M. & TSUJIMOTO, Y. 1999. Bcl-2 family proteins regulate the release of apoptogenic cytochrome c by the mitochondrial channel VDAC. *Nature,* 399**,** 483-7.

SHORT, D. M., HERON, I. D., BIRSE-ARCHBOLD, J. L., KERR, L. E., SHARKEY, J. & MCCULLOCH, J. 2007. Apoptosis induced by staurosporine alters chaperone and endoplasmic reticulum proteins: Identification by quantitative proteomics. *Proteomics,* 7**,** 3085-96.

SHOSHAN-BARMATZ, V., DE PINTO, V., ZWECKSTETTER, M., RAVIV, Z., KEINAN, N. & ARBEL, N. 2010. VDAC, a multi-functional mitochondrial protein regulating cell life and death. *Mol Aspects Med,* 31**,** 227-85.

SIMZAR, S., ELLYIN, R., SHAU, H. & SARAFIAN, T. A. 2000. Contrasting antioxidant and cytotoxic effects of peroxiredoxin I and II in PC12 and NIH3T3 cells. *Neurochem Res,* 25**,** 1613-21.

SINGH, R., KAUSHIK, S., WANG, Y., XIANG, Y., NOVAK, I., KOMATSU, M., TANAKA, K., CUERVO, A. M. & CZAJA, M. J. 2009. Autophagy regulates lipid metabolism. *Nature,* 458**,** 1131-5.

SIZOVA, D., CHARBAUT, E., DELALANDE, F., POIRIER, F., HIGH, A. A., PARKER, F., VAN DORSSELAER, A., DUCHESNE, M. & DIU-HERCEND, A. 2007. Proteomic analysis of brain tissue from an Alzheimer's disease mouse model by two-dimensional difference gel electrophoresis. *Neurobiol Aging,* 28**,** 357-70.

SPIRES-JONES, T. L., STOOTHOFF, W. H., DE CALIGNON, A., JONES, P. B. & HYMAN, B. T. 2009. Tau pathophysiology in neurodegeneration: a tangled issue. *Trends Neurosci,* 32**,** 150-9.

SU, B., WANG, X., LEE, H. G., TABATON, M., PERRY, G., SMITH, M. A. & ZHU, X. 2010. Chronic oxidative stress causes increased tau phosphorylation in M17 neuroblastoma cells. *Neurosci Lett,* 468**,** 267-71.

SUN, G. Y., XU, J., JENSEN, M. D. & SIMONYI, A. 2004. Phospholipase A2 in the central nervous system: implications for neurodegenerative diseases. *J Lipid Res,* 45**,** 205-13.

SUN, Y., DAY, R. N. & PERIASAMY, A. 2011. Investigating protein-protein interactions in living cells using fluorescence lifetime imaging microscopy. *Nat Protoc,* 6**,** 1324-40.

TAMAGNO, E., PAROLA, M., BARDINI, P., PICCINI, A., BORGHI, R., GUGLIELMOTTO, M., SANTORO, G., DAVIT, A., DANNI, O., SMITH, M. A., PERRY, G. & TABATON, M. 2005. Beta-site APP cleaving enzyme up-regulation induced by 4-hydroxynonenal is mediated by stress-activated protein kinases pathways. *J Neurochem,* 92**,** 628-36.

TAMPI, R. R. & VAN DYCK, C. H. 2007. Memantine: efficacy and safety in mild-to-severe Alzheimer's disease. *Neuropsychiatr Dis Treat,* 3**,** 245-58.

TANZI, R. E. & BERTRAM, L. 2005. Twenty Years of the Alzheimer's Disease Amyloid Hypothesis: A Genetic Perspective. *Cell,* 120**,** 545-555.

TAYLOR, J. P., HARDY, J. & FISCHBECK, K. H. 2002. Toxic proteins in neurodegenerative disease. *Science,* 296**,** 1991-5.

TAYLOR, R. W. & TURNBULL, D. M. 2005. Mitochondrial DNA mutations in human disease. *Nat Rev Genet,* 6**,** 389-402.

TIWARI, V., VASHISTT, J., KAPIL, A. & MOGANTY, R. R. 2012. Comparative proteomics of inner membrane fraction from carbapenem-resistant Acinetobacter baumannii with a reference strain. *PLoS One,* 7**,** e39451.

TURRENS, J. F. 2003. Mitochondrial formation of reactive oxygen species. *J Physiol,* 552**,** 335-44.

UEHARA, T., NAKAMURA, T., YAO, D., SHI, Z. Q., GU, Z., MA, Y., MASLIAH, E., NOMURA, Y. & LIPTON, S. A. 2006. S-nitrosylated protein-disulphide isomerase links protein misfolding to neurodegeneration. *Nature,* 441**,** 513-7.

VALERA, A. G., DIAZ-HERNANDEZ, M., HERNANDEZ, F., ORTEGA, Z. & LUCAS, J. J. 2005. The ubiquitin-proteasome system in Huntington's disease. *Neuroscientist,* 11**,** 583-94.
VAN DER WORP, H. B. & VAN GIJN, J. 2007. Clinical practice. Acute ischemic stroke. *N Engl J Med,* 357**,** 572-9.
VAN REMMEN, H. & RICHARDSON, A. 2001. Oxidative damage to mitochondria and aging. *Exp Gerontol,* 36**,** 957-68.
VERKHRATSKY, A. 2005. Physiology and pathophysiology of the calcium store in the endoplasmic reticulum of neurons. *Physiol Rev,* 85**,** 201-79.
VINCENT, I., JICHA, G., ROSADO, M. & DICKSON, D. W. 1997. Aberrant expression of mitotic cdc2/cyclin B1 kinase in degenerating neurons of Alzheimer's disease brain. *J Neurosci,* 17**,** 3588-98.
VOELKER, D. R. 2005. Bridging gaps in phospholipid transport. *Trends Biochem Sci,* 30**,** 396-404.
VORNOV, J. J., TASKER, R. C. & COYLE, J. T. 1994. Delayed protection by MK-801 and tetrodotoxin in a rat organotypic hippocampal culture model of ischemia. *Stroke,* 25**,** 457-64; discussion 464-5.
WALSH, D. M., KLYUBIN, I., FADEEVA, J. V., CULLEN, W. K., ANWYL, R., WOLFE, M. S., ROWAN, M. J. & SELKOE, D. J. 2002. Naturally secreted oligomers of amyloid beta protein potently inhibit hippocampal long-term potentiation in vivo. *Nature,* 416**,** 535-9.
WANG, C., NGUYEN, H. N., MAGUIRE, J. L. & PERRY, D. C. 2002. Role of intracellular calcium stores in cell death from oxygen-glucose deprivation in a neuronal cell line. *J Cereb Blood Flow Metab,* 22**,** 206-14.
WANG, H., CHANG-WONG, T., TANG, H. Y. & SPEICHER, D. W. 2010. Comparison of extensive protein fractionation and repetitive LC-MS/MS analyses on depth of analysis for complex proteomes. *J Proteome Res,* 9**,** 1032-40.
WANG, J., GAO, Q. S., WANG, Y., LAFYATIS, R., STAMM, S. & ANDREADIS, A. 2004. Tau exon 10, whose missplicing causes frontotemporal dementia, is regulated by an intricate interplay of cis elements and trans factors. *J Neurochem,* 88**,** 1078-90.
WARNER, D. S., SHENG, H. & BATINIC-HABERLE, I. 2004. Oxidants, antioxidants and the ischemic brain. *J Exp Biol,* 207**,** 3221-31.
WATANABE, T., HIKICHI, Y., WILLUWEIT, A., SHINTANI, Y. & HORIGUCHI, T. 2012. FBL2 regulates amyloid precursor protein (APP) metabolism by promoting ubiquitination-dependent APP degradation and inhibition of APP endocytosis. *J Neurosci,* 32**,** 3352-65.
WEBSTER, N. J., GREEN, K. N., PEERS, C. & VAUGHAN, P. F. 2002. Altered processing of amyloid precursor protein in the human neuroblastoma SH-SY5Y by chronic hypoxia. *J Neurochem,* 83**,** 1262-71.
WIEDEMANN, N., FRAZIER, A. E. & PFANNER, N. 2004. The protein import machinery of mitochondria. *J Biol Chem,* 279**,** 14473-6.
WISHART, T. M., ROONEY, T. M., LAMONT, D. J., WRIGHT, A. K., MORTON, A. J., JACKSON, M., FREEMAN, M. R. & GILLINGWATER, T. H. 2012. Combining comparative proteomics and molecular genetics uncovers regulators of synaptic and axonal stability and degeneration in vivo. *PLoS Genet,* 8**,** e1002936.
XIE, F., LIU, T., QIAN, W. J., PETYUK, V. A. & SMITH, R. D. 2011. Liquid chromatography-mass spectrometry-based quantitative proteomics. *J Biol Chem,* 286**,** 25443-9.
XIE, H. R., HU, L. S. & LI, G. Y. SH-SY5Y human neuroblastoma cell line: in vitro cell model of dopaminergic neurons in Parkinson's disease. *Chin Med J (Engl),* 123**,** 1086-92.
XUN, Z., LEE, D. Y., LIM, J., CANARIA, C. A., BARNEBEY, A., YANONNE, S. M. & MCMURRAY, C. T. 2012. Retinoic acid-induced differentiation increases the rate

of oxygen consumption and enhances the spare respiratory capacity of mitochondria in SH-SY5Y cells. *Mech Ageing Dev,* 133**,** 176-85.

YAN, S. D., FU, J., SOTO, C., CHEN, X., ZHU, H., AL-MOHANNA, F., COLLISON, K., ZHU, A., STERN, E., SAIDO, T., TOHYAMA, M., OGAWA, S., ROHER, A. & STERN, D. 1997. An intracellular protein that binds amyloid-beta peptide and mediates neurotoxicity in Alzheimer's disease. *Nature,* 389**,** 689-95.

YAN, S. D., SHI, Y., ZHU, A., FU, J., ZHU, H., ZHU, Y., GIBSON, L., STERN, E., COLLISON, K., AL-MOHANNA, F., OGAWA, S., ROHER, A., CLARKE, S. G. & STERN, D. M. 1999. Role of ERAB/L-3-hydroxyacyl-coenzyme A dehydrogenase type II activity in Abeta-induced cytotoxicity. *J Biol Chem,* 274**,** 2145-56.

YANG, W., THOMPSON, J. W., WANG, Z., WANG, L., SHENG, H., FOSTER, M. W., MOSELEY, M. A. & PASCHEN, W. 2012. Analysis of oxygen/glucose-deprivation-induced changes in SUMO3 conjugation using SILAC-based quantitative proteomics. *J Proteome Res,* 11**,** 1108-17.

YANKNER, B. A. 1996. Mechanisms of Neuronal Degeneration in Alzheimer's Disease. *Neuron,* 16**,** 921-932.

YANKNER, B. A., DAWES, L. R., FISHER, S., VILLA-KOMAROFF, L., OSTER-GRANITE, M. L. & NEVE, R. L. 1989. Neurotoxicity of a fragment of the amyloid precursor associated with Alzheimer's disease. *Science,* 245**,** 417-20.

YAO, J., CHEN, S., MAO, Z., CADENAS, E. & BRINTON, R. D. 2011. 2-Deoxy-D-glucose treatment induces ketogenesis, sustains mitochondrial function, and reduces pathology in female mouse model of Alzheimer's disease. *PLoS One,* 6**,** e21788.

YAO, J., IRWIN, R. W., ZHAO, L., NILSEN, J., HAMILTON, R. T. & BRINTON, R. D. 2009. Mitochondrial bioenergetic deficit precedes Alzheimer's pathology in female mouse model of Alzheimer's disease. *Proc Natl Acad Sci U S A,* 106**,** 14670-5.

YAO, J., TAYLOR, M., DAVEY, F., REN, Y., AITON, J., COOTE, P., FANG, F., CHEN, J. X., YAN, S. D. & GUNN-MOORE, F. J. 2007. Interaction of amyloid binding alcohol dehydrogenase/Abeta mediates up-regulation of peroxiredoxin II in the brains of Alzheimer's disease patients and a transgenic Alzheimer's disease mouse model. *Mol Cell Neurosci,* 35**,** 377-82.

YORIMITSU, T., NAIR, U., YANG, Z. & KLIONSKY, D. J. 2006. Endoplasmic reticulum stress triggers autophagy. *J Biol Chem,* 281**,** 30299-304.

YU, J. & ZHANG, L. 2008. PUMA, a potent killer with or without p53. *Oncogene,* 27 Suppl 1**,** S71-83.

ZECHNER, R. & MADEO, F. 2009. Cell biology: Another way to get rid of fat. *Nature,* 458**,** 1118-9.

ZHANG, K. & KAUFMAN, R. J. 2006. The unfolded protein response: A stress signaling pathway critical for health and disease. *Neurology,* 66**,** S102-S109.

ZHIYOU, C., YONG, Y., SHANQUAN, S., JUN, Z., LIANGGUO, H., LING, Y. & JIEYING, L. 2009. Upregulation of BACE1 and beta-amyloid protein mediated by chronic cerebral hypoperfusion contributes to cognitive impairment and pathogenesis of Alzheimer's disease. *Neurochem Res,* 34**,** 1226-35.

ZHOU, J., YU, Q. & ZOU, T. 2008. Alternative splicing of exon 10 in the tau gene as a target for treatment of tauopathies. *BMC Neurosci,* 9 Suppl 2**,** S10.

Appendix A

Calculating an appropriate enrichment ratio for the identification of putative ABAD interacting proteins

Step 1. Identify the number of proteins quantified with 2 or more peptides in each sample

_____ **proteins**

Step 2. Calculate protein enrichment ratio for each protein

$$\frac{\text{abundance in sample}}{\text{abundance in negative control}}$$

Step 3. Plot the frequency distribution of log enrichment ratios

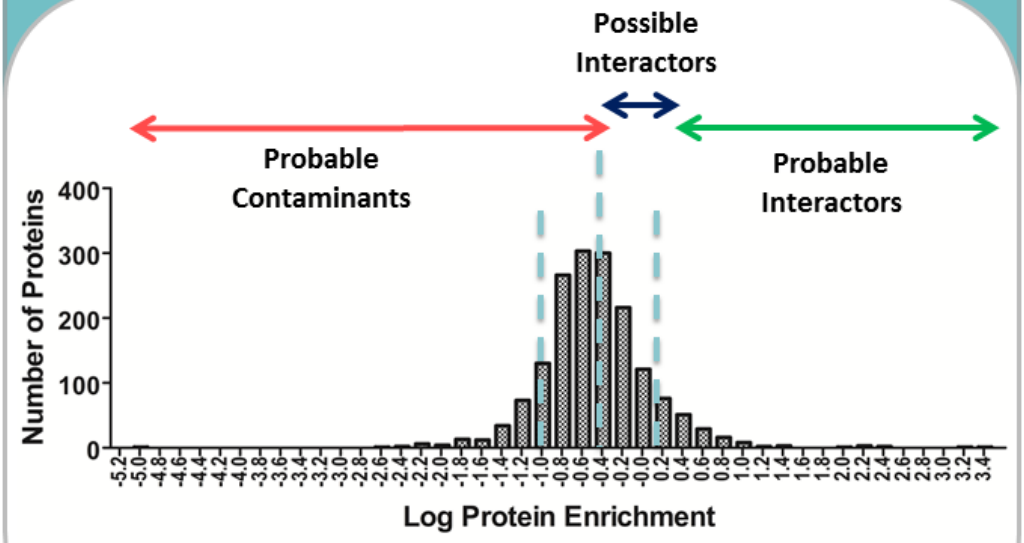

Appendix B

Total proteins detected in all samples with liquid chromatography mass spectrometry (LC-MS). 958 proteins were detected with 2 or more peptides. 14 proteins were significantly altered following 6h OGD ($p<0.01$). 193 proteins were significantly altered following 18h OGD ($p<0.01$). Significant protein changes are designated by **bold typescript**. Proteins are displayed alphabetically with p value, fold change, and direction of the protein change reported.

		6h OGD			18h OGD		
NCBI Accession No.	**Protein Name**	**P Value**	**Fold Change**	**Direction**	**P Value**	**Fold Change**	**Direction**
NP_002148.1	**10 kDa heat shock protein, mitochondrial**	0.879	1.01	Down	**0.00001**	**1.51**	**Up**
NP_004238.3	**116 kDa U5 small nuclear ribonucleoprotein component isoform a**	0.420	1.03	Up	**0.007**	**1.19**	**Up**
NP_054891.2	**14 kDa phosphohistidine phosphatase isoform 3**	0.493	1.09	Up	**0.004**	**1.21**	**Up**
NP_003395.1	14-3-3 protein beta/alpha	0.569	1.03	Down	0.242	1.13	Up
NP_006752.1	**14-3-3 protein epsilon**	0.725	1.02	Down	**0.006**	**1.30**	**Up**
NP_003396.1	14-3-3 protein eta	0.495	1.05	Down	0.174	1.18	Up
NP_036611.2	**14-3-3 protein gamma**	0.802	1.01	Down	**0.004**	**1.15**	**Up**
NP_006817.1	14-3-3 protein theta	0.832	1.01	Down	0.098	1.19	Up
NP_003397.1	14-3-3 protein zeta/delta	0.992	1.00	Up	0.061	1.21	Up
NP_002797.3	26S protease regulatory subunit 10B	0.409	1.04	Up	0.040	1.11	Up
NP_002793.2	26S protease regulatory subunit 4	0.796	1.01	Up	0.646	1.07	Up
NP_002795.2	**26S protease regulatory subunit 6A**	0.414	1.06	Down	**0.007**	**1.27**	**Up**
NP_006494.1	**26S protease regulatory subunit 6B isoform 1**	0.706	1.03	Down	**0.001**	**1.20**	**Up**
NP_002794.1	26S protease regulatory subunit 7	0.886	1.02	Down	0.395	1.09	Up
NP_002796.4	26S protease regulatory subunit 8 isoform 1	0.240	1.06	Down	0.012	1.13	Up
NP_002798.2	**26S proteasome non-ATPase regulatory subunit 1 isoform 1**	0.271	1.03	Up	**0.0002**	**1.18**	**Up**
NP_002806.2	**26S proteasome non-ATPase regulatory subunit 11**	0.765	1.02	Down	**0.001**	**1.18**	**Up**
NP_002807.1	26S proteasome non-ATPase regulatory subunit 12 isoform 1	0.527	1.04	Up	0.183	1.15	Up
NP_002808.3	26S proteasome non-ATPase regulatory subunit 13 isoform 1	0.674	1.03	Up	0.094	1.11	Up
NP_005796.1	26S proteasome non-ATPase regulatory subunit 14	0.045	1.07	Down	0.144	1.13	Up

NP_002799.3	**26S proteasome non-ATPase regulatory subunit 2**	0.816	1.01	Down	**0.001**	**1.22**	**Up**
NP_002800.2	26S proteasome non-ATPase regulatory subunit 3	0.299	1.09	Up	0.011	1.32	Up
NP_002801.1	26S proteasome non-ATPase regulatory subunit 4	0.086	1.13	Down	0.263	1.10	Down
NP_055629.1	**26S proteasome non-ATPase regulatory subunit 6**	0.471	1.02	Up	**0.005**	**1.61**	**Up**
NP_002802.2	26S proteasome non-ATPase regulatory subunit 7	0.475	1.06	Up	0.018	1.21	Up
NP_055706.1	28 kDa heat- and acid-stable phosphoprotein	0.457	1.07	Up	0.776	1.04	Up
NP_055899.2	28S ribosomal protein S27, mitochondrial	0.916	1.01	Down	0.571	1.06	Down
NP_006076.4	3'(2'),5'-bisphosphate nucleotidase 1	0.893	1.02	Down	0.052	1.21	Up
NP_002940.2	39S ribosomal protein L12, mitochondrial precursor	0.506	1.06	Down	0.157	1.23	Up
NP_004484.1	**3-hydroxyacyl-CoA dehydrogenase type-2 isoform 1**	0.370	1.05	Down	**0.004**	**1.27**	**Up**
NP_064524.3	3-hydroxybutyrate dehydrogenase type 2	0.766	1.02	Up	0.016	1.17	Up
NP_006102.2	**3-ketoacyl-CoA thiolase, mitochondrial**	0.190	1.09	Down	**0.007**	**1.26**	**Up**
NP_001013454.1	**3-mercaptopyruvate sulfurtransferase isoform 2**	0.863	1.01	Down	**0.001**	**1.25**	**Up**
NP_001005.1	40S ribosomal protein S10	0.615	1.06	Up	0.027	1.16	Down
NP_001006.1	40S ribosomal protein S11	0.713	1.04	Up	0.093	1.22	Down
NP_001007.2	40S ribosomal protein S12	0.152	1.09	Down	0.025	1.16	Up
NP_001008.1	40S ribosomal protein S13	0.676	1.05	Up	0.108	1.29	Down
NP_005608.1	**40S ribosomal protein S14**	0.615	1.04	Down	**0.0004**	**1.35**	**Down**
NP_001009.1	**40S ribosomal protein S15**	**0.002**	**1.20**	**Down**	**0.048**	**1.22**	**Down**
NP_001010.2	40S ribosomal protein S15a	0.952	1.01	Down	0.185	1.13	Down
NP_001011.1	**40S ribosomal protein S16**	0.832	1.02	Up	**0.0001**	**1.43**	**Down**
NP_001012.1	**40S ribosomal protein S17**	0.052	1.16	Down	**0.0005**	**1.25**	**Down**
NP_072045.1	40S ribosomal protein S18	0.170	1.12	Down	0.018	1.34	Down
NP_001013.1	40S ribosomal protein S19	0.562	1.07	Up	0.043	1.28	Down
NP_002943.2	40S ribosomal protein S2	0.671	1.03	Down	0.048	1.34	Down
NP_001014.1	40S ribosomal protein S20 isoform 2	0.914	1.01	Up	0.190	1.15	Down
NP_001015.1	40S ribosomal protein S21	0.111	1.12	Down	0.981	1.00	Up
NP_001016.1	**40S ribosomal protein S23**	0.740	1.04	Up	**0.0004**	**1.32**	**Down**
NP_001017.1	40S ribosomal protein S24 isoform c	0.503	1.05	Up	0.763	1.03	Down
NP_001019.1	40S ribosomal protein S25	0.960	1.00	Down	0.449	1.08	Down
NP_001020.2	40S ribosomal protein S26	0.879	1.01	Down	0.311	1.06	Down
NP_001021.1	40S ribosomal protein S27	0.943	1.01	Up	0.119	1.17	Down
NP_001023.1	40S ribosomal protein S29 isoform 1	0.652	1.04	Down	0.077	1.14	Down

NP_000996.2	40S ribosomal protein S3	0.786	1.03	Down	0.696	1.03	Down
NP_000997.1	40S ribosomal protein S3a	0.808	1.02	Down	0.651	1.07	Down
NP_000998.1	40S ribosomal protein S4, X isoform X isoform	0.697	1.03	Up	0.137	1.13	Down
NP_001000.2	40S ribosomal protein S5	0.910	1.01	Up	0.430	1.04	Down
NP_001001.2	40S ribosomal protein S6	0.812	1.03	Up	0.138	1.14	Down
NP_001002.1	40S ribosomal protein S7	0.086	1.08	Down	0.474	1.05	Down
NP_001003.1	40S ribosomal protein S8	0.797	1.01	Up	0.672	1.03	Down
NP_001004.2	**40S ribosomal protein S9**	0.904	1.01	Down	**0.0002**	**1.29**	**Down**
NP_002286.2	40S ribosomal protein SA	0.374	1.05	Down	0.243	1.09	Up
NP_065737.2	4-aminobutyrate aminotransferase, mitochondrial precursor	0.921	1.01	Down	0.357	1.06	Up
NP_000687.3	4-trimethylaminobutyraldehyde dehydrogenase	0.433	1.06	Up	0.385	1.07	Up
NP_036387.2	5'-3' exoribonuclease 2	0.193	1.07	Down	0.694	1.05	Down
NP_002147.2	**60 kDa heat shock protein, mitochondrial**	0.302	1.08	Down	**0.001**	**1.31**	**Up**
NP_004591.2	60 kDa SS-A/Ro ribonucleoprotein isoform 2	0.091	1.08	Down	0.987	1.00	Down
NP_000993.1	60S acidic ribosomal protein P0	0.972	1.00	Down	0.026	1.17	Up
NP_000994.1	60S acidic ribosomal protein P1 isoform 1	0.201	1.07	Down	0.261	1.06	Up
NP_000995.1	60S acidic ribosomal protein P2	0.042	1.11	Down	0.060	1.13	Up
NP_006004.2	60S ribosomal protein L10	0.275	1.06	Down	0.012	1.13	Down
NP_009035.3	60S ribosomal protein L10a	0.910	1.01	Down	0.107	1.23	Up
NP_000966.2	60S ribosomal protein L11 isoform 1	0.337	1.09	Down	0.394	1.13	Down
NP_000967.1	60S ribosomal protein L12	0.635	1.03	Down	0.061	1.25	Up
NP_150254.1	**60S ribosomal protein L13**	0.818	1.02	Down	**0.0004**	**1.19**	**Down**
NP_036555.1	60S ribosomal protein L13a	0.305	1.04	Down	0.406	1.06	Up
NP_003964.3	60S ribosomal protein L14	0.237	1.46	Up	0.566	1.10	Up
NP_002939.2	60S ribosomal protein L15	0.693	1.05	Up	0.321	1.06	Up
NP_000976.1	60S ribosomal protein L17 isoform a	0.668	1.04	Down	0.882	1.02	Down
NP_000970.1	60S ribosomal protein L18	0.369	1.07	Down	0.165	1.12	Down
NP_000971.1	60S ribosomal protein L18a	0.246	1.07	Down	0.215	1.07	Down
NP_000972.1	60S ribosomal protein L19	0.454	1.05	Down	0.057	1.13	Down
NP_000973.2	60S ribosomal protein L21	0.335	1.05	Down	0.433	1.07	Down
NP_000974.1	60S ribosomal protein L22 proprotein	0.595	1.05	Up	0.120	1.09	Down
NP_000969.1	**60S ribosomal protein L23**	0.498	1.12	Up	**0.0001**	**1.35**	**Down**
NP_000975.2	60S ribosomal protein L23a	0.947	1.00	Up	0.233	1.09	Down

NP_000977.1	60S ribosomal protein L24	0.588	1.08	Up	0.042	1.24	Down
NP_000978.1	60S ribosomal protein L26	0.624	1.04	Up	0.036	1.18	Down
NP_000979.1	60S ribosomal protein L27	0.017	1.16	Down	0.616	1.04	Up
NP_000981.1	60S ribosomal protein L27a	0.575	1.03	Down	0.469	1.03	Up
NP_000982.2	60S ribosomal protein L28 isoform 2	0.549	1.06	Up	0.117	1.20	Down
NP_000983.1	60S ribosomal protein L29	0.418	1.06	Down	0.605	1.04	Up
NP_000958.1	60S ribosomal protein L3 isoform a	0.615	1.04	Down	0.397	1.03	Down
NP_000980.1	60S ribosomal protein L30	0.740	1.03	Up	0.021	1.28	Up
NP_000984.1	60S ribosomal protein L31 isoform 1	0.812	1.03	Up	0.075	1.14	Down
NP_000985.1	60S ribosomal protein L32	0.244	1.05	Up	0.643	1.05	Down
NP_000986.2	60S ribosomal protein L34	0.729	1.05	Up	0.270	1.13	Up
NP_009140.1	**60S ribosomal protein L35**	0.766	1.03	Up	**0.002**	**1.22**	**Down**
NP_000987.2	60S ribosomal protein L35a	0.102	1.16	Down	0.083	1.26	Down
NP_056229.2	60S ribosomal protein L36	0.120	1.12	Down	0.186	1.20	Down
NP_000990.1	**60S ribosomal protein L38**	0.279	1.16	Up	**0.0001**	**1.55**	**Down**
NP_000959.2	60S ribosomal protein L4	0.750	1.01	Up	0.355	1.06	Down
NP_000960.2	60S ribosomal protein L5	0.918	1.00	Down	0.288	1.06	Down
NP_000961.2	60S ribosomal protein L6	0.140	1.06	Down	0.156	1.08	Up
NP_000962.2	60S ribosomal protein L7	0.411	1.04	Down	0.802	1.01	Down
NP_000963.1	60S ribosomal protein L7a	0.921	1.00	Up	0.298	1.05	Up
NP_000964.1	60S ribosomal protein L8	0.440	1.03	Down	0.791	1.03	Up
NP_000652.2	60S ribosomal protein L9	0.710	1.03	Down	0.123	1.11	Down
NP_002618.1	6-phosphofructokinase type C	0.296	1.05	Up	0.205	1.10	Up
NP_000280.1	6-phosphofructokinase, muscle type isoform 2	0.916	1.01	Down	0.045	1.16	Down
NP_002622.2	6-phosphogluconate dehydrogenase, decarboxylating	0.749	1.03	Up	0.893	1.01	Down
NP_036220.1	6-phosphogluconolactonase	0.775	1.02	Down	0.489	1.04	Up
NP_005338.1	**78 kDa glucose-regulated protein precursor**	0.268	1.10	Up	**0.00004**	**1.53**	**Up**
NP_005882.2	acetyl-CoA acetyltransferase, cytosolic	0.843	1.01	Up	0.016	1.12	Up
NP_000010.1	**acetyl-CoA acetyltransferase, mitochondrial precursor**	0.646	1.04	Down	**0.0001**	**1.38**	**Up**
NP_006296.1	acidic leucine-rich nuclear phosphoprotein 32 family member A	0.574	1.04	Up	0.678	1.02	Up
NP_006392.1	acidic leucine-rich nuclear phosphoprotein 32 family member B	0.316	1.05	Down	0.347	1.17	Down
NP_112182.1	**acidic leucine-rich nuclear phosphoprotein 32 family member E isoform 1**	0.218	1.04	Up	**0.003**	**1.08**	**Up**

NP_001089.1	aconitate hydratase, mitochondrial precursor	0.983	1.00	Down	0.190	1.27	Up
NP_005150.1	actin, alpha cardiac muscle 1 proprotein	0.834	1.05	Up	0.613	1.20	Down
NP_001092.1	actin, cytoplasmic 1	0.702	1.03	Down	0.201	1.17	Up
NP_004292.1	actin-like protein 6A isoform 1	0.251	1.12	Down	0.283	1.20	Up
NP_005713.1	actin-related protein 2 isoform b	0.438	1.03	Up	0.280	1.05	Up
NP_006400.2	actin-related protein 2/3 complex subunit 1A isoform 1	0.663	1.02	Down	0.943	1.00	Up
NP_005711.1	actin-related protein 2/3 complex subunit 1B	0.766	1.02	Up	0.480	1.11	Up
NP_005722.1	actin-related protein 2/3 complex subunit 2	0.338	1.06	Down	0.542	1.08	Down
NP_005710.1	actin-related protein 2/3 complex subunit 3	0.915	1.01	Down	0.161	1.26	Up
NP_005709.1	actin-related protein 2/3 complex subunit 4 isoform a	0.124	1.13	Down	0.624	1.05	Down
NP_005712.1	actin-related protein 3	0.912	1.00	Up	0.043	1.08	Up
NP_006704.3	activated RNA polymerase II transcriptional coactivator p15	0.820	1.02	Down	0.178	1.15	Down
NP_036243.1	activator of 90 kDa heat shock protein ATPase homolog 1	0.695	1.03	Up	0.111	1.11	Up
NP_004994.1	acyl carrier protein, mitochondrial precursor	0.111	1.13	Down	0.020	1.23	Up
NP_009191.1	acyl-protein thioesterase 2	0.249	1.06	Up	0.135	1.09	Up
NP_005197.3	adapter molecule crk isoform b	0.246	1.12	Down	0.137	1.11	Up
NP_000476.1	**adenine phosphoribosyltransferase isoform a**	0.199	1.06	Up	**0.004**	**1.24**	**Up**
NP_000678.1	adenosylhomocysteinase isoform 1	0.738	1.02	Down	0.032	1.15	Up
NP_001616.1	adenylate kinase 2, mitochondrial isoform a	0.535	1.05	Down	0.900	1.01	Down
NP_000467.1	adenylate kinase isoenzyme 1	0.118	1.10	Down	0.022	1.13	Up
NP_006358.1	**adenylyl cyclase-associated protein 1**	0.034	1.16	Down	**0.000005**	**1.42**	**Down**
NP_001627.2	ADP/ATP translocase 3	0.674	1.11	Down	0.013	2.79	Down
NP_001649.1	ADP-ribosylation factor 1	0.355	1.08	Down	0.129	1.17	Down
NP_001651.1	ADP-ribosylation factor 4	0.660	1.03	Down	0.117	1.09	Down
NP_001653.1	ADP-ribosylation factor 5	0.736	1.04	Up	0.342	1.14	Down
NP_004302.1	**ADP-ribosylation factor-like protein 3**	0.263	1.08	Down	**0.007**	**1.23**	**Up**
NP_054861.2	ADP-sugar pyrophosphatase	0.414	1.04	Up	0.024	1.22	Up
NP_001596.2	**alanyl-tRNA synthetase, cytoplasmic**	0.457	1.05	Down	**0.008**	**1.11**	**Up**
NP_000662.3	alcohol dehydrogenase class-3	0.172	1.04	Up	0.010	1.19	Up
NP_000681.2	aldehyde dehydrogenase, mitochondrial precursor	0.518	1.05	Down	0.024	1.32	Up
NP_001619.1	aldose reductase	0.358	1.04	Up	0.187	1.15	Up
NP_001093.1	alpha-actinin-1 isoform b	0.715	1.04	Down	0.060	1.21	Up
NP_004915.2	alpha-actinin-4	0.572	1.03	Up	0.319	1.08	Up

NP_005727.1	**alpha-centractin**	0.585	1.03	Up	**0.003**	**1.23**	**Up**
NP_001419.1	alpha-enolase	0.690	1.02	Down	0.011	1.18	Up
NP_116116.1	**alpha-internexin**	0.560	1.04	Down	**0.00005**	**1.24**	**Up**
NP_001073901.1	alpha-ketoglutarate-dependent dioxygenase FTO	0.797	1.01	Down	0.933	1.00	Up
NP_003818.2	**alpha-soluble NSF attachment protein**	0.565	1.03	Down	**0.0003**	**1.35**	**Up**
NP_002694.3	amidophosphoribosyltransferase proprotein	0.175	1.11	Up	0.013	1.41	Up
NP_004030.1	**annexin A2 isoform 2**	0.204	1.14	Down	**0.004**	**2.06**	**Down**
NP_001145.1	annexin A5	0.485	1.08	Down	0.381	1.13	Up
NP_001146.2	**annexin A6 isoform 1**	0.483	1.07	Down	**0.007**	**1.18**	**Up**
NP_663782.2	AP-1 complex subunit beta-1 isoform b	0.884	1.03	Up	0.019	1.40	Down
NP_055018.2	AP-2 complex subunit alpha-1 isoform 1	0.099	1.14	Up	0.371	1.10	Up
NP_001273.1	AP-2 complex subunit beta isoform b	0.962	1.01	Down	0.073	1.15	Down
NP_004635.2	AP-3 complex subunit beta-2	0.157	1.25	Down	0.430	1.21	Down
NP_658985.2	apolipoprotein A-I-binding protein precursor	0.901	1.01	Down	0.012	1.36	Up
NP_004315.1	apoptosis regulator BAX isoform beta	0.312	1.14	Down	0.138	1.22	Down
NP_055792.1	apoptotic chromatin condensation inducer in the nucleus isoform 1	0.580	1.03	Up	0.045	1.09	Up
NP_002878.2	arginyl-tRNA synthetase, cytoplasmic	0.648	1.04	Up	0.306	1.09	Down
NP_000781.1	aromatic-L-amino-acid decarboxylase	0.957	1.01	Up	0.026	1.38	Up
NP_004530.1	asparaginyl-tRNA synthetase, cytoplasmic	0.802	1.01	Up	0.012	1.11	Down
NP_002071.2	aspartate aminotransferase, mitochondrial precursor	0.761	1.05	Up	0.026	1.85	Up
NP_001340.2	aspartyl-tRNA synthetase, cytoplasmic	0.619	1.02	Down	0.363	1.06	Up
NP_003759.1	astrocytic phosphoprotein PEA-15	0.248	1.11	Down	0.135	1.14	Down
NP_037368.1	**ataxin-10 isoform 1**	0.207	1.11	Down	**0.0001**	**1.49**	**Down**
NP_004037.1	**ATP synthase subunit alpha, mitochondrial precursor**	0.369	1.09	Down	**0.002**	**1.21**	**Up**
NP_001677.2	ATP synthase subunit beta, mitochondrial precursor	0.241	1.10	Down	0.030	1.26	Up
NP_005165.1	ATP synthase subunit gamma, mitochondrial isoform H (heart) precursor	0.986	1.00	Up	0.145	1.18	Up
NP_001688.1	ATP synthase subunit O, mitochondrial precursor	0.807	1.03	Up	0.329	1.15	Up
NP_001676.2	**ATP synthase-coupling factor 6, mitochondrial isoform a precursor**	0.232	1.11	Down	**0.002**	**1.44**	**Up**
NP_004308.2	ATPase ASNA1	0.694	1.03	Up	0.032	1.24	Up
NP_001087.2	**ATP-citrate synthase isoform 1**	0.102	1.11	Down	**0.0005**	**1.47**	**Down**

NP_001348.2	ATP-dependent RNA helicase A	0.509	1.04	Up	0.598	1.02	Up
NP_004930.1	ATP-dependent RNA helicase DDX1	0.946	1.00	Up	0.973	1.00	Down
NP_006764.3	ATP-dependent RNA helicase DDX18	0.606	1.05	Down	0.068	1.25	Down
NP_060802.1	ATP-dependent RNA helicase DDX19A	0.410	1.14	Down	0.792	1.07	Up
NP_005795.2	**ATP-dependent RNA helicase DDX39**	0.203	1.07	Down	**0.00003**	**1.48**	**Down**
NP_001347.3	**ATP-dependent RNA helicase DDX3X isoform 1**	0.294	1.15	Down	**0.001**	**1.45**	**Down**
NP_003851.1	**barrier-to-autointegration factor**	0.393	1.12	Up	**0.004**	**1.46**	**Up**
NP_055485.2	basic leucine zipper and W2 domain-containing protein 1	0.239	1.07	Down	0.049	1.22	Down
NP_055554.1	bcl-2-associated transcription factor 1 isoform 1	0.393	1.05	Down	0.983	1.00	Down
NP_110517.2	beta-catenin-like protein 1	0.311	1.13	Up	0.257	1.18	Down
NP_001187.1	BH3-interacting domain death agonist isoform 2	0.141	1.19	Down	0.974	1.00	Down
NP_004437.2	bifunctional aminoacyl-tRNA synthetase	0.509	1.07	Down	0.012	1.30	Down
NP_004035.2	bifunctional purine biosynthesis protein PURH	0.753	1.01	Up	0.293	1.12	Up
NP_000703.2	biliverdin reductase A precursor	0.543	1.04	Up	0.051	1.18	Up
NP_001026997.1	BolA-like protein 2	0.177	1.09	Up	0.162	1.35	Up
NP_006308.3	brain acid soluble protein 1	0.519	1.08	Up	0.302	1.11	Down
NP_653296.2	BRO1 domain-containing protein BROX	0.316	1.05	Up	0.014	1.16	Up
NP_005947.3	C-1-tetrahydrofolate synthase, cytoplasmic	0.218	1.08	Down	0.094	1.08	Up
NP_004332.2	CAD protein	0.558	1.18	Up	0.729	1.25	Down
NP_055066.1	calcium-binding mitochondrial carrier protein Aralar2 isoform 2	0.667	1.11	Down	0.011	2.82	Down
NP_001035941.1	calcium-regulated heat stable protein 1	0.225	1.06	Up	0.037	1.19	Up
NP_055227.1	calcyclin-binding protein isoform 1	0.788	1.03	Up	0.581	1.10	Up
NP_004333.1	caldesmon isoform 2	0.407	1.10	Up	0.046	1.23	Down
NP_001734.1	**calmodulin**	0.815	1.01	Up	**0.006**	**1.17**	**Up**
NP_001737.1	calnexin precursor	0.169	1.21	Up	0.120	1.26	Down
NP_001740.1	calpain small subunit 1	0.679	1.02	Down	0.951	1.00	Up
NP_001830.1	calponin-3	0.079	1.12	Down	0.500	1.04	Down
NP_004334.1	**calreticulin precursor**	0.096	1.12	Up	**0.0000001**	**1.56**	**Up**
NP_001210.1	calumenin isoform a precursor	0.374	1.05	Up	0.011	1.28	Up
NP_002727.2	cAMP-dependent protein kinase type II-beta regulatory subunit	0.638	1.03	Up	0.224	1.11	Up
NP_005889.3	**caprin-1 isoform 1**	0.131	1.16	Down	**0.00004**	**1.45**	**Down**
NP_001748.1	carbonyl reductase [NADPH] 1	0.483	1.03	Down	0.351	1.10	Up
NP_001886.1	**casein kinase II subunit alpha isoform a**	0.631	1.03	Up	**0.008**	**1.27**	**Up**

NP_001899.1	**cathepsin B preproprotein**	0.813	1.01	Down	**0.005**	**1.18**	**Down**
NP_001782.1	cell division control protein 42 homolog isoform 1	0.828	1.03	Down	0.216	1.13	Down
NP_060707.2	cell division cycle and apoptosis regulator protein 1	0.056	1.11	Up	0.225	1.10	Up
NP_001777.1	**cell division protein kinase 1 isoform 1**	0.541	1.08	Down	**0.002**	**1.75**	**Down**
NP_004926.1	cell division protein kinase 5 isoform 1	0.245	1.26	Down	0.014	2.31	Down
NP_003409.1	cellular nucleic acid-binding protein isoform 3	0.156	1.13	Down	0.122	1.08	Down
NP_001869.1	cellular retinoic acid-binding protein 2	0.963	1.01	Down	0.244	1.38	Up
NP_057494.3	charged multivesicular body protein 5 isoform 1	0.903	1.01	Down	0.180	1.07	Up
NP_001279.2	chloride intracellular channel protein 1	0.981	1.00	Up	0.139	1.15	Up
NP_039234.1	**chloride intracellular channel protein 4**	**0.008**	**1.19**	**Down**	0.018	1.16	Down
NP_006798.1	chromobox protein homolog 1	0.832	1.01	Up	0.365	1.08	Up
NP_009207.2	chromobox protein homolog 3	0.226	1.07	Down	0.862	1.01	Up
NP_036249.1	chromobox protein homolog 5	0.927	1.01	Up	0.078	1.20	Up
NP_004068.2	citrate synthase, mitochondrial precursor	0.288	1.12	Down	0.458	1.10	Up
NP_004850.1	**clathrin heavy chain 1**	0.778	1.01	Up	**0.00005**	**1.16**	**Up**
NP_001824.1	clathrin light chain A isoform a	0.190	1.09	Down	0.201	1.17	Up
NP_008937.1	cleavage and polyadenylation specificity factor subunit 5	0.442	1.03	Down	0.965	1.00	Up
NP_008938.2	cleavage and polyadenylation specificity factor subunit 6	0.368	1.02	Down	0.021	1.19	Up
NP_001129512.1	cleavage and polyadenylation specificity factor subunit 7 isoform 2	0.668	1.03	Up	0.455	1.06	Up
NP_057535.1	coatomer subunit beta	0.761	1.02	Down	0.294	1.10	Down
NP_004757.1	coatomer subunit beta'	0.300	1.06	Down	0.016	1.18	Up
NP_001646.2	coatomer subunit delta isoform 1	0.166	1.13	Down	0.889	1.01	Up
NP_009194.2	coatomer subunit epsilon isoform a	0.467	1.05	Down	0.184	1.13	Down
NP_057212.1	**coatomer subunit gamma**	**0.004**	**1.34**	**Down**	0.066	1.28	Down
NP_036265.3	coatomer subunit gamma-2	0.267	1.09	Down	0.716	1.04	Down
NP_057141.1	coatomer subunit zeta-1	0.285	1.13	Down	0.887	1.02	Up
NP_005498.1	cofilin-1	0.136	1.07	Up	0.018	1.18	Up
NP_057223.1	**coiled-coil-helix-coiled-coil-helix domain-containing protein 2, mitochondrial precursor**	0.581	1.06	Up	**0.010**	**1.43**	**Down**
NP_009089.4	**cold shock domain-containing protein E1 isoform 2**	0.019	1.31	Down	**0.000001**	**1.61**	**Down**
NP_001271.1	cold-inducible RNA-binding protein	0.467	1.04	Down	0.508	1.07	Down

NP_001203.1	complement component 1 Q subcomponent-binding protein, mitochondrial precursor	0.385	1.05	Down	0.037	1.33	Up
NP_997657.1	COP9 signalosome complex subunit 1 isoform 1	0.401	1.09	Down	0.707	1.04	Up
NP_057213.2	COP9 signalosome complex subunit 4	0.568	1.04	Down	0.080	1.15	Up
NP_006824.2	COP9 signalosome complex subunit 6	0.801	1.02	Up	0.521	1.05	Up
NP_690902.1	copine-1 isoform a	0.086	1.09	Down	0.842	1.01	Up
NP_004884.1	core histone macro-H2A.1 isoform 2	0.288	1.33	Up	0.229	1.27	Down
NP_055140.1	coronin-1C isoform 1	0.567	1.09	Up	0.539	1.10	Up
NP_001814.2	**creatine kinase B-type**	0.986	1.00	Up	**0.003**	**1.16**	**Up**
NP_066270.1	creatine kinase U-type, mitochondrial precursor	0.243	1.10	Up	0.580	1.05	Up
NP_005198.1	crk-like protein	0.170	1.17	Up	0.036	1.20	Up
NP_001319.1	C-terminal-binding protein 1 isoform 1	0.860	1.01	Up	0.652	1.05	Down
NP_001896.2	CTP synthase 1	0.212	1.06	Down	0.591	1.04	Down
NP_060918.2	cullin-associated NEDD8-dissociated protein 1	0.689	1.01	Down	0.053	1.11	Up
NP_000062.1	**cystathionine beta-synthase**	0.421	1.03	Up	**0.008**	**1.20**	**Up**
NP_001303.1	cysteine-rich protein 2	0.153	1.07	Up	0.280	1.17	Up
NP_003356.2	**cytochrome b-c1 complex subunit 1, mitochondrial precursor**	0.339	1.20	Down	**0.010**	**2.17**	**Down**
NP_003357.2	**cytochrome b-c1 complex subunit 2, mitochondrial precursor**	0.571	1.16	Down	**0.002**	**3.26**	**Down**
NP_004246.2	cytochrome c oxidase subunit 5A, mitochondrial precursor	0.108	1.17	Down	0.347	1.19	Down
NP_001854.1	cytochrome c oxidase subunit 6B1	0.030	1.31	Down	0.169	1.16	Down
NP_001367.2	cytoplasmic dynein 1 heavy chain 1	0.991	1.00	Up	0.927	1.02	Down
NP_006132.1	cytoplasmic dynein 1 light intermediate chain 2	0.420	1.05	Up	0.159	1.08	Up
NP_863654.1	**cytosolic acyl coenzyme A thioester hydrolase isoform hBACHb**	0.467	1.06	Up	**0.001**	**1.19**	**Up**
NP_060705.2	cytosolic non-specific dipeptidase isoform 1	0.698	1.03	Up	0.019	1.20	Up
NP_006614.2	D-3-phosphoglycerate dehydrogenase	0.073	1.10	Down	0.079	1.13	Up
NP_061832.2	DAZ-associated protein 1 isoform b	0.741	1.02	Down	0.060	1.24	Up
NP_077001.1	dCTP pyrophosphatase 1	0.521	1.07	Up	0.983	1.00	Down
NP_001346.1	D-dopachrome decarboxylase	0.999	1.00	Up	0.022	1.27	Up
NP_001389.2	**delta(3,5)-Delta(2,4)-dienoyl-CoA isomerase, mitochondrial precursor**	0.153	1.09	Down	**0.005**	**1.28**	**Up**

NP_002851.2	delta-1-pyrroline-5-carboxylate synthase isoform 1	0.967	1.00	Up	0.212	1.10	Up
NP_001939.1	deoxyuridine 5'-triphosphate nucleotidohydrolase, mitochondrial isoform 2	0.376	1.07	Down	0.462	1.07	Down
NP_006861.1	destrin isoform a	0.821	1.02	Down	0.952	1.01	Up
NP_000099.2	**dihydrolipoyl dehydrogenase, mitochondrial precursor**	0.836	1.02	Up	**0.005**	**1.36**	**Up**
NP_001924.2	dihydrolipoyllysine-residue succinyltransferase component of 2-oxoglutarate dehydrogenase complex, mitochondrial	0.922	1.01	Down	0.185	1.36	Up
NP_001304.1	dihydropyrimidinase-related protein 1 isoform 2	0.655	1.02	Down	0.532	1.03	Up
NP_001184222.1	dihydropyrimidinase-related protein 2 isoform 1	0.722	1.02	Down	0.069	1.11	Up
NP_001378.1	dihydropyrimidinase-related protein 3 isoform 2	0.471	1.04	Down	0.390	1.09	Up
NP_006417.2	dihydropyrimidinase-related protein 4	0.593	1.06	Up	0.442	1.07	Up
NP_064519.2	dihydropyrimidinase-related protein 5	0.792	1.01	Down	0.033	1.09	Up
NP_005691.2	dipeptidyl peptidase 3	0.588	1.06	Up	0.057	1.27	Up
NP_001914.3	DNA damage-binding protein 1	0.365	1.03	Down	0.455	1.03	Up
NP_000242.1	DNA mismatch repair protein Msh2	0.388	1.04	Down	0.167	1.08	Down
NP_000170.1	DNA mismatch repair protein Msh6	0.919	1.01	Up	0.017	1.65	Down
NP_004517.2	DNA replication licensing factor MCM2	0.277	1.08	Down	0.019	1.26	Down
NP_002379.2	DNA replication licensing factor MCM3	0.677	1.05	Up	0.023	1.32	Down
NP_877423.1	DNA replication licensing factor MCM4	0.136	1.10	Down	0.067	1.16	Down
NP_005906.2	DNA replication licensing factor MCM6	0.459	1.03	Down	0.103	1.07	Down
NP_005907.3	DNA replication licensing factor MCM7 isoform 1	0.108	1.11	Down	0.033	1.18	Down
NP_001632.2	DNA-(apurinic or apyrimidinic site) lyase	0.317	1.11	Up	0.913	1.01	Down
NP_008835.5	DNA-dependent protein kinase catalytic subunit isoform 1	0.230	2.46	Up	0.314	1.57	Up
NP_002686.2	DNA-directed RNA polymerases I, II, and III subunit RPABC1	0.437	1.11	Down	0.362	1.11	Down
NP_001530.1	**dnaJ homolog subfamily A member 1**	**0.006**	**1.18**	**Down**	0.089	1.24	Down
NP_005871.1	**dnaJ homolog subfamily A member 2**	0.353	1.08	Down	**0.002**	**1.25**	**Up**
NP_002941.1	**dolichyl-diphosphooligosaccharide--protein glycosyltransferase subunit 1 precursor**	0.722	1.09	Up	**0.009**	**1.46**	**Down**
NP_002942.2	dolichyl-diphosphooligosaccharide--protein glycosyltransferase subunit 2 isoform 1 precursor	0.856	1.04	Up	0.170	1.18	Down
NP_000778.3	dopamine beta-hydroxylase precursor	0.170	1.11	Down	0.037	1.18	Down
NP_001102.2	double-stranded RNA-specific adenosine deaminase isoform a	0.798	1.03	Up	0.010	1.25	Down
NP_004386.2	drebrin isoform a	0.922	1.01	Up	0.030	1.18	Up

NP_054782.2	**drebrin-like protein isoform a**	0.531	1.05	Up	**0.010**	**1.18**	**Up**
NP_001177765.1	dynactin subunit 1 isoform 5	0.263	1.17	Down	0.467	1.03	Up
NP_006391.1	dynactin subunit 2	0.780	1.03	Up	0.120	1.31	Up
NP_001005336.1	dynamin-1 isoform 2	0.393	1.06	Down	0.827	1.02	Down
NP_036192.2	dynamin-1-like protein isoform 1	0.202	1.08	Down	0.560	1.02	Up
NP_003737.1	dynein light chain 1, cytoplasmic	0.370	1.08	Up	0.137	1.18	Up
NP_054902.1	dynein light chain roadblock-type 1	0.649	1.03	Down	0.211	1.17	Up
NP_006510.1	dynein light chain Tctex-type 1	0.952	1.00	Up	0.353	1.05	Up
NP_113584.3	E3 ubiquitin-protein ligase HUWE1	0.863	1.02	Down	0.852	1.03	Up
NP_055063.1	E3 ubiquitin-protein ligase RBX1	0.651	1.03	Down	0.407	1.09	Up
NP_009143.1	E3 ubiquitin-protein ligase RING2	0.744	1.03	Up	0.874	1.01	Down
NP_061936.2	echinoderm microtubule-associated protein-like 4 isoform a	0.436	1.24	Up	0.392	1.17	Down
NP_001410.2	ELAV-like protein 1	0.497	1.07	Up	0.047	1.23	Up
NP_001411.2	ELAV-like protein 3 isoform 1	0.990	1.00	Down	0.103	1.16	Up
NP_068771.2	**ELAV-like protein 4 isoform 1**	0.664	1.05	Up	**0.006**	**1.55**	**Up**
NP_000117.1	**electron transfer flavoprotein subunit alpha, mitochondrial isoform a**	0.715	1.02	Down	**0.0005**	**1.33**	**Up**
NP_001393.1	elongation factor 1-alpha 1	0.696	1.03	Down	0.048	1.16	Down
NP_001949.1	elongation factor 1-alpha 2	0.967	1.00	Up	0.045	1.24	Down
NP_001950.1	elongation factor 1-beta	0.583	1.03	Down	0.801	1.02	Up
NP_001951.2	elongation factor 1-delta isoform 2	0.028	1.15	Down	0.874	1.02	Up
NP_001395.1	elongation factor 1-gamma	0.514	1.03	Down	0.674	1.04	Down
NP_001952.1	**elongation factor 2**	**0.007**	**1.14**	**Down**	0.056	1.08	Down
NP_003312.3	elongation factor Tu, mitochondrial precursor	0.682	1.03	Down	0.582	1.06	Up
NP_006808.1	**endoplasmic reticulum resident protein 29 isoform 1 precursor**	0.484	1.05	Down	**0.0003**	**1.23**	**Up**
NP_055866.1	**endoplasmic reticulum resident protein 44 precursor**	0.233	1.21	Up	**0.001**	**1.23**	**Up**
NP_003290.1	**endoplasmin precursor**	0.338	1.06	Up	**0.0001**	**1.49**	**Up**
NP_004441.1	**enhancer of rudimentary homolog**	0.699	1.03	Down	**0.004**	**1.46**	**Up**
NP_004083.3	**enoyl-CoA hydratase, mitochondrial precursor**	0.913	1.01	Down	**0.004**	**1.33**	**Up**
NP_055399.1	ERO1-like protein alpha precursor	0.387	1.06	Up	0.018	1.25	Up
NP_004640.3	ES1 protein homolog, mitochondrial isoform Ia precursor	0.272	1.21	Up	0.060	1.27	Up
NP_001407.1	**eukaryotic initiation factor 4A-I**	**0.00003**	**1.30**	**Down**	**0.00004**	**1.52**	**Down**

NP_001958.2	eukaryotic initiation factor 4A-II	0.014	1.32	Down	0.028	1.38	Down
NP_055555.1	eukaryotic initiation factor 4A-III	0.830	1.02	Down	0.362	1.10	Up
NP_002085.2	eukaryotic peptide chain release factor GTP-binding subunit ERF3A isoform 1	0.345	1.05	Down	0.203	1.13	Up
NP_004721.1	eukaryotic peptide chain release factor subunit 1	0.643	1.05	Down	0.015	1.27	Down
NP_004271.1	eukaryotic translation elongation factor 1 epsilon-1 isoform 1	0.759	1.03	Up	0.142	1.12	Down
NP_005792.1	**eukaryotic translation initiation factor 1**	**0.003**	**1.38**	**Down**	**0.000002**	**2.00**	**Down**
NP_004085.1	eukaryotic translation initiation factor 2 subunit 1	0.490	1.05	Down	0.438	1.10	Down
NP_001406.1	eukaryotic translation initiation factor 2 subunit 3	0.321	1.12	Up	0.058	1.28	Down
NP_003741.1	eukaryotic translation initiation factor 3 subunit A	0.512	1.05	Down	0.062	1.22	Down
NP_003742.2	eukaryotic translation initiation factor 3 subunit B	0.819	1.02	Down	0.472	1.10	Down
NP_003743.1	eukaryotic translation initiation factor 3 subunit C	0.234	1.12	Down	0.242	1.12	Down
NP_001559.1	eukaryotic translation initiation factor 3 subunit E	0.536	1.04	Down	0.615	1.02	Up
NP_003745.1	eukaryotic translation initiation factor 3 subunit F	0.086	1.11	Down	0.567	1.03	Up
NP_003747.1	eukaryotic translation initiation factor 3 subunit H	0.076	1.10	Down	0.366	1.10	Up
NP_003748.1	**eukaryotic translation initiation factor 3 subunit I**	**0.002**	**1.17**	**Down**	**0.009**	**1.12**	**Down**
NP_057175.1	eukaryotic translation initiation factor 3 subunit L	0.097	1.19	Up	0.971	1.00	Up
NP_006351.2	eukaryotic translation initiation factor 3 subunit M	0.705	1.02	Down	0.335	1.06	Down
NP_937884.1	**eukaryotic translation initiation factor 4 gamma 1 isoform 5**	0.271	1.15	Down	**0.008**	**1.29**	**Down**
NP_001408.2	eukaryotic translation initiation factor 4B	0.073	1.20	Down	0.777	1.01	Down
NP_001959.1	eukaryotic translation initiation factor 4E isoform 1	0.500	1.05	Down	0.264	1.18	Up
NP_071496.1	eukaryotic translation initiation factor 4H isoform 1	0.418	1.04	Down	0.612	1.03	Down
NP_001960.2	eukaryotic translation initiation factor 5	0.230	1.06	Down	0.929	1.01	Up
NP_001961.1	eukaryotic translation initiation factor 5A-1 isoform B	0.952	1.00	Down	0.023	1.12	Up
NP_002203.1	eukaryotic translation initiation factor 6 isoform a	0.132	1.07	Down	0.012	1.11	Up
NP_852480.1	exosome complex exonuclease RRP43	0.746	1.04	Down	0.823	1.02	Down
NP_005024.2	exosome complex exonuclease RRP45 isoform 2	0.741	1.04	Up	0.653	1.05	Up
NP_003391.1	exportin-1	0.801	1.01	Up	0.779	1.03	Up
NP_001307.2	exportin-2	0.443	1.04	Up	0.271	1.06	Up
NP_065801.1	exportin-5	0.953	1.01	Down	0.658	1.07	Up
NP_056107.1	extended synaptotagmin-1 isoform 2	0.518	1.16	Up	0.615	1.07	Up
NP_003370.2	ezrin	0.026	1.17	Down	0.328	1.10	Down
NP_009123.1	FACT complex subunit SPT16	0.760	1.02	Up	0.916	1.01	Up

NP_003137.1	FACT complex subunit SSRP1	0.652	1.02	Up	0.152	1.11	Up
NP_006126.1	**F-actin-capping protein subunit alpha-1**	0.127	1.10	Up	**0.004**	**1.35**	**Up**
NP_004921.1	**F-actin-capping protein subunit beta**	0.533	1.10	Up	**0.00003**	**1.25**	**Up**
NP_003893.2	far upstream element-binding protein 1	0.784	1.02	Down	0.038	1.20	Up
NP_003676.2	far upstream element-binding protein 2	0.305	1.05	Down	0.075	1.15	Up
NP_003925.1	far upstream element-binding protein 3	0.172	1.09	Down	0.932	1.01	Down
NP_001995.1	farnesyl pyrophosphate synthase isoform a	0.582	1.06	Up	0.123	1.18	Up
NP_003079.1	**fascin**	0.896	1.00	Up	**0.002**	**1.18**	**Up**
NP_004095.4	fatty acid synthase	0.114	1.08	Down	0.048	1.20	Down
NP_001435.1	fatty acid-binding protein, epidermal	0.315	1.10	Down	0.607	1.07	Up
NP_078941.2	**F-box-like/WD repeat-containing protein TBL1XR1**	0.917	1.01	Down	**0.005**	**1.17**	**Up**
NP_001447.2	filamin-A isoform 1	0.740	1.04	Down	0.553	1.08	Down
NP_001448.2	filamin-B isoform 2	0.843	1.03	Up	0.726	1.04	Down
NP_004102.1	flap endonuclease 1	0.681	1.04	Up	0.300	1.09	Down
NP_001440.2	four and a half LIM domains protein 1 isoform 2	0.514	1.02	Up	0.230	1.12	Up
NP_005078.2	fragile X mental retardation syndrome-related protein 1 isoform a	0.880	1.01	Down	0.013	1.27	Down
NP_000025.1	fructose-bisphosphate aldolase A	0.986	1.00	Down	0.013	1.20	Up
NP_005156.1	**fructose-bisphosphate aldolase C**	0.738	1.03	Up	**0.006**	**1.34**	**Up**
NP_000134.2	**fumarate hydratase, mitochondrial precursor**	0.409	1.05	Up	**0.004**	**1.27**	**Up**
NP_002296.1	galectin-1	0.512	1.07	Down	0.299	1.13	Down
NP_001966.1	**gamma-enolase**	0.977	1.00	Down	**0.0001**	**1.23**	**Up**
NP_076956.1	gamma-glutamylcyclotransferase isoform 1	0.165	1.19	Down	0.084	1.55	Up
NP_127492.1	general transcription factor II-I isoform 1	0.414	1.18	Down	0.011	1.57	Down
NP_003706.1	general vesicular transport factor p115	0.912	1.01	Up	0.739	1.03	Up
NP_001035810.1	glucose-6-phosphate 1-dehydrogenase isoform b	0.585	1.03	Up	0.475	1.04	Up
NP_000166.2	**glucose-6-phosphate isomerase isoform 2**	0.077	1.07	Up	**0.001**	**1.27**	**Up**
NP_002734.2	**glucosidase 2 subunit beta isoform 1**	0.666	1.03	Down	**0.002**	**1.33**	**Up**
NP_005262.1	glutamate dehydrogenase 1, mitochondrial precursor	0.701	1.04	Down	0.073	1.28	Up
NP_055720.3	glutaminase kidney isoform, mitochondrial precursor	0.802	1.02	Down	0.941	1.01	Up
NP_006532.2	glutaredoxin-3	0.921	1.00	Down	0.894	1.01	Up
NP_000628.2	glutathione reductase, mitochondrial isoform 1 precursor	0.606	1.03	Down	0.446	1.13	Up
NP_000840.2	**glutathione S-transferase Mu 3**	**0.009**	**1.08**	**Up**	0.101	1.17	Up

NP_004823.1	glutathione S-transferase omega-1 isoform 1	0.504	1.08	Up	0.135	1.10	Up
NP_000843.1	**glutathione S-transferase P**	0.467	1.03	Up	**0.001**	**1.20**	**Up**
NP_002037.2	glyceraldehyde-3-phosphate dehydrogenase	0.729	1.01	Up	0.014	1.10	Up
NP_002038.2	glycyl-tRNA synthetase	0.130	1.06	Down	0.014	1.14	Up
NP_057164.3	glyoxalase domain-containing protein 4	0.510	1.05	Down	0.058	1.15	Up
NP_003866.1	GMP synthase [glutamine-hydrolyzing]	0.462	1.06	Down	0.353	1.11	Down
NP_002083.3	G-rich sequence factor 1 isoform 1	0.174	1.11	Down	0.781	1.03	Down
NP_002077.1	growth factor receptor-bound protein 2 isoform 1	0.179	1.14	Down	0.882	1.01	Up
NP_006316.1	GTP-binding nuclear protein Ran	0.665	1.02	Down	0.245	1.03	Up
NP_064535.1	GTP-binding protein SAR1a	0.186	1.07	Down	0.389	1.09	Up
NP_002065.1	guanine nucleotide-binding protein G(I)/G(S)/G(T) subunit beta-1	0.321	1.07	Up	0.451	1.13	Down
NP_005264.2	guanine nucleotide-binding protein G(I)/G(S)/G(T) subunit beta-2	0.930	1.00	Down	0.455	1.08	Down
NP_006089.1	guanine nucleotide-binding protein subunit beta-2-like 1	0.105	1.08	Down	0.079	1.09	Up
NP_001354.1	H/ACA ribonucleoprotein complex subunit 4 isoform 1	0.296	1.21	Down	0.490	1.09	Down
NP_005337.2	heat shock 70 kDa protein 1A/1B	0.666	1.03	Up	0.531	1.03	Down
NP_002145.3	heat shock 70 kDa protein 4	0.821	1.02	Up	0.025	1.18	Up
NP_006588.1	heat shock cognate 71 kDa protein isoform 1	0.594	1.03	Down	0.232	1.05	Down
NP_006635.2	heat shock protein 105 kDa	0.787	1.02	Down	0.294	1.04	Up
NP_057376.2	heat shock protein 75 kDa, mitochondrial precursor	0.363	1.09	Down	0.772	1.03	Down
NP_001531.1	heat shock protein beta-1	0.987	1.00	Down	0.506	1.12	Up
NP_005339.3	**heat shock protein HSP 90-alpha isoform 2**	0.677	1.02	Up	**0.003**	**1.11**	**Up**
NP_031381.2	heat shock protein HSP 90-beta	0.671	1.02	Down	0.222	1.05	Up
NP_057269.1	hematological and neurological expressed 1 protein isoform 1	0.306	1.06	Down	0.306	1.09	Down
NP_653171.1	hematological and neurological expressed 1-like protein	0.636	1.03	Down	0.109	1.19	Up
NP_000508.1	**hemoglobin subunit alpha**	0.085	1.48	Up	**0.0003**	**1.97**	**Up**
NP_004485.1	hepatoma-derived growth factor isoform a	0.842	1.01	Down	0.140	1.12	Up
NP_057371.2	heterochromatin protein 1-binding protein 3	0.313	1.58	Up	0.390	1.24	Down
NP_004490.2	heterogeneous nuclear ribonucleoprotein A/B isoform b	0.979	1.00	Up	0.015	1.16	Down
NP_006796.1	heterogeneous nuclear ribonucleoprotein A0	0.494	1.06	Up	0.088	1.28	Down
NP_002127.1	heterogeneous nuclear ribonucleoprotein A1 isoform a	0.641	1.04	Up	0.761	1.03	Up
NP_919223.1	heterogeneous nuclear ribonucleoprotein A3	0.419	1.09	Up	0.273	1.08	Up

NP_002129.2	heterogeneous nuclear ribonucleoprotein D0 isoform c	0.589	1.04	Up	0.016	1.14	Down
NP_112740.1	heterogeneous nuclear ribonucleoprotein D-like	0.420	1.04	Down	0.893	1.01	Up
NP_004957.1	heterogeneous nuclear ribonucleoprotein F	0.563	1.04	Down	0.286	1.12	Up
NP_002130.2	heterogeneous nuclear ribonucleoprotein G isoform 1	0.328	1.13	Up	0.726	1.04	Down
NP_005511.1	heterogeneous nuclear ribonucleoprotein H	0.998	1.00	Up	0.410	1.12	Up
NP_062543.1	heterogeneous nuclear ribonucleoprotein H2	0.516	1.06	Down	0.554	1.12	Up
NP_036339.1	heterogeneous nuclear ribonucleoprotein H3 isoform a	0.111	1.08	Up	0.260	1.06	Up
NP_112552.1	heterogeneous nuclear ribonucleoprotein K isoform b	0.269	1.05	Down	0.036	1.10	Up
NP_001524.2	heterogeneous nuclear ribonucleoprotein L isoform a	0.700	1.01	Down	0.545	1.03	Down
NP_612403.2	heterogeneous nuclear ribonucleoprotein L-like isoform 1	0.131	1.09	Up	0.807	1.02	Down
NP_005959.2	heterogeneous nuclear ribonucleoprotein M isoform a	0.425	1.05	Down	0.536	1.04	Up
NP_006363.4	heterogeneous nuclear ribonucleoprotein Q isoform 1	0.515	1.10	Up	0.191	1.14	Down
NP_005817.1	heterogeneous nuclear ribonucleoprotein R isoform 2	0.686	1.06	Up	0.589	1.04	Down
NP_004492.2	heterogeneous nuclear ribonucleoprotein U isoform b	0.618	1.04	Up	0.011	1.26	Down
NP_001073027.1	heterogeneous nuclear ribonucleoprotein U-like protein 2	0.077	1.07	Up	0.059	1.07	Up
NP_112533.1	heterogeneous nuclear ribonucleoproteins A2/B1 isoform B1	0.874	1.01	Up	0.065	1.11	Up
NP_112604.2	**heterogeneous nuclear ribonucleoproteins C1/C2 isoform a**	0.561	1.04	Down	**0.001**	**1.24**	**Down**
NP_000179.2	hexokinase-1 isoform HKI	0.603	1.04	Up	0.248	1.08	Down
NP_002119.1	high mobility group protein B1	0.174	1.24	Up	0.316	1.13	Down
NP_002120.1	high mobility group protein B2	0.167	1.30	Up	0.312	1.14	Down
NP_665906.1	high mobility group protein HMG-I/HMG-Y isoform a	0.396	1.21	Up	0.446	1.07	Down
NP_002140.2	hippocalcin-like protein 1	0.378	1.12	Down	0.866	1.04	Down
NP_005331.1	**histidine triad nucleotide-binding protein 1**	0.606	1.01	Up	**0.0002**	**1.15**	**Up**
NP_002100.2	histidyl-tRNA synthetase, cytoplasmic	0.302	1.06	Down	0.417	1.06	Down
NP_001518.3	histone deacetylase 2	0.152	1.06	Down	0.847	1.02	Down
NP_005309.1	histone H1.0	0.264	2.32	Up	0.864	1.03	Down
NP_005310.1	histone H1.2	0.291	3.56	Up	0.077	1.62	Down
NP_005312.1	histone H1.4	0.281	4.29	Up	0.086	1.47	Down
NP_005313.1	histone H1.5	0.296	3.71	Up	0.314	1.31	Down
NP_006017.1	histone H1x	0.136	1.47	Up	0.936	1.01	Up
NP_003507.1	histone H2A type 2-A	0.518	1.13	Up	0.020	1.81	Down
NP_002097.1	histone H2A.Z	0.802	1.04	Up	0.075	1.35	Down
NP_003509.1	histone H2B type 1-C/E/F/G/I	0.287	1.19	Up	0.913	1.01	Down

NP_003520.1	histone H3.1	0.292	3.26	Up	0.406	1.34	Down
NP_003529.1	histone H4	0.294	4.16	Up	0.476	1.28	Down
NP_005601.1	histone-binding protein RBBP4 isoform a	0.815	1.01	Down	0.841	1.01	Up
NP_002884.1	histone-binding protein RBBP7 isoform 2	0.417	1.07	Down	0.806	1.03	Up
NP_057123.1	homeobox prox 1	0.691	1.01	Down	0.064	1.12	Up
NP_005325.2	host cell factor 1	0.292	1.05	Up	0.647	1.03	Down
NP_003923.2	hsc70-interacting protein	0.236	1.07	Up	0.320	1.13	Up
NP_036399.3	hsp70-binding protein 1	0.388	1.09	Down	0.328	1.17	Down
NP_008996.1	hsp90 co-chaperone Cdc37	0.685	1.02	Down	0.167	1.08	Up
NP_001171634.2	hydroxyacyl-coenzyme A dehydrogenase, mitochondrial isoform 1 precursor	0.163	1.09	Down	0.113	1.22	Up
NP_055121.1	hypothetical protein LOC51493	0.239	1.02	Down	0.641	1.04	Down
NP_061980.1	**hypothetical protein LOC56005 precursor**	0.430	1.07	Up	**0.001**	**1.73**	**Up**
NP_000185.1	**hypoxanthine-guanine phosphoribosyltransferase**	0.351	1.05	Up	**0.0005**	**1.24**	**Up**
NP_006380.1	hypoxia up-regulated protein 1 precursor	0.553	1.04	Down	0.578	1.05	Up
NP_001007562.1	immunity-related GTPase family Q protein	0.244	1.14	Up	0.699	1.02	Down
NP_002257.1	**importin subunit alpha-2**	0.028	1.25	Down	**0.0001**	**1.44**	**Down**
NP_002258.2	importin subunit alpha-3	0.491	1.05	Up	0.179	1.09	Up
NP_002256.2	importin subunit beta-1	0.184	1.07	Down	0.042	1.08	Up
NP_078934.3	importin-4	0.970	1.01	Up	0.735	1.05	Down
NP_002262.3	importin-5	0.510	1.03	Down	0.221	1.12	Up
NP_006382.1	importin-7	0.937	1.00	Down	0.966	1.00	Up
NP_060555.2	importin-9	0.879	1.01	Up	0.017	1.12	Up
NP_066952.1	**inorganic pyrophosphatase**	0.822	1.01	Down	**0.003**	**1.24**	**Up**
NP_258412.1	inosine triphosphate pyrophosphatase isoform a	0.569	1.03	Down	0.228	1.10	Up
NP_000875.2	**inosine-5'-monophosphate dehydrogenase 2**	0.276	1.07	Up	**0.0001**	**1.48**	**Up**
NP_005527.1	inositol monophosphatase 1 isoform 1	0.731	1.02	Down	0.485	1.10	Up
NP_004506.2	interleukin enhancer-binding factor 2	0.072	1.10	Down	0.046	1.15	Up
NP_060090.2	interleukin enhancer-binding factor 3 isoform d	0.560	1.04	Down	0.016	1.13	Up
NP_057132.2	isochorismatase domain-containing protein 1	0.765	1.03	Up	0.287	1.08	Up
NP_005887.2	isocitrate dehydrogenase [NADP] cytoplasmic	0.808	1.02	Down	0.218	1.15	Up
NP_002159.2	isocitrate dehydrogenase [NADP], mitochondrial precursor	0.933	1.01	Down	0.450	1.14	Up
NP_060530.3	isoleucyl-tRNA synthetase, mitochondrial precursor	0.587	1.06	Down	0.045	1.50	Up

NP_006112.3	keratin, type II cytoskeletal 1	0.990	1.00	Up	0.973	1.01	Up
NP_006550.1	KH domain-containing, RNA-binding, signal transduction-associated protein 1	0.645	1.04	Up	0.060	1.24	Down
NP_891556.1	kinectin isoform a	0.025	1.63	Up	0.885	1.02	Down
NP_004513.1	kinesin heavy chain isoform 5C	0.809	1.02	Down	0.469	1.06	Up
NP_005543.2	kinesin light chain 1 isoform 1	0.871	1.01	Down	0.252	1.06	Up
NP_004512.1	kinesin-1 heavy chain	0.731	1.05	Up	0.630	1.08	Down
NP_006699.2	lactoylglutathione lyase	0.262	1.08	Down	0.449	1.07	Down
NP_005564.1	lamin-B1 isoform 1	0.431	1.11	Up	0.999	1.00	Up
NP_116126.2	**lamin-B2**	0.403	1.06	Up	**0.008**	**1.24**	**Up**
NP_056238.2	L-aminoadipate-semialdehyde dehydrogenase-phosphopantetheinyl transferase	0.872	1.03	Down	0.402	2.46	Up
NP_006046.1	lanC-like protein 1	0.926	1.01	Down	0.014	1.20	Up
NP_542433.1	large proline-rich protein BAT3 isoform b	0.041	1.20	Down	0.010	1.30	Down
NP_573566.2	leucine-rich PPR motif-containing protein, mitochondrial precursor	0.490	1.05	Down	0.761	1.03	Up
NP_065761.1	**leucine-rich repeat-containing protein 47**	0.889	1.01	Down	**0.005**	**1.22**	**Down**
NP_060979.2	**leucine-rich repeat-containing protein 59**	0.508	1.26	Up	**0.005**	**1.57**	**Down**
NP_064502.9	leucyl-tRNA synthetase, cytoplasmic	0.389	1.20	Up	0.092	1.24	Down
NP_000886.1	leukotriene A-4 hydrolase	0.865	1.01	Down	0.081	1.23	Up
NP_005557.1	**L-lactate dehydrogenase A chain isoform 1**	0.385	1.04	Up	**0.005**	**1.22**	**Up**
NP_002291.1	L-lactate dehydrogenase B chain	0.258	1.05	Down	0.061	1.08	Up
NP_004784.2	lon protease homolog, mitochondrial precursor	0.963	1.01	Down	0.943	1.01	Down
NP_004291.1	low molecular weight phosphotyrosine protein phosphatase isoform c	0.295	1.05	Down	0.016	1.14	Up
NP_057508.2	luc7-like protein 3	0.335	1.09	Down	0.111	1.18	Up
NP_003133.1	lupus La protein	0.220	1.04	Down	0.680	1.03	Up
NP_057370.1	L-xylulose reductase isoform 1	0.505	1.04	Down	0.610	1.06	Up
NP_005031.1	lysosomal Pro-X carboxypeptidase isoform 1 preproprotein	0.068	1.12	Down	0.335	1.07	Up
NP_005497.1	lysosome membrane protein 2	0.562	1.05	Down	0.014	1.43	Down
NP_005552.3	lysosome-associated membrane glycoprotein 1 precursor	0.562	1.07	Down	0.027	1.19	Down
NP_005539.1	lysyl-tRNA synthetase isoform 2	0.607	1.03	Down	0.680	1.03	Down
NP_002406.1	macrophage migration inhibitory factor	0.358	1.10	Down	0.246	1.15	Up

NP_005908.1	malate dehydrogenase, cytoplasmic isoform 2	0.538	1.04	Down	0.770	1.01	Up
NP_005909.2	**malate dehydrogenase, mitochondrial precursor**	0.657	1.03	Down	**0.001**	**1.32**	**Up**
NP_075385.1	**MARCKS-related protein**	0.014	1.22	Up	**0.009**	**1.40**	**Up**
NP_061322.2	matrin-3 isoform a	0.452	1.04	Down	0.016	1.16	Down
NP_000007.1	**medium-chain specific acyl-CoA dehydrogenase, mitochondrial isoform a precursor**	0.064	1.20	Down	**0.008**	**1.27**	**Down**
NP_004981.2	**methionyl-tRNA synthetase, cytoplasmic**	0.608	1.04	Down	**0.0004**	**1.28**	**Down**
NP_001284.1	methylosome subunit pICln	0.333	1.07	Down	0.087	1.16	Down
NP_005900.2	microtubule-associated protein 1B	0.939	1.01	Up	0.408	1.11	Up
NP_002365.3	microtubule-associated protein 2 isoform 1	0.135	1.13	Up	0.592	1.08	Up
NP_036457.1	microtubule-associated protein RP/EB family member 1	0.417	1.11	Up	0.026	1.22	Up
NP_057152.2	mitochondrial fission 1 protein	0.211	1.20	Down	0.523	1.15	Up
NP_036590.1	mitochondrial import inner membrane translocase subunit Tim13	0.386	1.05	Down	0.033	1.09	Down
NP_001001563.1	mitochondrial import inner membrane translocase subunit TIM50	0.181	1.73	Down	0.044	1.77	Down
NP_064628.1	**mitochondrial import receptor subunit TOM22 homolog**	0.334	1.22	Down	**0.003**	**2.16**	**Down**
NP_055635.3	mitochondrial import receptor subunit TOM70	0.751	1.07	Down	0.046	1.45	Down
NP_001093639.1	mitochondrial inner membrane protein isoform 2	0.524	1.13	Down	0.055	1.37	Down
NP_004716.1	mitotic checkpoint protein BUB3 isoform a	0.038	1.10	Down	0.957	1.00	Down
NP_071757.4	MMS19 nucleotide excision repair protein homolog	0.169	1.19	Down	0.553	1.07	Down
NP_006443.1	**multifunctional protein ADE2 isoform 2**	0.787	1.01	Down	**0.001**	**1.21**	**Up**
NP_055335.2	myb-binding protein 1A isoform 2	0.708	1.16	Up	0.951	1.02	Up
NP_066299.2	myosin light polypeptide 6 isoform 1	0.148	1.11	Down	0.724	1.03	Up
NP_006462.1	myosin regulatory light chain 12A	0.369	1.06	Down	0.136	1.15	Up
NP_005955.1	myosin-10	0.999	1.00	Down	0.098	1.15	Up
NP_002464.1	myosin-9	0.441	1.04	Down	0.961	1.00	Down
NP_036355.2	myosin-Ib isoform 2	0.399	1.06	Up	0.016	1.25	Down
NP_665807.1	**myotrophin**	0.273	1.05	Up	**0.001**	**1.13**	**Up**
NP_002347.5	myristoylated alanine-rich C-kinase substrate	0.309	1.13	Up	0.044	1.33	Up
NP_036269.1	N(G),N(G)-dimethylarginine dimethylaminohydrolase 1 isoform 1	0.992	1.00	Down	0.038	1.14	Up
NP_039268.1	N(G),N(G)-dimethylarginine dimethylaminohydrolase 2	0.540	1.03	Up	0.047	1.19	Up

NP_002387.1	NAD-dependent malic enzyme, mitochondrial isoform 1 precursor	0.427	1.07	Down	0.535	1.06	Down
NP_004991.1	**NADH dehydrogenase [ubiquinone] 1 alpha subcomplex subunit 5**	0.988	1.00	Down	**0.002**	**1.20**	**Up**
NP_004542.1	**NADH dehydrogenase [ubiquinone] iron-sulfur protein 3, mitochondrial precursor**	0.790	1.02	Down	**0.003**	**1.38**	**Up**
NP_004997.4	NADH-ubiquinone oxidoreductase 75 kDa subunit, mitochondrial isoform 1 precursor	0.910	1.01	Up	0.200	1.16	Up
NP_005585.1	nascent polypeptide-associated complex subunit alpha isoform b	0.348	1.05	Down	0.061	1.09	Down
NP_006147.1	**NEDD8 precursor**	0.755	1.02	Up	**0.008**	**1.16**	**Up**
NP_003960.1	NEDD8-conjugating enzyme Ubc12	0.275	1.07	Down	0.251	1.11	Up
NP_006608.1	nestin	0.160	1.16	Down	0.950	1.01	Down
NP_000606.3	**neural cell adhesion molecule 1 isoform 1**	0.021	1.45	Down	**0.0002**	**2.11**	**Down**
NP_005373.2	neurofilament medium polypeptide isoform 1	0.560	1.03	Down	0.045	1.13	Up
NP_835364.1	neuronal migration protein doublecortin isoform c	0.925	1.01	Up	0.011	1.38	Down
NP_003369.2	**neurosecretory protein VGF precursor**	0.331	1.10	Up	**0.003**	**1.39**	**Up**
NP_938148.1	**neutral alpha-glucosidase AB isoform 2**	0.535	1.05	Up	**0.002**	**1.27**	**Up**
NP_004999.1	NHP2-like protein 1	0.286	1.07	Down	0.328	1.09	Up
NP_005737.1	nicotinamide phosphoribosyltransferase precursor	0.692	1.02	Down	0.681	1.03	Down
NP_001018146.1	NME1-NME2 protein	0.924	1.01	Down	0.013	1.09	Up
NP_031389.3	non-POU domain-containing octamer-binding protein isoform 1	0.196	1.09	Down	0.115	1.11	Down
NP_004394.1	non-syndromic hearing impairment protein 5 isoform a	0.666	1.06	Down	0.063	1.25	Up
NP_057227.2	NSFL1 cofactor p47 isoform a	0.814	1.02	Up	0.489	1.07	Up
NP_002473.2	nuclear autoantigenic sperm protein isoform 2	0.514	1.03	Down	0.038	1.07	Up
NP_002477.1	nuclear cap-binding protein subunit 1	0.423	1.13	Up	0.218	1.22	Up
NP_006591.1	nuclear migration protein nudC	0.486	1.06	Down	0.261	1.15	Up
NP_006176.2	nuclear mitotic apparatus protein 1	0.910	1.01	Down	0.051	1.23	Down
NP_065134.1	nuclear pore complex protein Nup107	0.958	1.01	Down	0.174	1.09	Down
NP_004289.1	nuclear pore complex protein Nup155 isoform 2	0.561	1.04	Up	0.193	1.06	Up
NP_056046.1	nuclear pore complex protein Nup160	0.905	1.01	Down	0.586	1.06	Up
NP_079120.1	nuclear pore complex protein Nup85	0.124	1.19	Down	0.345	1.25	Up
NP_055484.3	nuclear pore complex protein Nup93	0.637	1.03	Down	0.208	1.10	Up
NP_036478.2	nuclear pore glycoprotein p62	0.490	1.06	Down	0.024	1.27	Up

NP_005787.1	nuclear transport factor 2	0.051	1.20	Down	0.969	1.00	Up
NP_073568.2	nuclear ubiquitous casein and cyclin-dependent kinases substrate	0.538	1.10	Down	0.590	1.13	Down
NP_004550.2	nuclease-sensitive element-binding protein 1	0.564	1.06	Down	0.148	1.14	Up
NP_004732.2	**nucleolar and coiled-body phosphoprotein 1**	0.168	1.08	Down	**0.007**	**1.28**	**Down**
NP_036473.2	**nucleolar GTP-binding protein 1**	0.488	1.08	Down	**0.001**	**2.10**	**Down**
NP_056277.2	nucleolar protein 11	0.342	1.06	Down	0.198	1.15	Up
NP_057018.1	nucleolar protein 58	0.689	1.05	Up	0.561	1.09	Up
NP_004719.2	**nucleolar RNA helicase 2**	0.412	1.41	Up	**0.002**	**1.44**	**Down**
NP_005372.2	nucleolin	0.710	1.03	Up	0.034	1.25	Up
NP_002511.1	nucleophosmin isoform 1	0.184	1.08	Down	0.012	1.15	Up
NP_076962.2	**nucleoporin Nup37**	0.010	1.30	Up	**0.006**	**1.52**	**Up**
NP_003283.2	**nucleoprotein TPR**	0.411	1.06	Up	**0.0001**	**1.24**	**Up**
NP_000260.1	nucleoside diphosphate kinase A isoform b	0.346	1.06	Down	0.016	1.16	Up
NP_004528.1	nucleosome assembly protein 1-like 1	0.866	1.01	Down	0.118	1.10	Up
NP_005960.1	**nucleosome assembly protein 1-like 4**	0.585	1.02	Down	**0.001**	**1.20**	**Up**
NP_116258.2	nudC domain-containing protein 1 isoform 1	0.671	1.02	Down	0.147	1.11	Up
NP_056147.2	nudC domain-containing protein 3	0.574	1.10	Down	0.030	1.27	Down
NP_037473.3	obg-like ATPase 1 isoform 1	0.856	1.01	Up	0.490	1.06	Down
NP_000265.1	**ornithine aminotransferase, mitochondrial isoform 1 precursor**	0.987	1.00	Down	**0.001**	**1.30**	**Up**
NP_066997.3	p30 DBC protein	0.119	1.08	Down	0.378	1.05	Up
NP_001035879.1	**paraspeckle component 1**	0.699	1.03	Up	**0.001**	**1.23**	**Up**
NP_066953.1	peptidyl-prolyl cis-trans isomerase A	0.987	1.00	Up	0.015	1.14	Up
NP_000933.1	peptidyl-prolyl cis-trans isomerase B precursor	0.188	1.16	Up	0.314	1.85	Up
NP_005029.1	peptidyl-prolyl cis-trans isomerase D	0.423	1.11	Up	0.941	1.01	Up
NP_002004.1	**peptidyl-prolyl cis-trans isomerase FKBP3**	0.992	1.00	Up	**0.002**	**1.28**	**Down**
NP_002005.1	peptidyl-prolyl cis-trans isomerase FKBP4	0.260	1.07	Down	0.438	1.03	Up
NP_006338.1	peptidyl-prolyl cis-trans isomerase H	0.309	1.11	Down	0.973	1.00	Up
NP_057161.1	**peptidyl-tRNA hydrolase 2, mitochondrial precursor**	0.956	1.02	Up	**0.004**	**1.96**	**Down**
NP_005808.3	**perilipin-3 isoform 1**	0.512	1.09	Up	**0.007**	**1.37**	**Up**
NP_002565.1	**peroxiredoxin-1**	0.878	1.01	Down	**0.001**	**1.20**	**Up**
NP_005800.3	**peroxiredoxin-2 isoform a**	0.638	1.02	Down	**0.001**	**1.14**	**Up**

NP_036226.1	**peroxiredoxin-5, mitochondrial isoform a precursor**	0.579	1.03	Up	**0.001**	**1.26**	**Up**
NP_004896.1	peroxiredoxin-6	0.360	1.04	Up	0.011	1.16	Up
NP_000405.1	peroxisomal multifunctional enzyme type 2 isoform 2	0.041	1.15	Up	0.016	1.17	Up
NP_065090.1	PEST proteolytic signal-containing nuclear protein	0.214	1.07	Down	0.732	1.05	Up
NP_116147.1	PHD finger-like domain-containing protein 5A	0.672	1.03	Up	0.016	1.30	Up
NP_005678.3	phenylalanyl-tRNA synthetase beta chain	0.394	1.06	Up	0.162	1.15	Up
NP_002626.1	phosphate carrier protein, mitochondrial isoform b precursor	0.818	1.05	Down	0.189	1.46	Down
NP_002558.1	**phosphatidylethanolamine-binding protein 1**	0.771	1.02	Up	**0.007**	**1.24**	**Up**
NP_036531.1	phosphatidylinositol transfer protein beta isoform	0.827	1.06	Up	0.571	1.10	Down
NP_002624.2	phosphoglucomutase-1 isoform 1	0.464	1.07	Down	0.058	1.22	Up
NP_060760.2	phosphoglucomutase-2	0.938	1.01	Down	0.587	1.07	Up
NP_000282.1	**phosphoglycerate kinase 1**	0.227	1.06	Up	**0.001**	**1.40**	**Up**
NP_002620.1	**phosphoglycerate mutase 1**	0.652	1.03	Up	**0.0001**	**1.25**	**Up**
NP_001026866.1	**phospholipase D3**	**0.001**	**1.32**	**Down**	**0.002**	**1.63**	**Down**
NP_006547.1	phosphomevalonate kinase	0.923	1.01	Up	0.616	1.06	Up
NP_036525.1	phosphoribosylformylglycinamidine synthase	0.845	1.02	Up	0.405	1.12	Down
NP_066977.1	phosphoserine aminotransferase isoform 2	0.022	1.22	Down	0.307	1.08	Up
NP_001018077.1	**plasminogen activator inhibitor 1 RNA-binding protein isoform 1**	0.255	1.27	Up	**0.00003**	**1.25**	**Down**
NP_000421.1	platelet-activating factor acetylhydrolase IB subunit alpha	0.699	1.02	Down	0.023	1.26	Up
NP_002563.1	**platelet-activating factor acetylhydrolase IB subunit beta isoform a**	0.928	1.00	Down	**0.0002**	**1.17**	**Up**
NP_002564.1	**platelet-activating factor acetylhydrolase IB subunit gamma**	0.800	1.01	Down	**0.002**	**1.10**	**Up**
NP_001609.2	poly	0.336	1.52	Up	0.052	1.37	Down
NP_006187.2	**poly(rC)-binding protein 1**	**0.003**	**1.09**	**Down**	0.077	1.09	Down
NP_114366.1	poly(rC)-binding protein 2 isoform b	0.019	1.13	Down	0.551	1.04	Down
NP_055096.2	poly(U)-binding-splicing factor PUF60 isoform b	0.209	1.07	Down	0.230	1.10	Up
NP_002559.2	polyadenylate-binding protein 1	0.039	1.15	Down	0.216	1.07	Down
NP_004634.1	polyadenylate-binding protein 2	0.791	1.03	Up	0.399	1.06	Up
NP_003810.1	polyadenylate-binding protein 4 isoform 2	0.156	1.14	Down	0.402	1.20	Down
NP_005701.1	polyglutamine-binding protein 1 isoform 1	0.330	1.06	Down	0.098	1.29	Down
NP_002810.1	polypyrimidine tract-binding protein 1 isoform a	0.520	1.02	Down	0.042	1.08	Down
NP_036526.2	prefoldin subunit 2	0.381	1.07	Down	0.992	1.00	Down

NP_003363.1	prefoldin subunit 3	0.119	1.11	Down	0.190	1.10	Up
NP_002615.2	prefoldin subunit 5 isoform alpha	0.094	1.11	Down	0.136	1.06	Up
NP_055075.1	prefoldin subunit 6	0.965	1.00	Down	0.286	1.07	Up
NP_005563.1	prelamin-A/C isoform 2	0.695	1.04	Down	0.229	1.13	Down
NP_055317.1	pre-mRNA-processing factor 19	0.816	1.01	Up	0.021	1.09	Up
NP_060362.3	pre-mRNA-processing factor 40 homolog A	0.909	1.01	Down	0.036	1.35	Up
NP_006436.3	pre-mRNA-processing-splicing factor 8	0.396	1.07	Up	0.891	1.01	Up
NP_002769.1	proactivator polypeptide isoform a preproprotein	0.112	1.13	Down	0.691	1.03	Up
NP_006377.2	probable ATP-dependent RNA helicase DDX17 isoform 1	0.613	1.04	Down	0.142	1.14	Down
NP_004387.1	**probable ATP-dependent RNA helicase DDX5**	0.162	1.15	Down	**0.000003**	**1.71**	**Down**
NP_001075.1	**procollagen-lysine,2-oxoglutarate 5-dioxygenase 3 precursor**	0.049	1.30	Up	**0.0001**	**1.87**	**Up**
NP_005013.1	profilin-1	0.427	1.05	Down	0.014	1.15	Up
NP_002619.1	profilin-2 isoform b	0.798	1.02	Up	0.271	1.11	Up
NP_037506.2	programmed cell death 6-interacting protein isoform 1	0.509	1.02	Down	0.018	1.15	Up
NP_004699.1	programmed cell death protein 5	0.250	1.08	Down	0.113	1.18	Up
NP_037364.1	programmed cell death protein 6	0.557	1.05	Down	0.037	1.24	Up
NP_002625.1	prohibitin	0.764	1.02	Down	0.057	1.15	Up
NP_009204.1	prohibitin-2 isoform 2	0.605	1.07	Down	0.016	1.24	Down
NP_002583.1	proliferating cell nuclear antigen	0.089	1.12	Down	0.176	1.11	Down
NP_006182.2	proliferation-associated protein 2G4	0.447	1.05	Down	0.856	1.02	Up
NP_055204.2	proline-, glutamic acid- and leucine-rich protein 1	0.445	1.07	Down	0.278	1.11	Up
NP_002717.3	prolyl endopeptidase	0.141	1.11	Up	0.063	1.21	Up
NP_006592.3	prostaglandin E synthase 3	0.833	1.01	Down	0.603	1.05	Down
NP_008933.2	proteasomal ubiquitin receptor ADRM1 precursor	0.848	1.04	Up	0.016	1.26	Up
NP_006254.1	proteasome activator complex subunit 1 isoform 1	0.597	1.02	Up	0.183	1.27	Up
NP_002809.2	proteasome activator complex subunit 2	0.083	1.07	Up	0.588	1.04	Up
NP_005780.2	proteasome activator complex subunit 3 isoform 1	0.310	1.08	Down	0.717	1.03	Down
NP_002777.1	proteasome subunit alpha type-1 isoform 2	0.940	1.00	Down	0.100	1.14	Up
NP_002778.1	proteasome subunit alpha type-2	0.777	1.01	Up	0.179	1.08	Up
NP_002779.1	proteasome subunit alpha type-3 isoform 1	0.831	1.02	Down	0.056	1.11	Up
NP_002780.1	proteasome subunit alpha type-4 isoform 1	0.987	1.00	Down	0.015	1.07	Up
NP_002781.2	**proteasome subunit alpha type-5 isoform 1**	0.628	1.02	Down	**0.004**	**1.16**	**Up**
NP_002782.1	proteasome subunit alpha type-6	0.893	1.01	Down	0.076	1.09	Up

NP_002783.1	proteasome subunit alpha type-7	0.405	1.05	Down	0.352	1.06	Up
NP_002784.1	proteasome subunit beta type-1 precursor	0.989	1.00	Down	0.170	1.21	Up
NP_002785.1	proteasome subunit beta type-2 isoform 1	0.991	1.00	Down	0.141	1.11	Up
NP_002786.2	proteasome subunit beta type-3	0.381	1.04	Up	0.068	1.09	Up
NP_002787.2	proteasome subunit beta type-4	0.280	1.09	Down	0.138	1.07	Up
NP_002788.1	proteasome subunit beta type-5 isoform 1	0.712	1.03	Down	0.806	1.02	Down
NP_002789.1	proteasome subunit beta type-6 precursor	0.572	1.02	Up	0.553	1.04	Up
NP_002790.1	proteasome subunit beta type-7 proprotein	0.670	1.03	Up	0.166	1.12	Up
NP_000507.1	protein ALEX GNASL	0.048	1.13	Down	0.015	1.25	Down
NP_938074.2	protein arginine N-methyltransferase 1 isoform 3	0.462	1.06	Down	0.181	1.11	Down
NP_006100.2	protein arginine N-methyltransferase 5 isoform a	0.620	1.04	Down	0.051	1.16	Up
NP_055070.1	**protein canopy homolog 2 isoform 1 precursor**	0.405	1.08	Up	**0.005**	**1.38**	**Up**
NP_057005.1	protein CutA isoform 2	0.860	1.01	Down	0.418	1.07	Up
NP_005304.3	**protein disulfide-isomerase A3 precursor**	0.162	1.09	Up	**0.00003**	**1.45**	**Up**
NP_004902.1	**protein disulfide-isomerase A4 precursor**	0.627	1.03	Up	**0.00001**	**1.38**	**Up**
NP_005733.1	**protein disulfide-isomerase A6 precursor**	0.523	1.04	Up	**0.00001**	**1.36**	**Up**
NP_000909.2	**protein disulfide-isomerase precursor**	0.767	1.03	Up	**0.007**	**1.25**	**Up**
NP_009193.2	protein DJ-1	0.978	1.00	Up	0.046	1.13	Up
NP_115963.1	protein dpy-30 homolog	0.422	1.10	Down	0.930	1.01	Up
NP_060682.2	protein enabled homolog isoform b	0.907	1.01	Up	0.988	1.00	Up
NP_002728.1	protein kinase C alpha type	0.401	1.07	Up	0.330	1.07	Down
NP_002361.1	protein mago nashi homolog	0.072	1.08	Up	0.071	1.23	Up
NP_003625.2	protein NipSnap homolog 1	0.732	1.03	Down	0.057	1.13	Up
NP_619634.1	protein phosphatase 1 regulatory subunit 14B	0.490	1.09	Up	0.542	1.07	Down
NP_002697.1	protein phosphatase 1B isoform 1	0.810	1.04	Up	0.797	1.05	Down
NP_817092.1	protein phosphatase 1G	0.207	1.06	Down	0.473	1.06	Up
NP_057231.1	protein phosphatase methylesterase 1	0.724	1.02	Up	0.955	1.00	Down
NP_061185.1	protein RCC2	0.363	1.09	Up	0.343	1.17	Down
NP_055776.1	protein RUFY3 isoform 2	0.310	1.07	Up	0.024	1.18	Up
NP_899195.1	protein SEC13 homolog isoform 1	0.203	1.06	Down	0.052	1.17	Up
NP_003002.2	protein SET isoform 2	0.555	1.04	Up	0.788	1.02	Up
NP_006314.2	protein transport protein Sec24B isoform a	0.902	1.04	Down	0.677	1.18	Up
NP_004913.2	protein transport protein Sec24C	0.232	1.12	Down	0.406	1.05	Down

NP_055748.2	protein transport protein Sec31A isoform 1	0.648	1.07	Down	0.339	1.18	Up
NP_002814.3	prothymosin alpha isoform 2	0.291	1.08	Up	0.977	1.00	Up
NP_000261.2	purine nucleoside phosphorylase	0.934	1.01	Up	0.215	1.09	Up
NP_006301.3	puromycin-sensitive aminopeptidase	0.518	1.03	Down	0.078	1.06	Up
NP_001349.2	**putative pre-mRNA-splicing factor ATP-dependent RNA helicase DHX15**	0.855	1.02	Up	**0.00001**	**1.29**	**Down**
NP_006734.1	**putative RNA-binding protein 3**	0.254	1.13	Down	**0.00004**	**1.84**	**Down**
NP_057103.2	putative RNA-binding protein Luc7-like 2	0.682	1.02	Down	0.069	1.08	Up
NP_060117.3	putative rRNA methyltransferase 3	0.770	1.02	Down	0.024	1.70	Down
NP_722546.1	pyrroline-5-carboxylate reductase 1, mitochondrial isoform 2	0.908	1.01	Up	0.054	1.32	Up
NP_000916.2	pyruvate dehydrogenase E1 component subunit beta, mitochondrial isoform 1 precursor	0.463	1.06	Down	0.017	1.59	Up
NP_002645.3	pyruvate kinase isozymes M1/M2 isoform M2	0.192	1.04	Up	0.119	1.17	Up
NP_001880.2	quinone oxidoreductase isoform a	0.623	1.09	Up	0.163	1.42	Up
NP_001484.1	**rab GDP dissociation inhibitor alpha**	0.361	1.07	Down	**0.003**	**1.19**	**Up**
NP_001485.2	rab GDP dissociation inhibitor beta isoform 1	0.214	1.07	Down	0.037	1.13	Up
NP_002897.1	radixin	0.331	1.07	Up	0.796	1.03	Up
NP_002874.1	ran GTPase-activating protein 1	0.976	1.00	Down	0.761	1.02	Down
NP_015561.1	ran-binding protein 3 isoform RANBP3-d	0.580	1.07	Down	0.705	1.11	Down
NP_002873.1	**ran-specific GTPase-activating protein**	0.520	1.02	Down	**0.003**	**1.15**	**Up**
NP_001093896.1	rap1 GTPase-GDP dissociation stimulator 1 isoform 1	0.981	1.00	Down	0.155	1.07	Up
NP_005745.1	**ras GTPase-activating protein-binding protein 1**	0.065	1.15	Down	**0.001**	**1.34**	**Down**
NP_036429.2	ras GTPase-activating protein-binding protein 2 isoform a	0.034	1.16	Down	0.863	1.01	Up
NP_008839.2	ras-related C3 botulinum toxin substrate 1 isoform Rac1	0.657	1.05	Down	0.013	1.39	Down
NP_057215.3	ras-related protein Rab-10	0.230	1.15	Up	0.370	2.03	Up
NP_004654.1	**ras-related protein Rab-11A**	0.363	1.05	Down	**0.003**	**1.31**	**Down**
NP_057406.2	ras-related protein Rab-14	0.605	1.04	Up	0.831	1.02	Down
NP_112243.1	ras-related protein Rab-1B	0.186	1.09	Up	0.202	1.08	Down
NP_002856.1	ras-related protein Rab-2A	0.701	1.03	Down	0.676	1.05	Up
NP_004574.2	ras-related protein Rab-5C isoform b	0.680	1.02	Down	0.717	1.03	Down
NP_002860.2	ras-related protein Rab-6A isoform a	0.549	1.08	Down	0.828	1.03	Down
NP_004628.4	ras-related protein Rab-7a	0.341	1.08	Up	0.367	1.11	Up
NP_002938.1	**replication protein A 14 kDa subunit**	0.354	1.06	Down	**0.008**	**1.11**	**Up**

NP_002937.1	**replication protein A 32 kDa subunit**	0.658	1.03	Up	**0.004**	**1.19**	**Up**
NP_002936.1	replication protein A 70 kDa DNA-binding subunit	0.788	1.01	Down	0.026	1.16	Up
NP_002893.1	reticulocalbin-2 precursor	0.769	1.03	Up	0.761	1.04	Up
NP_996734.1	**reticulon-1 isoform C**	0.577	1.10	Up	**0.006**	**1.41**	**Up**
NP_722550.1	**reticulon-4 isoform B**	0.501	1.09	Up	**0.003**	**1.32**	**Up**
NP_002890.2	retinol-binding protein 1 isoform a	0.797	1.01	Down	0.030	1.24	Up
NP_001128360.1	**retrotransposon-like protein 1**	**0.002**	**1.34**	**Down**	**0.00005**	**1.58**	**Down**
NP_004300.1	rho GDP-dissociation inhibitor 1 isoform a	0.180	1.05	Up	0.017	1.19	Up
NP_002930.2	ribonuclease inhibitor	0.673	1.02	Down	0.432	1.04	Up
NP_002755.1	ribose-phosphate pyrophosphokinase 1	0.819	1.01	Up	0.014	1.28	Up
NP_056474.2	ribosomal L1 domain-containing protein 1	0.582	1.06	Up	0.018	1.23	Down
NP_006319.1	**RNA-binding protein 14 isoform 1**	0.419	1.05	Down	**0.009**	**1.18**	**Down**
NP_004893.1	RNA-binding protein 39 isoform b	0.575	1.02	Down	0.339	1.04	Up
NP_002887.2	RNA-binding protein 4 isoform 1	0.588	1.03	Down	0.857	1.02	Down
NP_005096.1	RNA-binding protein 8A	0.362	1.09	Down	0.456	1.08	Down
NP_055124.1	RNA-binding protein 9 isoform 2	0.428	1.35	Up	0.730	1.11	Down
NP_005234.1	RNA-binding protein EWS isoform 2	0.904	1.01	Up	0.246	1.17	Up
NP_004951.1	RNA-binding protein FUS isoform 1	0.311	1.07	Down	0.802	1.02	Up
NP_620412.1	RNA-binding protein Musashi homolog 2 isoform a	0.643	1.04	Down	0.020	1.35	Up
NP_057951.1	**RNA-binding protein Raly long isoform**	0.902	1.01	Down	**0.001**	**1.51**	**Down**
NP_006702.1	RNA-binding protein with serine-rich domain 1	0.738	1.02	Down	0.019	1.20	Up
NP_001427.2	rRNA 2'-O-methyltransferase fibrillarin	0.901	1.01	Up	0.398	1.10	Down
NP_003698.1	**ruvB-like 1**	0.544	1.02	Down	**0.0001**	**1.29**	**Up**
NP_006657.1	**ruvB-like 2**	0.671	1.04	Down	**0.004**	**1.31**	**Up**
NP_005902.1	S-adenosylmethionine synthase isoform type-2	0.057	1.11	Down	0.809	1.01	Up
NP_149073.1	SAP domain-containing ribonucleoprotein	0.928	1.01	Down	0.797	1.03	Down
NP_055581.3	secernin-1 isoform a	0.393	1.05	Up	0.055	1.31	Up
NP_005689.2	secretory carrier-associated membrane protein 3 isoform 1	0.566	1.05	Up	0.413	1.13	Up
NP_060713.1	septin-11	0.918	1.01	Up	0.014	1.23	Up
NP_004395.1	septin-2	0.571	1.02	Up	0.013	1.19	Up
NP_055944.2	septin-6 isoform B	0.359	1.09	Up	0.112	1.20	Up
NP_001011553.2	septin-7 isoform 2	0.449	1.05	Up	0.289	1.14	Down
NP_001106965.1	septin-9 isoform b	0.420	1.04	Down	0.931	1.01	Up

NP_005403.2	serine hydroxymethyltransferase, mitochondrial isoform 1 precursor	0.515	1.06	Down	0.047	1.18	Up
NP_005830.2	serine/arginine repetitive matrix protein 1	0.614	1.05	Up	0.393	1.16	Up
NP_057417.3	serine/arginine repetitive matrix protein 2	0.934	1.01	Down	0.173	1.14	Down
NP_008855.1	**serine/arginine-rich splicing factor 1 isoform 1**	0.849	1.01	Up	**0.00001**	**1.42**	**Up**
NP_006616.1	serine/arginine-rich splicing factor 10 isoform 1	0.793	1.02	Up	0.091	1.10	Up
NP_004759.1	serine/arginine-rich splicing factor 11 isoform 1	0.392	1.06	Down	0.222	1.16	Up
NP_003007.2	serine/arginine-rich splicing factor 2	0.071	1.13	Down	0.145	1.14	Up
NP_003008.1	**serine/arginine-rich splicing factor 3**	0.408	1.11	Up	**0.001**	**1.22**	**Up**
NP_006266.2	**serine/arginine-rich splicing factor 6**	0.510	1.07	Up	**0.003**	**1.28**	**Up**
NP_001026854.1	**serine/arginine-rich splicing factor 7 isoform 1**	0.854	1.01	Up	**0.001**	**1.34**	**Up**
NP_003760.1	**serine/arginine-rich splicing factor 9**	0.493	1.08	Up	**0.003**	**1.16**	**Up**
NP_005100.1	serine/threonine-protein kinase OSR1	0.539	1.18	Up	0.694	1.20	Up
NP_002568.2	serine/threonine-protein kinase PAK 2	0.347	1.07	Down	0.326	1.10	Up
NP_055040.2	serine/threonine-protein phosphatase 2A 65 kDa regulatory subunit A alpha isoform	0.313	1.05	Down	0.781	1.01	Up
NP_002712.1	serine/threonine-protein phosphatase 6 catalytic subunit isoform b	0.824	1.03	Up	0.626	1.07	Down
NP_001164014.1	serine/threonine-protein phosphatase PGAM5, mitochondrial isoform 1	0.906	1.01	Down	0.915	1.01	Down
NP_002699.1	serine/threonine-protein phosphatase PP1-alpha catalytic subunit isoform 1	0.956	1.00	Down	0.291	1.06	Up
NP_009109.3	serine-threonine kinase receptor-associated protein	0.386	1.06	Down	0.129	1.11	Up
NP_001226.2	serpin H1 precursor	0.986	1.00	Up	0.317	1.07	Up
NP_056992.4	serrate RNA effector molecule homolog isoform a	0.743	1.03	Up	0.890	1.01	Up
NP_006504.2	seryl-tRNA synthetase, cytoplasmic	0.765	1.03	Up	0.482	1.08	Down
NP_001975.1	S-formylglutathione hydrolase	0.506	1.02	Down	0.024	1.12	Up
NP_112576.1	SH3 domain-binding glutamic acid-rich-like protein 3	0.622	1.06	Up	0.212	1.11	Up
NP_073591.2	sideroflexin-1	0.684	1.08	Up	0.100	1.53	Down
NP_003125.3	signal recognition particle 14 kDa protein	0.605	1.03	Up	0.079	1.16	Down
NP_055045.2	signal recognition particle 68 kDa protein	0.046	1.11	Up	0.794	1.02	Up
NP_008878.3	signal recognition particle 72 kDa protein	0.104	1.06	Down	0.713	1.03	Down
NP_003124.1	signal recognition particle 9 kDa protein isoform 2	0.466	1.05	Up	0.132	1.11	Down

NP_003012.1	small glutamine-rich tetratricopeptide repeat-containing protein alpha	0.539	1.06	Down	0.631	1.06	Up
NP_003085.1	small nuclear ribonucleoprotein E	0.447	1.05	Down	0.110	1.10	Up
NP_003086.1	small nuclear ribonucleoprotein F	0.050	1.19	Down	0.544	1.06	Up
NP_003087.1	small nuclear ribonucleoprotein G	0.100	1.08	Down	0.651	1.02	Up
NP_008869.1	small nuclear ribonucleoprotein Sm D1	0.438	1.05	Down	0.523	1.06	Up
NP_004588.1	small nuclear ribonucleoprotein Sm D2 isoform 1	0.347	1.08	Down	0.527	1.05	Down
NP_004166.1	small nuclear ribonucleoprotein Sm D3	0.085	1.16	Down	0.822	1.04	Up
NP_003082.1	small nuclear ribonucleoprotein-associated proteins B and B' isoform B	0.969	1.00	Up	0.614	1.04	Up
NP_003343.1	small ubiquitin-related modifier 1 isoform a precursor	0.442	1.04	Down	0.055	1.18	Down
NP_008868.3	small ubiquitin-related modifier 2 isoform a precursor	0.956	1.00	Down	0.506	1.05	Up
NP_002442.2	**S-methyl-5'-thioadenosine phosphorylase**	0.579	1.03	Up	**0.001**	**1.22**	**Up**
NP_689509.1	**sodium/potassium-transporting ATPase subunit alpha-3**	0.103	1.18	Down	**0.001**	**1.49**	**Down**
NP_006507.2	solute carrier family 2, facilitated glucose transporter member 1	0.385	1.24	Up	0.375	1.27	Up
NP_003095.2	**sorbitol dehydrogenase**	0.872	1.01	Up	**0.001**	**1.20**	**Up**
NP_003121.1	sorcin isoform a	0.943	1.01	Up	0.558	1.10	Up
NP_037478.2	sorting nexin-12	0.602	1.11	Down	0.176	1.15	Down
NP_003118.2	spectrin alpha chain, brain isoform 2	0.207	1.08	Down	0.068	1.12	Down
NP_003119.2	**spectrin beta chain, brain 1 isoform 1**	0.180	1.10	Down	**0.009**	**1.24**	**Down**
NP_003123.2	**spermidine synthase**	0.906	1.01	Down	**0.001**	**1.58**	**Up**
NP_004586.2	spermine synthase	0.700	1.09	Down	0.601	1.12	Down
NP_008861.2	**S-phase kinase-associated protein 1 isoform a**	0.445	1.10	Down	**0.007**	**1.26**	**Down**
NP_004631.1	spliceosome RNA helicase BAT1	0.872	1.01	Up	0.674	1.02	Up
NP_973727.1	splicing factor 1 isoform 3	0.042	1.12	Down	0.860	1.02	Up
NP_005868.1	splicing factor 3A subunit 1 isoform 1	0.802	1.02	Down	0.765	1.03	Up
NP_006793.1	splicing factor 3A subunit 3	0.834	1.01	Down	0.418	1.07	Up
NP_036565.2	splicing factor 3B subunit 1 isoform 1	0.993	1.00	Up	0.704	1.09	Down
NP_006833.2	splicing factor 3B subunit 2	0.090	1.10	Down	0.751	1.02	Up
NP_036558.3	splicing factor 3B subunit 3	0.788	1.01	Up	0.162	1.14	Up
NP_005841.1	**splicing factor 3B subunit 4**	**0.0099**	**1.24**	**Down**	0.029	1.19	Down
NP_112577.1	splicing factor 3B subunit 5	0.571	1.08	Down	0.148	1.20	Up
NP_006749.1	**splicing factor U2AF 35 kDa subunit isoform a**	0.554	1.04	Up	**0.006**	**1.23**	**Up**

NP_009210.1	splicing factor U2AF 65 kDa subunit isoform a	0.444	1.06	Down	0.724	1.05	Up
NP_005057.1	splicing factor, proline- and glutamine-rich	0.244	1.09	Down	0.053	1.14	Down
NP_055521.1	squamous cell carcinoma antigen recognized by T-cells 3	0.100	1.15	Up	0.041	1.25	Up
NP_112487.1	SRA stem-loop-interacting RNA-binding protein, mitochondrial precursor	0.569	1.05	Down	0.454	1.08	Up
NP_055205.2	staphylococcal nuclease domain-containing protein 1	0.900	1.01	Down	0.024	1.16	Down
NP_005554.1	**stathmin isoform a**	0.054	1.10	Up	**0.003**	**1.32**	**Up**
NP_055892.2	sterile alpha and TIR motif-containing protein 1	0.664	1.06	Down	0.202	1.24	Down
NP_038470.1	**stomatin-like protein 2**	0.798	1.02	Down	**0.005**	**1.36**	**Up**
NP_004125.3	stress-70 protein, mitochondrial precursor	0.639	1.05	Down	0.084	1.16	Up
NP_006810.1	**stress-induced-phosphoprotein 1**	0.891	1.01	Up	**0.001**	**1.17**	**Up**
NP_005436.1	**structural maintenance of chromosomes protein 3**	0.641	1.07	Up	**0.008**	**1.41**	**Down**
NP_005491.1	SUMO-activating enzyme subunit 1 isoform a	0.490	1.04	Down	0.038	1.14	Up
NP_005490.1	SUMO-activating enzyme subunit 2	0.290	1.03	Down	0.938	1.00	Down
NP_000445.1	superoxide dismutase [Cu-Zn]	0.039	1.06	Up	0.190	1.07	Up
NP_006695.1	suppressor of G2 allele of SKP1 homolog isoform SGT1A	0.374	1.05	Up	0.653	1.05	Up
NP_149351.1	surfeit locus protein 4	0.750	1.04	Down	0.639	1.04	Down
NP_003065.3	SWI/SNF complex subunit SMARCC1	0.893	1.01	Down	0.013	1.16	Down
NP_003066.2	SWI/SNF complex subunit SMARCC2 isoform a	0.808	1.02	Down	0.134	1.17	Up
NP_003070.3	SWI/SNF-related matrix-associated actin-dependent regulator of chromatin subfamily E member 1	0.803	1.04	Up	0.812	1.02	Down
NP_006364.2	synaptic vesicle membrane protein VAT-1 homolog	0.785	1.02	Up	0.393	1.07	Up
NP_006280.3	talin-1	0.050	1.19	Down	0.207	1.10	Down
NP_031401.1	TAR DNA-binding protein 43	0.766	1.02	Up	0.467	1.03	Up
NP_003478.1	TATA-binding protein-associated factor 2N isoform 2	0.341	1.08	Down	0.788	1.03	Up
NP_110379.2	T-complex protein 1 subunit alpha isoform a	0.598	1.02	Down	0.049	1.09	Up
NP_006422.1	T-complex protein 1 subunit beta isoform 1	0.165	1.05	Down	0.107	1.08	Up
NP_006421.2	T-complex protein 1 subunit delta	0.941	1.00	Down	0.095	1.09	Up
NP_036205.1	T-complex protein 1 subunit epsilon	0.382	1.04	Down	0.020	1.10	Up
NP_006420.1	T-complex protein 1 subunit eta isoform a	0.287	1.03	Down	0.161	1.06	Up
NP_005989.3	T-complex protein 1 subunit gamma isoform a	0.016	1.11	Down	0.695	1.03	Down
NP_006576.2	T-complex protein 1 subunit theta	0.892	1.01	Up	0.014	1.13	Up
NP_001753.1	T-complex protein 1 subunit zeta isoform a	0.351	1.04	Down	0.336	1.04	Up

NP_003320.2	thioredoxin	0.503	1.13	Up	0.055	1.21	Up
NP_116120.1	thioredoxin domain-containing protein 17	0.728	1.02	Down	0.028	1.17	Up
NP_110437.2	**thioredoxin domain-containing protein 5 isoform 1 precursor**	0.141	1.12	Up	**0.002**	**1.40**	**Up**
NP_877393.1	**thioredoxin reductase 1, cytoplasmic isoform 2**	0.449	1.05	Down	**0.005**	**1.18**	**Up**
NP_006784.1	**thioredoxin-dependent peroxide reductase, mitochondrial isoform a precursor**	0.996	1.00	Up	**0.001**	**1.57**	**Up**
NP_004777.1	thioredoxin-like protein 1	0.214	1.12	Down	0.812	1.03	Up
NP_005773.3	**THO complex subunit 4**	0.477	1.11	Up	**0.001**	**1.33**	**Down**
NP_689508.3	threonyl-tRNA synthetase, cytoplasmic	0.779	1.02	Up	0.090	1.16	Down
NP_060206.2	THUMP domain-containing protein 1	0.358	1.19	Up	0.040	1.22	Up
NP_003267.1	**thymopoietin isoform alpha**	0.496	1.27	Up	**0.001**	**1.80**	**Down**
NP_066926.1	thymosin beta-10	0.174	1.09	Down	0.068	1.17	Down
NP_066932.1	thymosin beta-4	0.813	1.03	Up	0.852	1.02	Up
NP_005110.2	thyroid hormone receptor-associated protein 3	0.371	1.07	Up	0.651	1.06	Up
NP_690866.1	TIP41-like protein isoform 1	0.064	1.31	Down	0.923	1.01	Down
NP_006746.1	transaldolase	0.999	1.00	Up	0.107	1.15	Up
NP_006747.1	transcription elongation factor A protein 1 isoform 1	0.113	1.12	Down	0.105	1.09	Down
NP_005639.1	transcription elongation factor B polypeptide 1	0.248	1.09	Down	0.587	1.04	Up
NP_009039.1	**transcription elongation factor B polypeptide 2 isoform a**	0.789	1.02	Up	**0.008**	**1.13**	**Up**
NP_001198.2	**transcription factor BTF3 isoform B**	**0.001**	**1.30**	**Down**	**0.001**	**1.39**	**Down**
NP_005753.1	transcription intermediary factor 1-beta	0.119	1.06	Down	0.318	1.05	Up
NP_003225.2	**transferrin receptor protein 1**	0.552	1.09	Down	**0.0002**	**1.72**	**Down**
NP_004584.1	**transformer-2 protein homolog beta**	0.048	1.07	Up	**0.0001**	**1.31**	**Up**
NP_001655.1	transforming protein RhoA precursor	0.753	1.03	Down	0.027	1.27	Down
NP_003555.1	transgelin-2	0.691	1.02	Down	0.434	1.06	Up
NP_037391.2	**transgelin-3**	0.668	1.04	Up	**0.007**	**1.20**	**Up**
NP_009057.1	**transitional endoplasmic reticulum ATPase**	0.490	1.03	Down	**0.007**	**1.15**	**Up**
NP_001055.1	transketolase	0.978	1.00	Up	0.496	1.04	Down
NP_001405.1	translation initiation factor eIF-2B subunit alpha	0.467	1.08	Down	0.181	1.29	Up
NP_006827.1	translational activator GCN1	0.851	1.04	Down	0.474	1.07	Down
NP_003286.1	translationally-controlled tumor protein	0.018	1.13	Down	0.142	1.09	Down
NP_004613.1	translin	0.943	1.00	Up	0.060	1.14	Up

NP_694858.1	transportin-1 isoform 2	0.462	1.06	Up	0.391	1.03	Down
NP_036602.1	transportin-3 isoform 1	0.924	1.01	Down	0.743	1.02	Up
NP_000347.2	treacle protein isoform b	0.776	1.03	Down	0.131	1.36	Down
NP_000173.2	trifunctional enzyme subunit alpha, mitochondrial precursor	0.688	1.06	Down	0.795	1.03	Down
NP_000174.1	trifunctional enzyme subunit beta, mitochondrial precursor	0.691	1.06	Up	0.974	1.00	Up
NP_000810.1	trifunctional purine biosynthetic protein adenosine-3 isoform 1	0.180	1.05	Down	0.254	1.09	Up
NP_000356.1	triosephosphate isomerase isoform 1	0.457	1.18	Up	0.100	1.65	Up
NP_003282.2	tripeptidyl-peptidase 2	0.366	1.10	Down	0.062	1.22	Up
NP_057488.1	**tRNA methyltransferase 112 homolog**	0.016	1.73	Down	**0.001**	**2.43**	**Down**
NP_003266.1	**tropomodulin-1**	0.037	1.25	Down	**0.001**	**1.57**	**Down**
NP_001018004.1	tropomyosin alpha-1 chain isoform 3	0.949	1.01	Down	0.233	1.20	Down
NP_705935.1	tropomyosin alpha-3 chain isoform 2	0.947	1.01	Up	0.016	1.23	Up
NP_003281.1	tropomyosin alpha-4 chain isoform 2	0.789	1.02	Down	0.127	1.17	Up
NP_004175.2	tryptophanyl-tRNA synthetase, cytoplasmic isoform a	0.730	1.02	Down	0.079	1.09	Up
NP_006073.2	tubulin alpha-1B chain	0.968	1.00	Up	0.027	1.13	Up
NP_821133.1	**tubulin beta chain**	0.949	1.00	Down	**0.002**	**1.23**	**Up**
NP_821080.1	tubulin beta-2B chain	0.442	1.05	Down	0.017	1.14	Up
NP_006077.2	tubulin beta-3 chain isoform 1	0.698	1.03	Up	0.069	1.21	Up
NP_001272.2	tubulin-folding cofactor B	0.682	1.03	Up	0.086	1.16	Up
NP_004598.1	tubulin-specific chaperone A	0.322	1.06	Down	0.666	1.03	Down
NP_005984.3	tubulin-specific chaperone D	0.315	1.08	Down	0.151	1.12	Down
NP_003279.2	tumor protein D54 isoform e	0.129	1.10	Down	0.038	1.10	Up
NP_003671.1	tyrosyl-tRNA synthetase, cytoplasmic	0.284	1.11	Down	0.931	1.01	Up
NP_003080.2	U1 small nuclear ribonucleoprotein 70 kDa	0.740	1.02	Down	0.290	1.12	Up
NP_004587.1	U1 small nuclear ribonucleoprotein A	0.691	1.03	Up	0.011	1.33	Up
NP_003084.1	U1 small nuclear ribonucleoprotein C	0.279	1.06	Down	0.888	1.02	Down
NP_003081.2	U2 small nuclear ribonucleoprotein A'	0.353	1.06	Up	0.026	1.25	Up
NP_005137.1	U4/U6.U5 tri-snRNP-associated protein 1	0.613	1.07	Up	0.230	1.14	Up
NP_054733.2	U5 small nuclear ribonucleoprotein 200 kDa helicase	0.783	1.05	Down	0.036	1.41	Down
NP_004805.2	U5 small nuclear ribonucleoprotein 40 kDa protein	0.544	1.05	Down	0.029	1.28	Up
NP_067000.1	U6 snRNA-associated Sm-like protein LSm2	0.779	1.02	Up	0.092	1.43	Up
NP_055278.1	U6 snRNA-associated Sm-like protein LSm3	0.991	1.00	Down	0.163	1.16	Up
NP_009011.1	U6 snRNA-associated Sm-like protein LSm6	0.329	1.08	Down	0.069	1.17	Up

NP_005142.1	ubiquitin carboxyl-terminal hydrolase 14 isoform a	0.314	1.10	Down	0.042	1.24	Up
NP_003472.2	**ubiquitin carboxyl-terminal hydrolase 5 isoform 2**	0.600	1.01	Up	**0.00003**	**1.15**	**Up**
NP_003461.2	ubiquitin carboxyl-terminal hydrolase 7	0.869	1.01	Down	0.782	1.03	Up
NP_004172.2	**ubiquitin carboxyl-terminal hydrolase isozyme L1**	0.067	1.09	Up	**0.002**	**1.14**	**Up**
NP_060140.2	ubiquitin thioesterase OTUB1	0.555	1.02	Down	0.030	1.17	Up
NP_002945.1	ubiquitin-40S ribosomal protein S27a precursor	0.523	1.06	Up	0.493	1.06	Down
NP_001120792.1	ubiquitin-associated protein 2-like isoform b	0.976	1.01	Up	0.150	1.11	Down
NP_003338.1	ubiquitin-conjugating enzyme E2 L3	0.518	1.05	Down	0.054	1.32	Up
NP_003339.1	ubiquitin-conjugating enzyme E2 N	0.437	1.07	Down	0.032	1.14	Up
NP_001027459.1	ubiquitin-conjugating enzyme E2 variant 1 isoform d	0.839	1.02	Down	0.528	1.04	Up
NP_003325.2	**ubiquitin-like modifier-activating enzyme 1**	0.912	1.00	Up	**0.005**	**1.14**	**Up**
NP_001988.1	**ubiquitin-like protein fubi and ribosomal protein S30 precursor**	0.781	1.02	Up	**0.001**	**1.42**	**Down**
NP_056937.2	UBX domain-containing protein 1	0.324	1.13	Down	0.150	1.30	Up
NP_064505.1	**UDP-glucose:glycoprotein glucosyltransferase 1 precursor**	0.340	1.06	Up	**0.007**	**1.23**	**Up**
NP_000364.1	uridine 5'-monophosphate synthase	0.479	1.07	Down	0.044	1.19	Up
NP_002865.1	**UV excision repair protein RAD23 homolog B**	0.857	1.01	Up	**0.001**	**1.22**	**Up**
NP_060676.2	vacuolar protein sorting-associated protein 35	0.957	1.00	Up	0.209	1.10	Up
NP_006286.1	valyl-tRNA synthetase	0.373	1.07	Down	0.079	1.19	Down
NP_006169.2	vesicle-fusing ATPase	0.572	1.05	Up	0.958	1.00	Down
NP_003371.2	vimentin	0.874	1.01	Up	0.426	1.11	Down
NP_003364.1	**vinculin isoform VCL**	0.200	1.10	Down	**0.007**	**1.29**	**Down**
NP_003365.1	**voltage-dependent anion-selective channel protein 1**	0.734	1.12	Down	**0.008**	**3.89**	**Down**
NP_003366.2	voltage-dependent anion-selective channel protein 2 isoform 2	0.472	1.21	Down	0.015	2.32	Down
NP_001681.2	**V-type proton ATPase catalytic subunit A**	0.434	1.05	Down	**0.007**	**1.33**	**Up**
NP_001684.2	**V-type proton ATPase subunit B, brain isoform**	0.542	1.03	Down	**0.010**	**1.16**	**Up**
NP_059830.1	WD repeat-containing protein 1 isoform 1	0.463	1.03	Down	0.150	1.04	Up
NP_077005.2	WD repeat-containing protein 18	0.898	1.01	Up	0.012	1.40	Up
NP_079510.1	WD repeat-containing protein 61	0.392	1.04	Down	0.465	1.04	Down
NP_065116.3	xaa-Pro aminopeptidase 1 isoform 1	0.796	1.02	Up	0.014	1.33	Up
NP_000276.2	xaa-Pro dipeptidase isoform 1	0.060	1.35	Down	0.477	1.15	Down
NP_066964.1	X-ray repair cross-complementing protein 5	0.302	1.05	Down	0.208	1.06	Up
NP_001460.1	X-ray repair cross-complementing protein 6	0.508	1.17	Up	0.031	1.20	Down
NP_005446.2	zinc finger Ran-binding domain-containing protein 2 isoform 2	0.709	1.05	Down	0.125	1.33	Up

Appendix C

The top 10 protein interactomes obtained from the oxygen glucose deprivation (OGD) 18hr data. Functional protein-protein interactions for the 193 proteins altered with OGD (18h) were defined using Ingenuity Pathway Analysis (IPA) software. Upward arrows denote significantly increased proteins; downward arrows denote significantly decreased proteins; proteins names in plain type are proteins inserted into the network by IPA to augment functional coherence. The IPA generated score is a putative measure of network probability (see Deighton *et al*, 2010 for critical analysis). The focus molecules are the number of proteins identified by LC-MS contained within the network.

Interactome ID	Molecules in 18hr OGD Networks	Score	Focus Molecules
[1.] Energy Production	60S ribosomal subunit, Actin, ↑**ACTR1A**, ATP synthesis, ↑**ATP5A1**, ↑**ATP5J**, ↑**ATP6V1B2**, ↑**BANF1**, ↓**CAP1**, ↓**DDX5**, ↓**DDX21**, ↓**DDX3X**, ↑**EFTUD2**, H+-transporting two-sector ATPase, ↑**HINT1**, ↓**HNRNPC**, ↑**LMNB2**, Mediator, ↑**NAPA**, RNA polymerase II, ↓**RPL13**, ↓**RPL23**, ↓**RPL35**, ↓**RPL38**, ↑**RTN4**, ↑**RUVBL1**, ↑**RUVBL2**, ↓**SMC3**, ↑**SRSF6**, ↑**SRSF9**, TIP60, ↓**TMPO**, ↑**TRA2B**, ↓**UQCRC1**, ↓**UQCRC2**	56	28
[2.] 40s Ribosome	↑**CALR**, ↓**CDK1**, ↓**CSDE1**, ↓**DDX39A**, ↓**DHX15**, E2f, ↑**ERH**, ↑**FAU**, ↑**GSTP1**, ↓**GTPBP4**, Histone h3, Histone h4, ↑**P4HB**, peroxidase (miscellaneous), ↑**PGK1**, ↑**PRDX1**, ↑**PRDX2**, ↑**PRDX5**, Ribosomal 40s subunit, ↑**RPA2**, ↑**RPA3**, RPA, ↓**RPS9**, RPS13, ↓**RPS14**, ↓**RPS16**, RPS21, ↓**RPS23**, ↓**RPS17/RPS17L**, ↑**SRSF1**, ↑**SRSF3**, ↑**TBL1XR1**, ↓**THOC4**, ↑**YWHAE**, ↑**YWHAG**	53	27
[3.] Mitochondrial transport	Alpha Actinin, Alpha catenin, Alpha tubulin, ↓**ANXA2**, Calmodulin, ↑**CAPZA1**, ↑**CAPZB**, Ck2, ↑**CLTC**, ↑**CSNK2A1**, ↓**CTSB**, ↑**DBNL**, ↑**ECHS1**, F Actin, ↓**FKBP3**, ↑**FSCN1**, ↑**GANAB**, ↑**LDHA**, ↓**LRRC59**, ↑**MARCKSL1**, ↑**MTPN**, ↓**NCAM1**, ↓**NOLC1**, ↑**PRKCSH**, ↓**RBM3**, ↓**SPTBN1**, ↑**STMN1**, ↓**TFRC**, ↓**TMOD1**, ↓**TOMM22**, Tropomyosin, Tubulin, ↑**U1AF1**, ↓**VCL,** ↓**VDAC1**	51	27
[4.] Protein folding + protein degradation	19S proteasome, 20s proteasome, 26s proteasome, ↑**ANXA6**, ATPase, ↑**DNAJA2**, ↓**EIF3I**, ↑**GDI1**, Hsp70, Hsp90, ↑**HSP90AA1**, ↑**HSP90B1**, ↑**HSPA5**, ↑**HSPD1**, ↓**MARS**, MHC Class I (complex), ↑**PAICS**, ↑**PDIA3**, ↑**PDIA4**, ↑**PSMA5**, PSMA, ↑**PSMC3**, ↑**PSMC4**, ↑**PSMD1**, ↑**PSMD2**, ↑**PSMD6**, ↑**PSMD11**, PSMD, ↑**RAD23B**, ↑**STIP1**, Tap, ↑**TUBB**, Ubiquitin, ↑**USP5**, ↑**VCP**	45	24

[5.] MAPK-YWHAZ	↑**AARS**, ↑**APRT**, ↓**ATP1A3**, C22orf28, Creatine Kinase, ↑**ECH1**, ↑**ECHS1**, EDIL3, EEF1B2, ↓**EIF4A1**, FAM65B, FAM82A2, ↑**FSCN1**, ↑**HSPD1**, HSPH1, ↑**INA**, KIAA1949, ↑**LDHA**, ↓**LRRC47**, MAPK3, MAPK6, ↑**MPST**, PABPC4, ↑**PAFAH1B2**, ↑**PAFAH1B3**, ↑**PEBP1**, ↑**PGAM1**, ↑**PRDX3**, ↓**RPN1**, SNCA, ↓**UQCRC2**, UQCRQ, ↑**VGF**, YWHAZ, ZFP36L1	35	20
[6.] Transcription	↑**ANP32E**, ATP5I, ↑**ATP6V1A**, ↑**C19orf10**, ↓**CSDE1**, FOS, IGF2R, ↓**LRRC59**, M6PR, ↑**MTAP**, MYCN, NAE1, ↑**NEDD8**, NFYB, NUAK2, ↑**NUP37**, ↑**OAT**, ↑**PDIA4**, ↑**PDIA6**, ↑**PLIN3**, ↓**RPL35**, ↓**RPL38**, RPS7, ↓**RPS9**, RPS25, ↓**RPS17/RPS17L**, SMAD2, ↑**SORD**, TGFBR1, ↑**TPR**, TRAF6, TUFM, ↑**UBA1**, ↑**UCHL1**, ZFAND5	35	20
[7.] NF kappaB	↓**ACADM**, AHNAK, ALDH16A1, ↑**ATP5J**, BHMT, ↓**BTF3**, ↑**CALM1 (includes others)**, CCD15, ↑**CKB**, ↑**CNPY2**, EIF4B, ↑**ETFA**, ETFB, HNRNPK, ↑**HPRT1**, IKBKE, ↑**IMPDH2**, ↓**LOC728622/SKP1**, MATR3, MPG, MT-CO2, MYL6, NFKB1, ↓**PLD3**, PLS3, PTMS, ↓**PTRH2**, PYGM, ↑**RANBP1**, ↓**SERBP1**, ↓**SPTBN1**, ↑**SRM**, ↑**SRSF7**, UBE2M, ↑**UGGT1**	30	18
[8.] Lipid + Ketone metabolism	↑**ACAA2**, ↑**ACAT1**, ↓**ACLY**, ↑**ACOT7**, APP, BCL2L1, BNIP1, ↑**CBS**, ↓**CHCHD2**, ↓**CTSB**, DLG4, FAM160A2, FZD1, ↑**HBA1/HBA2**, HBQ1, HNF4A, MT-ND3, ↑**NDUFA5**, NDUFA6, NDUFAF1, NDUFB1, NDUFB6, ↑**NDUFS3**, NDUFS4, NDUFS7, palmitoyl-CoA hydrolase, ↑**PHPT1**, ↓**RAB11A**, ↑**RTN1**, ↑**STOML2**, TIMM23B, TOMM40, ↓**TRMT112**, ↑**TXNRD1**, ↓**VDAC1**	27	17
[9.] Protein synthesis	↓**CAPRIN1,** CELF1, ↓**EIF1**, ↓**EIF4A1**, EIF4A, ↓**EIF4G1**, EIF4G3, ↑**ELAVL4**, EP300, ERO1LB, ↑**ERP29**, ↑**ERP44**, FBXW8, ↓**G3BP1**, ↑**GPI**, IGK, INTS6, KIAA1524, ↓**KPNA2**, mir-127, miR-127/miR-127-3p, MYC, ↑**NAPIL4**, OGFOD1, ↑**PSPC1**, ↓**RBM14**, RELA, RPS13, ↓**RTL1**, ↑**TCEB2**, ↑**TXNDC5**, UPF2, USP10, XBP1	26	16
[10.] --------	↑**ALDOC**, ↑**ARL3**, ↓**ATXN10**, C4orf41, COL18A1, ↑**DLD**, DNAJB11, DNAJC1, DNAJC3, DNAJC6, DNAJC10, ↑**ENO2**, ↑**ERH**, ETFB, FBXO11, FDXR, ↑**FH**, ↑**HSD17B10**, HSP, HSPA14, HSPB6, ↑**HSPE1**, HTT, ILK, MCMBP, ↑**MDH2**, NDUFS7, ↑**PLOD3**, ↑**PPA1**, ↓**RALY**, SESN1, ST3GAL2, TP53, TRAPPC8, TTC15	18	13

Publications

Herrmann A, Gordon S, Le Bihan T, Spires-Jones T, Cousin M, McCulloch J, Deighton R. *Identification of novel ABAD protein interacting partners under conditions of metabolic stress.* (In Preparation)

Herrmann A, Searcy J, Le Bihan T, McCulloch J, Deighton R. (2013) *Total variance should drive data handling in third generation proteomics studies.* Proteomics, **13**, 3251-5

Herrmann A, Deighton R, Le Bihan T, McCulloch M, Searcy J, Kerr L, McCulloch J. (2013) *Adaptive changes in the Neuronal Proteome: Mitochondrial Energy Production, Endoplasmic Reticulum Stress and Ribosomal Dysfunction in the Cellular Response to Metabolic Stress.* Journal of Cerebral Blood Flow and Metabolism, **33**(5): 673-83

JCBFM Open

Journal of Cerebral Blood Flow & Metabolism (2013) 33, 673–683

www.jcbfm.com

ORIGINAL ARTICLE

Adaptive changes in the neuronal proteome: mitochondrial energy production, endoplasmic reticulum stress, and ribosomal dysfunction in the cellular response to metabolic stress

Abigail G Herrmann[1], Ruth F Deighton[1], Thierry Le Bihan[2,3], Mailis C McCulloch[4], James L Searcy[1], Lorraine E Kerr[2] and James McCulloch[1]

Impaired energy metabolism in neurons is integral to a range of neurodegenerative diseases, from Alzheimer's disease to stroke. To investigate the complex molecular changes underpinning cellular adaptation to metabolic stress, we have defined the proteomic response of the SH-SY5Y human neuroblastoma cell line after exposure to a metabolic challenge of oxygen glucose deprivation (OGD) *in vitro*. A total of 958 proteins across multiple subcellular compartments were detected and quantified by label-free liquid chromatography mass spectrometry. The levels of 130 proteins were significantly increased ($P<0.01$) after OGD and the levels of 63 proteins were significantly decreased ($P<0.01$) while expression of the majority of proteins (765) was not altered. Network analysis identified novel protein–protein interactomes involved with mitochondrial energy production, protein folding, and protein degradation, indicative of coherent and integrated proteomic responses to the metabolic challenge. Approximately one third (61) of the differentially expressed proteins was associated with the endoplasmic reticulum and mitochondria. Electron microscopic analysis of these subcellular structures showed morphologic changes consistent with the identified proteomic alterations. Our investigation of the global cellular response to a metabolic challenge clearly shows the considerable adaptive capacity of the proteome to a slowly evolving metabolic challenge.

Journal of Cerebral Blood Flow & Metabolism (2013) **33,** 673–683; doi:10.1038/jcbfm.2012.204; published online 16 January 2013

Keywords: Alzheimer's; cell culture; energy metabolism; mitochondria; neurodegeneration; proteomics

INTRODUCTION

Impaired energy metabolism in neurons is integral to many central nervous system diseases. An acute, intense metabolic challenge during conditions such as stroke and brain trauma can induce irreversible neuronal damage.[1] By contrast, age-related chronic metabolic impairment is thought to contribute to the evolution of neurodegenerative diseases such as Alzheimer's disease, Parkinson's disease, and Huntington's disease.[2,3] Neurochemical cascades initiated by both acute and prolonged metabolic challenges can induce cell death via an elevation of proapoptotic proteins. These metabolic challenges can also activate genomic and proteomic responses promoting cell survival in the immediate phase as well as preparing the cell to deal with similar challenges in the future (conditioning).[4]

Subcellular organelles display complex proteomic responses to impaired energy metabolism, with these responses ultimately determining the death or survival of the cell. In mitochondria, metabolic stress can disrupt energy generation, provoke mitochondrial swelling, and initiate apoptosis, all with potentially lethal consequences.[5] In response to cell stress, the endoplasmic reticulum (ER) detects and reconfigures misfolded proteins in a process known as the unfolded protein response (UPR). The UPR is integral to cell survival as excessive accumulation of these damaged proteins in the ER lumen can result in the suppression of protein synthesis and irreversible pathology.[6] In the nucleus and ribosomes, metabolic stress leads to a genomic response and the synthesis of proteins such as heat-shock proteins and trophic factors, which contribute to protein repair and neuronal survival.[7] The genomic response to metabolic challenge has been well characterized both *in vitro* and *in vivo*.[8–10] In the present study, we provide a comprehensive cellular proteomic response and explore the extent to which proteins are altered after a metabolic challenge.

Oxygen glucose deprivation (OGD) induces metabolic stress in neurons in culture.[11,12] The intensity of the metabolic challenge can be controlled by adjusting experimental conditions such as the choice of cell line and alterations in the duration of OGD. Mass spectrometry-based proteomics provides an excellent platform to quantify OGD-dependent protein changes and to gain a fresh perspective on adaptations that occur within the proteome in response to metabolic stress.[13] We have used human SH-SY5Y neuroblastoma cells and label-free liquid chromatography mass spectrometry (LC-MS) to define the integrated proteomic response to metabolic stress that induces severe mitochondrial dysfunction but only limited cell death. The majority of proteins analyzed (800 out of 1,000) were not significantly altered by OGD.

[1]Centre for Cognitive and Neural Systems, University of Edinburgh, Edinburgh, UK; [2]SynthSys, University of Edinburgh, Edinburgh, UK; [3]Institute of Structural and Molecular Biology, University of Edinburgh, Edinburgh, UK and [4]Applied Neurobiology Group, Institute of Infection, Immunity and Inflammation, College of Medical, Veterinary and Life Sciences, University of Glasgow, Glasgow, UK. Correspondence: Dr RF Deighton, University of Edinburgh, 1 George Square, Edinburgh EH8 9JZ, UK.
E-mail: ruth.deighton@ed.ac.uk
AGH is supported by the Medical Research Council. The research is supported by Age UK as part of the Disconnected Mind programme and performed under the aegis of the Centre for Cognitive Aging and Cognitive Epidemiology (part of the Lifelong Health and Wellbeing initiative of UK Research Councils). TLB and LEK are funded by SynthSys which is a Centre for Integrative Systems Biology (CISB) funded by BBSRC and EPSRC; reference BB/D019621/1.
Received 29 October 2012; revised 3 December 2012; accepted 5 December 2012; published online 16 January 2013

Protein increases after OGD was more than twice as frequent as was decreases, consistent with an integrated cellular survival response. Protein interactomes highlight coordinated proteomic responses after OGD in relation to mitochondrial energy production, ER stress, and ribosomal dysfunction.

MATERIALS AND METHODS

Reagents

All standard growth media used was obtained from Invitrogen (Paisley, UK), unless otherwise stated, and all procedures were conducted in compliance with all relevant legislation in the United Kingdom. Cells were routinely maintained in standard 75 cm^2 cell culture-treated flasks (Greiner Bio One, Stonehouse, UK) within a continuous flow incubator at 37°C, with 5% CO_2 in fully humidified air. All growth media and solutions were prewarmed to 37°C before contact with cells, unless otherwise stated. The acetonitrile and water used in the LC-MS buffer solutions were of HPLC grade (Fisher, Loughborough, UK). Formic acid was of 98% to 100% purity (Merck, Darmstadt, Germany) and trifluoroacetic acid was 99% sequencing grade (Sigma-Aldrich, Gillingham, UK). All other chemicals used in the processing of the protein samples were of reagent grade or better. The trypsin used for protein digestion was from Promega (Southampton, UK).

Cell Culture and Oxygen Glucose Deprivation

SH-SY5Y cells (ATCC, Manassas, VA, USA) were cultured in Dulbecco's Modified Eagle Medium: Nutrient Mixture F12 (DMEM/F12) supplemented with 2 mmol/L L-Glutamine, 100 U/mL Penicillin, 100 mg/mL Streptomycin, and fetal bovine serum. Cells were routinely maintained at 37°C, 5% CO_2, with culture medium replaced biweekly. Oxygen glucose deprivation (for 3, 6, 9, 12, and 18 hour durations) was achieved through incubation of the cells at 37°C in 95% N_2:5% CO_2. Aglycemia was induced by replacing standard culture medium with glucose-free DMEM supplemented with fetal bovine serum, after a glucose-free wash step. Control cells underwent the same glucose-free wash step, followed by incubation with glucose containing media (4,500 mg/L glucose). The osmolality of the DMEM solutions used was within the range of 300 to 340 mOsm/kg for the no glucose solutions, and 320 to 360 mOsm/kg for the glucose containing media. All media were equilibrated overnight before experimentation in either normoxic or anoxic chambers. Oxygen content in the media was recorded in preliminary studies using a fiber optic dual oxygen-temperature sensing probe (OxyLite 2000 E Series, Oxford Optronix, Oxford, UK). A rapid oxygen depletion phase was recorded, with oxygen partial pressure falling exponentially from 140 to 7 mm Hg over the initial 3 hours of OGD. Oxygen depletion plateaued and remained severely hypoxic between 4 and 18 hours with a recorded average partial pressure of 2 mm Hg.

Assessment of Mitochondrial Function (MTS Assay)

Cells were seeded onto poly-D-lysine coated flat-bottomed 96-well plates at a density of 125,000 cells per well overnight. After OGD, glucose-free DMEM was replaced with 200 μL glucose-containing DMEM and cell viability was assessed using 20 μL of CellTiter 96 AQueous One Solution Cell Proliferation Assay (MTS) (Promega, Madison, USA) as per the manufacturer's guidelines. Cells were incubated for 2 hours in glucose containing, normoxic media (37°C, 5% CO_2) to allow residual mitochondrial function after OGD to be assessed using a Dynex MRX plate reader (Dynex Technologies Ltd., Worthing, UK) at 490λ.

Assessment of Global Cell Death (Trypan Blue)

Trypan blue staining was carried out to assess the extent of cell death occurring after each OGD time point. Cells were collected immediately at the end of each time point by trypsinization, centrifugation (200 *g*, 7 minutes) and resuspension in glucose-containing DMEM. Cells were incubated with 0.1% trypan blue as per the manufacturer's instructions (Invitrogen). A hemocytometer was used to count stained and unstained cells. The percentage of stained cells in each OGD and time-matched control sample was calculated.

Preparation of Protein Samples for Liquid-Chromatography Mass Spectrometry

SH-SY5Y cells were treated with 6 hours OGD ($n = 6$ independent samples per group) and 18 hours OGD ($n = 6$), with a time-matched control for each sample. After OGD or 'control' incubations, SH-SY5Y cells were immediately scraped and centrifuged (200 *g*, 7 minutes). Cell pellets were washed in Hanks Buffered Saline Solution and recentrifuged. Washed cell pellets were resuspended in 1 ml Hanks Buffered Saline Solution and centrifuged (6,000 *g*, 3 minutes). Supernatants were removed and the pellets snap frozen for temporary storage at −80°C. Cell pellets were defrosted and lysed in 100 μL 8 M urea using a cordless motor pellet pestle (Sigma-Aldrich, Dorset, UK). Samples were then centrifuged (14,000 *g*, 15 minutes) and supernatants recovered. Total protein content was determined using the Pierce BCA Protein Assay Kit (Thermo-Fisher, Loughborough, UK). Protein extract (140 μg) from OGD and control samples were digested as previously described.[14]

Liquid Chromatography Mass Spectrometry

Label-free intensity-based LC-MS was used to identify proteins differentially expressed after 6 and 18 hours OGD relative to time-matched controls. Capillary LC-MS data were acquired on an online system consisting of a micro-pump (1200 binary HPLC system, Agilent, Edinburgh, UK) coupled to a hybrid LTQ-Orbitrap XL instrument controlled through Xcalibur 2.0.7 (Thermo-Fisher). Peptides were reconstituted in 20 μL of loading buffer before injection and 8 μL was loaded. The HPLC separation was provided by a gradient between buffer A (97.5% H_2O, 2.5% acetonitrile, 0.1% formic acid) and buffer B (90% acetonitrile, 10% H_2O, 0.025% trifluoroacetic acid, 0.1% formic acid). The peptide mixture was separated on a 140-minute gradient. The mass spectrometer was operated in 'data-dependent mode', with a single MS scan (400 to 2,000 *m/z*) followed by MS/MS scans in the linear ion trap on the five most abundant ions and excluded for 120 seconds.

Protein Identification and Quantification

All LC-MS runs were analyzed using a label-free intensity-based approach with Progenesis (version 4.0 Nonlinear Dynamics, Newcastle, UK), under randomized conditions. The MS/MS data were searched using MASCOT versions 2.3 (Matrix Science Ltd, London, UK) against a human subset of the NCBI database (downloaded on 12 January 2011) with 34,281 sequences using a maximum missed-cut of 2. Variable methionine oxidation, STY phosphorylation, protein N-terminal acetylation, and fixed cysteine carbamidomethylation were used in all searches.

LC-MS label-free quantification was performed using Progenesis 4.0 (Nonlinear Dynamics). Protein conflict (peptides shared between different proteins) was solved as followed: conflict resulting from multiple sequence assignment to the same peak; we kept only the sequence having the highest score. Conflict resulting from same peptide sequences assigned to different proteins, the assignment was singly attributed to the protein that had the highest number of peptides. Regarding the label-free quantitation, the total number of Features (i.e., intensity signal at a given retention time and *m/z*) was reduced to MSMS peaks with charge of 2, 3, or 4+ and we only kept the five most intense MSMS spectra per 'Feature'. The subset of multicharged ions (2+, 3+, and 4+) was extracted from each LC-MS run and the ions intensities summed for normalization. Protein quantitation was performed as follows; for a specific protein, the associated unique peptide ions were summed to generate an abundance value. The measured protein abundances were transformed using an ArcSinH function (as the method of detection can generate a significant amount of near zero measurement for which a log transform is not ideal). The within-group means were calculated to determine the fold change and the transformed data were then used to calculate the *P* values using one-way analysis of variance. Significant changes in protein expression ($P < 0.01$) between control and OGD experimental groups were determined for each time point (6 and 18 hours) using Student's *t*-test.

Analysis of Protein Subcellular Localization

All 958 proteins identified by LC-MS by at least two or more peptides were uploaded to the Database for Annotation, Visualization and Integrated Discovery (DAVID) (http://david.abcc.ncifcrf.gov[15]) to determine subcellular localization based on gene ontology (GO). Protein clusters founded on subcellular localization with DAVID scores >2 were used. Proteins significantly altered ($P < 0.01$) after 18 hours OGD were also assessed by DAVID according to subcellular localization.

Interactome Analysis of Proteins Altered with Oxygen Glucose Deprivation

Protein identifiers of all the proteins significantly altered after 18 hours OGD ($P < 0.01$) were uploaded with their corresponding fold change values

to Ingenuity Pathway Analysis software (IPA; http://www.ingenuity.com). Interactomes were algorithmically generated based on direct relationships (physical interactions and associations) between eligible proteins. The interactomes are color coded with green nodes representing proteins that were downregulated after 18 hours OGD and red protein nodes representing proteins that were upregulated after 18 hours OGD. The shading of the interactome nodes is positively correlated with the magnitude of fold change. The IPA generates a score for each interactome, which is a putative measure of probability (see Deighton *et al*[16] for critical analysis).

Subcellular Morphology with Electron Microscopy

SH-SY5Y cells were exposed to OGD using the same paradigm as the LC-MS study. Samples were collected immediately after 3, 9, and 18 hours of OGD and fixed for a minimum of 20 hours in aldehyde fixative (4% paraformaldehyde and 5% glutaradehyde in 0.08 M sodium cacodylate buffer, pH 7.2). Once fixed, cells were centrifuged at 100 *g*, the supernatant removed and replaced with a 3% solution of agar (type VII, low gelling temperature; Sigma-Aldrich, Gillingham, UK). The gels were set at 4°C for 5 minutes before being cut into 1 mm^3 blocks and processed for electron microscopy (EM). Processing, embedding, and staining were performed, as described previously.[17] Briefly, the blocks were cut into 70 nm thick sections, collected on 300 mesh copper grids, stained with Reynold's lead citrate and contrasted with uranyl acetate.

The EM sections were evaluated on a JEOL CX-100 II transmission electron microscope (Tokyo, Japan). The evaluator was blinded to the treatment condition of all samples. Cells were chosen from grid squares in a predetermined pattern. Fifty cells were assessed from each treatment. For each cell, the condition of mitochondria and rough ER was assessed. Mitochondria were graded as '*normal*' (cristae clearly visible across >50% of the matrix), '*swollen*' (with a proportion of the matrix lost) and '*abnormal*' (with most/ the entire matrix lost). The ER in each cell was graded similarly, i.e., '*normal*' (where ER outer membranes ran parallel to each other), '*swollen*' (where modest swelling of ER outer membrane was present), or '*abnormal*' where ER displayed extensive membrane swelling and distortions. A Chi-Squared 3×2 matrix was used to test the null hypothesis that OGD would have no effect on the ultrastructure of organelles.

RESULTS

Mitochondrial Function, Cell Viability, and Ultrastructure after Oxygen Glucose Deprivation

Normal mitochondrial function was significantly reduced in SH-SY5Y cells after OGD relative to time-matched control cells ($P<0.0001$, at each time point analyzed), with longer durations of OGD inducing more severe mitochondrial dysfunction (Figure 1A). Viability of SH-SY5Y cells treated with OGD was quantified using Trypan Blue staining (Figure 1B). Minimal cell death was detected after OGD, with 91% of cells remaining viable after 18 hours OGD.

Ultrastructural morphologic changes in subcellular organelles were analyzed relative to time-matched controls by EM after OGD. With increasing OGD duration, the number of cells displaying abnormal ER was significantly increased (Chi-Square, $P<0.01$) (Figures 2A and 2C). SH-SY5Y cells also showed changes in mitochondrial morphology with increasing OGD duration (Figures 2B and 2D). It should be noted that even after 18 hours OGD exposure, only 26% of cells displayed abnormal ER, and only 34% had abnormal mitochondria.

Global Proteomic Response after Oxygen Glucose Deprivation (6 and 18 hours)

A total of 958 proteins were identified across all samples with two or more peptides by LC-MS (Supplementary Table 1). Minimal protein changes were observed after 6 hours OGD, with only 14 proteins significantly altered in expression level ($P<0.01$). After 18 hours OGD, 193 proteins were significantly altered in expression level ($P<0.01$) with 130 proteins increased and 63 proteins decreased. For 765 proteins, no significant difference was observed between control and OGD samples after 18 hours OGD.

Subcellular distribution of all the 958 proteins identified by LC-MS was examined using DAVID software. Proteins were detected from across many subcellular compartments, including the nuclear lumen, cytoskeleton, mitochondria, ER, golgi apparatus, ribosomes, and vesicles (Figure 3A).

The ascribed subcellular locations of the significantly altered proteins with OGD (18 hours) indicate that organelles are not uniformly affected by the metabolic challenge. None of the 197 detected nuclear lumen proteins were significantly altered after OGD, while 41% of the 56 detected ER proteins and 32% of the 118 detected mitochondrial proteins were significantly altered (Figure 3B). The significantly increased and decreased proteins after OGD (18 hours) are listed by subcellular location in Table 1 and Table 2, respectively.

Functional protein–protein interactions for the 193 proteins altered with 18 hours OGD were defined using IPA software. IPA-generated 10 protein interactomes (Supplementary Table 2) and three high-scoring interactomes (IPA scores >40) are discussed in context below. These interactomes highlight a shift in mitochondrial energy production, enhanced ER stress, and ribosomal dysfunction.

Mitochondrial Protein Alterations after Oxygen Glucose Deprivation (18 hours)

In all, 38 mitochondrial proteins (out of 118 detected; assigned using the GO term *mitochondrion* GO:0005739) were significantly

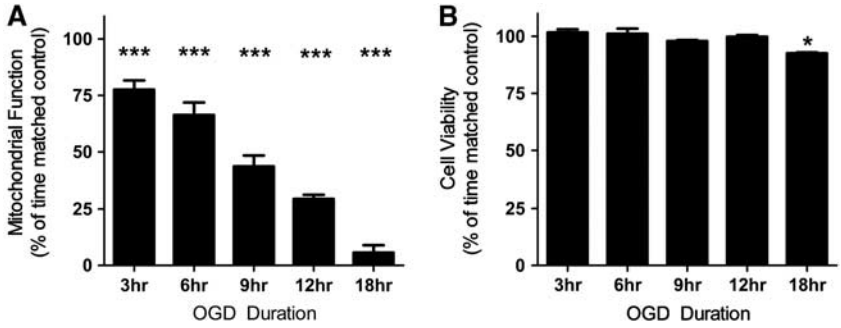

Figure 1. Mitochondrial function decreases after oxygen glucose deprivation (OGD), whereas cell viability is largely maintained. (**A**) Mitochondrial function is significantly decreased at each OGD time point compared with time-matched controls. Mitochondrial function was assessed using an MTS assay, with data presented as mean ± s.d., $n=8$ for each time point. (**B**) Cell viability is maintained up to 12 hours OGD, with an increase in cell death after 18 hours OGD. Cell viability was assessed using a trypan blue dye exclusion assay. Data are presented as mean ± s.d., $n=3$ for each time point. All data are expressed as a percentage of contemporaneous time matched controls (*$P<0.05$, ***$P<0.0001$, *T*-test).

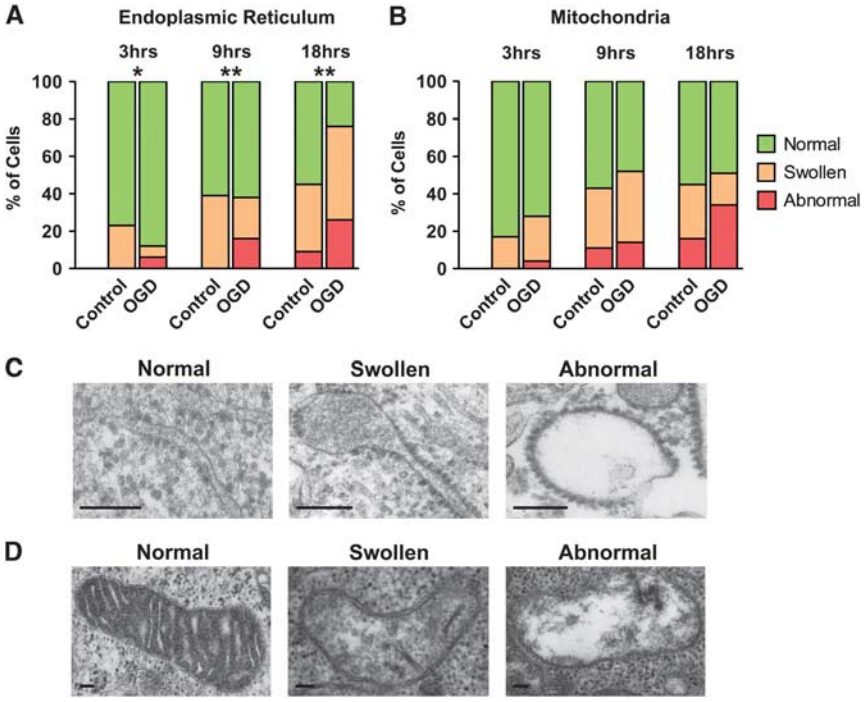

Figure 2. The endoplasmic reticulum (ER) and mitochondria display progressive morphologic changes after oxygen glucose deprivation (OGD). (**A**) OGD induced increases in the number of cells containing swollen and abnormal ER. Significant changes in the distribution of 'normal', 'swollen', and 'abnormal' ER within cells were seen after 3, 9, and 18 hours OGD compared with the time-matched controls (*$P<0.05$, **$P<0.01$, χ^2). (**B**) The occurrence of mitochondrial morphologic abnormality increases after longer OGD durations. (**C**) Representative electron micrographs of the three grades of ER morphology. Scale bar = 0.1 μm. (**D**) Representative electron micrographs of the three grades of mitochondrial morphology. Scale bar = 0.1 μm.

altered after OGD (18 hours): 29 were increased and 9 were decreased. VDAC1 and TOM22, proteins involved in mediating the movement of metabolites across the mitochondrial membrane, were significantly reduced after OGD. UQCRC1 and UQCRC2, integral components of complex III of the electron transport chain (ETC), were also significantly reduced (Figure 4A). Coordinated changes in other regions of the ETC were observed after 18 hours OGD treatment: ETC complex V proteins ATP5J and ATP5A1, and ETC complex I proteins NDUFS3 and NDUFA5 were all significantly increased ($P<0.01$).

Numerous mitochondrial proteins that have a role in lipid metabolism were also found to be altered after 18 hours OGD. ACADM, the enzyme involved in the first step of fatty acid beta oxidation was significantly decreased ($P<0.01$); and ECH1, HSD17B10 and ACAA2, enzymes downstream in the beta-oxidation process were significantly increased. ACAT1, a mitochondrial protein involved in ketone metabolism was also significantly increased.

The highest scoring protein interactome generated by IPA features some of the alterations in energy production described above, namely increases in Complex V proteins (including ATP5J and ATP5A1) and decreases in Complex III proteins (UQCRC1 and UQCRC2) (Figure 4B). This *Energy Production Interactome* also highlights interactions between altered components of the ETC and other cellular machinery. Both UQCRC1 and UQCRC2 interact with RTN4, a protein predominantly associated with regulating ER function that was significantly upregulated after OGD (Figure 4A). UQCRC2 is also shown to interact with upregulated RUVBL2, a cytoskeletal protein involved in numerous cellular activities including transcription and cellular transformation (Figure 4A). The *Energy Production Interactome* also contains a cluster of ribosomal proteins that are distinct but intersect with the ribosomal interactome described below.

Endoplasmic Reticulum Protein Alterations after Oxygen Glucose Deprivation (18 hours)

In all, 23 ER proteins (out of 56 detected; assigned using the GO term *Endoplasmic reticulum* GO:0005783) were significantly altered after 18 hours OGD: 19 were increased and 4 were decreased. A number of proteins centrally involved in the UPR were significantly increased, including, HSPA5, HSP90B1, PDIA3, and PDIA4 ($P<0.01$) (Figure 5A). Other proteins including CALR, UGGT1, ERP29, ERP44, and VCP that are integral to ER stress response and protein folding were significantly increased.

Multiple proteins that have a role in protein degradation were significantly altered after OGD (18 hours). Protein subunits of the 20S and 19S core structures of the 26S proteasome (PSMA5, PSMC3, PSMC4, PSMD1, PSMD2, PSMD6, and PSMD11) were increased. These proteasomal proteins, along with proteins involved in the UPR and heat-shock response after OGD dominate the high scoring, *Protein Folding and Degradation Interactome* generated by IPA (Figure 5B).

Ribosomal Protein Alterations after Oxygen Glucose Deprivation (18 hours)

In all, 11 ribosomal proteins (out of 82 detected; assigned using the GO term *Ribosome* GO:0005840) were significantly altered after 18 hours OGD: 1 was increased and 10 were decreased. The decreased ribosomal proteins were associated with both the 60S (RPL38, RPL23, RPL35, and RPL13) and 40S (RPS1, RPS14, RPS23, RPS9, and RPS17) ribosomal subunits (Figure 5C). These downregulated ribosomal proteins feature prominently in another of the high scoring protein interactomes generated by IPA (Figure 5D). An additionally important feature of this *Ribosomal Interactome* is the cluster of upregulated peroxidases (PRDX1, PRDX2, and PRDX5) (Figure 5C) involved in redox homeostasis and

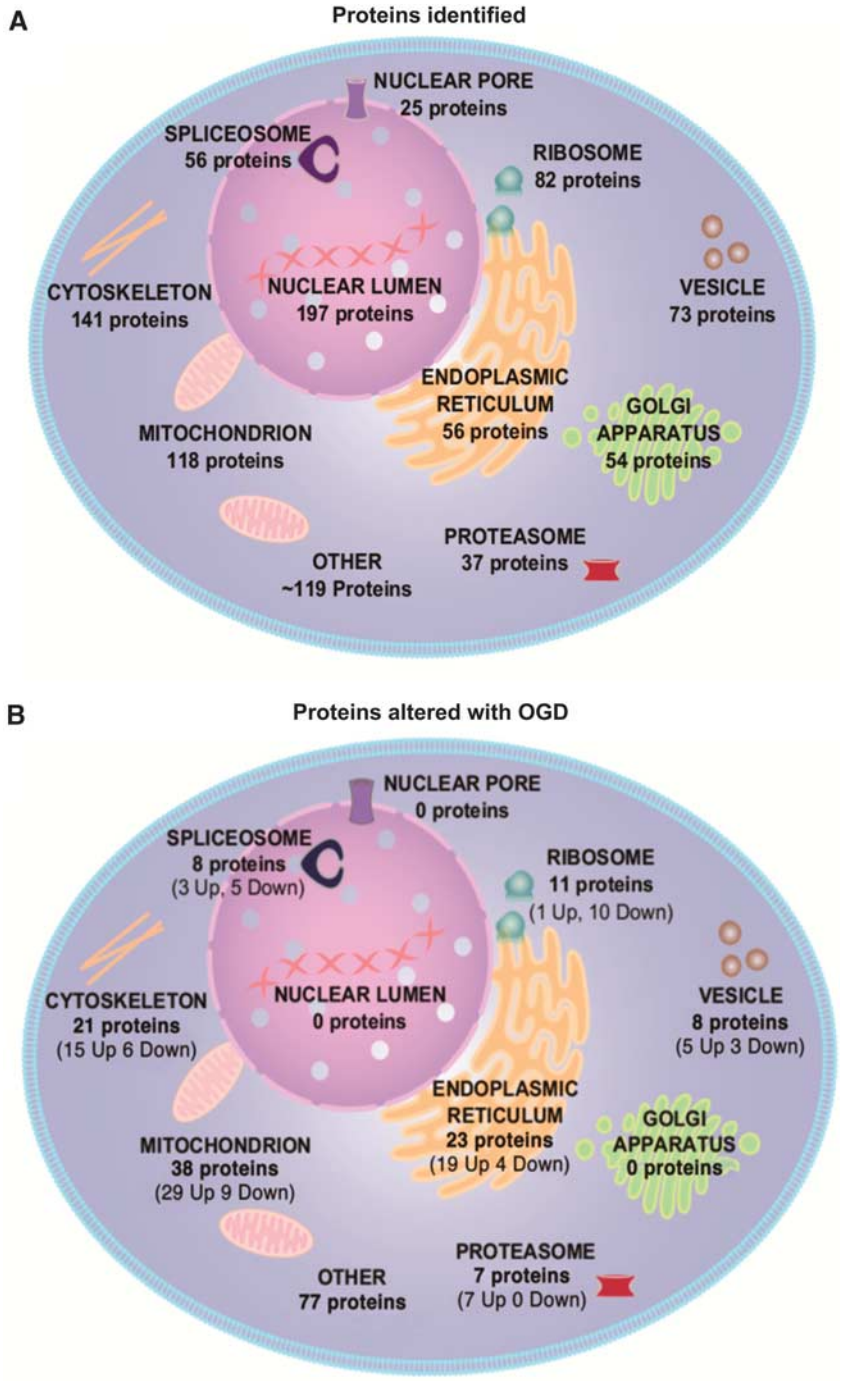

Figure 3. Subcellular distribution of detected proteins contrasted with subcellular distribution of proteins significantly altered after oxygen glucose deprivation (OGD). Proteins were ascribed to subcellular compartment by DAVID software based on gene ontology. Proteins were significantly altered after OGD ($P<0.01$) relative to their original levels in time-matched control samples. (**A**) Liquid chromatography mass spectrometry (LC-MS) detected 958 proteins from across many subcellular compartments, showing the utility of LC-MS in providing a global overview of cellular proteomics. (**B**) Organelles are differentially affected by 18 hours OGD. The 193 significant proteins changed ($P<0.01$) were not distributed evenly across subcellular compartments: the endoplasmic reticulum and the mitochondria contained the largest proportion of significantly altered proteins, whereas no significant protein changes were detected in the golgi apparatus or nuclear pore.

protecting neurons from oxidative insults (for a review, see Bell and Hardingham, 2011[18]).

DISCUSSION

This study provides the first comprehensive analysis of the proteomic and morphologic response of human SH-SY5Y cells to prolonged metabolic challenge. The robustness of SH-SY5Y cells to external stressors has allowed the evolving proteomic changes occurring in response to OGD induced metabolic stress to be defined, in the absence of cell death. The observed protein changes provide insight into the complex molecular alterations underpinning cellular adaptation to metabolic stress. The lack of acute ischemic cell death in our *in vitro* model of neuronal

Table 1. Proteins significantly increased with OGD (18 hours)

Uniprot accn no.	*Gene name*	*Protein name*	P *value*	*Fold change*	*Protein function*
Mitochondria					
P30048	*PRDX3*	Peroxiredoxin III	0.0006	1.57	Cell redox homeostasis
P61604	*HSPE1*	10 kDa heat-shock protein	6.1E-06	1.51	Stress response
P18859	*ATP5J*	ATP synthase-coupling factor 6	0.0016	1.44	ETC complex V
O75489	*NDUFS3*	NADH-ubiquinone oxidoreductase 30 kDa subunit	0.0030	1.38	ETC complex I
P24752	*ACAT1*	Acetyl-CoA acetyltransferase	9.1E-05	1.38	Ketone body metabolism
P09622	*DLD*	Dihydrolipoyl dehydrogenase	0.0051	1.36	Gycine cleavage
Q9UJZ1	*STOML2*	Stomatin-like protein 2	0.0052	1.36	Receptor binding
P09972	*ALDOC*	Fructose-bisphosphare aldolase C	0.0061	1.34	Glycolysis
P38606	*ATP6V1A*	V-type proton ATPase catalytic subunit A	0.0067	1.33	ATP hydrolysis transport
P13804	*ETFA*	Electron transfer flavoprotein subunit alpha	0.0005	1.33	Respiratory ETC
P30084	*ECHS1*	Enoyl-CoA hydratase	0.0043	1.33	Fatty acid metabolism
P40926	*MDH2*	Malate dehydrogenase	0.0009	1.32	Citric acid cycle
P10809	*HSPD1*	60 kDa heat-shock protein	0.0012	1.31	Protein folding
P62258	*YWHAE*	14-3-3 protein epsilon	0.0056	1.30	Apoptosis
P04181	*OAT*	Orthinine aminotransferase	0.0012	1.30	Amino acid biosynthesis
Q13011	*ECH1*	Delta (3,5)-delta(2,4)-dienoyl-CoA isomerase	0.0048	1.28	Lipid metabolism
Q99714	*HSD17B10*	3-hydroxyacyl-CoA dehydrogenase type 2	0.0037	1.27	Lipid metabolism
P07954	*FH*	Fumarate hydratase	0.0038	1.27	Citric acid cycle
P30044	*PRDX5*	Peroxiredoxin 5	0.0014	1.26	Redox homeostasis
P42765	*ACAA2*	3-ketoacyl-CoA thiolase	0.0067	1.26	Lipid metabolism
P25325	*MPST*	3-mercaptopyruvate sulfurtransferase	0.0012	1.25	Response to Toxins
P30086	*PEBP1*	Phosphatidylethanolamine binding protein 1	0.0067	1.24	Protease inhibition
P25705	*ATP5A1*	ATP synthase subunit alpha	0.0019	1.21	ETC complex V
Q06830	*PRDX1*	Peroxiredoxin 1	0.0009	1.20	Redox homeostasis
P43686	*PSMC4*	26S protease regulatory subunit 6B	0.0007	1.20	Protein degradation
Q16718	*NDUFA5*	NADH-ubiquinone oxidoreductase 13 kDa subunit	0.0022	1.20	ETC complex I
O00154	*ACOT7*	Cytosolic acyl-coenzyme A thioester hydrolase	0.0009	1.19	Acyl-CoA hydrolysis
Q00610	*CLTC*	Clathrin heavy chain 1	4.9E-05	1.16	Endocytosis
P12277	*CKB*	Creatine Kinase B type	0.0027	1.16	Creatine metabolism
Endoplasmic reticulum					
O60568	*PLOD3*	Procollagen-lysine 2-oxoglutarate 5-dioxygenase 3	7.7E-05	1.87	Lysyl hydroxylation
P27797	*CALR*	Calreticulin	1.0E-07	1.56	Protein folding
P11021	*HSPA5*	Heat-shock protein 5	3.9E-05	1.53	Protein complex assembly
P14625	*HSP90B1*	Heat-shock Protein 90 kDa beta member 1	5.5E-05	1.49	Protein transport
P30101	*PDIA3*	Protein disulfide isomerase A3	2.7E-05	1.45	Protein folding
Q16799	*RTN1*	Reticulon 1	0.0055	1.41	Neuron differentiation
Q8NBS9	*TXNDC5*	Thioredoxin-domain containing protein 5	0.0017	1.40	Cell redox homeostasis
P13667	*PDIA4*	Protein disulfide isomerase A4	1.4E-05	1.38	Cell redox homeostasis
Q9Y2B0	*CNPY2*	Protein canopy homolog 2	0.0051	1.38	Protein binding
Q15084	*PDIA6*	Protein disulfide isomerase A6	6.1E-06	1.37	Chaperone
P54920	*NAPA*	Alpha soluble NSF attachment protein	0.0003	1.35	ER-golgi vesicle transport
P14314	*PRKCSH*	Glucosidase 2 subunit beta	0.0016	1.33	Glycoprotein formation
Q9NQC3	*RTN4*	Reticulon 4	0.0033	1.32	Neurogenesis/apoptosis
Q14697	*GANAB*	Neutral alpha-glucosidase AB/GNAB protein	0.0018	1.27	Glycoprotein cleavage
P07237	*P4HB*	Protein disulfide isomerase	0.0073	1.25	Redox homeostasis
Q9BS26	*ERP44*	Endoplasmic reticulum resident protein 44	0.0007	1.23	ER stress response
Q9NYU2	*UGGT1*	UDP glucose:glycoprotein glucosyltransferase 1	0.0074	1.23	ER protein folding
P30040	*ERP29*	Endoplasmic reticulum resident protein 29	0.0003	1.23	ER protein folding
P55072	*VCP*	Valosin-containing protein	0.0069	1.15	ER stress response
Ribosomes					
P69905	*HBA1*	Hemoglobin subunit alpha	0.0003	1.97	O_2 transport
Vesicle					
O15240	*VGF*	Neurosecretory protein VGF	0.0035	1.39	Cell–cell interactions
P08133	*ANXA6*	Annexin 6	0.0075	1.18	Ca2+ binding
P21281	*ATP6V1B2*	V-type proton ATPase subunit B	0.0098	1.16	H+ ion transport
P07900	*HSP90AA1*	Heat Shock Protein HSP90-alpha	0.0030	1.11	Stress response
Q9BTT0	*ANP32E*	Acidic leucine-rich nuclear phosphoprotein 32E	0.0034	1.08	Phosphatase inhibitor
Cytoskeleton					
P52907	*CAPZA1*	F-actin capping protein subunit alpha 1	0.0039	1.35	Protein complex assembly
P16949	*STMN1*	Stathmin	0.0029	1.32	Microtubule disassembly
Q9Y230	*RUVBL2*	RuvB like 2	0.0037	1.31	Transcription
P47756	*CAPZB*	F-actin-capping protein subunit beta	3.2E-05	1.25	Protein complex assembly
Q03252	*LMNB2*	Lamin B2	0.0076	1.24	Cytoskeleton regulation
Q16352	*INA*	Alpha-internexin	4.9E-05	1.24	Neurogenesis
P07437	*TUBB*	Tubulin beta chain	0.0016	1.23	Microtubule constituent
P36405	*ARL3*	ADP-ribosylation factor-like protein 3	0.0071	1.23	Cell division
P61163	*ACTR1A*	Alpha centractin	0.0029	1.23	Vesicle mediated transport
Q9UJU6	*DBNL*	Debrin-like protein	0.0095	1.18	Endocytosis
Q16658	*FSCN1*	Fascin	0.0018	1.18	Cytoskeleton organization
P62158	*CALM*	Calmodulin	0.0059	1.17	Calcium modulation
Q9BZK7	*TBL1XR1*	F-box like/WD repeat containing protein TBL1XR1	0.0046	1.17	Protein degradation

Table 1. (Continued)

Uniprot accn no.	*Gene name*	*Protein name*	P *value*	*Fold change*	*Protein function*
P49773	*HINT1*	Histidine triad nucleotide-binding protein 1	0.0002	1.15	Signal transduction
P43487	*RANBP1*	Ran-specific GTPase-activating protein	0.0029	1.15	Signal transduction
Spliceosome					
Q07955	*SRSF1*	Serine/Arginine-rich splicing factor 1	1.1E-05	1.42	mRNA splicing
Q01081	*U2AF1*	Splicing factor U2AF 35 kDa subunit	0.0062	1.23	mRNA splicing
Q15029	*EFTUD2*	116 kDa U5 small nuclear ribonucleoprotein	0.0069	1.19	mRNA splicing
Proteosome					
Q15008	*PSMD6*	26s proteasome non ATPase regulatory subunit 6	0.0053	1.61	Protein degradation
P17980	*PSMC3*	26S protease regulatory subunit 6A	0.0071	1.27	Protein degradation
Q13200	*PSMD2*	26S proteasome non-ATPase regulatory subunit 2	0.0005	1.22	Protein degradation
P54727	*RAD23B*	UV excision protein RAD23 homolog B	0.0009	1.22	Protein degradation
Q99460	*PSMD1*	26S proteasome non-ATPase regulatory subunit 1	0.0002	1.18	Protein degradation
O00231	*PSMD11*	26S proteasome non-ATPase regulatory subunit 11	0.0008	1.18	Protein degradation
P28066	*PSMA5*	Proteasome subunit alpha type 5	0.0036	1.16	Protein degradation

ER, endoplasmic reticulum; ETC, electron transport chain; OGD, oxygen glucose deprivation.
Proteins are grouped according to subcellular compartment based on gene ontology and ranked according to magnitude of fold change. The significance threshold was set *a priori* at $P<0.01$.

Table 2. Proteins Significantly Decreased with OGD (18 hours)

Uniprot accn no.	*Gene name*	*Protein name*	P-*value*	*Fold change*	*Protein function*
Mitochondria					
P21796	*VDAC1*	Voltage-dependent anion selective channel protein 1	0.0079	0.26	Ion transport
P22695	*UQCRC2*	Cytochrome b-c1 complex subunit 2	0.0017	0.31	ETC complex III
P31930	*UQCRC1*	Cytochrome b-c1 complex subunit 1	0.0097	0.46	ETC complex III
Q9NS69	*TOM22*	Translocase of outer membrane 22 kDa subunit	0.0027	0.46	Protein transport
Q9Y3E5	*BIT1*	Peptidyl-tRNA hydrolase 2	0.0038	0.51	Apoptosis
P02786	*TFRC*	Transferrin receptor protein 1	0.0002	0.58	Endocytosis
O75534	*CSDE1*	Cold shock domain containing protein E1	1.0E-06	0.62	Transcription
Q9Y6H1	*CHCHD2*	Coiled-coil helix–coiled-coil helix domain protein 2	0.0099	0.70	*unknown*
P11310	*ACADM*	Medium chain specific acyl-CoA dehydrogenase	0.0084	0.79	Lipid metabolism
Endoplasmic reticulum					
Q81V08	*PLD3*	Phospholipase D3	0.0016	0.61	Lipid degradation
Q96AG4	*LRRC59*	Leucine rich repeat-containing protein 59	0.0048	0.64	ER membrane interactions
P13637	*ATP1A3*	$Na+/K+$ ATPase alpha (III) subunit	0.0008	0.67	ATP hydrolysis catalyst
P04843	*RPN1*	Ribophorin 1	0.0094	0.68	Glycosyltransferase activity
Ribosomes					
P63173	*RPL38*	60s ribosomal protein L38	0.0001	0.65	Protein biosynthesis
P62249	*RPS16*	40S ribosomal protein S16	7.9E-05	0.70	Protein biosynthesis
P35544	*FAU*	Ubiquitin-like protein FUB 1	0.0012	0.70	Ubiquitination modulation
P62263	*RPS14*	40S ribosomal protein S14	0.0004	0.74	Protein biosynthesis
P62829	*RPL23*	60S ribosomal protein L23	5.3E-05	0.74	Protein biosynthesis
P62266	*RPS23*	40S ribosomal protein S23	0.0004	0.76	Protein biosynthesis
P46781	*RPS9*	40S ribosomal protein S9	0.0002	0.78	Protein biosynthesis
P08708	*RPS17*	40S ribosomal protein S17	0.0004	0.80	Protein biosynthesis
P42766	*RPL35*	60S ribosomal protein L35	0.0018	0.82	Protein biosynthesis
P26373	*RPL13*	60S ribosomal protein L13	0.0004	0.84	Protein biosynthesis
Vesicle					
P07355	*ANXA2*	Annexin A2	0.0038	0.49	Ca^{2+} binding
P62491	*RAB11A*	Ras-related protein Rab 11A	0.0026	0.76	Endocytic cycling
P07858	*CTSB*	Cathepsin B	0.0053	0.85	Protein degradation
Cytoskeleton					
P06493	*CDK1*	Cyclin-dependent kinase 1	0.0022	0.57	Cell-cycle control
P28289	*TMOD1*	Tropomodulin 1	0.0005	0.64	Cytoskeleton organization
Q01518	*CAP1*	Adenylyl cyclase-associated protein 1	4.7E-06	0.70	Signal transduction
Q9UQE7	*SMC3*	Structural maintenance of chromosomes protein 3	0.0084	0.71	Cell cycle
P18206	*VCL*	Viniculin	0.0067	0.78	Cell adhesion
Q01082	*SPTBN1*	Spectrin beta chain brain 1	0.0092	0.81	Cytoskeleton movement
Spliceosome					
P17844	*DDX5*	Probable ATP-dependent RNA helicase DDX5	2.9E-06	0.58	mRNA processing
Q9UKM9	*RALY*	RNA-binding protein Raly	0.0014	0.66	mRNA splicing
Q86V81	*THOC4*	THO complex subunit 4	0.0007	0.75	mRNA splicing
O43143	*DHX15*	Pre-mRNA splicing factor ATP-dep. RNA helicase	5.5E-06	0.78	mRNA splicing
P07910	*HNRNPC*	Heterogeneous nuclear ribonucleoproteins Ca/C2	0.0005	0.81	mRNA splicing

ER, endoplasmic reticulum; ETC, electron transport chain; OGD, oxygen glucose deprivation.
Proteins are grouped according to subcellular compartment based on gene ontology and ranked according to magnitude of fold change. The significance threshold was set a priori at $P<0.01$.

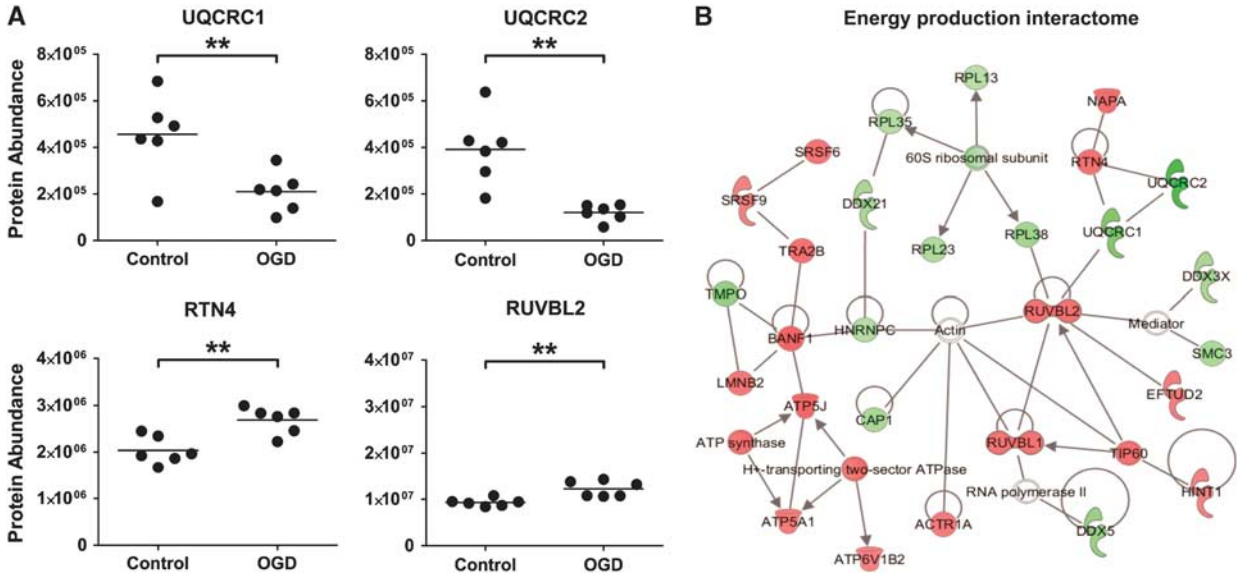

Figure 4. Mitochondrial energy production proteins and associated interacting partners are affected by oxygen glucose deprivation (OGD). (**A**) Key mitochondrial energy production proteins (UQCRC1/UQCRC2) and their putative interacting partners (RTN4/RUVBL2) are significantly altered by OGD (18 hours). Each data point represents an independent sample with the mean abundance line shown (**$P < 0.01$, *T*-test). (**B**) Energy Production Interactome. One of the highest scoring Ingenuity Pathway Analysis (IPA) networks gained from the 18-hour OGD proteomic data set is presented. The network contains numerous proteins involved in mitochondrial energy production, the colored nodes indicate proteins detected in our study as significantly altered by OGD. Red nodes are upregulated proteins and green nodes are downregulated. Unshaded nodes were manually inserted by IPA to augment functional coherence. Only direct protein–protein interactions were included in the analysis.

metabolic stress makes the proteomic results particularly pertinent to mild, sustained ischemia challenges and the compromised energy metabolism associated with slowly evolving neurodegenerative disorders such as Alzheimer's disease.[3]

Proteomics has showed alterations and interactions in mitochondrial, ER, and ribosomal proteins after OGD. The ETCproteins displayed bidirectional changes (Complex I and V proteins increased and Complex III proteins decreased) in response to OGD. Other mitochondrial proteins involved in lipid and ketone metabolism, including AD-related HSD17B10 (more commonly known as ABAD), were also increased after OGD (18 hours). The ER stress response proteins along with proteins involved in proteasomal/ubiquitination degradation also formed an important part of the upregulated proteomic response to the metabolic challenge of OGD.

A significant mitochondrial proteomic response was observed after OGD. Two of the most markedly decreased proteins after 18 hours OGD were subunits 1 and 2 (UQCRC1 and UQCRC2) of ETC complex III. Complex III is the third component of the ETC located within the inner mitochondrial membrane. Complex III mediates the transfer of electrons from ubiquinone to cytochrome C, and in doing so translocates a proton into the inner-membrane space and contributes to the generation of the electrochemical gradient used for the production of ATP.[19] Complex III is also intrinsically involved in the generation of reactive oxygen species from the mitochondria during hypoxia, and these reactive oxygen species work to stabilize HIF1α and initiate protein transcription.[20] A significant decrease in UQCRC1 and UQCRC2 might be an attempt by the cells to reduce the production of reactive oxygen species from the mitochondria under stress conditions. Interestingly, UQCRC1 has also been recorded as significantly decreased in the brains of AD patients.[21] The similar decrease in UQCRC1 expression observed in AD patients and cells *in vitro* after OGD may provide a link between chronic oxidative challenge and the onset and progression of AD.

The *Energy Production Interactome* (Figure 4B) also highlighted putative functional protein–protein interactions between UQCRC1, UQCRC2, and RTN4 (a protein increased after 18 hours OGD). RTN4 is increased in hippocampal neurons of AD patients[22] and is known to interact with BACE1, reducing AB40 and AB42 levels.[23] The dysregulation of RTN4 after a metabolic challenge (18 hours OGD), its interaction with complex III proteins, and its potential role in APP processing, highlights RTN4 protein as a compelling target for future investigation.

Mitochondrial complex I and V proteins were significantly increased in expression after OGD in sharp contrast to the reduction in complex III proteins after OGD. Complex I is the first protein complex of the ETC and initiates the transfer of electrons required for oxidative phosphorylation. The process is initiated through binding and oxidation of NADH, with the concurrent transfer of two electrons from NADH to ubiquinone, and the translocation of four protons into the intermembrane space.[24] An increase in Complex I proteins after OGD may reflect a compensatory mechanism to counteract the impact of decreased complex III proteins on energy production. Similarly, the increase in Complex V proteins may reflect a compensation for downregulated Complex III proteins or a general remodeling of the ETC, as has previously been shown in studies investigating ischemic preconditioning.[25] Functional assays of the five complexes that constitute the ETC, in ischemic conditions will need to be carried out to confirm whether such remodeling occurs. Determining the regulatory mechanisms of these protein changes could provide valuable insight that would allow therapeutic intervention to alter the course of mitochondrial dysfunction after OGD and metabolic challenges *in vivo*.

Concurrent with the dysregulation of the oxidative phosphorylation pathway, OGD (18 hours) induced an increase in mitochondrial proteins involved in lipid and ketone metabolism. The increase in these proteins (ACAT1 in ketone metabolism, and ACADM, ECH1, HSD17B10, and ACAA2 in lipid metabolism)

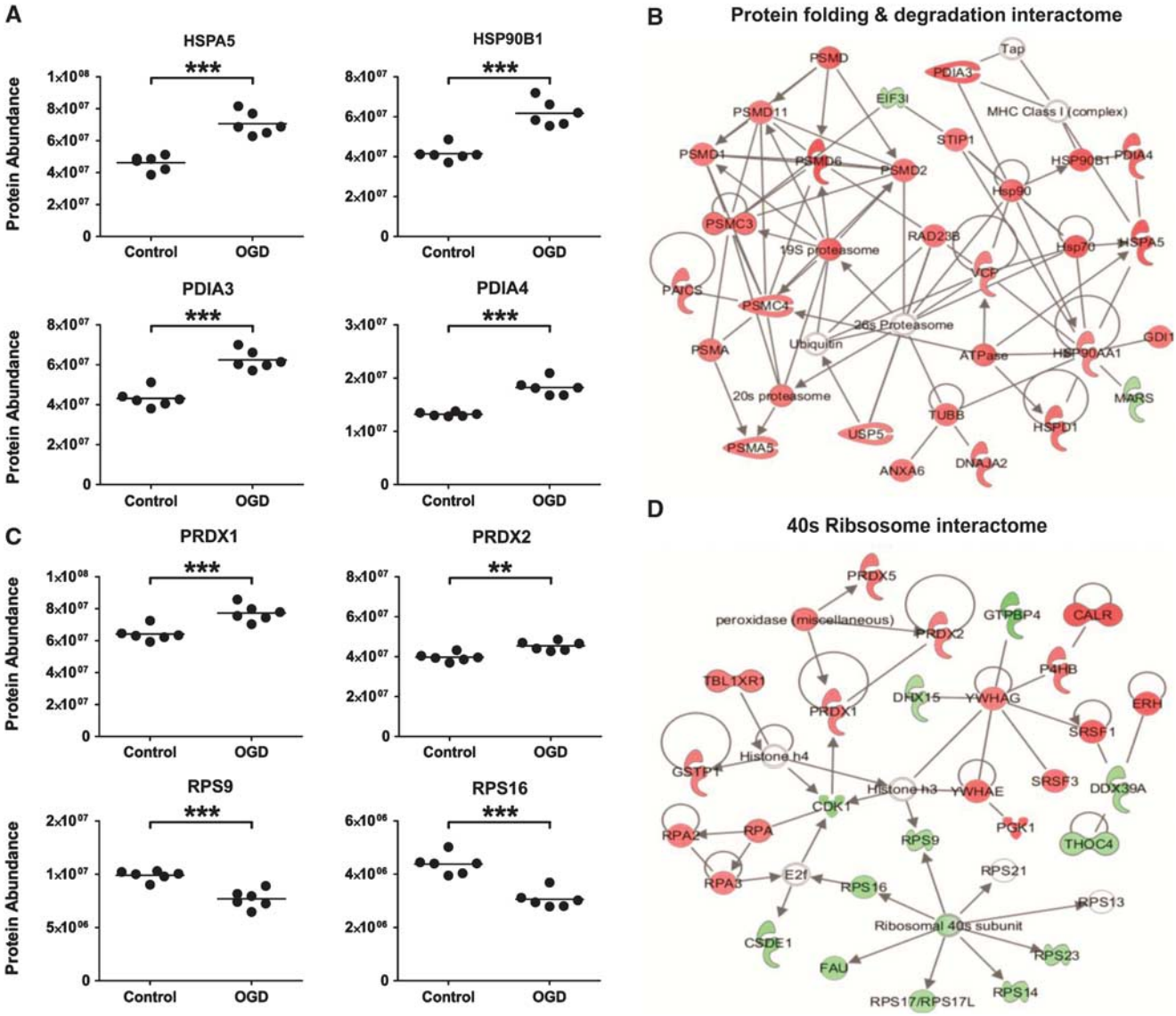

Figure 5. Protein production, folding, and degradation pathways are affected by oxygen glucose deprivation (OGD). (**A**) Key proteins involved in protein folding and the endoplasmic reticulum stress response (HSPA5/HSP90B1/PDIA3/PDIA4) are significantly altered by OGD (18 hours). (**B**) Protein Folding and Degradation Interactome. A high scoring Ingenuity Pathway Analysis (IPA) network generated from the 18-hour OGD proteomic data set contained numerous proteins involved in protein folding and degradation is presented. The colored nodes indicate proteins detected in our study as significantly altered by OGD. Red nodes are upregulated proteins and green nodes are downregulated proteins. Unshaded nodes were manually inserted by IPA to augment functional coherence. Only direct protein–protein interactions were included in the analysis. (**C**) Representative ribosomal proteins (RPS9/RPS16) and the cellular stress response proteins (PRDX1/PRDX2) are significantly altered by OGD (18 hours). Each data point represents an independent sample (**$P<0.01$, ***$P<0.0001$, *T*-test). (**D**) 40S Ribosomal Interactome. A further high scoring IPA network was dominated by the downregulation of 40S ribosomal proteins and cell stress response proteins.

indicates a shift toward using lipid and ketone bodies as alternative sources of energy for SH-SY5Y cells faced with glucose restriction. The availability of such alternative energy sources is likely to be important in preventing cells hitting the point where energy provision is insufficient for cell survival, leading to a downward spiral of metabolic and cognitive decline. A recent study using a triple transgenic model of AD showed an induction of ketogenesis after a 2-deoxy-D-glucose diet was introduced. This correlated with an increase in nonamyloidogenic APP processing pathways, reduced AD pathology and reduced oxidative stress,[26] indicating a potential therapeutic role for enhanced ketone metabolism.

To use ketones as an alternative energy source in the brain, acetoacetate and β-hydroxybutyrate (the main ketone bodies used for energy) need to be synthesized from acetyl-coA. Acetyl-coA is released after beta oxidation of fatty acids, a four step process within the mitochondrial matrix requiring beta-oxidation enzymes at each stage (namely, ACAD, ECH1, HSD17B10, and ACAA2). Each of these beta-oxidation enzymes, as noted above, was significantly altered after 18 hours OGD. Of note, the third beta-oxidative enzyme HSD17B10 (ABAD) is now emerging as an important player in AD. ABAD has been shown to directly interact with Aβ in the mitochondria of AD patients and AD transgenic mouse models. Inhibition of the ABAD-Aβ interaction suppresses

induced apoptosis by increasing levels of Aβ, and conversely overexpression of ABAD in transgenic mice with high levels of Aβ has been shown to cause heightened neuronal oxidative stress and memory impairments.[27] The direct involvement of ABAD in AD pathophysiology makes ABAD an interesting candidate to investigate further in terms of its upregulation upon metabolic challenge.

Pore forming proteins VDAC1 and TOM22 were significantly downregulated after OGD. VDAC1 is thought to be involved in the formation of the mPTP, which in turn allows calcium and solutes <1.5 kDa to pass across the mitochondrial membranes, resulting in osmotic swelling, loss of the mitochondrial membrane potential, and damage to the electron transport respiratory chain.[28] Mitochondrial swelling after OGD was clearly showed in the human cells under the electron microscope (Figure 2D). The role that these mitochondrial pore forming proteins have in mediating mitochondrial swelling after OGD needs to be defined to facilitate the discovery of novel pathways that might be manipulated to restore mitochondrial normality.

A major proteomic response in the ER was identified after OGD. The ER stress response (also known as the unfolded protein response, UPR) is a cellular reaction activated to clear misfolded proteins that accumulate upon ER stress, thus returning the cell to a state of proteostasis.[29] Two central molecular chaperones, HSPA5 and HSP90B1, involved in the early and late stages of the UPR respectively were upregulated after OGD in SH-SY5Y cells (as well as numerous other UPR proteins and ER stress proteins) (Figure 5A). These data are consistent with recent results from OGD in mixed primary cortical cultures where increases in both HSPA5 and HSP90B1 were detected.[30] The induction of the UPR in response to OGD was also implied in the electron microscopic data. The ER showed a progressive morphologic swelling that significantly increased after longer durations of OGD exposure compared with time-matched controls ($P<0.01$, Figure 2C). An expanded ER forms an important part of the UPR as it enables larger numbers of misfolded proteins to be incorporated within the ER membrane, thus increasing cellular capacity to deal with abundant protein damage.[31] A larger ER volume also reduces the concentration of protein intermediates, therefore reducing the risk of protein aggregate formation.[32] The morphologic observation of enlarged ER along with the significant increase in UPR proteins HSPA5 and HSP90B1 detected in our proteomic data provides telling insights into how the human neuronal cells respond to the metabolic challenge of OGD.

In accord with activation of the UPR, an upregulation of numerous proteins involved in proteasomal degradation was highlighted by the *Protein Folding and Degradation Interactome*. Subunits of the 20S and 19S (core and regulatory) particles that constitute the 26S proteasome were increased, suggesting 26S proteasomal degradation to be a fundamental mechanism for degrading the misfolded proteins that accumulate in response to metabolic challenge. There has been a long-standing hypothesis that protein aggregates in diseased brain impair the protein degradation function of the 26S proteasome.[33–35] Our proteomic data show proteasomal proteins to be upregulated after a metabolic challenge. It is therefore possible to hypothesize that any proteasomal response to metabolic challenge might be adversely affected in the presence of protein aggregates associated with neurodegenerative diseases such as AD. In this situation, the cellular capacity to cope with metabolic stress would be impaired, potentially leading to a deterioration in cellular function.

A coordinated response after OGD (18 hours) was also observed in the ribosomal proteome. Numerous ribosomal proteins that constitute the core ribosomal machinery were downregulated, and in line with this, several eukaryotic initiation factors central to protein synthesis were also decreased. It is well established that cells undergoing severe metabolic stress experience a downregulation of protein translation, which can be reversible in more resistant brain areas, and irreversible in vulnerable regions.[36] Further work involving a recovery phase would need to be undertaken to understand whether the decrease in protein synthesis machinery is a survival mechanism to conserve energy, or whether it ultimately pushes the cells down a cell death route. The proteomic data does suggest that activation of the UPR correlates with a decrease in global protein synthesis, perhaps to deal with the accumulation of misfolded proteins.[37]

Substrate deprivation both *in vivo* and *in vitro* has long been recognized to evoke a marked genomic response. Whether this genomic response translates into distinct alterations in protein expression has been a matter of debate. The present study clearly shows the considerable adaptive capacity of the SH-SY5Y proteome to a prolonged metabolic challenge *in vitro*, but caution must be exercised in the extrapolation of the present data to cerebral ischemia *in vivo*. No single cell culture system can model the complexity of the response of cerebral tissue to substrate deprivation. Astrocyte cultures and neuronal cells of neuroblastoma lineage (such as SH-SY5Y cells) can tolerate prolonged OGD, whereas primary neuronal and oligodendrocyte cultures are irreversibly damaged within a few hours.[38,39] The temporal susceptibility of these different cultures to metabolic challenge, their ability to generate energy from various sources (SH-SY5Y cells have considerable capacity to perform anaerobic glycolysis[40]) and their intrinsic energy demands will all impact on the evoked proteomic response to OGD.

Additional proteomic and biochemical analyses (not just LC-MS as in the present study) including protein–protein interaction assays, membrane potential recordings, and *in vitro* ATP levels across a range of different cell types would enhance our understanding of the true nature of the metabolic challenge posed by OGD. These studies would also provide more detail as to the subtleties of the proteomic changes, not only in terms of abundance, but also in cellular and subcellular localization, and the interacting partners of altered proteins.

DISCLOSURE/CONFLICT OF INTEREST

The authors declare no conflict of interest.

REFERENCES

1 van der Worp HB, van Gijn J. Acute Ischemic Stroke. *N Engl J Med* 2007; **357**: 572–579.
2 Beal MF, Hyman BT, Koroshetz W. Do defecs in mitochondrial energy metabolism underlie the pathology of neurodegenerative diseases? *Trends Neurosci* 1993; **16**: 125–131.
3 de la Torre JC. The vascular hypothesis of Alzheimer's disease: bench to bedside and beyond. *Neurodegener Dis* 2010; **7**: 116–121.
4 Liu XQ, Sheng R, Qin ZH. The neuroprotective mechanism of brain ischemic preconditioning. *Acta Pharmacol Sin* 2009; **30**: 1071–1080.
5 Soane L, Kahraman S, Kristian T, Fiskum G. Mechanisms of impaired mitochondrial energy metabolism in acute and chronic neurodegenerative disorders. *J Neurosci Res* 2007; **85**: 3407–3415.
6 Ron D, Walter P. Signal integration in the endoplasmic reticulum unfolded protein response. *Nat Rev Mol Cell Biol* 2007; **8**: 519–529.
7 Kogure K, Kato H. Altered gene expression in cerebral ischemia. *Stroke* 1993; **24**: 2121–2127.
8 Scandalios J. Oxidative stress responses - what have genome-scale studies taught us? *Genome Biol* 2002; **3**: 1–6.
9 Zou S, Meadows S, Sharp L, Jan LY, Jan YN. Genome-wide study of aging and oxidative stress response in Drosophila melanogaster. *Proc Natl Acad Sci* 2000; **97**: 13726–13731.
10 Reimer MM, McQueen J, Searcy L, Scullion G, Zonta B, Desmazieres A *et al*. Rapid disruption of axon–glial integrity in response to mild cerebral hypoperfusion. *J Neurosci* 2011; **31**: 18185–18194.
11 Webster NJ, Green KN, Peers C, Vaughan PF. Altered processing of amyloid precursor protein in the human neuroblastoma SH-SY5Y by chronic hypoxia. *J Neurochem* 2002; **83**: 1262–1271.

12 Almeida A, Delgado-Esteban M, Bolanos JP, Medina JM. Oxygen and glucose deprivation induces mitochondrial dysfunction and oxidative stress in neurones but not in astrocytes in primary culture. *J Neurochem* 2002; **81**: 207–217.
13 Bayes A, Grant SG. Neuroproteomics: understanding the molecular organization and complexity of the brain. *Nat Rev Neurosci* 2009; **10**: 635–646.
14 James R, Searcy JL, Le Bihan T, Martin SF, Gliddon CM, Povey J *et al.* Proteomic analysis of mitochondria in APOE transgenic mice and in response to an ischemic challenge. *J Cereb Blood Flow Metab* 2012; **32**: 164–176.
15 Dennis G, Sherman B, Hosack D, Yang J, Gao W, Lane H *et al.* DAVID: Database for annotation, visualization, and integrated discovery. *Genome Biol* 2003; **4**: R60.
16 Deighton RF, Kerr LE, Short DM, Allerhand M, Whittle IR, McCulloch J. Network generation enhances interpretation of proteomic data from induced apoptosis. *Proteomics* 2010; **10**: 1307–1315.
17 Griffiths IR, Duncan ID, McCulloch M. Shaking pups: a disorder of central myelination in the spaniel dog. II. Ultrastructural observations on the white matter of the cervical spinal cord. *J Neurocytol* 1981; **10**: 847–858.
18 Bell KF, Hardingham GE. CNS peroxiredoxins and their regulation in health and disease. *Antioxid Redox Signal* 2011; **14**: 1467–1477.
19 Iwata S, Lee JW, Okada K, Lee JK, Iwata M, Rasmussen B *et al.* Complete structure of the 11-subunit bovine mitochondrial cytochrome bc1 complex. *Science* 1998; **281**: 64–71.
20 Guzy RD, Hoyos B, Robin E, Chen H, Liu L, Mansfield KD *et al.* Mitochondrial complex III is required for hypoxia-induced ROS production and cellular oxygen sensing. *Cell Metab* 2005; **1**: 401–408.
21 Kim SH, Vlkolinsky R, Cairns N, Lubec G. Decreased levels of complex III core protein 1 and complex V beta chain in brains from patients with Alzheimer's disease and Down syndrome. *Cell Mol Life Sci* 2000; **57**: 1810–1816.
22 Gil V, Nicolas O, Mingorance A, Urena JM, Tang BL, Hirata T *et al.* Nogo-A expression in the human hippocampus in normal aging and in Alzheimer disease. *J Neuropathol Exp Neurol* 2006; **65**: 433–444.
23 Murayama KS, Kametani F, Saito S, Kume H, Akiyama H, Araki W. Reticulons RTN3 and RTN4-B/C interact with BACE1 and inhibit its ability to produce amyloid beta-protein. *Eur J Neurosci* 2006; **24**: 1237–1244.
24 Janssen RJ, Nijtmans LG, van den Heuvel LP, Smeitink JA. Mitochondrial complex I: structure, function and pathology. *J Inherit Metab Dis* 2006; **29**: 499–515.
25 Arrell DK, Elliott ST, Kane LA, Guo Y, Ko YH, Pedersen PL *et al.* Proteomic analysis of pharmacological preconditioning. *Circ Res* 2006; **99**: 706–714.
26 Yao J, Chen S, Mao Z, Cadenas E, Brinton RD. 2-Deoxy-D-glucose treatment induces ketogenesis, sustains mitochondrial function, and reduces pathology in female mouse model of Alzheimer's disease. *PLoS ONE* 2011; **6**: e21788.
27 Lustbader JW, Cirilli M, Lin C, Xu HW, Takuma K, Wang N *et al.* ABAD directly links Abeta to mitochondrial toxicity in Alzheimer's disease. *Science* 2004; **304**: 448–452.
28 Du H, Yan SS. Mitochondrial permeability transition pore in Alzheimer's disease: Cyclophilin D and amyloid beta. *Biochim Biophys Acta (BBA)* 2010; **1802**: 198–204.
29 Scheper W, Nijholt DA, Hoozemans JJ. The unfolded protein response and proteostasis in Alzheimer disease: preferential activation of autophagy by endoplasmic reticulum stress. *Autophagy* 2011; **7**: 910–911.
30 Badiola N, Penas C, Minano-Molina A, Barneda-Zahonero B, Fado R, Sanchez-Opazo G *et al.* Induction of ER stress in response to oxygen-glucose deprivation of cortical cultures involves the activation of the PERK and IRE-1 pathways and of caspase-12. *Cell Death Dis* 2011; **2**: e149.
31 Schuck S, Prinz WA, Thorn KS, Voss C, Walter P. Membrane expansion alleviates endoplasmic reticulum stress independently of the unfolded protein response. *J Cell Biol* 2009; **187**: 525–536.
32 Apetri AC, Horwich AL. Chaperonin chamber accelerates protein folding through passive action of preventing aggregation. *Proc Natl Acad Sci* 2008; **105**: 17351–17355.
33 Taylor JP, Hardy J, Fischbeck KH. Toxic proteins in neurodegenerative disease. *Science* 2002; **296**: 1991–1995.
34 Ciechanover A, Brundin P. The ubiquitin proteasome system in neurodegenerative diseases: sometimes the chicken, sometimes the egg. *Neuron* 2003; **40**: 427–446.
35 Valera AG, Diaz-Hernandez M, Hernandez F, Ortega Z, Lucas JJ. The ubiquitin-proteasome system in Huntington's disease. *Neuroscientist* 2005; **11**: 583–594.
36 Paschen W, Mengesdorf T, Aufenberg C. Suppression of protein synthesis after transient cerebral ischemia. *Int Congr Ser* 2003; **1252**: 179–191.
37 Zhang K, Kaufman RJ. The unfolded protein response: a stress signaling pathway critical for health and disease. *Neurology* 2006; **66**(2 Suppl 1): S102–S109.
38 Wetzel M, Li L, Harms KM, Roitbak T, Ventura PB, Rosenberg GA *et al.* Tissue inhibitor of metalloproteinases-3 facilitates Fas-mediated neuronal cell death following mild ischemia. *Cell Death Differ* 2008; **15**: 143–151.
39 Zhang J, Li Y, Zheng X, Gao Q, Liu Z, Qu R *et al.* Bone marrow stromal cells protect oligodendrocytes from oxygen-glucose deprivation injury. *J Neurosci Res* 2008; **86**: 1501–1510.
40 Mazzio EA, Soliman YI, Soliman KF. Variable toxicological response to the loss of OXPHOS through 1-methyl-4-phenylpyridinium-induced mitochondrial damage and anoxia in diverse neural immortal cell lines. *Cell Biol Toxicol* 2010; **26**: 527–539.

Supplementary Information accompanies the paper on the Journal of Cerebral Blood Flow & Metabolism website (http://www.nature.com/jcbfm)

VIEWPOINT

Total variance should drive data handling strategies in third generation proteomic studies

Abigail G. Herrmann[1], James L. Searcy[1]*, Thierry Le Bihan[2,3], James McCulloch[1] and Ruth F. Deighton[1]*

[1] Centre for Cognitive and Neural Systems, University of Edinburgh, Edinburgh, UK
[2] SynthSys, University of Edinburgh, Edinburgh, UK
[3] Institute of Structural and Molecular Biology, University of Edinburgh, Edinburgh, UK

Received: February 6, 2013
Revised: August 2, 2013
Accepted: August 21, 2013

Quantitative proteomics is entering its "third generation," where intricate experimental designs aim to increase the spatial and temporal resolution of protein changes. This paper re-analyses multiple internally consistent proteomic datasets generated from whole cell homogenates and fractionated brain tissue samples providing a unique opportunity to explore the different factors influencing experimental outcomes. The results clearly indicate that improvements in data handling are required to compensate for the increased mean CV associated with complex study design and intricate upstream tissue processing. Furthermore, applying arbitrary inclusion thresholds such as fold change in protein abundance between groups can lead to unnecessary exclusion of important and biologically relevant data.

Keywords:
Bioinformatics / Differential protein expression / LC-MS/MS / Protein marker discovery / Proteome analysis

Proteomics is entering its "third generation," where MS is increasingly being used, not only to quantify total protein levels, but also to investigate how proteins within specific cell types and subcellular organelles respond both spatially and temporally to a host of experimental stimuli. [1]. As proteomic studies embark on more intricate designs, it is essential to re-evaluate whether the currently used data-handling strategies remain appropriate. Fundamental weaknesses and arbitrary design decisions still permeate proteomic research, despite efforts to improve the rigor of data handling [2–7]. This article compares primary datasets generated contemporaneously in our laboratory using peak intensity based LC-MS to provide a novel perspective on the suitability of various inclusion criteria and data-handling strategies in analyzing third generation proteomic data.

Correspondence: Abigail Herrmann, University of Edinburgh, 1 George Square, Edinburgh, EH8 9JZ, UK
E-mail: A.G.Herrmann@sms.ed.ac.uk
Fax: +44-131-651-1835

Abbreviations: GRP78, glucose regulated protein 78; **GRP94**, glucose regulated protein 94; **OGD**, oxygen-glucose deprivation

Many quantitative LC-MS proteomic studies use an initial inclusion criterion that proteins should be identified with two or more peptides. Though seemingly arbitrary, this inclusion criterion is important for two reasons: first, removal of proteins identified with only one peptide increases the reliability of LC-MS protein identification and helps avoid false detections. A single peptide feature may be found in several proteins or protein isoforms, therefore a truly definitive identification is less likely [8]. Second, this cut-off of two peptides for identification purposes significantly reduces the overall variance within the dataset, defined as the mean of the coefficient of variances for all proteins in the dataset. This reduction is variance considerably increases the power to detect subtle protein changes (Fig. 1). There is clearly a trade-off between reducing variance and the number of proteins remaining for analysis. Extending the inclusion criterion to identification of proteins with three or more peptides further reduces variance, however, also drastically reduces the number of proteins by nearly half of those originally identified by one peptide.

*These authors contributed equally to this work.

VIEWPOINT

Correspondence concerning this and other Viewpoint articles can be accessed on the journals' home page at: http://viewpoint.proteomics-journal.de

Correspondence for posting on these pages is welcome and can also be submitted at this site.

Subcellular proteomics will be a dominant theme in third generation proteomic research, yet sample fractionation can greatly impact variance within protein datasets. Sample processing techniques including the enrichment of microvessels, mitochondria [9] or white matter [10] can be used upstream of proteomic analysis to provide a more in-depth proteomic profile of how individual cell types and subcellular compartments are responding to experimental stimuli. However, increasing technicality upstream of protein detection increases the total variance of the final dataset, as demonstrated by analysis of our own proteomic data generated using a range of enrichment techniques (Fig. 2). White matter enrichment via micropunches of the corpus callosum and microvessel enrichment using density gradient centrifugation, two intricate upstream tissue handling techniques, induce a 7 and 15% increase in total variance in control tissue, respectively, compared to whole brain homogenates. We hypothesise that this increase in variance might be linked to varying degrees of protein degradation occurring when samples are handled at room temperature for extended periods of time. Upstream tissue processing enriches samples with targeted proteins, improving the spatial resolution of detected protein changes. However, the associated increases in variance make detection of subtle protein changes more difficult.

The magnitude of the change in protein abundance (fold change) is a popular but arbitrary inclusion criterion often used to dissect proteomic data. Analysis of our in vitro human cell line data shows that employing an arbitrary fold change value as a data dissection tool can exclude important proteins from the final analysis. This in vitro study investigated the effects of a global metabolic challenge on mitochondrial function and cellular proteomics. A total of 958 proteins were identified with two or more peptides ($n = 6$/group). A stringent a priori inclusion criterion of a $p < 0.01$ was set for a protein change to be deemed significant, resulting in a final protein list of 193 significantly altered proteins [11] (Fig. 3A). However, as well as a *p*-value threshold, many investigators also utilize a fold change cut-off to rapidly identify the most "important" protein changes. Datasets with a low overall variance allow for the detection of subtle protein changes, however, employing an arbitrary fold change inclusion criterion such as the popular "minimum 1.5 fold change" on these low variance datasets excludes the subtle yet significant protein changes. The fold change cut-off drastically reduces the number of proteins included in the final analysis and increases the risk of creating false negatives (Fig. 3A).

A similar analysis of the impact of arbitrary fold change cut-offs was carried out on the more variable microvessel extraction data (Fig. 3B). Due to the increased variability of these data (as shown in Fig. 2C), employing a stringent alpha value of $p < 0.01$ significantly reduces the number of proteins in the final list for analysis from 653 identified with two or more peptides to only 12. In this more variable system, imposing a 1.5 fold change cut-off has no further effect on protein number, due to a large fold change required to overcome the variance for inclusion at the set alpha level. It is therefore concluded that inclusion of a fold change data cut-off is either dangerous in the creation of false negatives (in studies with low overall variance) or irrelevant (in studies with high overall variance).

Alternatively, power calculations can be used to determine the magnitude of change required to detect a significant

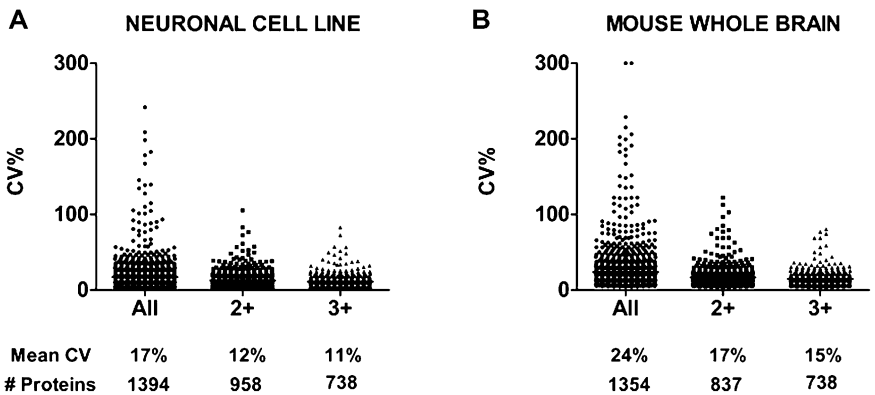

Figure 1. Variance structure is affected by the number of peptides used for protein identification. (A) Quantifying proteins with at least two peptides reduces the mean CV by 5% in a human cell line and (B) by 7% in mouse whole brain, reducing the total list of proteins by 31–38%. More stringent inclusion criteria (>3 peptides) has minimal effect on the variance but reduces the overall protein number by ~50%. A set initial inclusion criterion in proteomic data analysis should therefore be protein identification by at least two peptides. Each data point is the CV of the abundance measurements for each individual protein. The CV is calculated for individual proteins using abundance values from independent biological replicates.

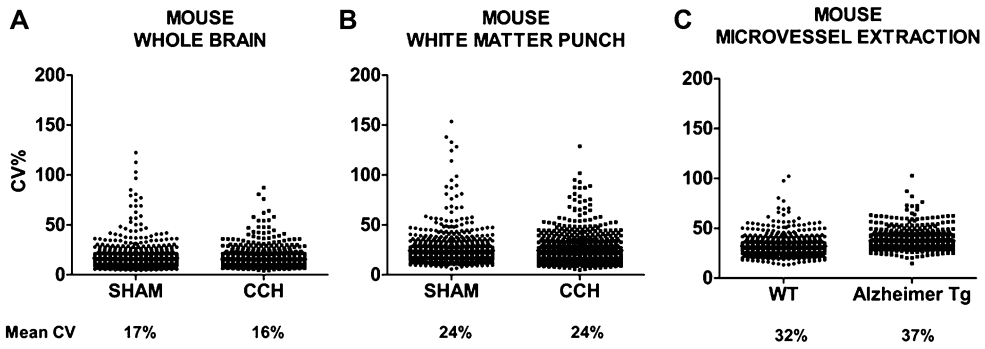

Figure 2. Complex tissue processing techniques have a direct effect on the total variance of the dataset. (A) Whole brain tissue samples show very similar overall CV in both sham and chronic cerebral hypoperfusion groups (17 and 16%, respectively). (B) White matter dissection introduces more variance into the system (24% for both sham and chronic cerebral hypoperfusion). (C) Technically demanding techniques such as microvessel dissection further increase variance (32 and 37% in wild type (WT) and transgenic (Tg) mice, respectively). Independent variables (surgery or transgene) have little effect on the variance structure of the data. The internal consistency of the three datasets controls for the technical variance introduced by the LC-MS technique, allowing the effect of tissue processing on the total variance to be assessed. Each data point represents the CV for the abundance measurement of individual proteins across independent replicates in each study, with the mean CV across all proteins shown.

difference between two populations given the technical and biological variance [5]. Used a priori, power calculations are beneficial in study design, guiding decisions regarding the number of replicates needed to obtain a set level of power [12]. However, the nature of a priori power calculations means these calculations are based on an estimate of overall biological and technical variance. Our analysis reveals that the CV is highly dependent upon the type of tissue being analyzed and the degree of upstream tissue processing involved (Fig. 2). Using a CV that is not specific to the dataset to decide detectable fold change can be problematic, and could lead to an over- or underestimation of proteins found to be differentially expressed. To ensure maximum accuracy in a priori power calculations, extensive and specific pilot data should be obtained.

The question of whether inclusion of fold change cut-offs in addition to a *p*-value cut-off adds biological value to proteomic data remains. To assess this, we identified two key proteins involved in the endoplasmic reticulum stress response: glucose regulated protein 78 (GRP78) and glucose regulated protein 94 (GRP94). In our in vitro study, experimental intervention with the metabolic challenge of oxygen-glucose deprivation (OGD) saw significant upregulation of GRP78 and GRP94 ($p < 0.01$). However, GRP78 underwent a fold change of 1.53, whereas GRP94 only had a fold change of 1.48 (Fig. 3C and D) [11]. The popular fold change cut-off of 2 would exclude both of these proteins from the analysis, and only GRP78 would be included if a fold change of 1.5 was used. The interplay between these two proteins is integral to the endoplasmic reticulum stress response; however, one or both of these proteins would be lost from the final dataset if an arbitrary fold change inclusion criterion was employed. Temporal evolution of protein level change is another important factor to be considered in understanding third generation proteomics. Data from the in vitro study demonstrate that following 6 h of OGD, small increases in protein levels of GRP78 and GRP94 predict larger increases following 18 h OGD (Fig. 3C and D). These results suggest that protein fold change should not be used as threshold for inclusion, but rather as an indicator of evolving events occurring within the cell. A protein exhibiting a small fold change at an early time point can be indicative of increasing abundance that might be detected as significant at a later time.

The ability to detect a fold change at a particular level of significance is intrinsically linked to the variance of the data, and this variance is dependent on tissue source and processing techniques (Fig. 2). It is therefore misguided to include fold change in the initial stages of data dissection. A protein reaching the threshold set by a stringent *p*-value (which in its nature incorporates the variance and the magnitude of change) should be sufficient for the initial inclusion criterion, resulting in a much reduced but relevant list of protein changes (Fig. 3).

The concept of excluding proteins based on fold change not only increases the likelihood of making type II errors, but is also fundamentally flawed given that the biological relevance of a change in protein abundance is likely to be protein specific. For example, proteins in the Bcl-2 family are important evolutionarily conserved regulators of apoptosis. However, even within this family, certain proteins are more influential than others: PUMA (p53 upregulated modulator of apoptosis) being one of the most potent [13]. Subtle changes in this protein are likely to have important cellular effects; however, may be ruled out if stringent fold change cut-offs are employed when analyzing data. The importance of subtle protein changes needs to be recognized in the analysis of large proteomic datasets to avoid the loss of valuable data through the use of inappropriate fold change cut-offs.

The issue of multiple hypothesis testing, where investigating changes in many separate proteins can lead to

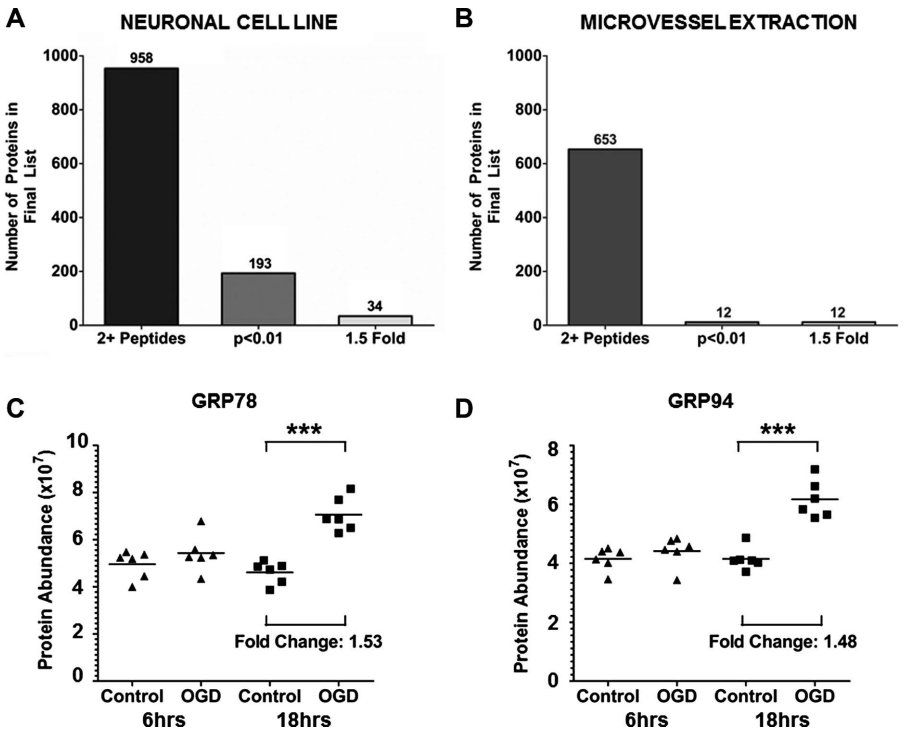

Figure 3. Arbitrary fold change cut-offs are associated with the increased likelihood false negatives. (A) Employing the common "minimum 1.5 fold change" inclusion criterion on datasets with low overall variance drastically reduces the number of proteins available for analysis. A stringent alpha value of $p < 0.01$ reduces the number of proteins in from 958 identified with two or more peptides to 193. Imposing an additional fold change cut-off of 1.5 on this reduced protein list results in a final list for analysis containing only 34 proteins. (B) Analysis of the more variable microvessel enrichment data demonstrates that a stringent alpha value of $p < 0.01$ reduces the number of proteins available for analysis from 653 identified with two or more peptides to only 12. Imposing a 1.5 fold change cut-off has no further effect on protein number, due to a large fold change required to overcome the variance for inclusion at the set alpha threshold. (C) Biologically relevant protein GRP78 is significantly increased following a severe metabolic challenge (18 h OGD), and undergoes a fold change increase of 1.53 from control to OGD samples. This protein would be included for further analysis in most proteomic studies (D) Biologically related protein GRP94 is also significantly increased following a severe metabolic challenge (18 h OGD), however, undergoes a fold change increase of 1.48. This protein would be excluded from further analysis in most proteomic studies, demonstrating the arbitrary and irrelevant nature of fold change inclusion criteria. Each data point in C and D represent an independent biological replicate ($n = 6$ for each condition).

significant results purely by chance, is an important and widely reviewed issue that is not formally dealt with in this article [4, 14–16]. However, consideration should be given to the fact that overly stringent corrections for multiple comparisons can limit the ability to glean biologically meaningful conclusions from data. Typical methods, such as the Bonferroni correction, are too stringent when studying changes in hundreds of gene or protein abundances in microarray and proteomic experiments. A less stringent method for dealing with multiple comparisons is to employ the false discovery rate, described by Benjamini and Hochberg, based on the frequency distribution of the statistically generated *p*-values [17]. It must be noted that a level of arbitrariness remains when implementing a false discovery rate. The rate of incorrectly rejecting the null hypotheses is chosen by the individual, depending on the perceived acceptability of false-positives remaining in the final dataset.

As proteomic technology advances, it is important to remember where the true power of proteomics lies: as a hypothesis generator and a tool for generating candidates of potential biomarkers and drug targets of disease. The utility of proteomics is greatest when a maximum number of proteins are identified and included for further analysis. Data processing techniques such as an initial inclusion of a protein identification threshold of two or more peptides give the researcher confidence in the protein identification. Statistical significance should then be considered as a sufficient threshold in detecting important protein changes. Pushing proteins to clear too many hurdles on their way to the final dataset increases the likelihood of omitting biologically interesting and relevant data.

AGH is supported by the MRC. This research is supported by Age UK as part of the Disconnected Mind programme, performed under the aegis of the Centre for Cognitive Aging and Cognitive Epidemiology. TLB is funded by SynthSys, a Centre for Integrative Systems Biology funded by BBSRC and EPSRC; reference BB/D019621/1. RD is funded by the Melville Trust.

The authors have declared no conflicts of interest.

References

[1] Lamond, A. I., Uhlen, M., Horning, S., Makarov, A. et al., Advancing Cell Biology Through Proteomics in Space and Time (PROSPECTS). *Mol. Cell. Proteomics* 2012, *11*, O112.017731.

[2] Podwojski, K., Stephan, C., Eisenacher, M., Important issues in planning a proteomics experiment: statistical considerations of quantitative proteomic data. *Methods Mol. Biol.* 2012, *893*, 3–21.

[3] Karp, N. A., Lilley, K. S., Design and analysis issues in quantitative proteomics studies. *Proteomics* 2007, *7*, 42–50.

[4] Diz, A. P., Carvajal-Rodriguez, A., Skibinski, D. O., Multiple hypothesis testing in proteomics: a strategy for experimental work. *Mol. Cell. Proteomics* 2011, *10*, M110 004374.

[5] Levin, Y., The role of statistical power analysis in quantitative proteomics. *Proteomics* 2011, *11*, 2565–2567.

[6] Deighton, R. F., Kerr, L. E., Short, D. M., Allerhand, M. et al., Network generation enhances interpretation of proteomic data from induced apoptosis. *Proteomics* 2010, *10*, 1307–1315.

[7] Karp, N. A., McCormick, P. S., Russell, M. R., Lilley, K. S., Experimental and statistical considerations to avoid false conclusions in proteomics studies using differential in-gel electrophoresis. *Mol. Cell. Proteomics* 2007, *6*, 1354–1364.

[8] Mallick, P., Kuster, B., Proteomics: a pragmatic perspective. *Nat. Biotechnol.* 2010, *28*, 695–709.

[9] James, R., Searcy, J. L., Le Bihan, T., Martin, S. F. et al., Proteomic analysis of mitochondria in APOE transgenic mice and in response to an ischemic challenge. *J. Cereb. Blood Flow Metab.* 2012, *32*, 164–176.

[10] Reimer, M. M., McQueen, J., Searcy, L., Scullion, G. et al., Rapid disruption of axon-glial integrity in response to mild cerebral hypoperfusion. *J. Neurosci.* 2011, *31*, 18185–18194.

[11] Herrmann, A. G., Deighton, R. F., Le Bihan, T., McCulloch, M. C. et al., Adaptive changes in the neuronal proteome: mitochondrial energy production, endoplasmic reticulum stress, and ribosomal dysfunction in the cellular response to metabolic stress. *J. Cereb. Blood Flow Metab.* 2013, *33*, 673–683.

[12] Bezeau, S., Graves, R., Statistical power and effect sizes of clinical neuropsychology research. *J. Clin. Exp. Neuropsychol.* 2001, *23*, 399–406.

[13] Yu, J., Zhang, L., PUMA, a potent killer with or without p53. *Oncogene* 2008, *27*, S71–S83.

[14] Storey, J. D., Tibshirani, R., Statistical significance for genomewide studies. *Proc. Natl. Acad. Sci.* 2003, *100*, 9440–9445.

[15] Almudevar, A., Multiple hypothesis testing: a methodological overview. *Methods Mol. Biol.* 2013, *972*, 37–55.

[16] Goloborodko, A. A., Mayerhofer, C., Zubarev, A. R., Tarasova, I. A. et al., Empirical approach to false discovery rate estimation in shotgun proteomics. *Rapid Commun. Mass Spectrom.* 2010, *24*, 454–462.

[17] Benjamini, Y., Hochberg, Y., Controlling the false discovery rate: a practical and powerful approach to multiple testing. *J. R. Stat. Soc Series B Methodol.* 1995, *57*, 289–300.

